

POLY(LACTIC ACID) BASED NANOCOMPOSITES: MECHANICAL,
THERMAL AND RHEOLOGICAL PROPERTIES AND MORPHOLOGY

A THESIS SUBMITTED TO
THE GRADUATE SCHOOL OF NATURAL AND APPLIED SCIENCES
OF
MIDDLE EAST TECHNICAL UNIVERSITY

BY

EDA AÇIK

IN PARTIAL FULFILLMENT OF THE REQUIREMENTS
FOR
THE DEGREE OF DOCTOR OF PHILOSOPHY
IN
CHEMICAL ENGINEERING

JULY 2014

Approval of the thesis:

**POLY(LACTIC ACID) BASED NANOCOMPOSITES: MECHANICAL,
THERMAL AND RHEOLOGICAL PROPERTIES AND MORPHOLOGY**

Submitted by **EDA AÇIK** in partial fulfillment of the requirements for the degree of
**Doctor of Philosophy in Chemical Engineering Department, Middle East
Technical University** by,

Prof. Dr. Canan Özgen

Dean, Graduate School of **Natural and Applied Sciences** _____

Prof. Dr. Halil Kalıpçılar

Head of Department, **Chemical Engineering** _____

Prof. Dr. Ülkü Yilmazer

Supervisor, **Chemical Engineering Dept., METU** _____

Examining Committee Members:

Prof. Dr. Erdal Bayramlı

Chemistry Dept., METU _____

Prof. Dr. Ülkü Yilmazer

Chemical Engineering Dept., METU _____

Prof. Dr. Göknur Bayram

Chemical Engineering Dept., METU _____

Assoc. Prof. Dr. Güralp Özkoç

Chemical Engineering Dept., Kocaeli Uni. _____

Assist. Prof. Dr. Erhan Bat

Chemical Engineering Dept., METU _____

Date: July 7, 2014

I hereby declare that all information in this document has been obtained and presented in accordance with academic rules and ethical conduct. I also declare that, as required by these rules and conduct, I have fully cited and referenced all material and results that are not original to this work.

Name, Last Name: EDA AÇIK

Signature

ABSTRACT

POLY(LACTIC ACID) BASED NANOCOMPOSITES: MECHANICAL,
THERMAL AND RHEOLOGICAL PROPERTIES AND MORPHOLOGY

Açık, Eda

Ph.D., Department of Chemical Engineering

Supervisor: Prof. Dr. Ülkü Yılmaz

July 2014, 261 pages

The aim of this study was to increase the potential applications of poly(lactic acid) (PLA) by incorporating reactive functionalities with different nano-scale fillers. To investigate the effects of nanoclay types, five different organically modified nanoclays (Cloisites®15A, 25A and 30B and Nanofils®5 and 8) were used. Two elastomeric compatibilizers, ethylene-glycidyl methacrylate (E-GMA) and ethylene-butyl acrylate-maleic anhydride (E-BA-MAH), were added to the nanocomposites produced via melt compounding. The degree of clay dispersion was determined by the chemical compatibility between the polymer matrix and the modifier. Compatibility between C25A, C30B and E-GMA resulted in better dispersion and thus, enhanced tensile modulus and toughness. The network structure formed owing

to the high reactivity of the epoxide group of GMA towards the PLA end groups resulted in high impact toughness and solid-like behavior in the melt state.

Effects of filler loadings with different production methods (melt compounding and solution mixing) were investigated with expanded graphite (EG) as the filler. Filler loading was kept below 2 wt. % to minimize the dispersion problem and solvent usage. No significant changes were observed in filler dispersion in both methods. However, when E-GMA was added, melt compounded blends had phase separated matrix morphology and solution mixed blends had continuous matrix morphology. Significant decreases in ultimate tensile strength and elastic modulus, but increased strain at failure were observed for samples prepared by solution mixing. Enhancements in elastic behavior and complex viscosity of composites in the melt state are other remarkable outcomes of addition of E-GMA by the solution mixing method.

Keywords: poly(lactic acid), organoclay, expanded graphite, compatibilizer, nanocomposite

ÖZ

POLİ(LAKTİK ASİT) BAZLI NANOKOMPOZİTLER: MEKANİK, ISISAL VE REOLOJİK ÖZELLİKLERİ VE MORFOLOJİSİ

Açık, Eda

Doktora, Kimya Mühendisliği Bölümü

Tez Yöneticisi : Prof. Dr. Ülkü Yılmaz

Temmuz 2014, 261 sayfa

Bu çalışmanın amacı poli(laktik asit)'in, (PLA), muhtemel kullanım alanlarının reaktif fonksiyonel gruplar ile çeşitli nano-boyutlu dolgu malzemeleri kullanılarak arttırılmasıdır. Farklı kil tiplerinin malzeme özelliklerine etkisinin incelenmesi amacıyla organik olarak modifiye edilmiş beş farklı kil (Cloisite® 15A, 25A ve 30B, ve Nanofiller® 5 ve 8) kullanılmıştır. Elastomerik yapıdaki iki farklı uyumlaştırıcı, etilen-gliseril metakrilat (E-GMA) ve etilen-bütül akrilat-maleik anhidrit (E-BA-MAH), eriyik karıştırma yöntemi ile üretilen nanokompozitlere eklenmiştir. Kil dağılımını belirleyen unsur polimer matrisi ile kil modifikasyonunun kimyasal uyumudur. C25A ve C30B ile E-GMA arasındaki polarite eşleşmesi bu killerin matris içinde daha iyi dağılması ve bunun sonucunda gerilim modülü ve

tokluğunun artması ile sonuçlanmıştır. GMA içindeki epoksi grubunun polimer matrisinin fonksiyonel gruplarına olan yüksek reaktivitesi nedeniyle oluşan ağsı yapı, darbe dayanımı ve eriyik haldeki katı-benzeri davranışta artış ile sonuçlanmıştır.

Dolgu malzemesi olarak tabaka aralıkları genişletilmiş grafit (EG) kullanımında nanokompozit üretim yöntemlerinin (eriyik karıştırma ve çözelti içinde karıştırma) etkileri araştırılmıştır. Malzeme içinde dağılım ve solvent kullanımı problemlerini en aza indirmek için dolgu malzemesi yüklemesi ağırlıkça % 2'nin altında tutulmuştur. İki yöntem arasında dolgu malzemesi dağılımı açısından büyük değişiklik olmamıştır. Ancak, E-GMA eklendiğinde eriyik harmanlama yöntemi ile üretilen karışım ve nanokompozitlerde faz ayrışımı morfoloji, çözelti içinde karıştırma ile hazırlananlarda ise kesiksiz (sürekli) morfoloji elde edilmiştir. Çözelti içinde karıştırma yöntemi ile hazırlanan numunelerin gerilme dayanımı ve modülünde önemli düşüş olmuş, ancak kopmadaki uzamada artış görülmüştür. Çözelti içinde karıştırma yöntemi ile hazırlanan kompozitlerin eriyik hallerinde elastik davranış ve viskozitede oluşan önemli artışlar göze çarpan bir diğer sonuçtur.

Anahtar Sözcükler: poly(laktik asit), organokil, grafit, uyumlaştırıcı, nanokompozit

To my beloved family

ACKNOWLEDGEMENTS

I wish to express my sincere gratitude to my supervisor Prof. Dr. Ülkü Yılmaz for his valuable guidance, advices, encouragements and support during this study. It was a pleasing honor for me to work with him and I sincerely appreciate the time and effort he has taken during my supervision.

I also wish to thank to Prof. Dr. Göknur Bayram for her positive attitude, helpful comments and suggestions about my studies and also for providing me every opportunity to use the instruments in her laboratory. I would also like to thank to Prof. Dr. Erdal Bayramlı for his valuable advices and critics for the completion of this work. I am thankful to Dr. Neşe Orbey from University of Massachusetts at Lowell for her hospitality, for giving me the opportunity to work in her laboratory and helping me in every possible way.

I would like to thank to especially Dr. Cevdet Öztin, Prof. Dr. Hayrettin Yücel, Prof. Dr. Deniz Üner, Prof. Dr. İnci Eroğlu, Prof. Dr. Pınar Çalık, Prof. Dr. Işık Önal, and Assoc. Prof. Dr. Çerağ Dilek Hacıhabiboğlu and all faculty members of Chemical Engineering Department. Each and every one of them, at some time during my study, helped me in different ways with their comments and suggestions or taught me something about research, academia or just about life.

During my early times in the polymer laboratory, Dr. Sertan Yeşil, Dr. Fatma Işık Coşkunes, Dr. Tijen Seyidoğlu, Dr. Ali Sinan Dike were very kind and full of help to me. I want to express my thanks to them.

My special thanks about getting acquainted with the equipment and doing the experiments goes to Touffik Baouz from Université Abderrahmane Mira and İrem Şengör. Without them it would be impossible for me to even start the experiments and the time I spent in the lab would not be enjoyable and memorable. I also would

like to thank my lab mates Miray Yaşar, Yüksel Sayın, Erdem Balık, Elif Yürekli, Fadile Ezeroğlu and my dear students Sevil Demirci, Tuğçe Özkurt and Gizem Güngör who helped me in every possible way and gave their valuable friendship throughout my thesis work.

I would like to thank to Mihrican Açıkgöz from Department of Chemical Engineering for DSC and FTIR analyses; Necmi Avcı from Department of Metallurgical and Materials Engineering, Ali Güzel and Pınar Tokmakkaya from METU Central Laboratories for the X-ray analyses; Seçkin Öztürk, Tuğba Endoğan and Sedat Canlı from METU Central Laboratories for SEM analyses; and Mustafa Güler from Bilkent University UNAM Laboratories for ultramicrotome and TEM analyses.

Heartfelt thanks to everyone who helped me about my studies during the time I spent in UMass Lowell. Prof. Dr. Robert Malloy and Dr. Meg Sobkowicz-Kline made invaluable comments on the problems I faced during rheology investigations and gave me the opportunity to use the instruments in their laboratories. Dr. Earl Ada, helped me in sample preparation and spent his valuable time for TEM trials. Nathanael Effendy helped in sample preparation, JeongIn Gug, and Xun Chen helped in molding and rheometer usage. Brian Pleskowicz, Thorsten Dieckow, Matt Gallant, and James Ogilvie-Battersby provided their support and friendship.

I am also thankful to all administrative and technical staff of Department of Chemical Engineering METU with special thanks to Turgut Aksakal, Süleyman Nazif Kuşhan, Yavuz Güngör, Gülüstan Görmez, Naciye Kaya, and Özlem Güven Pak for their help and support.

Above all, I had my friends with me in every single occasion. I should start with Merve Akkuş who witnessed everything about my life and my studies for more than eight years and it was a pleasure to work with her. Eda Bayraktar gave her endless friendship, support, and help in all parts of my life. Canan Yeniova Erpek, Özge Mercan and Miray Gezer are the ones with whom I shared the precious memories in that legendary office room, CZ-01. And I have lots of friends with whom I shared countless unforgettable memories in the department: Ayça Arınan, Emine Kurnaz,

Deniz Onay, Barış Erdoğan, İlker Tezsevin, Saltuk Pirgaliöđlu, Sevler Gökçe Avciođlu, İrfan Tuđçe Ersöz and many other teaching assistants and graduate students. For the time I spent in US, I wish to express my utmost appreciation to Fulya Sudur for her unlimited hospitality and friendship. Again during the time I spent in Lowell Tuđba Demirciođlu Arsava, Sarp Arsava, Umut Zalluhođlu, Ayhan Sebastian Bayırlı, Merve Tüccar, and Efe Burak gave me their invaluable friendship and made me feel like at home.

I wish to present my deepest gratitude to my bosom friend, Tuba Kâhya. I could not imagine how I would complete writing this thesis without her. She endeavored for every single line of this dissertation.

I would like to express my sincere appreciation to my beloved family. I am forever grateful for the love and support of my parents, İlkay and Turgut Açıık and my sister Hande İřman. At every step of my life they were just beside me with their endless support. And heartfelt thanks to my best friend and life companion Engin Çumkur for his unlimited love, patience and encouragement throughout my graduate studies. I am dedicating this work to them, whose love always encouraged me.

This study was partially supported by The Scientific and Technological Research Council of Turkey (TUBITAK) under scholarship code 2214-A International Research Fellowship Program and also supported by the Middle East Technical University Research Fund Project (BAP-03-04-2012-003).

TABLE OF CONTENTS

ABSTRACT	v
ÖZ	vii
ACKNOWLEDGEMENTS	x
TABLE OF CONTENTS	xiii
LIST OF TABLES	xviii
LIST OF FIGURES	xx
LIST OF SYMBOLS	xxxi

CHAPTERS

1. INTRODUCTION	1
2. BACKGROUND INFORMATION	7
2.1. Composite Materials.....	7
2.1.1 Polymer Matrix Composites	9
2.2. Nanocomposites	9
2.2.1 Polymer – Layered Silicate Nanocomposites	10
2.2.1.1 Structure of Layered Silicates	11
2.2.1.2 Organic Modification of Silicate Layers.....	13
2.2.1.3 Polymer Layered Silicate Nanocomposite Types	14
2.2.1.4 Thermodynamics of Nanocomposite Formation.....	15
2.2.2 Preparation of Polymer-Layered Silicate Nanocomposites	17
2.2.2.1 Solution Intercalation	17

2.2.2.2	In Situ Polymerization Method	18
2.2.2.3	Melt Intercalation	18
2.2.3	Polymer – Graphite Nanocomposites	19
2.2.3.1	Structure of Graphite.....	20
2.2.3.2	Production of Different Graphite Structures	22
2.2.4	Preparation of Polymer-Graphite Nanocomposites	25
2.3.	Biodegradable Polymers	26
2.3.1	Poly(lactic acid): Structure and Synthesis	27
2.3.2	Material Properties of PLA	29
2.3.3	Advantages and Limitations of PLA.....	30
2.4.	Polymer Processing Methods	32
2.4.1	Extrusion	32
2.4.2	Solvent Assisted Ultrasonication	35
2.4.3	Injection Molding.....	36
2.4.4	Compression Molding.....	38
2.5.	Experimental Techniques for Material Characterization	38
2.5.1	Mechanical Properties.....	39
2.5.1.1	Tensile Test.....	39
2.5.1.2	Impact Test.....	42
2.5.2	Thermal Properties	44
2.5.2.1	Differential Scanning Calorimetry.....	44
2.5.3	Morphological Analyses	46
2.5.3.1	X-Ray Diffraction	46
2.5.3.2	Scanning Electron Microscopy	48
2.5.3.3	Transmission Electron Microscopy	50
2.5.4	Spectroscopic Analyses	51
2.5.4.1	Fourier Transform Infrared Spectroscopy	51
2.5.5	Rheological Analyses.....	52

2.6.	Previous Studies	54
3.	EXPERIMENTAL METHODS	69
3.1.	Materials	69
3.1.1	Polymer Matrix	69
3.1.2	Compatibilizers	70
3.1.3	Fillers	72
3.1.3.1	Organoclays.....	72
3.1.3.2	Expanded Graphite.....	75
3.2.	Nanocomposite Preparation	76
3.2.1.	Melt Compounding	76
3.2.2.	Solution Mixing	77
3.2.3.	Composite Compositions	79
3.2.4.	Sample Preparation	82
3.2.4.1	Injection Molding.....	83
3.2.4.2	Compression Molding.....	83
3.3.	Characterization of Nanocomposites.....	84
3.3.1.	Analysis of Morphology	85
3.3.1.1	X-Ray Diffraction	85
3.3.1.2	Scanning Electron Microscopy	85
3.3.1.3	Transmission Electron Microscopy.....	86
3.3.2	Spectroscopic Analysis	86
3.3.2.1	Fourier Transform Infrared Spectroscopy.....	86
3.3.3	Thermal Analysis	86
3.3.3.1	Differential Scanning Calorimetry.....	86
3.3.4	Mechanical Tests.....	87
3.3.4.1	Tensile Test.....	87
3.3.4.2	Impact Test.....	88

3.3.5	Rheological Analysis (UMass-Lowell).....	89
4.	RESULTS AND DISCUSSION.....	91
4.1.	PLA/Layered Silicate Nanocomposites	91
4.1.1	Determination of Processing Parameters	92
4.1.1.1	Dispersion of Clay	92
4.1.1.2	Mechanical Properties.....	93
4.1.2	Effects of Clay Type and Compatibilizer Structure.....	95
4.1.2.1	Morphological Analyses	95
4.1.2.2	Spectroscopic Analyses	117
4.1.2.3	Mechanical Analyses	119
4.1.2.4	Rheological Analyses.....	128
4.1.2.5	Thermal Analyses	139
4.2.	PLA/Expanded Graphite Nanocomposites.....	140
4.2.1	Characterization of Expanded Graphite	141
4.2.1.1	Energy-Dispersive X-Ray Spectroscopy	141
4.2.1.2	Brunauer–Emmett–Teller (BET) Surface Area Analyses.....	142
4.2.1.3	X-Ray Diffraction	142
4.2.2	Characterization of PLA/Expanded Graphite Composites	143
4.2.2.1	Morphological Analyses	143
4.2.2.2	Spectroscopic Analyses	163
4.2.2.3	Mechanical Analyses	164
4.2.2.4	Rheological Analyses.....	182
4.2.2.5	Thermal Analyses	197
5.	CONCLUSIONS	199
	REFERENCES	205

APPENDICES

A.	SPECTROSCOPIC ANALYSIS	225
B.	MECHANICAL ANALYSES	229
C.	DSC ANALYSES	231
D.	RHEOLOGY ANALYSES	249
E.	IMAGE ANALYSES	255
	CURRICULUM VITAE	259

LIST OF TABLES

TABLES

Table 2.1 Structure and chemistry of mica-type layered silicates [6].....	12
Table 2.2 Material properties of two commercial PLAs [50].....	30
Table 3.1 Properties of PLA (NaturePlast PLI-005) [123].....	69
Table 3.2 Properties of the impact modifier Lotader® AX8840 (E-GMA) [124].....	70
Table 3.3 Properties of the impact modifier Lotader® 2210 (E-BA-MAH) [124]....	71
Table 3.4 Properties of Cloisites® [125]	74
Table 3.5 Properties of Nanofils® [125]	75
Table 3.6 Properties of Timrex® C-Therm 001 [126].....	75
Table 3.7 Sample compositions prepared to investigate the effects of organoclays and compatibilizers	81
Table 3.8 Sample compositions prepared to investigate the effects of different production methods for PLA/EG composites	82
Table 3.9 Tensile test specimen dimensions according to ISO 527-2 Standards	88
Table 4.1 Mechanical properties of PLA/E-GMA/C30B (88/10/2) nanocomposites at different processing conditions	94
Table 4.2 Average domain sizes of all samples	108
Table 4.3 Characteristic bands in IR spectrum of PLA [137, 140].....	118
Table 4.4 Thermal properties of neat PLA, PLA/compatibilizer binary blends, PLA/organoclay and PLA/compatibilizer/organoclay nanocomposites determined by DSC.....	140
Table 4.5 Thermal properties of PLA, PLA/E-GMA binary blend, PLA/EG binary composites and PLA/E-GMA/EG ternary composites determined by DSC	198

Table B.1 Tensile test results of neat PLA, PLA/compatibilizer binary blends, PLA/organoclay binary nanocomposites and PLA/compatibilizer/organoclay ternary nanocomposites	229
Table B.2 Tensile test results of neat PLA, PLA/compatibilizer binary blends, PLA/EG binary nanocomposites and PLA/compatibilizer/EG ternary nanocomposites	230

LIST OF FIGURES

FIGURES

Figure 2.1 The structure of 2:1 layered silicates [6]	12
Figure 2.2 Schematic representation of a cation-exchange reaction between the silicate and alkylammonium salt [30]	13
Figure 2.3 Orientations of alkylammonium ions in the layered silicates galleries [32]	14
Figure 2.4 Schematic illustrations of A: conventional; B: intercalated; C: ordered exfoliated; and D: disordered exfoliated polymer–clay nanocomposites [32]	15
Figure 2.5 Schematic representation of the system components before and after the intercalation takes place [31]	16
Figure 2.6 Solution intercalation method for polymer-layered silicate nanocomposite preparation [36].....	17
Figure 2.7 In situ polymerization method for polymer-layered silicate nanocomposite preparation [36].....	18
Figure 2.8 Melt intercalation method for polymer-layered silicate nanocomposite preparation [36].....	19
Figure 2.9 Structures of diamond and graphite [40]	20
Figure 2.10 Crystal structure of graphite showing ABAB stacking sequence and unit cell [38]	21
Figure 2.11 Schematic representation of acid intercalation of graphite sheets.....	22
Figure 2.12 Schematic representation of graphite intercalation using alkali metals [41].....	23
Figure 2.13 SEM image of expanded graphite [43].....	24
Figure 2.14 Lactic acid optical monomers [51]	28
Figure 2.15 Synthesis routes of PLA [53]	29

Figure 2.16 Schematic representation of an extrusion line [58]	33
Figure 2.17 Parts of an extruder [58]	33
Figure 2.18 Parts of an extruder screw [58]	34
Figure 2.19 Screw configurations for twin screw extrusion [61].....	35
Figure 2.20 Schematic representation of thermoplastic injection molding machine [63]	36
Figure 2.21 Parts of a mold used for injection molding [63]	37
Figure 2.22 Pressure change during the injection molding cycle [65].....	37
Figure 2.23 Schematic representation of compression molding process [58]	38
Figure 2.24 Schematic representation of tensile test [58]	40
Figure 2.25 A typical dog-bone shaped tensile test specimen [67].....	40
Figure 2.26 Engineering data from tensile tests [58]	41
Figure 2.27 Typical stress–strain curves for polymeric materials [58].....	42
Figure 2.28 Schematic representation of Charpy and Izod impact tests [68]	43
Figure 2.29 Typical DSC curve [70].....	45
Figure 2.30 Interaction of X-rays with materials: scattering and diffraction mechanisms [73]	47
Figure 2.31 Bragg's Law reflection [75]	48
Figure 2.32 Schematic representation of beam-specimen interactions in SEM [78].	49
Figure 2.33 Layout of SEM instrument [79].....	49
Figure 2.34 The optical electron beam diagram of TEM [82]	51
Figure 2.35 Schematic representation of FTIR [85]	52
Figure 2.36 Schematic representation of a typical rheometer setup with the sample placed between two plates [88]	53
Figure 3.1 Chemical structure of PLA	70
Figure 3.2 Chemical structure of Lotader® AX8840	71
Figure 3.3 Chemical structure of Lotader® 2210	72
Figure 3.4 Chemical structure of organic modifier of Cloisite®15A	73
Figure 3.5 Chemical structure of organic modifier of Cloisite®25A	73
Figure 3.6 Chemical structure of organic modifier of Cloisite®30B	74
Figure 3.7 Thermoprism TSE 16 TC twin screw extruder.....	76

Figure 3.8 Preparation of nanocomposites through melt blending method	77
Figure 3.9 Preparation of PLA nanocomposites through solution mixing method ...	79
Figure 3.10 Flowchart of the study	80
Figure 3.11 A photograph of injection molding device	83
Figure 3.12 A photograph of the compression molding device.....	84
Figure 3.13 A photograph of the tensile testing machine	87
Figure 3.14 A photograph of the impact testing machine.....	89
Figure 3.15 A photograph of Ares G2 Rheometer.....	89
Figure 4.1 XRD patterns at different processing conditions.....	93
Figure 4.2 XRD patterns of neat PLA, C15A and PLA/C15A nanocomposites	96
Figure 4.3 XRD patterns of neat PLA, C25A and PLA/C25A nanocomposites	97
Figure 4.4 XRD patterns of neat PLA, C30B and PLA/C30B nanocomposites.....	97
Figure 4.5 XRD patterns of neat PLA, N5 and PLA/N5 nanocomposites	98
Figure 4.6 XRD patterns of neat PLA, N8 and PLA/N8 nanocomposites	98
Figure 4.7 SEM micrographs of neat PLA with (a) x500 and (b) x3000 magnifications.....	100
Figure 4.8 SEM micrographs of PLA/C15A nanocomposite with (a) x500 and (b)x3000 magnifications	101
Figure 4.9 SEM micrographs of PLA/C25A nanocomposite with (a) x500 and (b)x3000 magnifications	102
Figure 4.10 SEM micrographs of PLA/C30B nanocomposite with (a) x500 and (b)x3000 magnifications	102
Figure 4.11 SEM micrographs of PLA/N5 nanocomposite with (a) x500 and (b)x3000 magnifications	103
Figure 4.12 SEM micrographs of PLA/N8 nanocomposite with (a) x500 and (b)x3000 magnifications	103
Figure 4.13 SEM micrographs of PLA/E-GMA blend with (a) x500 and (b) x3000 magnifications.....	104
Figure 4.14 SEM micrographs of PLA/E-BA-MAH blend with (a) x500 and (b)x3000 magnifications	104

Figure 4.15 SEM micrographs of PLA/E-GMA/C15A nanocomposite with (a) x500 and (b) x3000 magnifications	105
Figure 4.16 SEM micrographs of PLA/E-GMA/C25A nanocomposite with (a) x500 and (b) x3000 magnifications	105
Figure 4.17 SEM micrographs of PLA/E-GMA/C30B nanocomposite with (a) x500 and (b) x3000 magnifications	106
Figure 4.18 SEM micrographs of PLA/E-GMA/N5 nanocomposite with (a) x500 and (b) x3000 magnifications	106
Figure 4.19 SEM micrographs of PLA/E-GMA/N8 nanocomposite with (a) x500 and (b) x3000 magnifications	106
Figure 4.20 SEM micrographs of PLA/E-BA-MAH/C25A nanocomposite with...	109
Figure 4.21 SEM micrographs of PLA/E-BA-MAH/N5 nanocomposite with.....	109
Figure 4.22 Low magnification TEM micrograph of PLA/C25A nanocomposite ..	110
Figure 4.23 High magnification TEM micrographs of PLA/C25A: (A) tactoids, (B)intercalated and (C) exfoliated clay nanoplatelets	111
Figure 4.24 Low magnification TEM micrograph of PLA/E-GMA/C25A nanocomposite.....	112
Figure 4.25 High magnification TEM micrograph of PLA/E-GMA/C25A nanocomposite.....	113
Figure 4.26 Low magnification TEM micrographs of PLA/N5 nanocomposite	114
Figure 4.27 High magnification TEM micrographs of PLA/N5 nanocomposite.....	115
Figure 4.28 Low magnification TEM micrographs of PLA/E-GMA/N5 nanocomposite.....	116
Figure 4.29 High magnification TEM micrographs of PLA/E-GMA/N5 nanocomposite.....	117
Figure 4.30 FTIR spectra of (a) PLA, (b) E-GMA, (c) E-BA-MAH, (d) PLA/C15A, (e) PLA/E-GMA/C15A, (f) PLA/E-BA-MAH/C15A.....	119
Figure 4.31 Typical stress-strain curve of neat PLA.....	120
Figure 4.32 Effect of organoclay and compatibilizer types on tensile strength.....	122
Figure 4.33 Effect of organoclay and compatibilizer types on Young's modulus...	123

Figure 4.34 Effect of organoclay and compatibilizer types on percent elongation at break.....	125
Figure 4.35 Effect of organoclay and compatibilizer types on impact strength	127
Figure 4.36 Time sweep curves of processed neat PLA, and PLA/E-GMA and PLA/E-BA-MAH blends at 170°C, at 5% strain amplitude and 10 rad/s.....	129
Figure 4.37 Strain sweep curves of processed neat PLA, PLA blends and, binary and ternary nanocomposites produced with C25A	130
Figure 4.38 Storage modulus as a function of frequency for PLA/organoclay nanocomposites produced with different clay types	132
Figure 4.39 Loss modulus as a function of frequency for PLA/organoclay nanocomposites produced with different clay types	132
Figure 4.40 Complex viscosity as a function of frequency for PLA/organoclay nanocomposites produced with different clay types	133
Figure 4.41 Storage modulus as a function of frequency for neat PLA, PLA blends and, binary and ternary nanocomposites produced with C25A	134
Figure 4.42 Loss modulus as a function of frequency for neat PLA, PLA blends and, binary and ternary nanocomposites produced with C25A	136
Figure 4.43 Complex viscosity as a function of frequency for neat PLA, PLA blends and, binary and ternary nanocomposites produced with C25A	136
Figure 4.44 Storage modulus as a function of frequency for neat PLA, PLA blends and, binary and ternary nanocomposites produced with N5.....	137
Figure 4.45 Loss modulus as a function of frequency for neat PLA, PLA blends and, binary and ternary nanocomposites produced with N5.....	138
Figure 4.46 Complex viscosity as a function of frequency for neat PLA, PLA blends and, binary and ternary nanocomposites produced with N5	138
Figure 4.47 EDX spectrum of EG (Timrex® C-Therm 001)	142
Figure 4.48 XRD pattern of pure EG (Timrex® C-Therm 001).....	143
Figure 4.49 XRD patterns of PLA/EG nanocomposites prepared by extrusion	144
Figure 4.50 XRD patterns of PLA/EG nanocomposites prepared by solution mixing	144

Figure 4.51 SEM micrographs of PLA/EG-0.5 prepared via extrusion at (a) x500 and (b), (c) and (d) x3000 magnifications.....	147
Figure 4.52 SEM micrographs of PLA/EG-2 prepared via extrusion at (a) x500 and (b), (c) and (d) x3000 magnifications	148
Figure 4.53 SEM micrographs of PLA/EG (90/10) binary blend prepared via extrusion at (a) x500 and (b) x3000 magnifications	150
Figure 4.54 SEM micrographs of PLA/E-GMA/EG-0.5 prepared via extrusion at (a)x250 and (b), (c) and (d) x3000 magnifications	151
Figure 4.55 SEM micrographs of PLA/EG-0.5 prepared via solution mixing at (a)x500 and (b), (c) and (d) x3000 magnifications	152
Figure 4.56 SEM micrographs of PLA/EG-2 prepared via solution mixing at (a)x500 and (b), (c) and (d) x3000 magnifications.....	153
Figure 4.57 SEM micrographs of PLA/E-GMA (90/10) binary blend prepared via solution mixing at (a) x500 and (b) x3000 magnifications	155
Figure 4.58 SEM micrographs of PLA/E-GMA/EG-0.5 prepared via solution at (a)x250 and (b), (c) and (d) x3000 magnifications	156
Figure 4.59 TEM micrographs of PLA/EG-2 produced via melt blending at different magnifications	158
Figure 4.60 TEM micrographs of PLA/E-GMA/EG-2 produced via melt blending at different magnifications	159
Figure 4.61 TEM micrographs of PLA/EG-2 produced via solution mixing at different magnifications	161
Figure 4.62 TEM micrographs of PLA/E-GMA/EG-2 produced via solution mixing at different magnifications	162
Figure 4.63 FTIR spectra of E-GMA, PLA and their binary blends prepared via melt blending or solution mixing	163
Figure 4.64 Tensile strength of neat PLA, PLA/E-GMA binary blend and PLA/E-GMA/EG ternary composites prepared via melt blending.....	165
Figure 4.65 Young's modulus of neat PLA, PLA/E-GMA binary blend and PLA/E-GMA/EG ternary composites prepared via melt blending.....	166

Figure 4.66 Elongations at break of neat PLA, PLA/E-GMA binary blend and PLA/E-GMA/EG ternary composites prepared via melt blending	167
Figure 4.67 Impact strength of neat PLA, PLA/E-GMA binary blend and PLA/E-GMA/EG ternary composites prepared via melt blending	169
Figure 4.68 Tensile strength of neat PLA, PLA/E-GMA binary blend and PLA/E-GMA/EG ternary composites prepared via solution mixing	170
Figure 4.69 Young's modulus of neat PLA, PLA/E-GMA binary blend and PLA/E-GMA/EG ternary composites prepared via solution mixing	170
Figure 4.70 Elongations at break of neat PLA, PLA/E-GMA binary blend and PLA/E-GMA/EG ternary composites prepared via solution mixing.....	172
Figure 4.71 Impact strength of neat PLA, PLA/E-GMA binary blend and PLA/E-GMA/EG ternary composites prepared via solution mixing.....	173
Figure 4.72 Comparison of tensile strength values of PLA/EG binary composites prepared via extrusion and solution mixing.....	175
Figure 4.73 Comparison of tensile strength values of PLA/E-GMA/EG ternary composites prepared via extrusion and solution mixing.....	176
Figure 4.74 Comparison of Young's modulus values of PLA/EG binary composites prepared via extrusion and solution mixing.....	177
Figure 4.75 Comparison of Young's modulus values of PLA/E-GMA/EG ternary composites prepared via extrusion and solution mixing.....	178
Figure 4.76 Comparison of elongations at break of PLA/EG binary composites prepared via extrusion and solution mixing.....	179
Figure 4.77 Comparison of elongations at break of PLA/E-GMA/EG ternary composites prepared via extrusion and solution mixing.....	179
Figure 4.78 Comparison of impact strength values of PLA/EG binary composites prepared via extrusion and solution mixing.....	181
Figure 4.79 Comparison of impact strength of PLA/E-GMA/EG ternary composites prepared via extrusion and solution mixing.....	181
Figure 4.80 Time sweep curves obtained at 170°C, at 5% strain amplitude and 10 rad/s for processed neat PLA, and PLA/E-GMA blends prepared via extrusion and solution mixing	183

Figure 4.81 Strain sweep curves of processed neat PLA, PLA/E-GMA binary blend, PLA/EG binary composites and PLA/E-GMA/EG ternary composites prepared via melt blending.....	184
Figure 4.82 Strain sweep curves of processed neat PLA, PLA/E-GMA binary blend, PLA/EG binary composites and PLA/E-GMA/EG ternary composites prepared via solution mixing	184
Figure 4.83 Storage modulus as a function of frequency for PLA, PLA/E-GMA binary blend, PLA/EG binary composites and PLA/E-GMA/EG ternary composites prepared produced via melt blending method.....	186
Figure 4.84 Loss modulus as a function of frequency for PLA, PLA/E-GMA binary blend, PLA/EG binary composites and PLA/E-GMA/EG ternary composites prepared produced via melt blending method.....	187
Figure 4.85 Complex viscosity as a function of frequency for PLA, PLA/E-GMA binary blend, PLA/EG binary composites and PLA/E-GMA/EG ternary composites prepared produced via melt blending method.....	188
Figure 4.86 Storage modulus as a function of loss modulus for PLA, PLA/E-GMA binary blend, PLA/EG binary composites and PLA/E-GMA/EG ternary composites prepared produced via melt blending method.....	189
Figure 4.87 Storage modulus as a function of frequency for PLA, PLA/E-GMA binary blend, PLA/EG binary composites and PLA/E-GMA/EG ternary composites prepared produced via solution mixing method.....	191
Figure 4.88 Loss modulus as a function of frequency for PLA, PLA/E-GMA binary blend, PLA/EG binary composites and PLA/E-GMA/EG ternary composites prepared produced via solution mixing method.....	192
Figure 4.89 Complex viscosity as a function of frequency for PLA, PLA/E-GMA binary blend, PLA/EG binary composites and PLA/E-GMA/EG ternary composites prepared produced via solution mixing method.....	194
Figure 4.90 Storage modulus as a function of loss modulus for PLA, PLA/E-GMA binary blend, PLA/EG binary composites and PLA/E-GMA/EG ternary composites prepared produced via solution mixing method.....	195

Figure 4.91 Comparison of storage modulus of binary and ternary nanocomposites with respect to the preparation methods	196
Figure 4.92 Comparison of complex viscosity of binary and ternary nanocomposites with respect to the preparation methods	197
Figure A.1 The FTIR spectra of neat PLA	225
Figure A.2 FTIR spectra of (a) PLA, (b) E-GMA, (c) E-BA-MAH, (d) PLA/C25A, (e) PLA/E-GMA/C25A, (f) PLA/E-BA-MAH/C25A	226
Figure A.3 FTIR spectra of (a) PLA, (b) E-GMA, (c) E-BA-MAH, (d) PLA/C30B, (e) PLA/E-GMA/ C30B, (f) PLA/E-BA-MAH/ C30B.....	226
Figure A.4 FTIR spectra of (a) PLA, (b) E-GMA, (c) E-BA-MAH, (d) PLA/N5, (e)PLA/E-GMA/N5, (f) PLA/E-BA-MAH/N5.....	227
Figure A.5 FTIR spectra of (a) PLA, (b) E-GMA, (c) E-BA-MAH, (d) PLA/N8, (e)PLA/E-GMA/N8, (f) PLA/E-BA-MAH/N8.....	227
Figure C.1 DSC curve of E-GMA performed under He purge between -180°C and 150°C at an heating rate of 10°C/min.....	231
Figure C.2 DSC curve of E-BA-MAH performed under He purge between -180°C and 150°C at an heating rate of 10°C/min	232
Figure C.3 DSC curve for A-00.....	232
Figure C.4 DSC curve for A-01	233
Figure C.5 DSC curve for A-1	233
Figure C.6 DSC curve for A-2.....	234
Figure C.7 DSC curve for A-3.....	234
Figure C.8 DSC curve for A-4.....	235
Figure C.9 DSC curve for A-5.....	235
Figure C.10 DSC curve for B-1	236
Figure C.11 DSC curve for B-2	236
Figure C.12 DSC curve for B-3	237
Figure C.13 DSC curve for B-4	237
Figure C.14 DSC curve for B-5	238
Figure C.15 DSC curve for C-1	238
Figure C.16 DSC curve for C-2	239

Figure C.17 DSC curve for C-3	239
Figure C.18 DSC curve for C-4	240
Figure C.19 DSC curve for C-5	240
Figure C.20 DSC curve for E-0	241
Figure C.21 DSC curve for E-1	241
Figure C.22 DSC curve for E-2	242
Figure C.23 DSC curve for E-3	242
Figure C.24 DSC curve for E-4	243
Figure C.25 DSC curve for E-5	243
Figure C.26 DSC curve for E-6	244
Figure C.27 DSC curve for E-7	244
Figure C.28 DSC curve for S-1.....	245
Figure C.29 DSC curve for S-2.....	245
Figure C.30 DSC curve for S-3.....	246
Figure C.31 DSC curve for S-5.....	246
Figure C.32 DSC curve for S-6.....	247
Figure C.33 DSC curve for S-7.....	247
Figure D.1 Frequency dependence of G' , G'' and η^* of E-GMA.....	249
Figure D.2 Frequency dependence of G' , G'' and η^* of E-BA-MAH.....	250
Figure D.3 Storage modulus as a function of frequency for neat PLA, and binary and ternary nanocomposites produced with C15A	250
Figure D.4 Complex viscosity as a function of frequency for neat PLA, and binary and ternary nanocomposites produced with C15A	251
Figure D.5 Storage modulus as a function of frequency for neat PLA, and binary and ternary nanocomposites produced with C30B	251
Figure D.6 Complex viscosity as a function of frequency for neat PLA, and binary and ternary nanocomposites produced with C30B.....	252
Figure D.7 Storage modulus as a function of frequency for neat PLA, and binary and ternary nanocomposites produced with N8.....	252
Figure D.8 Complex viscosity as a function of frequency for neat PLA, and binary and ternary nanocomposites produced with N8	253

Figure E.1 SEM image of a binary blend with x3000 magnification 256
Figure E.2 SEM image of a binary blend after thresholding 256
Figure E.3 SEM image of a binary blend with the identified rubber domains 257
Figure E.4 Description of a box plot [192] 258

LIST OF SYMBOLS

A_0	Initial cross-sectional area	m^2
d	Inter-planar spacing of atoms	\AA
E	Elastic modulus (Young's modulus)	MPa
F	Force	N
G'	Storage modulus	Pa
G''	Loss modulus	Pa
L	Instantaneous length	mm
L_0	Original gauge length	mm
M_w	Average molecular weight	g/mol
M_w/M_n	Polydispersity	
n	Integer representing the order of the diffraction peak	
T_c	Cold crystallization temperature	$^{\circ}\text{C}$
T_g	Glass transition temperature	$^{\circ}\text{C}$
T_m	Melting temperature	$^{\circ}\text{C}$
UTS	Ultimate tensile strength	MPa
w_{poly}	Fraction of polymer phase in the composite	
X_c	Percent crystallinity of the polymer phase	
ΔH_m°	Heat of fusion of the 100% crystal structure	J/g
ΔH_c	Cold crystallization energy	J/g
ΔH_m	Melting energy obtained from the DSC analysis of the sample	J/g
ΔL	Change in gauge length	mm
$\Delta L \%$	Percent elongation	mm

Symbols

σ_y	Yield strength or yield point	MPa
σ	Engineering (nominal) stress	MPa
ε	Engineering (nominal) strain	MPa
λ	Wavelength of the X-ray	nm
θ	Scattering angle	°
ω	Frequency of the oscillation	rad/s
$\gamma(t)$	Rotation of the bottom plate with a time dependent strain	%
$\sigma(t)$	Time dependent stress	Pa
$\tan \delta$	Loss tangent	
η^*	Complex viscosity	Pa.s

Abbreviations

2MHTL8	2-ethylhexyl quaternary ammonium
3HA	3-hydroxyalkanoate
3HB	3-hydroxybutyrate
ABS	Acrylonitrile-butadiene-styrene
APP	Ammonium polyphosphate
AS	Acrylonitrile-styrene copolymer
ATR	Attenuated total reflectance
BA	Butyl acrylate
BET	Brunauer–Emmett–Teller surface area
C15A	Cloisite®15A
C25A	Cloisite®25A
C30B	Cloisite®30B
CVD	Chemical vapor deposition
DCP	Dicumyl peroxide
DSC	Differential scanning calorimetry
E	Ethylene
EDX	Energy dispersive X-ray spectroscopy
EG	Expanded graphite

EP-g-MA	Maleated ethylene-propylene copolymer
FTIR	Fourier transform infrared spectroscopy
GIC	Graphite intercalate compound
GMA	Glycidyl methacrylate
GN	Graphite nanosheet
GNF	Graphite nanoflake
GNP	Graphite nanoplatelet
GO	Graphite oxide
HDPE	High density polyethylene
H-PLA	High molecular weight PLA
IR	Infrared spectroscopy
LA	Lactide
LDI	Lysine diisocyanate
LLDPE	Linear low density polyethylene
L-PLA	Low molecular weight PLA
LTI	Lysine triisocyanate
LVR	Linear viscoelastic range
MAH	Maleic anhydride
MMT	Montmorillonite
MT2EtOH	Bis-2-hydroxyethyl quaternary ammonium
N5	Nanofil®5
N8	Nanofil®8
NPCC	Nanosized precipitated calcium carbonate
ODA	Octadecylamine
OMLS	Organically modified layered silicate
OMMT	Organically modified montmorillonite
PA	Polyamide
PBAT	Poly(butylene adipate-co-terephthalate)
PBS	Poly(butylene succinate)
PBSA	Poly[(butylene succinate)-co-adipate]
PC	Polycarbonate

PCL	Poly(ϵ -caprolactone)
PE	Polyethylene
PEG	Poly(ethylene glycol)
PET	Polyethylene terephthalate
PHA	Polyhydroxyalkanoates
PHB	Polyhydroxybutyrate
PHV	Polyhydroxyvalerate
PLA	Poly(lactic acid)
PLA-g-MA	Maleic anhydride grafted PLA
PLC	Polycaprolactone
PLLA	Poly-L-lactide
PLLA-b-PE	Poly(lactide)-block-polyethylene
PMC	Polymer matrix composite
PMMA	Poly(methyl methacrylate)
PP	Polypropylene
PP-g-MAH	Maleic anhydride grafted polypropylene
PS	Polystyrene
PU	Polyurethane
PVC	Polyvinyl chloride
SAXD	Small angle X-ray diffraction
SEBS	Styrene-b-butadiene-b-styrene copolymer
SEM	Scanning electron microscopy
SR	Silicone rubber
SSSP	Solid-state shear pulverization
TCA	Tricarboxylic acid
TEM	Transmission electron microscopy
TPP	Triphenyl phosphate
WAXD	Wide angle X-ray diffraction
xGnP	Exfoliated graphite nanoplatelets
XRD	X-ray diffraction

CHAPTER 1

INTRODUCTION

Throughout the history of polymeric materials, almost all of the attempts were made to develop stable and durable polymeric structures that can withstand natural destructive forces such as sunlight, oxygen, water and heat. Conventional petroleum based plastics such as polyethylene (PE), polypropylene (PP), polyethylene terephthalate (PET) and polyvinyl chloride (PVC) are strong, relatively cheap, easily processible and durable. However, durability causes difficulties when these materials are sent to waste stream. Since these materials end up with non-degradable wastes both industry and academia share similar concerns about the environmental issues [1].

Today, two approaches are applied to eliminate the undegradable plastic wastes from the environment. The first one is the storage of wastes at landfill sites, however, landfill sites are limited, and they become insufficient day by day compared to the very fast development of society. The second approach can be considered in two stages: incineration and recycling. The first step usually produces large amounts of carbon dioxide and sometimes toxic gases which have adverse effects on global warming and pollution. The second step, recycling is rather benign, but requires substantial cost of labor and energy for removal of the wastes, separation according to their types and other processed to obtain a final product [2].

Biodegradable polymers have the potential to be a solution to the solid waste problem associated with the decreasing availability of landfills, global warming caused by increasing amounts of carbon dioxide in the atmosphere and the attempts

to find sustainable or renewable raw material sources [3]. Among a number of commercially available bio-based thermoplastic polymers, poly(lactic acid) (PLA) is one of the mostly investigated alternatives. Decreased production cost of this promising polymer with the recent advances in polymerization technologies makes it economically competitive with petroleum based commercial polymers. Thus, it becomes attractive for several industrial applications such as packaging, textile, and automotive industries [4]. Even though it has numerous advantages in terms of being eco-friendly, having comparable cost with petroleum based polymers, having high strength and modulus, its intrinsic brittleness restricts its utilization in pristine form.

Similar to the conventional plastics, blending or making composites using inorganic or natural filler materials are the potential methods to improve the properties of biodegradable polymers according to the desired area of usage. Reinforcement of biodegradable polymers through the addition of nano-scale reinforcements can be a useful method in production of eco-friendly nanocomposites for various applications [2].

Nanocomposites are a particular class of polymer matrix composites. They contain fillers whose one dimension is at least in the nanometer (10^{-9}) scale [5]. These materials are popular because of the enhanced properties obtained by effective dispersion of the nano-sized fillers [6]. Various types of nano-sized fillers such as layered silicates, graphite nanosheets, carbon nanotubes (CNTs), nanofibers, metal oxide nanoparticles and layered titanate have been used to prepare variety of polymer nanocomposites for many industrial applications [7]. Certainly, layered silicates are the most popular ones among these other alternatives owing to their easy accessibility, low price and being environmentally friendly [2].

The pioneering study in the field of nanocomposites is performed by Kojimo et al. of Toyota in which the tensile modulus and strength of nylon was doubled with the incorporation of 2 % clay [8]. Continued progress in production and utilization of nanosized fillers with polymeric materials improved understanding of the physicochemical phenomena at the nanometer scale and thus led to the rapid development of new polymer-layered silicate nanocomposites. The first effort to

prepare PLA nanocomposites using an organically modified layered silicate was performed by Ogata and coworkers [9]. The results were not promising in terms of mechanical properties, but after that many successful studies reporting well dispersion of layered silicates in PLA matrix have been published until today, some focusing on thermal and mechanical properties, some on morphology and rheology and some on biodegradability.

In recent literature, graphite is shown to be promising alternative to nanoclays to produce nanocomposites. This material has low mass density compared to the conventional fillers. Additionally, they are highly electrically and thermally conductive [10]. The main advantage of utilizing thermally and electrically conductive nano-scale filler materials with polymeric matrices is that the final product is usually light in weight with relatively low cost and easy processibility. Such multifunctional composites can be used in a wide range of applications including energy harvesting, flexible electronics, thermal interphase materials and structural components for automotive and aerospace vehicles [11].

Among the possible graphitic structures so called expanded graphite (EG) has different names reported in the literature such as graphite nanosheets (GN), graphite nanoflakes (GNF), graphite nanoplatelets (GNPs), or simply exfoliated graphite. It is a type of two-dimensional nanofiller containing many graphene layers one on the top of the other. These layers are interacting by Van der Waals forces and the interlayer distance between the layers is constant (0.34 nm) [10]. Additionally, the production of expanded graphite does not require expensive and complicated equipment like other carbonaceous nanofillers such as carbon nanotubes and/or carbon nanofibers. Furthermore, these fillers can be produced from abundant resources of natural graphite by fairly convenient methods [10, 12].

Several studies published in the literature can be found on the possibility of increasing mechanical and the electrical properties of various polymer matrices via addition of carbon based nanofillers. There are also some studies on effective distribution of these graphitic fillers in various polymer matrices. However, information on the effects of the manufacturing process on the multifunctional

properties of the prepared composites is relatively limited [11]. Comparisons are mainly based on the previously reported results. Furthermore, EG was usually studied to produce hybrid nanocomposites to improve various properties of the final composite material to obtain multifunctional structures.

Polymer nanocomposites with very low filler contents have been shown to possess various property enhancements mainly including increased tensile strength, modulus, hardness and fracture toughness, decreased gas permeability and flammability, improved thermal stability, and electrical properties. These property improvements highly depend on effective polymer particle interactions and effective dispersion of the filler in the matrix. The degree of dispersion is sensitive to the forces acting between the dispersed particles [7]. This phenomenon is valid for both layered silicates and graphitic fillers like expanded graphite. In order to investigate and improve dispersion and distribution of nanofillers several approaches can be followed such as incorporation of low molecular weight compatibilizers and modification of the filler surface with organophilic moieties. The synthesis of nanocomposites is also an important factor to achieve desired dispersion and properties. The most commonly used nanocomposite production methods are melt compounding, in situ synthesis, solution mixing, gas phase processing, living polymerization, etc. All methods employed to modify the filler surface as well as to synthesize nanocomposites should be supported by characterizations of the final product in order to have deeper information on the microstructure and properties.

Under the light of these discussions, this study is mainly aimed to investigate the properties of PLA nanocomposites produced with various additives. Two different road maps were followed to achieve this aim. In the first one, it was aimed to increase PLA processibility by incorporating epoxy and maleic anhydride functionalities together with nanoclays to improve toughness. The main idea was to pursue the changes in material properties with the changes in types of nanoclays at relatively low clay loadings with the idea that the structure of modifier is the key parameter in nanocomposites. Five different organically modified commercial nanoclays were used as nanofillers. In addition to that, presence of an elastomeric phase which is supposed to act as a compatibilizer was investigated. For this purpose

two different commercial elastomers with different functional groups (ethylene-glycidyl methacrylate and ethylene-butyl acrylate-maleic anhydride) were selected as compatibilizers. Both the clay and the compatibilizer contents were kept constant in order to pursue the changes in some properties of the nanocomposites with changes in structures of additives. Conventional twin-screw extrusion was used as the production method for nanocomposites and the articles for testing were prepared by injection and compression molding techniques. In order to see the dispersion of clay particles in the polymer matrix X-ray diffraction (XRD), scanning electron microscopy (SEM) and transmission electron microscopy (TEM) analyses were performed. Mechanical properties of the specimens were evaluated by tensile and impact tests. The thermal behaviors of the samples were investigated using differential scanning calorimetry analysis, and rheological behaviors were determined with by dynamic oscillatory rheometry. Finally, the interactions between the polymer matrix and the elastomeric additives were investigated via Fourier Transform Infrared Spectroscopy (FTIR).

Concurrently, graphite was used as an alternative to the conventional layered fillers. To see the effects of different production methods on the dispersion problem of the expanded graphite (EG) structure used in this study, extrusion and solution mixing techniques were compared. Loading of the filler was kept below 2 wt. % in order to minimize the dispersion problem and to minimize the solvent usage. High amounts of organic solvents are necessary to dissolve each constituent in the final product. In this respect, influence of EG contents (below 2 wt. %) in the composites and addition of E-GMA as impact modifier were investigated for both production methods. To the best of our knowledge, addition of a ternary elastomeric polymer was tried, especially in the solution mixing method, for the first time in this study.

The expanded graphite used (Timrex® C-Therm 001) in this study was provided from the manufacturer as a confidential product, there are limited technical data about this filler. Hence, EG itself was characterized first via energy dispersive X-Ray spectroscopy (EDX), Brunauer–Emmett–Teller (BET) surface area analyses and XRD. After production of nanocomposites at different concentrations with different production methods, the dispersion of EG in the polymer matrix was investigated via

XRD, SEM and TEM. Potential reactive interactions between PLA and the rubber were investigated via FTIR. Mechanical properties of the specimens were determined by tensile and impact tests. The thermal behaviors of the samples were investigated by using differential scanning calorimetry analysis, and rheological behaviors were determined using dynamic oscillatory rheometry.

CHAPTER 2

BACKGROUND INFORMATION

2.1. Composite Materials

A composite material can be defined as a combination of two or more materials which results in better material properties than those of the individual components. In composite materials, each constituent retains its separate chemical, physical and mechanical properties [13]. In other words, these constituents do not dissolve or merge completely in each other; they can be physically identified; however, they act together [14]. The main advantages of composite materials are their high strength and stiffness, combined with low density, when compared with bulk materials [13].

The two constituents in a composite material are the reinforcement and matrix. The reinforcing phase might be in shape like fiber, flake or particles. In most cases, the reinforcement is harder, stronger, and stiffer than the matrix. The matrix or continuous phase can be polymer, metal, or ceramic [13]. The matrix acts as binder holding the components together, and transmitting and distributing the stresses; therefore it determines the mechanical properties of the materials. Composite materials are not only man-made, but also naturally exist. For example, wood is composed of lignin as matrix reinforced with cellulose fibers. Bones are also composite materials in which the bone-salt plates made of calcium and phosphate ions reinforce soft collagen [15].

In addition to the type and quantity of the reinforcement, the most important factor determining the properties of composite material is the interface interactions.

Interface is defined as the region through which material parameters, such as concentrations of components, crystallinity, physical and mechanical properties can change from one side to another [16]. In most cases, there are multiple bonding types on the interface. These are mechanical, chemical, and physical bondings. Mechanical bonding is effective in load transfer when the force is applied parallel to the interface. Chemical bonding, which includes bonding by direct reactions, coupling agents, molecular chain entanglements, is stronger than mechanical bonding. Physical bonding, on the other hand, involves relatively weak secondary interactions such as van der Waals forces, dipolar interactions and hydrogen bonding. As in mechanical bonding, physical bonding is not enough for most of the cases, since it is effective only over small distances [15, 16].

Composites can be classified from two different perspectives: according to the type of reinforcement or according to the type of matrix material. Reinforcements can be in particulate, flake or fiber form. Particulate composites are composed of particles immersed in alloys and ceramics as matrix, such as aluminum particles in rubber or sand in concrete. Flake materials are flat in shape, such as glass and mica resulting in higher strength with low cost. However, flakes cannot be oriented easily and there are limitations of alternative reinforcements. Fiber reinforcements can either be continuous (long) or discontinuous (short) and are generally anisotropic having different properties in different directions. Most common fiber reinforcements are carbon fibers and glass fibers. From the point of matrix materials, four major classes can be mentioned: polymer, metal, ceramic or carbon matrix composites. In metal matrix composites, reinforcement improves strength and stiffness together with abrasion and creep resistances. Additionally, it can enhance thermal conductivity. For ceramic matrix composites, the incorporation of fibers enables high processing temperatures and resilience to oxidation and deterioration [15]. Carbon matrix composites usually consist of carbon fiber reinforcements in a carbonaceous matrix. These materials are usually used where resistance to very high temperatures are required [17]. In this study, the main focus is on polymer matrices. Below fundamental information can be found by narrowing down from the polymer matrix

composites to specific properties of polymer and reinforcement materials used in this study.

2.1.1 Polymer Matrix Composites

Polymer matrix composites (PMCs) are the most common type of composite materials consisting of a polymeric matrix such as epoxy, polyester or urethane, reinforced by several different types of fillers. Among the other possible matrices, polymers have many advantages, since processing does not require high pressure and high temperatures, and the processing cost is low [18]. Additionally, since diverse alternatives are available, they can satisfy required mechanical characteristics, such as tensile strength, modulus, elongation and impact strength. In some cases, high thermal and moisture expansion coefficients and low elastic properties in certain directions for some polymeric materials could be considered as drawbacks depending on the particular application [15].

Polymeric materials can be classified as thermoplastics and thermosets. Thermoplastics would soften upon heating and can be made to flow when a stress is applied. When they are cooled, they reversibly regain their solid or rubbery nature. Thermosets, on the other hand, might be heated to a point where they would soften and could be made to flow under stress once, but this process is not reversible. In fact, heating causes them to undergo a curing reaction in which cross-linking of polymer chains results in toughening or hardening of the material. Further heating of this type of polymers leads to degradation [19].

2.2. Nanocomposites

Conventional composite materials consist of fillers on the microscale (10^{-6} m). Nanocomposites, on the other hand, consist of materials that are on the scale of nanometers (10^{-9} m). In order to be accepted as a nanocomposite, one of the constituents should be at least 100 nm. At this scale, the properties of materials are

different from those of the bulk material. Most of the properties of the nanocomposites are better than the ones at the microscale [15].

Nanocomposites can be classified into three main groups depending on the number of dimensions at the nanoscale.

- **Isodimensional nanoparticles:** Three dimensions of the filler are in the order of nanometers. Spherical silica nanoparticles obtained by in situ sol–gel methods or by polymerization promoted directly from their surface can be given as examples [20, 21, 22].
- **Two–dimensional nanoparticles:** When two dimensions are in the nanometer scale and the third is larger, it forms an elongated structure, such as nanotubes or whiskers. For example, carbon nanotubes or cellulose whiskers, which are extensively studied as reinforcing nanofillers are two-dimensional nanoparticles [23, 24].
- **One–dimensional nanoparticles:** This third type is characterized by only one dimension in the nanometer range. In this case, the filler is present in the form of sheets of one to a few nanometers thick, to hundreds to thousands nanometers long [5]. Layered silicates can be given as an example to this group.

2.2.1 Polymer – Layered Silicate Nanocomposites

For improving mechanical properties of conventional petroleum based polymers, forming nanocomposites has been used extensively, since the researchers at the Toyota research center in Japan showed that the tensile modulus and strength were doubled for nylon-layered silicate nanocomposites containing 2 vol.% clay. They also showed that the heat distortion temperature of the nanocomposites increased by 87%, extending the use of this polymer to under-the-hood structural parts in the engine compartment [8].

The use of layered silicates as a reinforcing phase is one of the most successful ways of designing polymer nanocomposites with a broad range of markedly modified properties in comparison to classical micrometer scale particulate filled materials

[25]. Layered silicates are lighter in weight compared to conventional composites and they exhibit exceptional barrier properties. Also, the mechanical properties are usually remarkably higher compared to those of polymers reinforced with unidirectional fibers. The main reason is that reinforcement from the inorganic layers will occur in two dimensions rather than in one dimension [6]. Furthermore, fabrication techniques of polymer-layered silicate are much easier and cheaper than the fabrication of conventional composites, since they can attain the composite properties with low volume fraction of reinforcement.

2.2.1.1 Structure of Layered Silicates

Clay minerals are called as layered silicates because of the stacked structure of almost 1 nm thick silicate layers with variable interlayer distances [26]. They are widely used for improving properties of polymeric materials due to two distinguishing properties: 1- formation of fine particles yielding large surface areas; 2- possibility to alter the chemistry of their surface via some the exchange reactions with organic or inorganic cations [27].

The most frequently used layered silicates in the polymer matrix nanocomposites are members of phyllosilicates group. The structure, which is designated as 2:1 layered family, is composed of two-dimensional layers where a central octahedral sheet of alumina or magnesia is fused to two external silica tetrahedron by the tip so that the oxygen ions of the octahedral sheet are also shared by the tetrahedral sheets. The lateral dimensions range from 300 Å to several microns or even larger due to particular silicate type, and the layer thickness is about 1 nm (Figure 2.1). These layers form stacks with a regular Van der Waals gaps in between. These gaps are named as interlayer galleries or basal spacing.

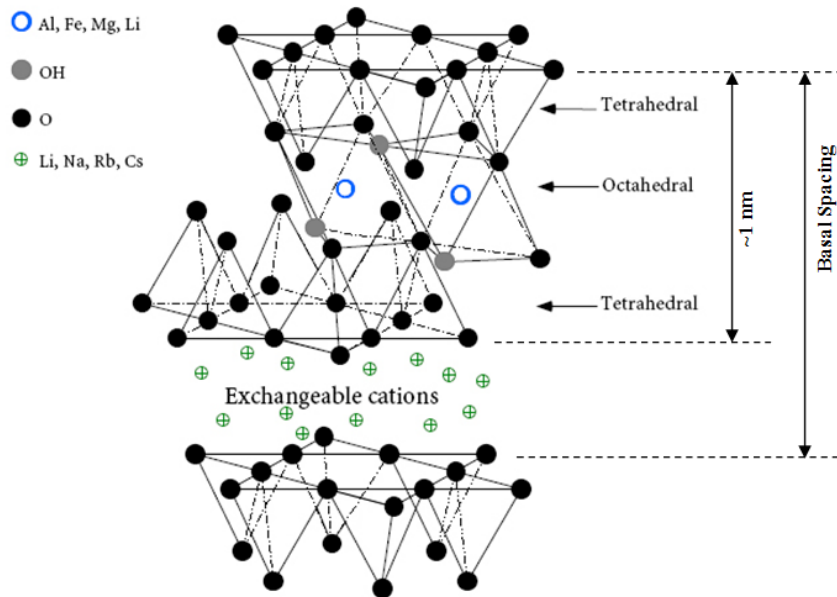


Figure 2.1 The structure of 2:1 layered silicates [6]

The phyllosilicate 2:1 layered clays include mica, smectite, vermiculite, and chlorite. Smectite group can be further divided into montmorillonite (MMT), saponite and hectorite species, and these are the most commonly used layered silicates [6, 28]. Details about the structures and surface chemistry of these layered silicates can be seen in Table 2.1.

Table 2.1 Structure and chemistry of mica-type layered silicates [6]

Silicate	Location of isomorphous substitution	Formula
Montmorillonite	Octahedral	$M_x[Al_{4-x}Mg_x](Si_8)O_{20}(OH)_4$
Hectorite	Octahedral	$M_x[Mg_{6-x}Li_x](Si_8)O_{20}(OH)_4$
Saponite	Tetrahedral	$M_x[Mg_6](Si_{8-x}Al_x)O_{20}(OH)_4$

2.2.1.2 Organic Modification of Silicate Layers

Pristine layered silicates usually contain hydrated Na^+ or K^+ ions and they are only miscible with hydrophilic polymers. Layered silicates are made miscible with many other polymer matrices by converting hydrophilic silicate surface to organophilic structures by ion-exchange reactions with cationic surfactants including primary, secondary, tertiary and quaternary alkylammonium or alkylphosphonium cations (Figure 2.2).

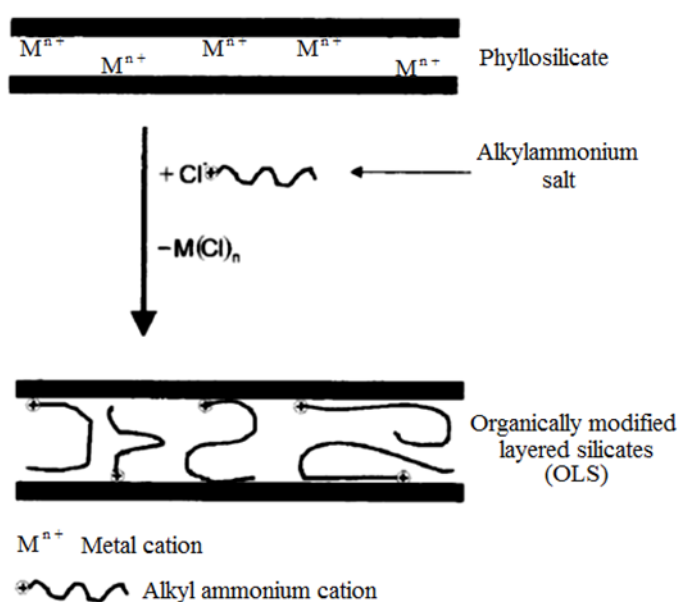


Figure 2.2 Schematic representation of a cation-exchange reaction between the silicate and alkylammonium salt [29]

Organic modification of layered silicates makes intercalation of polymers possible via lowering the surface energy of the inorganic filler and improving the wetting features of the polymer. Furthermore, the alkyl ammonium cations provide moieties that can react with the polymer or initiate polymerization reactions. Therefore, they

enhance the interface interactions between the inorganic filler and the polymer matrix [30]. This replacement of exchange cations by organic onium ions on the gallery surfaces also expands the clay galleries. This facilitates the penetration of polymer chains to the gallery space. Various arrangements of the ions are possible depending on the charge density of clay and the onium ion surfactant. These arrangements are shown in Figure 2.3.

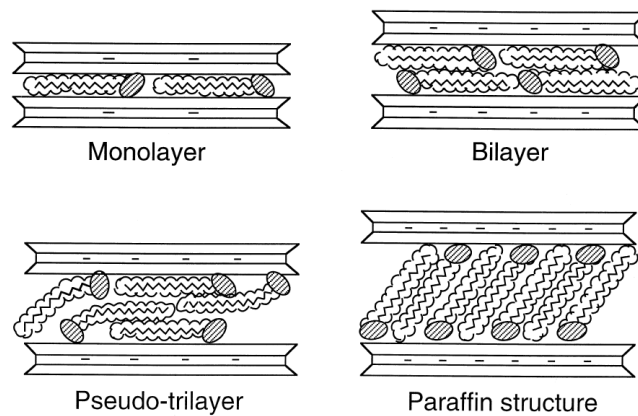


Figure 2.3 Orientations of alkylammonium ions in the layered silicates galleries [31]

2.2.1.3 Polymer Layered Silicate Nanocomposite Types

Depending on the arrangement of clay nanoplatelets in the polymer matrix, composite materials can be classified under three essential titles; phase separated composites, intercalated nanocomposites, and exfoliated (delaminated) nanocomposites where the third group can also be categorized as ordered and disordered (Figure 2.4).

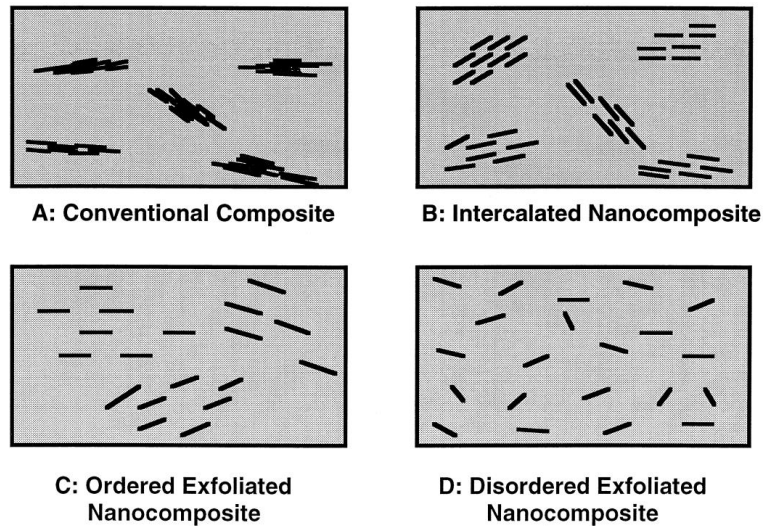


Figure 2.4 Schematic illustrations of A: conventional; B: intercalated; C: ordered exfoliated; and D: disordered exfoliated polymer–clay nanocomposites [31]

Formation of these structures depends on the nature of the polymer and the layered silicate, nanocomposite synthesizing methods, interfacial interactions and the filler loading. Conventional composite structure occurs if the polymer matrix and organoclay are incompatible so that the clay layers remain as big stacks with no polymer chain diffused through the layers. This structure can be said to be a phase-separated microcomposite. In the intercalated structure, on the other hand, clay platelets remain as well ordered stacks, although some polymer chains diffuse into the layers. The purpose of many nanocomposite applications is to achieve exfoliated structure due to the highest property improvements such as barrier characteristics, chemical resistance, reduced solvent uptake and flame retardancy [31]. This structure is obtained when both the clay surfaces and the polymer matrix have polar groups that have favorable interaction [32].

2.2.1.4 Thermodynamics of Nanocomposite Formation

Nanocomposite formation and its equilibrium state for polymer-layered silicate nanocomposites are highly dependent on the polymer structure, the charge carrying

capacity of the layered silicate, chain length and structure of the organic modifier [33]. In fact, the factors determining the polymer intercalation are enthalpic and entropic. Impoundment of the polymer chains in the silicate layers results in a reduction in the overall entropy of the polymer chains. However, polymer confinement in the silicate layers is accompanied with enhanced conformational freedom of surfactant chains in a less confined environment. As for small rises in the interlayer spacing the total entropy change is small, moderate changes in the total enthalpy will regulate whether intercalation is thermodynamically possible or not.

The enthalpy of mixing could be categorized into two subtitles: apolar and polar. Polar enthalpy of mixing is considered more favorable for intercalation. Hence, number of favorable polymer-surface interactions should be maximized while minimizing the magnitude and number of unfavorable apolar interactions between the polymer and the functionalizing aliphatic chains. A schematic representation of polymer-modifier interactions during nanocomposite preparation can be seen in Figure 2.5.

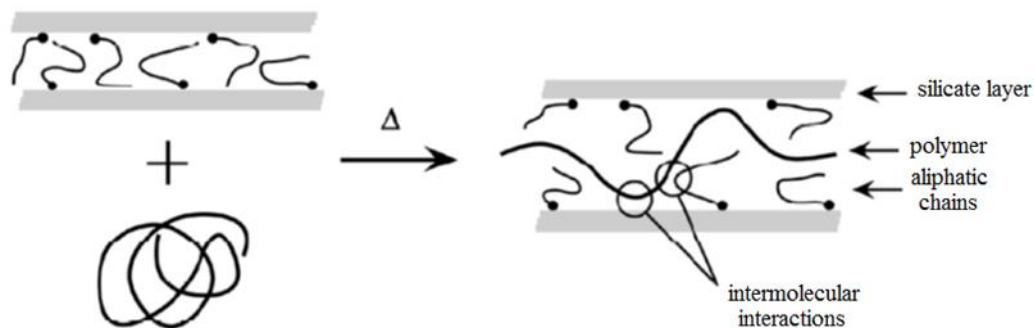


Figure 2.5 Schematic representation of the system components before and after intercalation takes place [30]

2.2.2 Preparation of Polymer-Layered Silicate Nanocomposites

There are three conventional methods to produce polymer matrix composites in which layered silicates are used as fillers. These are in situ intercalative polymerization, solution intercalation and melt intercalation methods. Each of these methods can be used for other nano-fillers with some minor modifications in application details.

2.2.2.1 Solution Intercalation

Solution intercalation method is based on a polymer-solvent system in which the polymer or pre-polymer is soluble and the silicate layers are swellable. First, the layered silicate is swollen in the solvent (i.e., water, chloroform, or toluene). As the polymer chains and the filler are mixed in the solvent, the polymer chains intercalate within the interlayer of the silicate. Then the remaining structure is solution intercalated upon removal of the solvent from the environment [34]. A schematic representation of this process can be seen in Figure 2.6. The solution intercalation method is not preferably used in industrial applications due the high amounts of solvent used which makes it environmentally detrimental and economically unfavorable.

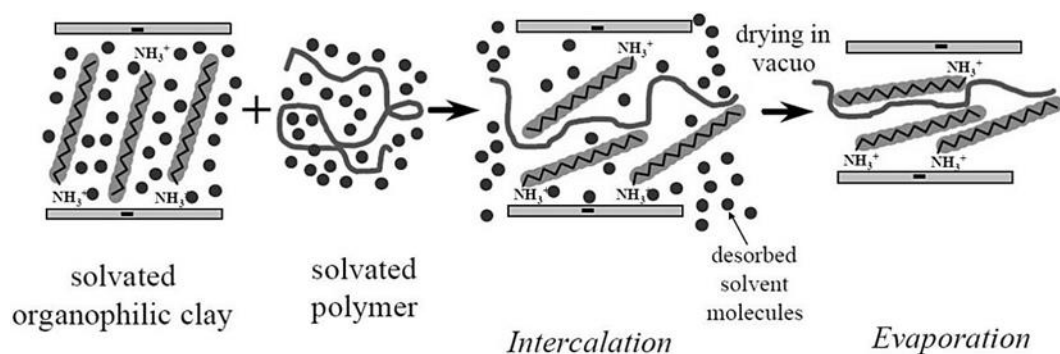


Figure 2.6 Solution intercalation method for polymer-layered silicate nanocomposite preparation [35]

2.2.2.2 In Situ Polymerization Method

In this method, polymerization reaction takes place within the silicate layers. First the layered silicate is swollen within the liquid monomer or a monomer solution. Then the reaction can be initiated by various different methods: by heat or radiation, by the diffusion of a suitable initiator, by an organic initiator or catalyst fixed through cation exchange inside the interlayer before the swelling step [34]. A schematic representation of this process can be seen in Figure 2.7.

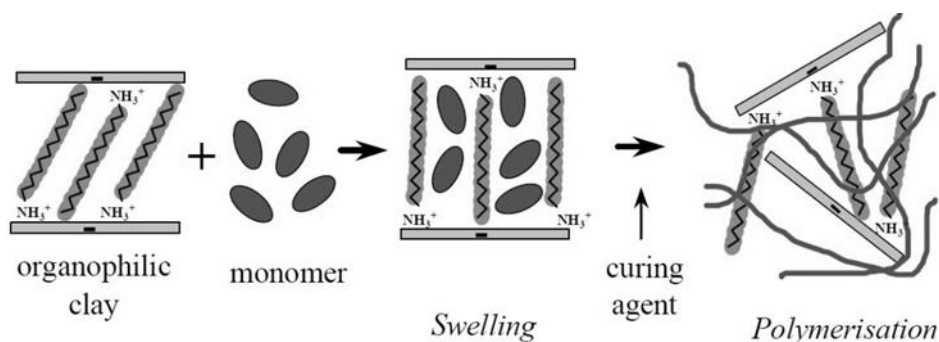


Figure 2.7 In situ polymerization method for polymer-layered silicate nanocomposite preparation [35]

Nanocomposites prepared with via in situ polymerization can possess remarkably improved properties, however the amount of final product is usually limited to small size reactors. Furthermore, the presence of additives in the system results in complexities in both process control and the contaminations in the final product. Thus, bulk production of the nanocomposites by this method is very unlikely in industry.

2.2.2.3 Melt Intercalation

Melt intercalation method basically involves annealing of a polymer and organically modified layered silicate mixture under shear above the softening point of the

polymer [34]. The main difference between melt processing and other preparation methods is that high shear forces on the system enhances the clay dispersion. Other parameters that affect degree of the dispersion are matrix viscosity and the mean residence time [36]. A simple schematic representation of the melt intercalation process can be seen in Figure 2.8.

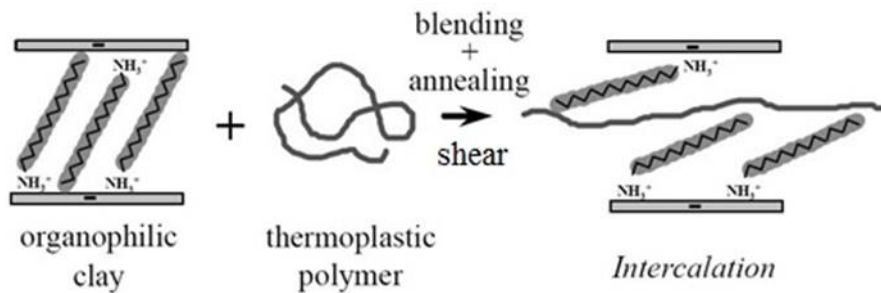


Figure 2.8 Melt intercalation method for polymer-layered silicate nanocomposite preparation [35]

This method has great advantages over the other two conventional methods. First of all, it is environmentally benign due to the absence of organic solvents. Additionally, it is compatible with current industrial process, such as extrusion and injection molding. Finally, the melt intercalation method allows the use of polymers which are not suitable for in situ polymerization or solution intercalation methods [34].

2.2.3 Polymer – Graphite Nanocomposites

In the literature, graphite is shown to be promising alternative to nanoclays to produce nanocomposites, due to its low mass density compared to that of conventional fillers, and its highly electrical and thermal conductivity. The graphene is also reported possesses superior mechanical properties compared to many other filler materials [10].

2.2.3.1 Structure of Graphite

The origin of the word “graphite” is the Greek word “graphein” which means “to write”. Actually, graphite has been used for writing and drawing purposes since the ancient times and the first pencils were manufactured in England in the 15th century. In the 18th century, it was demonstrated that graphite actually is an allotrope of carbon [37].

Carbon is polymorphic. It exists in three forms, namely diamond, graphite and fullerenes. The main difference between diamond and graphite is that the carbon bonding involves sp^3 (tetrahedral) hybridization in diamond and sp^2 (trigonal) hybridization in graphite. As a result, diamond has a three-dimensional crystal structure or covalent network solid. Graphite, on the other hand, consists of carbon layers (with covalent and metallic bonding within each layer) which are stacked in an AB sequence and linked by a weak Van der Waals force (Figure 2.9) [38].

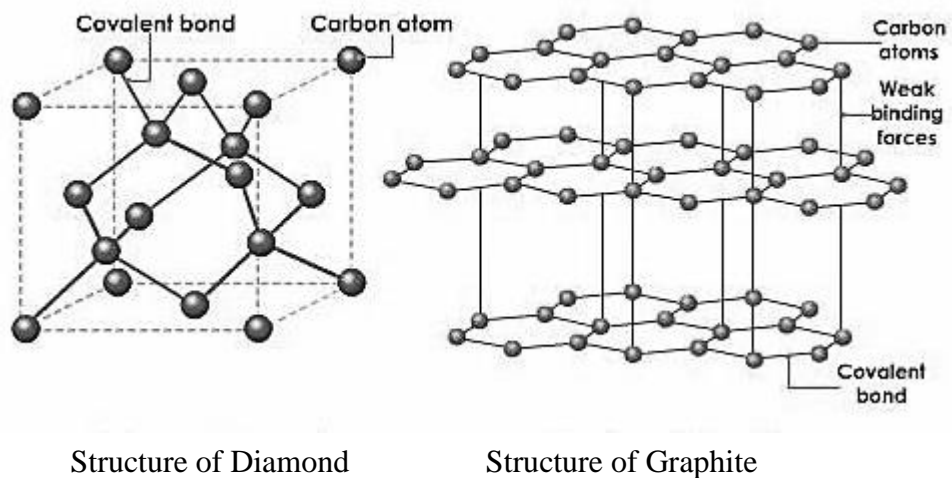


Figure 2.9 Structures of diamond and graphite [39]

The carbon layers in graphite are known as graphene layers in which the atoms are arranged in a hexagonal pattern within each layer and the layers are stacked in the AB sequence (Figure 2.10) [38]. Within each layer plane, the carbon atom is bonded to three others, forming a series of continuous hexagons in what can be considered as an essentially infinite two-dimensional molecule. The hybridized fourth valence electron is paired with another delocalized electron of the adjacent plane by a much weaker Van der Waals bond (a secondary bond arising from structural polarization). Carbon is the only element to have this particular layered hexagonal structure [37].

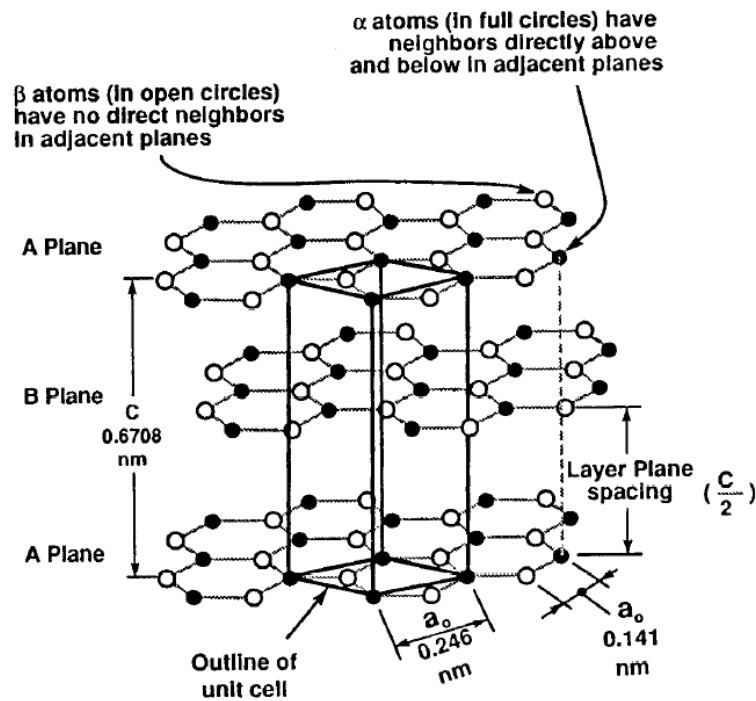


Figure 2.10 Crystal structure of graphite showing ABAB stacking sequence and unit cell [37]

2.2.3.2 Production of Different Graphite Structures

Graphite structures utilized in scientific research and industrial applications can be referred as graphite nanoplatelets (GNPs) or exfoliated or expanded graphite (EG) [10]. Some of these terms are used interchangeably but some of them refer to different structures. Therefore in order to differentiate those structures, production procedures should be known.

Two main fabrication approaches for the preparation of GNPs are mechanical milling and graphite intercalation. The first one starts with breaking up the bulk graphite by breaking the Van der Waals forces between the graphene layers. Resulting large particle sizes with broad size distribution are the two main drawbacks of mechanical milling. Graphite-intercalation approach is shown to be a candidate to solve these problems. In the beginning, the graphite is intercalated to obtain graphite intercalate compound (GIC). The principle of intercalation is to put some chemicals within the graphite layers. These chemicals can react and produce a large volume of gas or heat to separate the graphene layers. The most frequently employed method is acid intercalation (Figure 2.11).

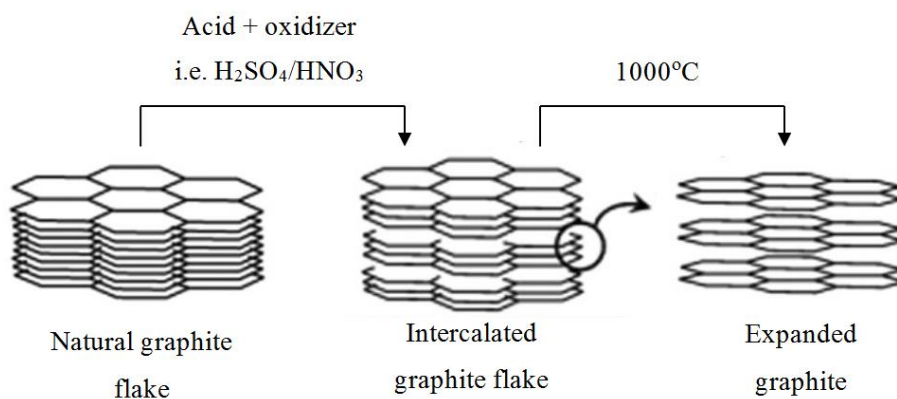


Figure 2.11 Schematic representation of acid intercalation of graphite sheets

The acids involved in forming GICs include nitric acid, sulfuric acid, perchloric acid and selenic acid together with some oxidizers such as HNO_3 , KMnO_4 , H_2O_2 , O_3 , etc.

[10, 40]. A rapid heating of GIC to relatively high temperatures cause an expansion of intercalated layers resulting in the structure named as expanded graphite. It is claimed that microwave can also produce enough energy to promote expansion of GICs [10].

Using alkali compounds is another alternative to prepare the GICs. Usually, KC_8 obtained by heating the graphite powder and potassium (K) seems as shown in Figure 2.12. Then, the expansion of GIC can be achieved in exfoliating agents in aqueous phase like water and alcohol. Hydrogen gas produced by the reaction can break the weak Van der Waals bonds between the graphite sheets and lead to further separation of the graphene sheets [10].

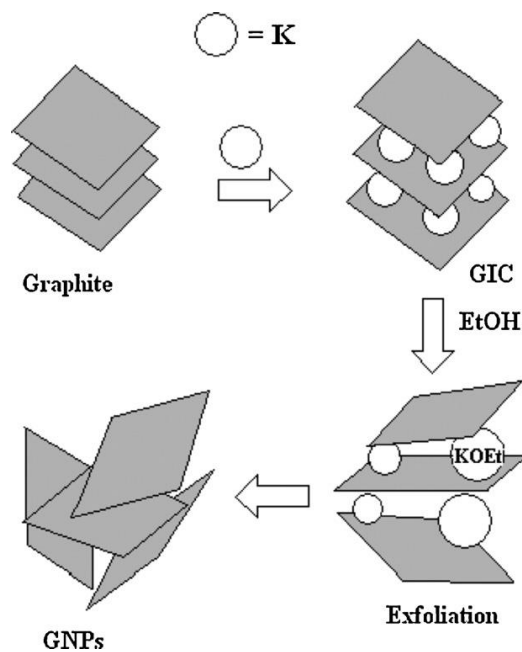


Figure 2.12 Schematic representation of graphite intercalation using alkali metals [40]

The structure obtained after the expansion of graphite sheets in GICs is named as expanded graphite and it has a worm-like morphology (Figure 2.13). EG is composed of stacks of nanosheets that may vary from 100 to 400 nm [41].



Figure 2.13 SEM image of expanded graphite [41]

Going one step further and separating the single carbon layers results in graphene that is one atom thick and therefore acquiring importance in materials sciences [42]. There are five ways to produce graphene sheets, only two of which are suitable for bulk quantity production. The first route involves chemical vapor deposition (CVD) of monolayer of graphite on transition metal surfaces. Micromechanical exfoliation of graphite is the second alternative and involves peeling of the graphene from graphite using “Scotch” tape. The third route involves the epitaxial growth of graphene on electrically insulating substrates like silicon carbide. Preparation of bulk quantities of graphene for the time being is possible from graphite oxide (GO) and GICs. As a fourth method, hydroxyl and epoxide groups on the edges of GO layers make it water dispersible which results in colloidal suspensions of single graphene oxide layers upon ultrasonication. In the final method bulk quantities of graphene can be prepared is by thermal reduction of GO [40].

2.2.4 Preparation of Polymer-Graphite Nanocomposites

Similar to all other nanofillers, the main difficulty in manufacturing polymer/graphite nanocomposites is the dispersion and distribution of the fillers in the polymer matrix. Three conventional techniques are mainly employed to provide good dispersion and distribution. These are in situ polymerization, solution compounding and melt blending. Details of these methods are virtually the same with the methods used for preparation of polymer-layered silicate nanocomposites explained in Section 2.2.2. When the filler is graphite, in situ polymerization and solution mixing methods are employed together with ultrasonication for better dispersion of the filler in the polymer matrix. However, these two methods have some serious problems. First, hazardous chemicals such as monomers for polymerization or organic solvents as processing medium are involved; second, they are not ideal for industrial production, due to the low yield and high production cost [10]. These two important hitches reveal the fact that there is a big demand for production methods based on melt mixing. Generally, melt mixing is not adequate to obtain good dispersion and properties of final graphitic composites [10, 40]. As a result, different modified melt compounding techniques have been developed. These modified procedures generally involve two steps, first of which can be said to be the premixing step followed by the melt mixing. The premixing step can be performed in liquid, melt, and solid phases. Premixing in solution can be achieved by preparing high filler content masterbatches or by first powdering the polymer matrix and dispersing the graphite on the polymer powder. In the latter method, removal of the solvent from the environment results in filler-coated polymer powder which can be further melt extruded [43]. Premixing in melt state can also be performed via master batch filling technique. Mechanical mixing is another premixing step which is performed in solid state. In fact, this technique is named as solid-state shear pulverization (SSSP) [44]. In this method, the polymer matrix and filler are co-pulverized in a continuously cooled pulverizer with a very similar configuration to twin-screw extruder. However, specially designed screws are used to yield moderately harsh shear/compression conditions. The resulting powder is a

homogeneous mixture of the polymer and the filler which can be further melt processed.

2.3. Biodegradable Polymers

It is difficult to find an exact definition for the biodegradability term, since it is not used consistently. For instance, it has been used to indicate hydrolysis in the medical field for sutures, bone reconstruction and drug delivery; however, it is used to indicate fragmentation, loss of mechanical properties, or sometimes degradation through the action of living organisms for environmentally degradable plastics. Jamshidian et al. [45] summarized biodegradation as changes in chemical structure, loss of mechanical and structural properties, and finally, changing into other compounds such as water, carbon dioxide, minerals, and intermediate products like biomass and humic materials under the action of naturally occurring microorganisms such as bacteria, fungi, and algae. However, a world-wide valid definition for biodegradable polymers has not yet been declared, and all the present definitions correlate the degradability of a material to a specific disposal environment and to specific test methods which simulate the alternative disposal environments [46].

Biopolymers, whose biodegradation takes place in the nature, can be classified under four main types [45]:

- Biopolymers extracted directly from natural raw materials, such as polysaccharides like starch and cellulose; proteins like gelatin, casein, and silk; and marine prokaryotes;
- Biopolymers produced by chemical synthesis from bio-derived monomers such as poly(lactic acid) (PLA);
- Biopolymers produced by microorganisms or genetically modified bacteria such as polyhydroxyalkanoates (PHA), polyhydroxybutyrate (PHB), polyhydroxyl-valerate (PHV), bacterial cellulose, xanthan, and pullan;
- Biopolymers produced from crude oil like aliphatic and aromatic polyesters, polyvinyl alcohol, and modified polyolefins.

The best known petroleum source-derived biodegradable polymers are aliphatic polyesters such as polycaprolactone (PCL), polybutylene succinate (PBS) and their copolymers or aliphatic-aromatic copolyesters such as poly(butylene adipate-co-terephthalate) (PBAT) [2, 47]. However, biodegradable polymers produced from totally renewable sources are attracting attention due to their more environmentally friendly origin contrary to the petroleum-based polymers.

2.3.1 Poly(lactic acid): Structure and Synthesis

Poly(lactic acid) is a biodegradable, linear, aliphatic polyester. In its monomer, lactic acid, there are four unique groups attached to the central carbon atom, therefore it is a chiral molecule (Figure 2.14). Chiral molecules exist as ‘mirror images’ or stereoisomers. The optically active forms are “L” and “D” forms and by convention D=R=right handed and L=S=left handed. Chemically synthesized lactic acid gives the racemic mixture of approximately 50% L- and 50% D-isomers where lactic acid produced by fermentation typically consists of 99.5% of the L-isomer and the rest is D-isomer. Production of the cyclic lactide dimer might result in three different forms such as D, D-lactide (called D-lactide), L, L-lactide (called L-lactide) and L, D or D, L lactide called meso lactide. D and L forms of cyclic lactide are optically active whereas meso-form is not [48].

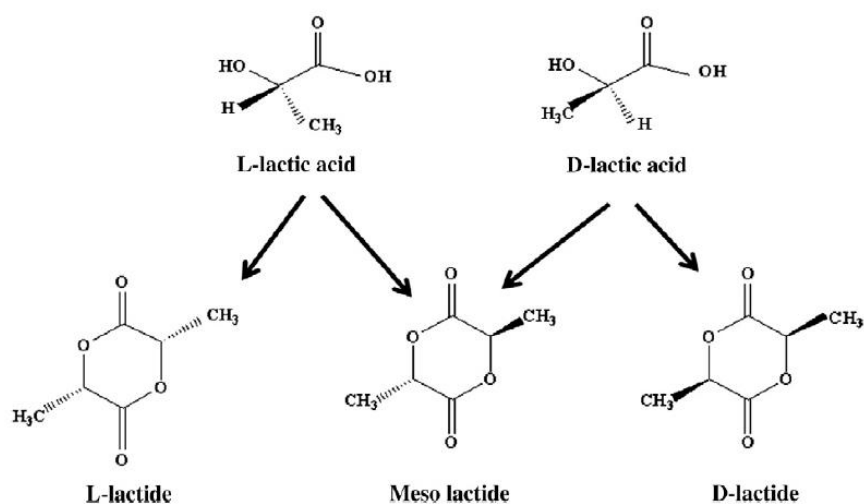


Figure 2.14 Lactic acid optical monomers [49]

Polymerization of lactic acid monomer can be performed using two different methods: in direct condensation process which involves solvents under high vacuum or in a solvent-free process, a cyclic dimer intermediate called lactide is formed followed by catalytic ring opening polymerization of the cyclic lactide [1]. The direct condensation route is an equilibrium reaction, and there are difficulties of removing water and impurities. Hence, the final product usually has low molecular weights ($M_w \sim 2-10$ kDa) [1, 50]. Because of the problems faced in direct condensation method, the commercial production processes are based upon lactide ring-opening polymerization. Both methods are shown in Figure 2.15.

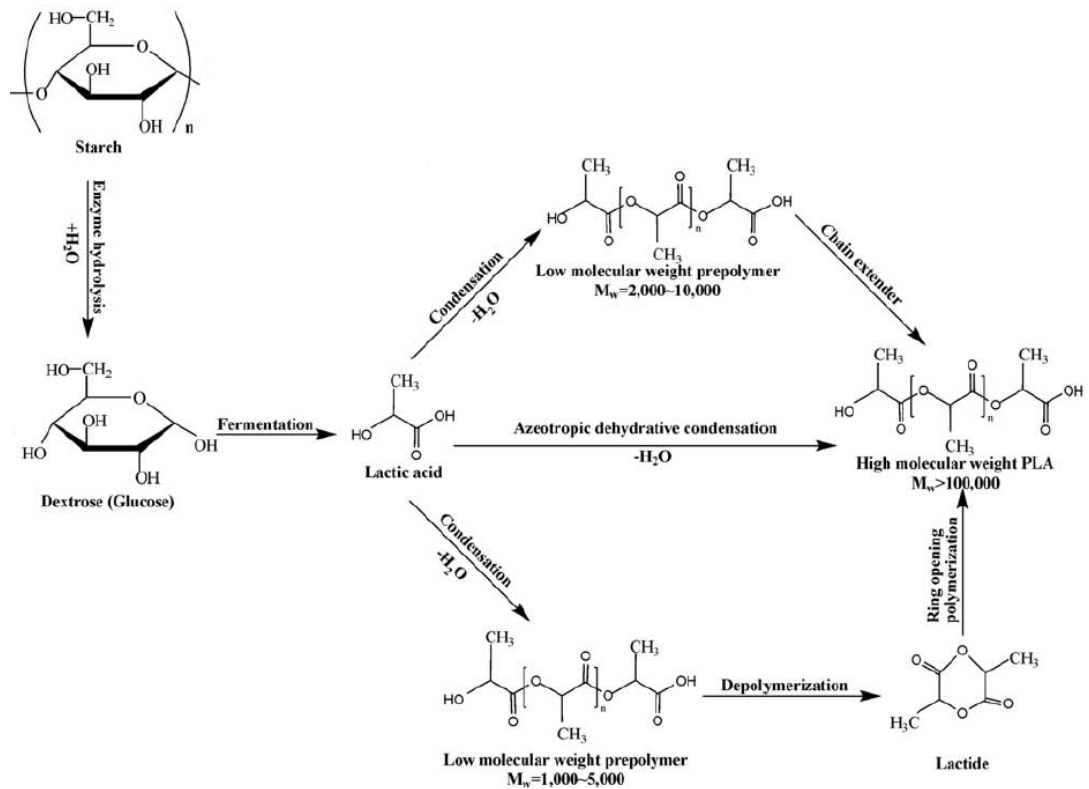


Figure 2.15 Synthesis routes of PLA [4]

2.3.2 Material Properties of PLA

Material properties of PLA such as density, heat capacity, and mechanical and rheological behaviors depend strongly on its transition temperatures. PLA structures with high L-lactide contents can be used to produce crystalline polymers while the higher-D-lactide PLAs are more amorphous. For amorphous PLAs, the glass transition (T_g); for semi-crystalline PLAs both the T_g and melting point (T_m), determine the temperature limitations for commercial uses [51]. In addition to the optical composition, these transition temperatures depend also on primary structure, thermal history, and molecular weight.

PLA is a clear, colorless thermoplastic when quenched from the melt, and it is similar in many respects to polystyrene. It can be processed like most thermoplastic polymers into fiber and film. However, regardless of optical content, both

amorphous and crystalline PLA show brittle behavior at room and body temperatures [49, 52].

Physical, mechanical and thermal properties of commercial PLA grades also differ significantly. Properties of two commercial PLA grades summarized by Nampoothiri et al. [49] are shown in Table 2.2.

Table 2.2 Material properties of two commercial PLAs [49]

	Nature Works	Biomer
<i>Physical Properties</i>		
Melt flow rate (g/10 min)	4.3-2.4	3.6
Density (g/cm ³)	1.25	1.25
Haze	2.2	
Yellowness index	20-60	
<i>Mechanical Properties</i>		
Tensile strength at yield (MPa)	53	70
Elongation at Yield (%)	10-100	2.4
Flexural Modulus (MPa)	350-450	3600
<i>Thermal Properties</i>		
Heat deflection temperature (°C)	40-45, 135	
VICAT softening point (°C)		56
T _g (°C)	55-56	55
Melting point (°C)	120-170	

2.3.3 Advantages and Limitations of PLA

Biodegradable polymers can be a solution to the solid waste problem associated with the decreasing availability of landfills, global warming caused by increasing amounts of carbon dioxide in the atmosphere and the attempts to find sustainable or renewable raw material sources [3]. Among the available biodegradable polymers in

the market, PLA has the following advantages and limitations summarized by Rasal et al. [1]:

Advantages

- **Eco-friendliness:** Being biodegradable, recyclable, and compostable makes PLA eco-friendly. Fixation of significant quantities of carbon dioxide via corn production also makes it valuable against global warming [45, 53]. Moreover, when burned, it produces no nitrogen oxide (NO_x) gases.
- **Biocompatibility:** It is an important material for biomedical applications. PLA hydrolyzes to its constituent α -hydroxy acid, which is assimilated in the tricarboxylic acid cycle (TCA) and expelled from the body. α -hydroxy acid is naturally produced by eukaryotic organisms and it is non-toxic at low concentrations. Thus, PLA is a suitable choice for applications of polymeric materials in biomedical field.
- **Processibility:** It has good thermal processibility compared to many commercially available bio-based polymers such as PHAs, poly(ethylene glycol) (PEG), poly(ϵ -caprolactone) (PCL), etc. PLA can be processed by almost all industrially available techniques.
- **Energy savings:** In the past, production procedures of biopolymers were costly. However, together with the new production techniques patented by Cargill Dow LLC, PLA requires 25–55% less energy to produce compared to many petroleum-based polymers. It is foreseen that production cost can be further reduced in the future [48].

Limitations

- **Toughness:** PLA is inherently brittle with elongation at break value less than 10%. Its poor toughness is an important limitation for applications that necessitate plastic deformation at high stresses.
- **Degradation rate:** Degradation of PLA occurs through the hydrolysis of ester groups. The rate of degradation depends on the global crystallinity, molecular weight, morphology of the sample, rate of water diffusion, and the

stereoisomeric content [54]. Slow degradation might be a problem for medical applications.

- Hydrophobicity: PLA is relatively hydrophobic, with a static water contact angle of approximately 80° which results in low cell affinity. This might cause inflammatory response of the living host upon direct contact with biological fluids [1].
- Reactive side-chain groups: Applications of PLA is also limited due to its chemical structure involving no chemically modifiable side-chain groups.

2.4. Polymer Processing Methods

Polymer matrix blends and composites can be produced by various polymer processing methods. The methods for thermoplastic polymers can be classified under two extensive subtitles. In the first step, the neat polymer is converted into a blend and/or composite. The second one describes the process of converting polymeric materials into desired shapes for necessary characterizations or applications. Two different polymer composite preparation methods and two different specimen preparation methods were used in this dissertation. PLA/organically modified clay nanocomposites were prepared by twin screw extrusion. PLA/expanded graphite nanocomposites were prepared both by extrusion and solvent assisted ultrasonication. Specimens for characterizations were prepared using injection and compression molding methods.

2.4.1 Extrusion

Extrusion is a polymer processing technique in which thermoplastic materials are converted to a continuous uniform melt from powdered or granular form and then shaped into items of uniform cross-sectional area by forcing it through a die [55]. Auxiliary equipment for cooling, stretching and cutting can be added to the whole extrusion system as shown in Figure 2.16.

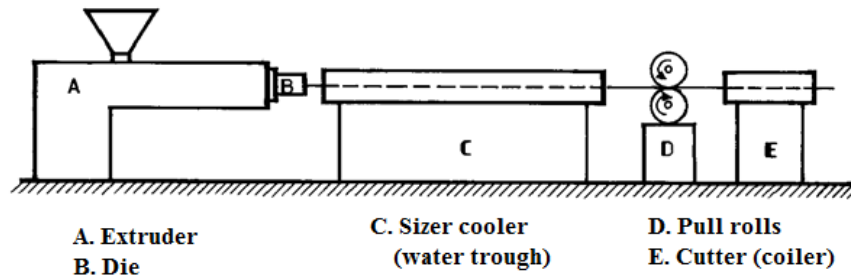


Figure 2.16 Schematic representation of an extrusion line [55]

Major parts of an extruder can be seen in Figure 2.17. There is a barrel through which the polymer is fed from the feeder to the die. The screw placed inside the barrel is the moving part of the extruder and it is designed to pick up, mix, compress, and carry the polymer from the hopper to the die as it changes from solid particles to a viscous melt. The screw turns in the barrel with power supplied by a motor operating through a gear reducer [55].

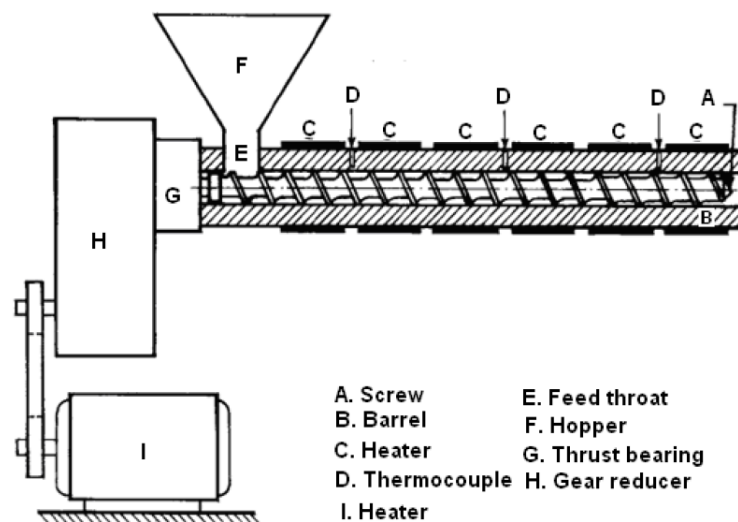


Figure 2.17 Parts of an extruder [55]

The regions in the barrel can be named as follows: feeding, compression (transition) and metering (Figure 2.18). The feed material is carried from the feed section to the transition section by the rotation of the screw. The electric heaters on to the barrel enable melting of the feed material. The polymer is totally melted as it reaches to the metering section and the shear applied by the screw forces the polymer melt to come out of the die. The melt material is given the desired by the die and cooled properly [56].

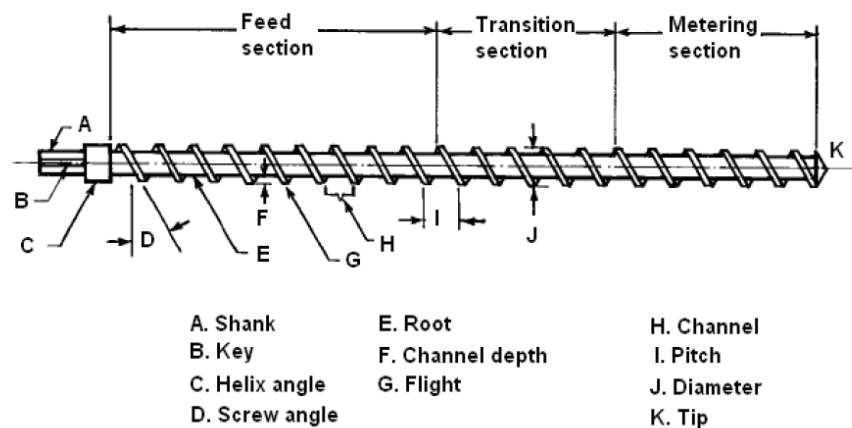


Figure 2.18 Parts of an extruder screw [55]

The most commonly used extruder type is the single screw extruder. A number of modifications of the single screw designs are available. Currently, multi-screw extruders are in use for particular applications where the single screw configurations are ineffective. The motion of the screw in a twin-screw extruder may be either co-rotating or counter-rotating. This type of extruders is appropriate for processing materials which are hard to supply owing to its positive displacement features in the intermeshing section. The maximum positive displacement is applied by counter-rotating twin-screw extruders. This feature makes them the principal choice for many extrusion applications. On the other hand, co-rotating twin-screw extruders are employed for applications such as compounding, mixing, devolatilization and

chemical reaction because of the complex flow in the intermeshing region [57]. Possible screw configurations for twin-screw extruders can be seen in Figure 2.19.

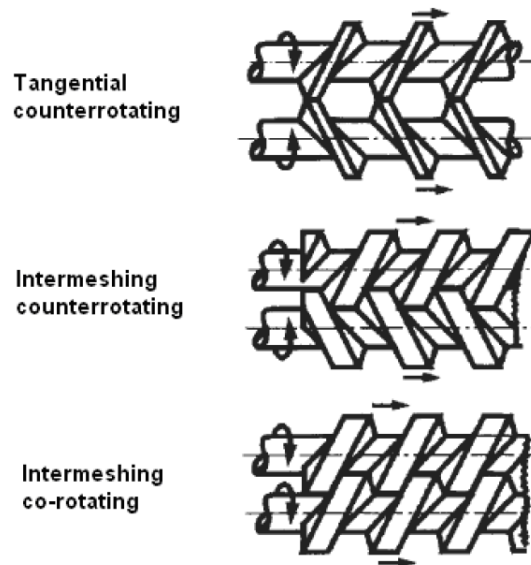


Figure 2.19 Screw configurations for twin screw extrusion [58]

2.4.2 Solvent Assisted Ultrasonication

Solution mixing has been widely used in order to produce composites of graphite derivatives and graphene. However, as in the case of carbon nanotubes, graphite derivatives are very cohesive materials due to the Van der Waals bonds between the carbon atoms. Achieving desired dispersion of these carbonaceous materials is not easy in the liquids owing to their strong tendency for agglomeration [59]. Agglomeration of these carbonaceous materials can be reduced by ultrasonication. Therefore, polymer/expanded graphite composites are prepared by solvent assisted ultrasonication method which involves mainly three steps. First, the polymer matrix and the filler are dissolved in solvent where, at this step only, the filler solution is exposed to ultrasonication. After that, these two solutions are mixed together and high energy ultrasonication is applied together with mechanical mixing until it

becomes a homogenous mixture. As the final step, the solvent is evaporated from the suspension [10, 59].

2.4.3 Injection Molding

Injection molding is the most common means of fabricating thermoplastic articles. The compound to be molded, usually in the form of pellets, is fed with the help of a hopper into an electrically heated barrel in which the material is melted [19]. This melt material is sent into the mold with high pressure and cooled under pressure until it solidifies. Then by opening the mold product is obtained. The parameters that affect the quality of injection molded articles are injection and back pressures, melt and temperatures, and the sample size. Injection molding equipment has injection and clamp units in order to do the cyclical steps during the process (Figure 2.20) [55, 59]. A typical mold for preparing dog-bone shaped specimens used in this study and its sections can also be seen in Figure 2.21.

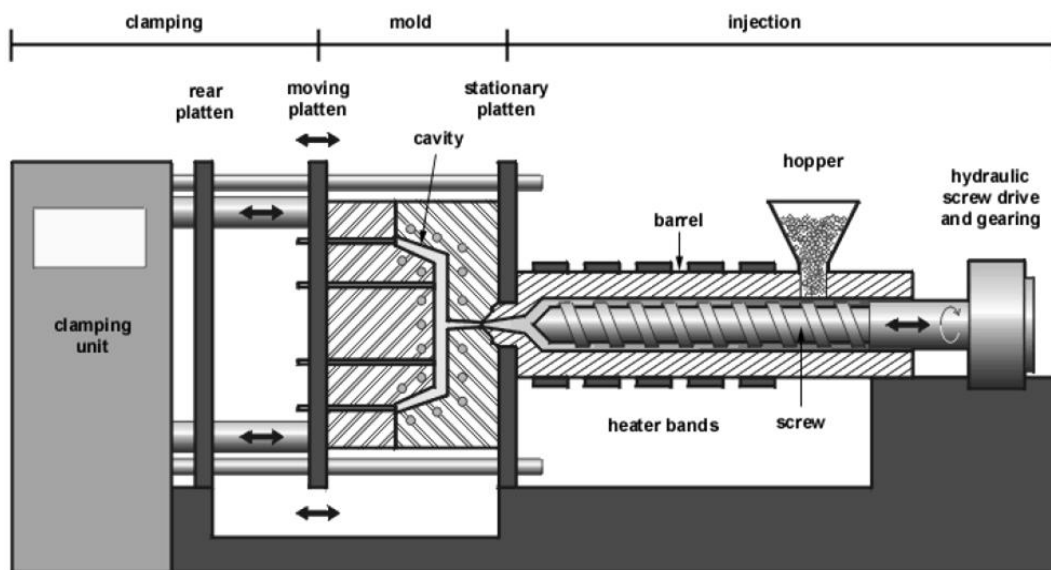


Figure 2.20 Schematic representation of thermoplastic injection molding machine [60]

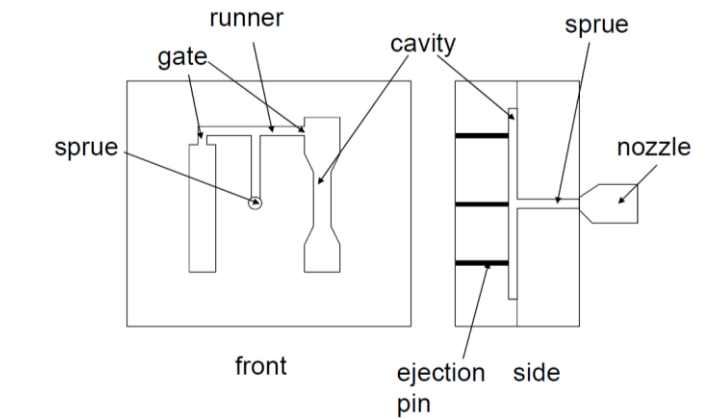


Figure 2.21 Parts of a mold used for injection molding [60]

The molding cycle is composed of three basic steps: filling, packing and cooling. The pressure rise is slow in the first cycle. The shrinkage is balanced by the high pressure applied at the packing stage. In order to have minimum shrinkage, the pressure on the cavity is very high during the cooling stage. Then the pressure is decreased gradually. The main step affecting the overall processing time is the cooling step and the thickness of the molded piece is the most important parameter. Poorly conductive polymers constitute the resistance to cooling, therefore prolong the total processing time [61]. The change in pressure during the injection molding process can be illustrated as in Figure 2.22.

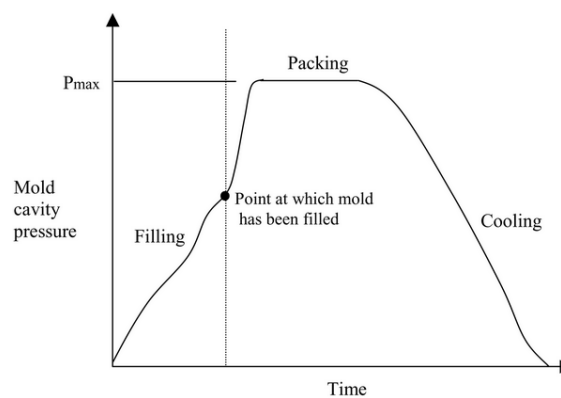


Figure 2.22 Pressure change during the injection molding cycle [62]

2.4.4 Compression Molding

In compression molding process, a predetermined amount of material is loaded into the lower half of a heated mold or cavity. Then, the top half of the mold is placed over the bottom half. The force plug is lowered into the cavity, and pressure, which can range from 20 to 1000 tons, is applied to the powdered or granular polymer. Under heat and pressure, the material melts and fills the mold cavity. After a suitable time period, the mold is opened, and the part is ejected while it is still hot. The sample is allowed to cool outside the mold [55]. In some cases, the gases produced upon heating and moisture trapped in the material cause bubbles in the molded sample. This can be eliminated by repeated compression/decompression cycles. A schematic representation of the compression molding process can be seen in Figure 2.23.

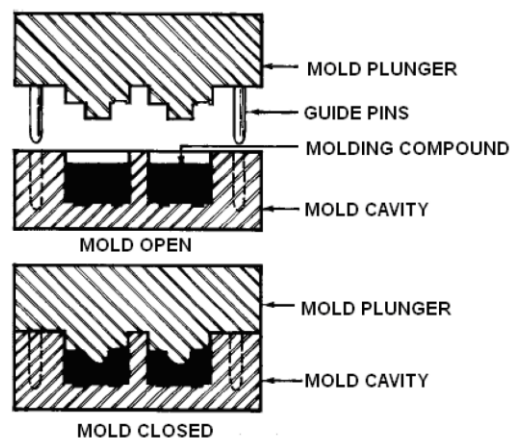


Figure 2.23 Schematic representation of compression molding process [55]

2.5. Experimental Techniques for Material Characterization

Mechanical, thermal, morphological, spectroscopic and rheological characterization methods were applied to the nanocomposites prepared in this dissertation.

2.5.1 Mechanical Properties

Mechanical testing plays an important role in evaluating fundamental properties of engineering materials as well as in developing new materials and controlling the quality of materials for use in design and construction. If a material is to be used as a part of an engineering structure that will be subjected to a load, it is important to know that the material is strong and rigid enough to withstand the loads that it will experience in service. A variety of methods can be used to determine mechanical performance under a variety of loading conditions. These methods can be classified under four main titles [63]:

- Static (i.e., tensile and shear)
- Transient (i.e., creep and stress relaxation)
- Impact (Izod and Charpy)
- Cyclic (Fatigue Test)

In this study, static (tensile) and impact (Charpy) tests are applied to the specimens prepared from PLA nanocomposites. Static tests are used to measure the force response when a sample is exposed to a strain, compression or shear at constant rate. The response of the material is characterized in terms of modulus, strain and elongation at break [63].

2.5.1.1 Tensile Test

Tensile test is probably the most common type of test used to measure the mechanical properties of a material. In this test, the specimen is deformed (pulled) at a constant rate, and the stress required for this deformation is measured simultaneously as shown in Figure 2.24 [55].

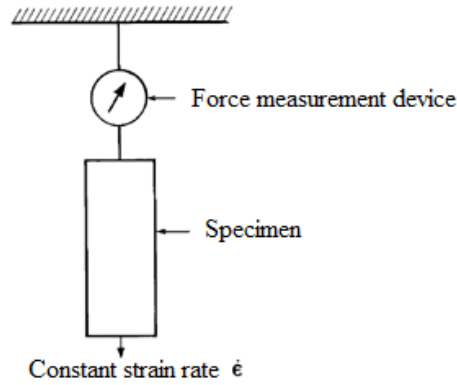


Figure 2.24 Schematic representation of tensile test [55]

In this test, a dog-bone shaped specimen, which is suitable for gripping into the jaws of the testing machine, is used (Figure 2.25).

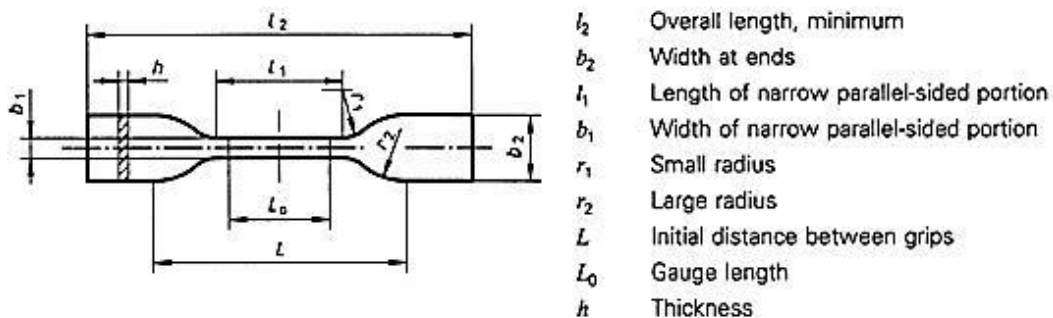


Figure 2.25 A typical dog-bone shaped tensile test specimen [64]

A stress-strain curve is obtained after the measurements. The major parameters that describe the stress-strain curve are the ultimate tensile strength (UTS), yield strength or yield point (σ_y), elastic modulus (E), and percent elongation (ΔL %). Toughness, resilience and Poisson's ratio can also be found using this testing technique.

Usually, the experimental data are presented as engineering (nominal) stress (σ) vs. engineering (nominal) strain (ϵ) as shown in Figure 2.26.

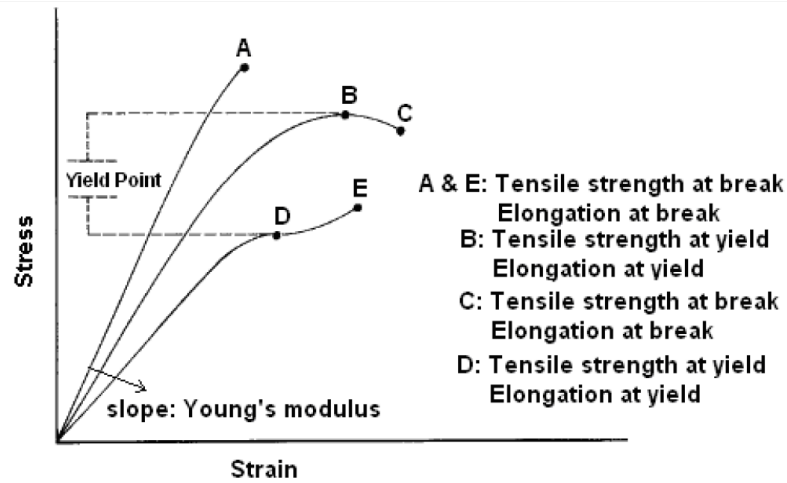


Figure 2.26 Engineering data from tensile tests [55]

The engineering stress (σ) is defined as:

$$\sigma = \frac{F}{A_0} \quad (2.1)$$

where F is the force measured during testing and A_0 is the initial cross-sectional area.

Engineering strain is given by:

$$\epsilon = \frac{L - L_0}{L_0} = \frac{\Delta L}{L_0} \quad (2.2)$$

In Equation (2.2), L_0 is the original gauge length, ΔL is the change in gauge length and L is the instantaneous gauge length. The elastic modulus (or Young's modulus)

E (MPa) is the ratio of the stress to the strain where the relationship between stress and strain is linear and it can be defined by Hooke's law as shown in Equation (2.3).

$$\sigma = E \cdot \varepsilon \quad (2.3)$$

Behavior of polymeric materials under tensile stress can be categorized as shown in Figure 2.27. The elastic modulus defines if the material is soft or hard. The ability of the tested material to absorb energy and undergo plastic deformation without failure is defined as toughness. It can be calculated from the area under the stress-strain curve.

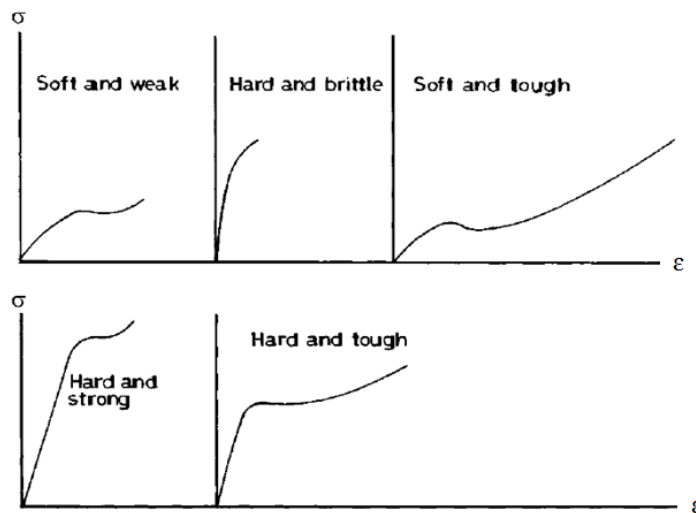


Figure 2.27 Typical stress–strain curves for polymeric materials [55]

2.5.1.2 Impact Test

The impact properties of a material signify its capacity to absorb and dissipate energies under impact loadings [17]. A number of testing methods have been developed for impact testing of polymeric materials. Calculation of the area under the stress-strain curve for a rapid tensile test can be an alternative. Falling ball or dart

test is another alternative in which the energy required to break a specimen is measured with the help of a falling ball of known weight released from a predetermined height. However, the most popular methods for impact testing are Charpy and Izod tests (Figure 2.28). In the Charpy test, a specimen of known dimensions (either notched or unnotched) that is rigidly held from its ends is broken by a hammer like weight. The energy required to break the specimen is obtained from the loss in kinetic energy of the hammer. In case of Izod test, the energy to break a notched specimen of known dimensions is measured again, but the specimen is clamped rigidly at one end and then struck at the other end by a pendulum weight [55].

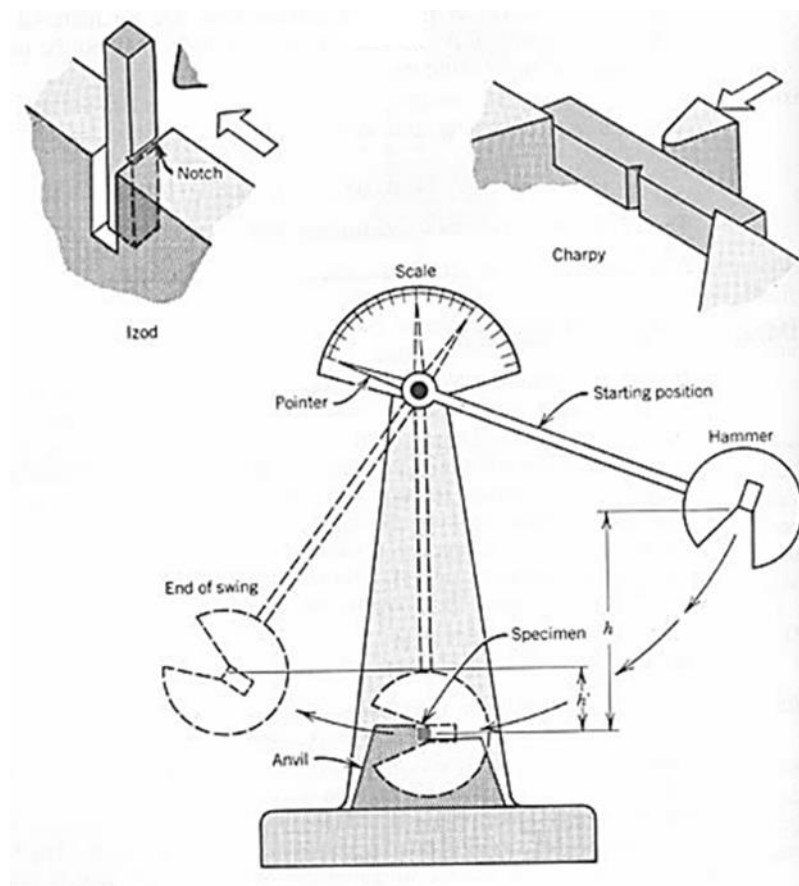


Figure 2.28 Schematic representation of Charpy and Izod impact tests [65]

2.5.2 Thermal Properties

Thermal analyses cover a number of methods in which changes in physical properties of a material are measured as the temperature varies [66]. In this thesis, differential scanning calorimetry (DSC) is used to determine the thermal properties of the produced nanocomposites.

2.5.2.1 Differential Scanning Calorimetry

In DSC analyses, the amount of heat required to increase the temperature of a sample and a reference pan are measured as a function time. Temperatures of the sample and the reference are kept almost at the same temperature. The basic principle applied in this technique is that when the sample undergoes a physical change like phase transition, the amount of heat to provide this transition would be more (or less) than the heat required to keep the reference at the same temperature. The transitions of a material can be either endothermic or exothermic. Melting of a solid material, for example, is an endothermic process requiring more heat flow to the sample. Crystallization, on the other hand, is an exothermic process which requires less heat to raise the temperature of the sample. By observing the difference in heat flow between the reference pan and the sample, it is possible to measure the amount of energy required for particular phase transitions. A sample curve obtained from DSC analyses can be seen Figure 2.29.

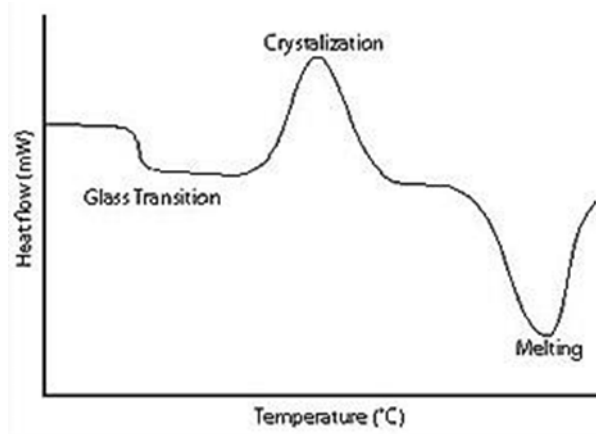


Figure 2.29 Typical DSC curve [67]

Transition temperatures that can be determined via DSC are glass transition temperature (T_g), cold crystallization temperature (T_c) and melting temperature (T_m). The glass transition is a reversible transition in amorphous materials or in amorphous regions within semi-crystalline materials from a hard and relatively brittle state into a molten or rubber-like state [68]. The temperature at which this transition occurs is called the glass transition temperature. T_m is the melting temperature. At this temperature the crystals in the sample disintegrate and liquefy. Heat required for the cold crystallization and melting of semi-crystalline materials can be used to determine initial % crystallinity (X_c) of the polymer phase, if the heat of fusion for the 100 % crystalline polymer is known (2.4).

$$X_c = \left[\frac{(\Delta H_m - \Delta H_c)}{(\Delta H_m^o w_{poly})} \right] \times 100 \quad (2.4)$$

where ΔH_m^o (J/g) is the heat of fusion of the 100% crystal structure, ΔH_c (J/g) is the cold crystallization energy, ΔH_m (J/g) is the melting energy obtained from the DSC curve. Additionally, w_{poly} is the fraction of polymer phase in the composite.

2.5.3 Morphological Analyses

Morphology can be defined as the study of form and structure. For polymer science, it is the study of order within the macromolecular structures. In this thesis, X-ray diffraction (XRD), scanning electron microscopy (SEM) and transmission electron microscopy (TEM) are used to investigate the morphologies of the nanocomposites.

2.5.3.1 X-Ray Diffraction

X-rays are very frequently used in the analyses of interatomic distances in solids, since their wavelengths (0.5-2.5 Å) are at the same order magnitude of atomic configurations [69]. The most basic application is the determination of crystal lattice spacings but many other information can be derived such as crystal size and perfection, lamellar thickness and interlamellar region of lamellar polymers, degree of crystallization in semi-crystal polymers and, using suitable computational methods, the conformation of chains in amorphous polymers [66].

X-rays are produced by bombarding a metal target with high energy electrons. The target material is kept in vacuum to avoid scattering of the electrons by gas atoms. When X-rays interact with a single particle, it scatters the incident beam in all directions but when they interact with a solid material the scattered beams can add together in a few directions and reinforce each other to yield diffraction. The regularity of the material is responsible for the diffraction of the beams. The diffraction and scattering mechanisms can be seen in Figure 2.30.

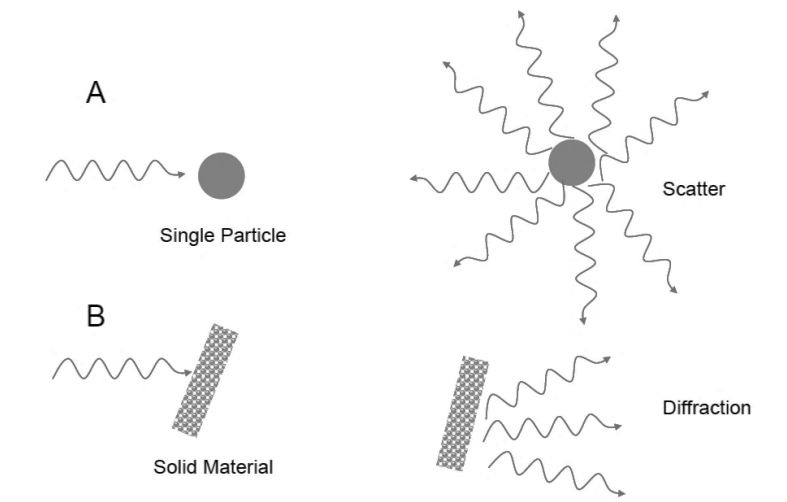


Figure 2.30 Interaction of X-rays with materials: scattering and diffraction mechanisms [70]

In order to describe the position of the X-ray diffraction peaks in angular space a relationship discovered by Sir William H. Bragg and Sir W. Lawrence Bragg can be used. This relation is known as Bragg's Law (2.5).

$$n\lambda = 2d\sin\theta \quad (2.5)$$

where λ is the wavelength of the X-ray, θ is the scattering angle, n is an integer representing the order of the diffraction peak and d is the inter-planar spacing of atoms [71]. The Bragg's Law is based upon the diffraction of X-rays as shown in Figure 2.31.

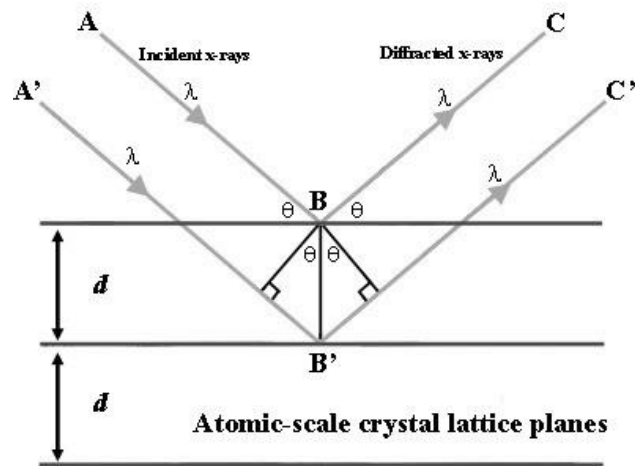


Figure 2.31 Bragg's Law reflection [72]

Depending on the scope of X-ray analyses, two different methods can be applied. Wide angle X-ray diffraction (WAXD) involves scattering with 2θ values typically in the range of $10\text{-}40^\circ$. If much smaller angles are involved, small angle X-ray diffraction (SAXD) should be used. In general, WAXD detects the changes in crystallinity and orientation by which spatial arrangement of atoms is described, whereas SAXD detects fibrillar and lamellar structures and cavities [73].

2.5.3.2 Scanning Electron Microscopy

Electron microscopy has emerged as a powerful tool for investigation of polymer morphology. The information obtained from this technique is in the form of magnified images which are relatively easy to interpret. In this technique, an incident electron beam is scanned across the sample surface, and the resulting electrons emitted from the sample are collected to form an image of the surface. In order to get SEM images of a surface, the first requirement is a monoenergetic beam of electrons. For the best resolution, the electron beam must be as narrow as possible. The electron beam is focused on the specimen with the help of a system of lenses. Various detectors such as secondary electron detectors, backscattered electron detectors and X-ray detectors are arranged in the instrument for the measurement of

different signals [66]. These detectors are necessary due to the beam-specimen interactions shown in Figure 2.32 and the layout of the SEM instrument can be seen in Figure 2.33. Imaging is typically obtained using secondary electrons for the best resolution of fine surface topographical features. Alternatively, imaging with backscattered electrons gives contrast based on atomic number to resolve microscopic composition variations, as well as, topographical information [74].

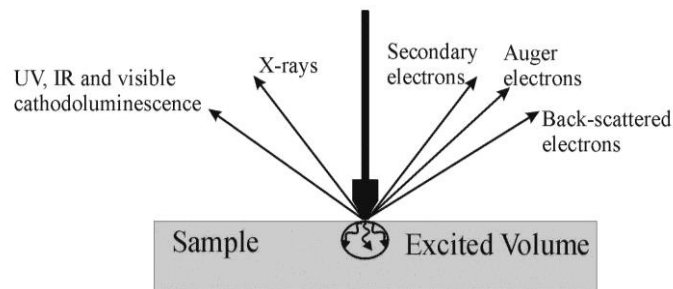


Figure 2.32 Schematic representation of beam-specimen interactions in SEM [75]

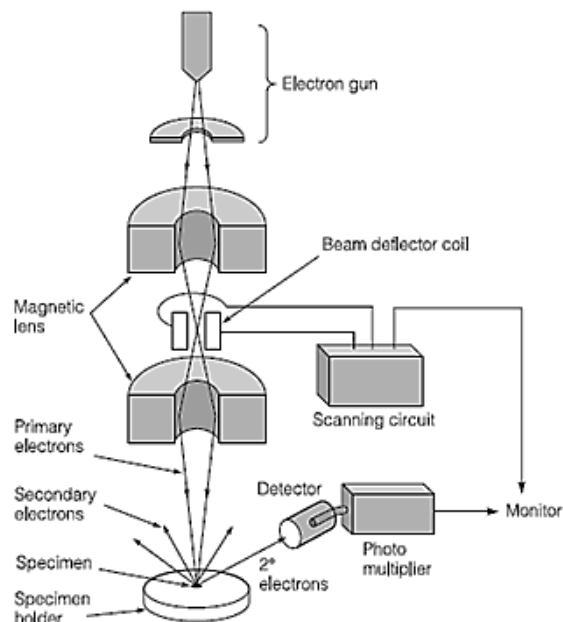


Figure 2.33 Layout of SEM instrument [76]

Two major problems are observed in imaging of polymers with SEM. Firstly, since the polymers are poor conductors charge build up on the polymer surface happens as the electron beams are sent to the sample, which affects the incoming beam. In order to eliminate this problem, a conductive coating (i.e., gold, carbon, etc.) can be applied to the sample surface. Secondly, polymers can be damaged by the energetic imprinting electrons, restricting the operating conditions [66].

2.5.3.3 Transmission Electron Microscopy

The transmission electron microscope (TEM) provides valuable information about the structural information of the sample to be investigated at levels of atomic dimensions. Under optimum conditions information within a range of 1-100 nm can be obtained. However, the main shortcoming in TEM imaging is that very thin samples (less than 1 μm thick) should be prepared requiring special sample preparation techniques [66].

Operation principle of TEM is very similar to light microscope however in this method electrons are used instead of light. In the TEM instrument, an electron source at the top of the microscope emits monoenergetic electrons which travel in the vacuum. Because of strong interactions of electron with matter, gas particles must be totally evacuated from the column. The required high vacuum is maintained by a vacuum system typically containing a rotary pump, a diffusion pump and one or more ion getter pumps. Instead of glass lenses focusing the light in the light microscope, TEM uses electromagnetic lenses to focus the electrons into a very thin beam. Some of the electrons coming to the specimen are scattered depending on the material density. The unscattered electrons reach to a fluorescent screen placed at the bottom of the microscope. The image obtained from TEM is actually a shadow image with its different parts displayed in varied darkness according to their density [77, 78]. The optical electron beam diagram of TEM can be seen in Figure 2.34.

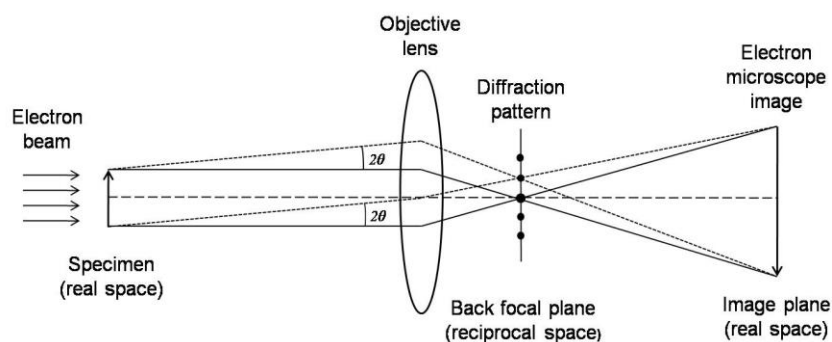


Figure 2.34 The optical electron beam diagram of TEM [79]

2.5.4 Spectroscopic Analyses

Spectroscopic techniques are widely used to identify the structure of a completely unknown chemical or to determine configurational states (i.e., cis-trans isomers) or presence of a particular functional group. Interpretation of the spectroscopic data can be performed by comparison with known standard samples. In this dissertation Fourier Transform Infrared Spectroscopy (FTIR) was used to investigate chemical interactions between the functional groups of polymer matrix and additives.

2.5.4.1 Fourier Transform Infrared Spectroscopy

Infrared spectroscopy is a vibrational spectroscopic technique where molecular vibrations are analyzed. In this technique, infrared radiation (IR) is passed through a sample. Some of it is absorbed and the rest is transmitted. The spectrum obtained after analyses shows the molecular absorption and transmission of the IR and this spectra is considered as the molecular fingerprint of the material [80]. In fact, all chemical bonds vibrate at a characteristic frequency depending on their structure, bond length and angle. Therefore, they interact with incident radiation by absorbing the radiation at specific wavelengths. By observing the energy absorption of a particular sample, a spectrum can be obtained through which individual absorption

peaks can be identified based on known structures. This enables the determination of interactions between complex systems [81].

The heart of the FTIR is a Michelson interferometer. It splits a beam of radiation into two paths having different lengths, and then recombines them. A detector measures the intensity variations of the exit beam as a function of path difference. A basic representation of this method can be seen in Figure 2.35.

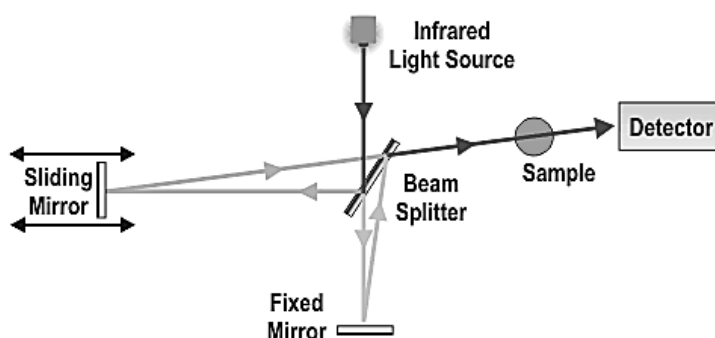


Figure 2.35 Schematic representation of FTIR [82]

2.5.5 Rheological Analyses

Rheology is the science of deformation and flow of materials [63]. As opposed to the traditional engineering practice, behavior of polymeric materials cannot be classified as elastic solids or viscous liquids. The behavior of polymeric materials falls between these two extremes [55]. For describing this behavior of polymers the word “viscoelastic” is used since they can behave like a solid or a fluid depending on the time scale of applied shear and/or the temperature [83].

Materials of the same grade might show different flow behavior under stress only because of the small changes in the structure. Because of the sensitivity of rheology of the condensed phase to structure, rheology is a highly convenient method to characterize polymers [84]. In this dissertation, dynamic oscillatory shear

measurements were used to investigate melt rheological behavior of polymer nanocomposites.

In oscillatory rheometer, a sinusoidal shear deformation is applied on the sample and the resultant stress response is measured. As mentioned, the behavior is depends on the time scale of the applied shear, which is determined by the frequency of the oscillation (ω). For the measurements, the sample is placed between two heated plates (Figure 2.36). As the polymer melts and the thickness is adjusted accurately, the oscillatory shear is applied by the rotation of the bottom plate with a time dependent strain, $\gamma(t)=\gamma_0.\sin(\omega t)$. When the bottom plate is moving, the top plate is stationary and the time dependent stress, $\sigma(t)$, on this stationary plate is obtained by measuring the torque [85].

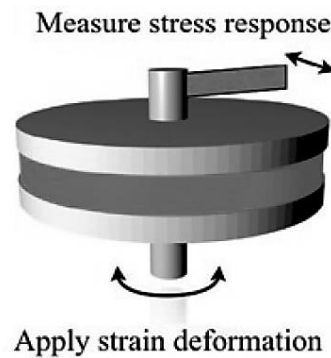


Figure 2.36 Schematic representation of a typical rheometer setup with the sample placed between two plates [85]

The viscoelastic behavior of a polymeric sample is determined by two main material functions: the storage modulus (G') and the loss modulus (G''), which characterize the solid-like and fluid-like behaviors, respectively. G' represents the stored elastic energy and G'' represents the energy dissipated in one cycle of deformation [86]. The stress response of the material resulting from a sinusoidal strain deformation is expressed as:

$$\sigma(t) = G'(\omega)\gamma_0 \sin(\omega t) + G''(\omega)\gamma_0 \cos(\omega t) \quad (2.6)$$

Usually in a dynamic oscillatory experiment, G' and G'' values are obtained as a function of frequency. By using these properties, loss tangent, $\tan \delta$, and complex viscosity, η^* , can be determined as shown in Equations (2.7) and (2.8), respectively [86].

$$\tan \delta = \frac{G''}{G'} \quad (2.7)$$

$$\eta^* = [(G'/\omega)^2 + (G''/\omega)^2]^{1/2} \quad (2.8)$$

2.6. Previous Studies

High strength and high modulus of PLA makes it very attractive among the other bioplastics, but its intrinsic brittleness limits its industrial applications. One of the mainstream thermoplastics used in wide range of applications, polystyrene (PS), has comparable strength and modulus when compared to PLA. Additionally, these two thermoplastic polymers also have similar brittleness. Historically, brittle nature of PS led to the products modified with rubber modified and having high impact strength values [4]. Similar attempts are common for PLA for the past few years.

In order to achieve desired mechanical properties and impact resistance using biodegradable and non-biodegradable fillers and plasticizers or blending of PLA with other polymers are the principal routes that have been followed. Particularly, improving impact toughness through melt blending with flexible polymers is an easy-to-apply and promising approach. Variation in stereochemistry, molecular weight and crystallinity of neat PLA were also reported to have influence on ductility and impact resistance however these effects are insufficient for industrial purposes [4]. Additionally, synthesis of PLA copolymers to achieve desired properties is another method but it is the less industrially preferred one.

Toughening PLA

Plasticizers

The main objective in plasticization is to decrease the glass transition temperature (T_g) and to increase the tensile toughness. Additionally, a good plasticizer for PLA applications is preferred to be biodegradable, nonvolatile, nontoxic and shows minimum migration during aging [4]. In the literature, different biodegradable and non-biodegradable plasticizers have been used with PLA.

A monomeric plasticizer used with PLA is lactide (LA), which enhanced elongation at break, but due to its low molecular weight showed migration towards the surface hence caused stiffening during aging [87, 88]. In order to eliminate the migration problem, oligomeric plasticizers were utilized such as oligomeric LA, citrate esters, PEG, etc. Matrin and Avérous [89] reported that oligomeric LA and low molecular weight PEG gave the best results in terms of lowering the glass transition temperature (from 58°C to 12°C and 18°C, respectively).

Many other oligomeric and polymeric plasticizers were investigated in the literature. Some of them are tailored according to the needs of PLA and some of them are commercial plasticizers. Liu and Zhang [4], in their recent review on toughening of PLA, summarized the drawbacks of plasticization. It is revealed that high amounts of plasticizers (15-20%) are required to achieve a significant decrease in T_g . The same situation is valid for improvements in ductility and tensile toughness. High percentages of plasticizers bring reductions in strength and modulus, even though elongation at break increases. Additionally, phase separation and increase in chain mobility require careful optimization of processing parameters and material contents in achieving the desired material properties [4].

Biodegradable Polymer Blends

Development of polymer blends of PLA with other biodegradable polymers have been extensively studied, since obtaining the desired material properties without any negative effect on natural degradability is a major issue for many applications.

Polyhydroxyalkanoates (PHAs) are bacterially produced alternatives to blend with PLA with a wide range of properties changing according to their chemical structure. An interesting and promising study was performed with a commercial PHA copolymer, Nodax, a copolymers having 3-hydroxybutyrate (3HB) and 3-hydroxyalkanoate (3HA) units with side groups greater than or equal to three carbons. It was reported that in PLA/NodaxH6 (10 wt. %) blend, elongation at break was higher than 100% and tensile toughness was almost 10 times that of neat PLA. In terms of morphology, NodaxH6 was dispersed in PLA matrix as rubbery amorphous droplets when its concentration was less than 20 % [90].

Polycaprolactone (PLC), an aliphatic polyester, is another widely investigated biodegradable polymer in PLA blends. Since PLA and PLC are immiscible, compatibilizers are usually utilized. Triphenyl phosphate (TPP) [91], dicumyl peroxide (DCP) [92], lysine diisocyanate (LDI) and lysine triisocyanate (LTI) [93] are some of the compatibilizers. Due to presence of hydroxyl and carboxyl end groups in PLA, compatibilizers containing isocyanate groups (LDI, LTI, etc.) are also used in other polymer blends such as copolymers of poly(butylene succinate) (PBS) [94].

Biodegradable polyurethane (PU) and polyamide (PA) elastomers were also used to toughen PLA. Since PU and PA elastomers are partially miscible with PLA without any need of compatibilizers, blends with some improved properties could be obtained. For instance, Li and Shimizu [95] reported that an increase in the PU content resulted in a gradual increase in toughness. Moreover, blends with 30 wt. % PU content showed higher elongation at break and impact strength, but lower tensile strength.

Non-Biodegradable Polymer Blends

Although it is desirable to produce totally biodegradable polymer blends, non-biodegradable polymers might also help researchers to obtain toughened PLA meeting the needs of consumers. As in the case of biodegradable polymer blends, problem of immiscible phases appear for non-biodegradable polymers therefore compatibilizers are utilized in a number of cases.

Linear low density PE (LLDPE) was melt blended with PLA in the presence of PLLA-b-PE diblock copolymers as a compatibilizer at a constant ratio of 80 wt. % of PLA and 20 wt. % of LLDPE [96]. According to the SEM images, addition of PLLA-b-PE block copolymer into the binary blend yielded in enhanced interfacial adhesion and as a result better dispersion of LLDPE in PLA matrix. In addition, toughness of the blend was found to be affected by the crystallinity of PLA such that semi-crystalline PLA blends revealed toughening even in the absence of PLLA-b-PE block copolymer.

In order to have enhanced interactions and fine dispersion between the materials, chemically complementary groups are preferred in the structure of either modifier or compatibilizer in reactive blending. For instance, epoxide group is reactive towards the functional end groups of PLA (hydroxyl and carboxyl groups). This knowledge leads to the utilization of glycidyl methacrylate (GMA) copolymers in PLA blends. For instance, Oyama [97] studied toughening of PLA via melt blending with poly(ethylene-co-glycidyl methacrylate). In this study, it was reported that the blend of low molecular weight PLA (L-PLA) with 20 wt. % E-GMA had a much higher elongation (>200%) relative to pristine L-PLA (5%). The increase in the notched Charpy impact strength was not as significant as of elongation at break, and it was only two times that of neat L-PLA. One distinct result obtained in that study is the increase in impact strength after the annealing of injection molded specimens. The annealing step was performed at 90°C for 2.5 hours and as a result the impact strength was considerably increased to 72 kJ/m² which is about 50-fold higher than that of pristine L-PLA. With the higher molecular weight PLA (H-PLA) effect of annealing on impact strength seemed to be comparatively less outstanding.

Most recently, PLA was toughened using hydrogenated styrene-b-butadiene-b-styrene copolymer (SEBS) and E-GMA [98]. Notched Izod impact strength of 92 kJ/m² and an elongation at break of 185% were achieved with PLA/SEBS/E-GMA (70/20/10, w/w) blend. Similar to the previously mentioned work of Oyama [97], samples were annealed in this study for 48 hours at 80°C. Annealing resulted in decrease in both impact strength and elongation at break. Going one step further, quaternary blends with the addition of polycarbonate (PC) were produced. For

PLA/PC/SEBS/E-GMA (40/40/15/5, w/w) blends, it was reported that the heat deflection temperature and aging resistance were improved, but the notched impact strength was relatively decreased compared to those of ternary blends.

Besides the particular attempts in designing PLA blends, many commercial impact modifiers are available in the market. These modifiers are either linear elastomers with low T_g or crosslinked core-shell polymers [4]. For example, a commercial acrylonitrile-butadiene-styrene (ABS) resin, BlendexTM 338, was used to toughen PLA by NatureWorks and at 20% BlendexTM 338 content notched Izod impact strength of 518 J/m and an elongation of 281% was achieved, whereas the corresponding values of neat PLA were 26.7 J/m and 10%, respectively. On the other hand, tensile strength of the blend reduced 30% compared to neat PLA. Biomax[®] Strong series, which are ethylene-acrylate copolymers, are produced by DuPont particularly to enhance toughness without major transparency loss. Sukano[®], OnCapTM BIO are other elastomeric impact modifiers which are commercially available. BiostrengthTM, on the other hand, is a core-shell impact modifier produced by Arkema.

PLA-Organoclay Nanocomposites

Nanoparticles have been extensively used in the property improvement of engineering plastics for some decades. Based on the experiences gained with petroleum based plastics, over the last decade, PLA has been reinforced with various nanoparticles, including clays, carbon based nanofillers, metal oxides, polysaccharide nanoparticles, etc. Among all these alternatives, probably the most popular and promising nanofiller for PLA have been layered silicates.

The first attempt to prepare PLA nanocomposite using organophilic montmorillonite was performed by Ogata and coworkers [9]. Solution intercalation method was utilized in that study, but the results were not promising. The layered silicates were not well dispersed, but rather formed tactoids consisting of several stacked silicate monolayers. As a result, although the geometrical structure of the tactoids caused improved Young's modulus with increasing clay content, the goal of producing

nanocomposites were not achieved. After that many successful studies reporting well dispersion of layered silicates in PLA matrix have been published until today, some focusing on thermal and mechanical properties, some on morphology and rheology, and some on biodegradability.

In one of the PLA nanocomposite studies, PLA/clay nanocomposites loaded with 3 wt. % organomodified montmorillonite (dimethyl 2-ethylhexyl (hydrogenated tallow alkyl) ammonium cation) and PLA/clay microcomposites containing 3 wt. % sodium montmorillonite were prepared by melt blending and the properties of these composites materials were compared with those of neat PLA processed in the manner. It was shown that the PLA-based microcomposite formed a phase-separated microstructure. According to the X-ray diffraction patterns, an increase in the interlayer spacing from 21.0 Å in the nanoclay filler to 31.4 Å is said to be a proof of some intercalation occurring during the component blending. Additionally, thermal investigations showed an improvement in the nanocomposite thermal stability under oxidative conditions in comparison to those for the microcomposite and unfilled PLA [99].

After that, Krikorian and Pochan [100], successfully prepared exfoliated materials via solvent intercalation in the presence of Cloiste 30B (C30B). It was discussed that, the long alkyl chain and hydroxyl groups of C30B enhanced the interactions between C=O functional groups of the PLA backbone, and hence favored exfoliation. As a result, the mechanical properties were improved such that the storage modulus increased by 61% with 15 wt. % of C30B.

Effect of forming nanocomposites on biodegradability of PLA is another issue that researchers have been focusing. Paul et al. [101] studied the hydrolytic degradation of PLA filled with organically modified montmorillonite (MMT) by hydrolysis test in a phosphate buffer medium. On the other hand, Ray et al. [102] investigated biodegradation of the PLA/MMT nanocomposites under composting conditions. According to these studies, the biodegradation of the nanocomposites occurs more rapidly than the biodegradation of unfilled PLA. In the former study, an increase in the opacity of the samples during degradation period was seen which was correlated

to an evolution in crystallinity of the polymer matrix. This result supports the claim that the hydrolytic degradation preferentially takes place in amorphous regions, leading therefore to an increase of the polymer global crystallinity. A conflicting result was reported by Pluta et al. [99], where both types of clay used in that study showed a tendency to limit PLA degradation. Recently, Ozkoc and Kemaloglu [103] also claimed that increasing crystallinity obtained by the inclusion of clay results in a lower biodegradation rate, 30% weight loss happens in the first 30 days for PLA, while only 10% is lost at the end of 100 days for PLA and plasticized nanocomposites. Furthermore, it was reported that the presence of organofiller does not improve the tensile strength of PLA whereas it gives a higher Young's modulus.

Blends of PLA with flexible polymers usually show toughening, however this enhancement comes together with reductions in tensile strength and tensile modulus. Contrarily, incorporation of rigid fillers results in improvement in modulus and reduction in elongation. Therefore, some researchers are trying to balance the outcomes of flexible polymers and rigid fillers by producing ternary composites [4].

One alternative was produced by Chen et al. [104] with Cloisite 25A (C25A) in PLA and poly(butylene succinate) (PBS) blends. 75 wt. % PLLA and 25 wt. % PBS blend containing 10 wt. % C25A showed almost 80% increase in tensile, but elongation at break decreased from 71.8% to 3.6%. Elongation at break of this nanocomposite was lower than that of pristine PLLA. In addition, using an organoclay with epoxy functionality resulted in approximately the same tensile modulus and increased elongation at break (118%).

A core-shell rubber impact modifier Paraloid™ EXL 2330 was utilized in PLA/clay/core-shell rubber ternary composites by Li et al. [105], but the results were not very promising. With 20% EXL 2330 and 5 wt. % C30B clay, the notched Izod impact strength increased from 2.2 kJ/ m² of neat PLA to 5.2 kJ/m², which is more than twice. However, the tensile modulus decreased from 1.81 MPa to 1.79 MPa accompanied with a decrease in tensile strength from 61.0 MPa of neat PLA to 43.8 MPa. Elongation at break showed little change, being 7% compared to 6.6% of neat PLA.

Jiang et al. [106] investigated the effects of organically modified clay and nano-sized precipitated calcium carbonate (NPCC) on mechanical properties of ternary composites containing PLA, poly(butylene adipate-*co*-terephthalate) (PBAT) and nanofiller. Higher tensile strength and modulus were obtained for the composites containing OMMT, but elongation at break was lower compared to the elongation at break of NPCC containing composites. In the same study, by replacing 25 wt. % of the PLA by maleic anhydride grafted PLA (PLA-g-MA), significant increases were obtained in the elongation at break. This might have been attributed to the improvement of surface interactions with the presence of epoxide functional groups. As a result, PLA/PBAT/OMMT (87.5/10/2.5 w/w) where 25 wt. % of PLA was replaced with PLA-g-MA gave the best results. The tensile strength was retained at 87% of neat PLA. Additionally, slightly higher modulus and notably increased strain at break (16.5 times higher than that of neat PLA) were obtained.

Finally, Martino et al. [107] produced nano-biocomposites based on PLA plasticized with 15 wt. % polyadipates to improve the polymer ductility. These materials showed enhanced ductility and barrier properties. In the production, the clay was swollen in liquid polyadipates prior to their blending with PLA. In certain processing conditions (melt blending at 100 rpm, 170°C and for 20 min.), homogeneous and exfoliated structures were obtained which was supported by X-ray diffraction (XRD) and transmission electronic microscopy (TEM) results. Without the addition of clay, plasticized PLA showed high deformation at break values, around 250–300% compared to 5% for the neat PLA. The incorporation of OMMT at 2.1 wt. % resulted in an increase in the elastic modulus values and decrease in the elongation at break, as usual for the composite materials.

Ternary nanocomposites of many commercial plastics with layered silicates were characterized in terms of mechanical properties, morphology and rheology. Determination of rheological behavior is important in order to enable effective processing. In addition, melt rheology can be used as a method to characterize the nanocomposite structure and filler dispersion, therefore rheology measurements of polymer nanocomposites are almost always coupled with morphology investigations. There are a number of studies concerning the rheological behavior of binary and

ternary PLA nanocomposites. Di and coworkers [11] studied PLA/organically modified clay nanocomposites with two different types of organoclays. Nanocomposites showed higher viscosity and noticeably higher elastic properties compared to those of pure PLA. Organoclay content was increased up to 10 wt. %, and higher values of viscosity (η^*), storage modulus (G') and loss modulus (G'') were obtained in the frequency range studied for all the nanocomposites prepared using Cloisite 30B (C30B) as the nanofiller. Furthermore, even at lowest the filler loadings, disappearance of Newtonian plateau at low frequencies was observed. These increases in modulus values and disappearance of Newtonian plateau at low frequencies were mainly attributed to the strong interaction between C30B and PLA molecules and effective nanodispersion of filler in polymer matrix. Recently, Singh et al. [12] extensively studied the rheological behavior of binary PLA nanocomposites with C30B as the filler material. As the nanoclay content increased, an increase of the values of η^* , G' and G'' was observed. In addition, thermal stability up to 100 seconds was reported. The stress relaxation data showed that the slopes of relaxation curves decreased with the increase in clay content indicating that the relaxation time increased with the clay content. Increases in the moduli and viscosity values were attributed to an interconnected structure and reinforcement of the molten PLA by C30B owing to hydrogen bonding of hydroxyl groups in the organic modifier of the nanoclay and carbonyl groups of PLA chains. More recently, rheological behavior of ternary PLA nanocomposites were also studied. Bhatia [13] examined the rheological behavior and thermal properties of ternary PLA, PBS, and C30B nanocomposites. At a constant PLA/PBS ratio, strain sweep measurements showed that the limit of linearity of viscoelastic region tended toward low strain amplitudes at high organoclay concentrations. Interestingly, storage modulus of PLA/PBS blend was always higher as compared to low filler content (1-3 wt. %) nanocomposites over the entire frequency range (0.1–100 rad/s). This situation is valid for G'' and η^* which was explained by the presence of little interparticle interactions compared to higher clay contents. Shear-thinning behavior at high shear rates and the change from Newtonian to pseudo-plastic behavior at high clay contents were emphasized. Another ternary blend of PLA with poly[(butylene

succinate)-co-adipate] (PBSA) and nanoclay was studied by Eslami and Kamal [14]. They used different PLA/PBSA ratios at a single clay concentration (3 wt.%) and investigated the rheological properties with a particular interest on elongational flow behavior. Blends with PBSA content higher than 25 wt. % exhibited distinct strain hardening behavior. Oscillatory shear experiments showed that above 50 wt. % PBSA, strong solid-like behavior is exhibited due to the large amounts of clay platelets located at the PLA/PBSA interface resulting in polymer–particle and particle–particle network-like structures.

There has been a considerable interest on PLA blends and nanocomposites. Their rheological behaviors have also been studied in some cases since it provides valuable information about the nanocomposite structure and the processibility of the final product. Majority of the studies concerning the rheology of PLA based binary or ternary organoclay nanocomposites investigated the effect of either nano-filler content or blending ratio. Studies concerning the effects of modifier structure are limited and all are focused on the morphology based on X-ray diffraction (XRD) patterns and thermal properties. Krikorian and Pochan [15] studied the effects of modifier miscibility and the extent of clay modification on overall nanocomposite formation with three commercial organophilic clay types (Cloisites 15A, 25A and 30B) using solution-intercalation film-casting method. Based on morphological studies, they claim that the degree of miscibility of the organic modifier and the PLLA is the key factor for good dispersion of the filler. Findings from both quantitative and qualitative analyses were supported with theoretical solubility parameters computations, and Cloisite 30B was selected as the most suitable organoclay for good dispersion and exfoliation due the enthalpic interaction between the diols in its modifier structure with the C=O bonds in the PLLA backbone. Pluta et al. [16] studied three different modified clays (Cloisites 20A, 25A and 30B) with poly(ethylene glycol) (PEG) plasticized PLA by considering the effects of the filler concentration, the nature of clay modifier and the effects of plasticization. The intercalation of silicate layers were shown to depend on the structure of organic modification. Among the three organoclays, C30B is more prone to get intercalate than the other types. Higher interaction of PLA with C30B was explained by

hydrogen-bonding between the carbonyl group in the main chain of PLA molecules and the hydroxyl group in the organic modifier of C30B [11].

Fabrication of Polymer/Graphite Nanocomposites

Carbonaceous nanofillers are also popular to be use with bio-based polymers. Especially carbon nanotubes and graphene sheets exhibit unique electrical, mechanical and thermal properties which make them attractive fillers for reinforcing polymers to form functional and structural composite materials [108]. In this study, expanded graphite (EG) is used as a filler to improve properties of PLA. EG is an industrial term for exfoliated graphite obtained from sulfuric acid-based graphite intercalation compound precursor [108].

As in the case of all other nanofillers, the main difficulty in manufacturing polymer/graphite nanocomposites is the dispersion and distribution of the fillers in the polymer matrix. Most of the studies published in the literature investigate effective distribution of these graphitic fillers in various polymer matrices. Three conventional techniques are mainly employed to provide good dispersion and distribution. These are in situ polymerization, solution compounding and melt blending.

In situ polymerization and solution mixing together with ultrasonication are reported to be effective in providing good dispersion and intercalation for a number of polymers such as poly(methyl methacrylate) (PMMA), poly(arylene disulfide), silicone rubber (SR) and Nafion [109, 110, 111, 112]. These two methods also appear to be adequate to process thermosetting polymer/GNP nanocomposites [113]. Particularly, the production of composites containing thermosetting polymers as matrix and GNPs as filler starts with dispersing GNPs in liquid monomers of the polymer via solution mixing. This is followed by in situ polymerization. However, in a recent review it was reported that these two methods face a number of important problems. First, hazardous chemicals are involved, second, these approaches are not suitable for industrial applications [10]. These two important hitches reveal the fact that there is a big demand for production methods based on melt mixing. In both of

the recent reviews on graphite based nanocomposites, it is indicated that the melt mixing is not enough for good dispersion and final material properties of the nanocomposite containing GNP [10, 40]. As a result, different melt blending methods with some alterations have been developed. These alterations generally involve two steps, first of which can be said to be the premixing step followed by the melt mixing. The mixing procedure before melt compounding can be either in solution, melt, and solid states. For example, Drzal et al. [43] developed a novel coating approach, in which, before melt compounding polypropylene (PP) powder and graphitic fillers are premixed in an alcohol solution with the help of sonication. It was reported that composites produced by this new technique had improved flexural properties compared to those produced by direct melt mixing. Improved electrical conductivity is another promising result obtained by the coating approach when compared to the solution method.

Another approach to provide good dispersion is the masterbatch filling technique. In this method, polymer masterbatch containing high amounts of nano scale graphitic fillers (70-80 wt. %) was prepared by dissolving acrylonitrile-styrene copolymer (AS) resin in 2-butanone at room temperature. After the addition of GNPs, the mixture was sonicated to form a homogeneous dispersion of graphite particles in AS solution. Aqueous alcoholic solution was added to precipitate the graphite particles coated with AS resin. Then, this precipitate is filtered and dried, and designated as the masterbatch which is then diluted in the polymer matrix by extrusion. High density polyethylene (HDPE)/GNP composites and acrylonitrile-styrene copolymer composites have been successfully produced with this approach [114].

Mechanical mixing is another premixing step reported in the literature. Solid-state shear pulverization (SSSP) has been shown to be a successful method to use with graphite-polymer nanocomposites [44]. Manually blended polypropylene (PP) and graphite mixture were co-pulverized in a continuously cooled pulverizer with a very similar configuration as a twin-screw extruder, but using specially designed screws to yield moderately harsh shear/compression conditions. The resulting powder is a homogeneous mixture of the polymer and the filler. The properties of the resultant nanocomposites were compared with the composite having the same filler content

fabricated via single-screw melt extrusion. Compression molded samples produced with SSSP showed superior tensile, impact and crystallization properties. Exfoliation of the graphite nanosheets were also proven via X-ray diffraction and transmission electron microscopy analysis.

In addition to the conventional techniques summarized above, surface modification of nanofillers can be used to provide better interaction between the polymer matrix and nanofillers. Surface modifications of GNPs usually result in oxidization, so that some hydroxyl moieties, epoxide functionalities, and carbonyl groups are attached to GNPs. These functional groups are able to form strong interactions with polymeric resins with polar groups, and they also provide sites for further modifications. Some of the chemicals used for GNP surface modifications of used in literature are octadecylamine (ODA) [109], maleated ethylene-propylene copolymer (EP-g-MA) [115], and PP-g-MAH [116]. The basis of modification of the surface based on the oxidized graphite. This usually results in poor physical properties because of the transformation from sp^2 to sp^3 carbons during acid oxidization. Sp^2 configuration is responsible for the electrical conductivity. Therefore, surface modifications cause a decrease in electrical conductivity. Meng et al. [117] suggested a new attitude to sustain the electrical conductivity property of nanocomposites produced with GNPs, by first producing GNP oxide nanocomposites. After that reducing the oxides via heat treatment under vacuum at 200°C. As a result, the electrical conductivity revealed a considerable increase from 10^{-7} S/cm to 0.51 S/cm.

PLA-Expanded Graphite Nanocomposites

There are some studies which employ EG as a reinforcement for PLA. Kim and Jeong [118] produced polylactide/exfoliated graphite (PLA/EG) nanocomposites by melt-compounding and investigated their morphology, structure, thermal stability, mechanical, and electrical properties. It was reported that EG was dispersed homogeneously in the PLA matrix without forming crystalline aggregates, unlike natural graphite. Thermal degradation temperatures of PLA/EG nanocomposites increased substantially with the EG content up to 3 wt. %. Mechanical properties

were also enhanced such that Young's moduli of PLA/EG nanocomposites increased noticeably with the EG content up to again 3 wt. %.

In another study, again melt compounding was used for the preparation of PLA based nanocomposites expanded graphite and organically modified montmorillonites [119]. It was reported that the addition and co-addition of these nanofillers to PLA result in nanocomposites that showed significant enhancements in rigidity, thermal stability and fire retardancy of the polymer matrix. For example in thermal analyses, it was observed that EG particles significantly accelerated the crystallization process of the PLA matrix. The synergistic effect of using both fillers were emphasized such that the Young's modulus and the tensile strength of PLA/EG/Clay nanocomposites were improved significantly compared to PLA/EG composites.

There are other studies investigating the synergistic effects of different fillers incorporated into PLA matrix. Zhu et al. [120] studied the expanded graphite (EG) and ammonium polyphosphate (APP) on flame retarded polylactide (PLA). Han et al. [121] studied the potential synergy between nanomaterials such as exfoliated graphite nanoplatelets (xGnP) and micro-size reinforcements such as kenaf natural fibers, in poly(lactic acid) based composites produced via melt compounding. Prior to melt-mixing the kenaf fibers were coated with xGnP using sonication. Morphological analyses revealed that the interfaces in ternary systems were void free and the reinforcement wetting by the polymer was better compared to PLA composites where only one reinforcement was used at a time. Dynamic viscosity of PLA was significantly altered upon addition of kenaf fibers with the viscosity increasing by three orders of magnitude for the highest loading of 40 wt. % fiber content. Furthermore, addition of xGnP up to 3 wt. % to neat PLA did not alter these properties. However, when both xGnP and kenaf fibers were added to PLA, the viscosity was lower compare to the viscosity of kenaf fiber-PLA composites. This result was explained such that xGnP promotes better dispersion of the kenaf fibers and the higher amount of xGnP contributes to good adhesion between kenaf fiber and the polymer matrix. Tait et al. [11] studied vapor grown carbon nanofibers and exfoliated graphite to prepare poly(lactic acid) composites at various concentrations varying from 0 to 20 wt. %. The synergistic effect of the two fillers were also

investigated, but differently two compounding processes, melt mixing and polymer dissolution, and two forming methods, injection and compression molding, were used to manufacture the composites. Various properties such as flexural behavior, impact strength, storage and loss modulus, and electrical conductivity of the neat matrix and composites were determined as a function of the filler type and content, and the processing method. It is reported that compounding by solution mixing followed by compression molding leads to composites with the lowest percolation threshold in terms of electrical conductivity and highest storage modulus, whereas extrusion injection molding results in composites with the highest mechanical properties. For example, exfoliated graphite improves the impact energy for all loadings with the largest increase in strength, by more than 65%, for 8 and 10 wt. % loadings. It is claimed that upon further addition of filler, homogeneous dispersion becomes challenging and filler agglomeration is unavoidable leading to decrease in impact energy.

CHAPTER 3

EXPERIMENTAL METHODS

3.1. Materials

3.1.1 Polymer Matrix

A transparent, injection grade of PLA with 5 % D-lactide stereoisomer content, weight average molecular weight (M_w) of 278000 and polydispersity (M_w/M_n) of 1.78 was purchased from NaturePlast, France. The properties of PLA provided by the manufacturer are listed below in Table 3.1, and the chemical formula of PLA is shown in Figure 3.1.

Table 3.1 Properties of PLA (NaturePlast PLI-005) [122]

Physical Properties	Method	Unit	Value
Density	ISO 1183	g/cm ³	1.25 (± 0.05)
Melt Index	ISO 1133	g/10 min	10-30
Melt Temperature	-	°C	144-155
Degradation Temperature	-	°C	240-250

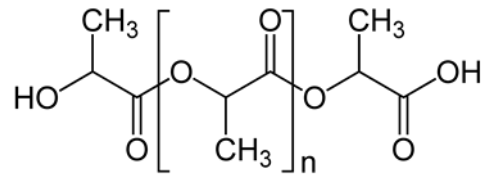


Figure 3.1 Chemical structure of PLA

3.1.2 Compatibilizers

A random copolymer of ethylene (E) and glycidyl methacrylate (GMA) with a trade name of Lotader® AX8840, and a terpolymer of ethylene (E) butyl acrylate (BA) and maleic anhydride (MAH) with a trade name of Lotader 2210 were used (Arkema Chemicals, France) as compatibilizers, which also act as impact modifiers. The chemical structure of Lotader® AX8840 and its properties are given in Table 3.2 and Figure 3.2, respectively.

Table 3.2 Properties of the impact modifier Lotader® AX8840 (E-GMA) [123]

Property	Unit	Value
GMA Content	% wt.	8
Melt Index	g/10 min	5
Melting Point	°C	105
Tensile Strength	MPa	8
Young's Modulus	MPa	104
Elongation at Break	%	420
Density	g/cm ³	0.94
Hardness	Shore D	92

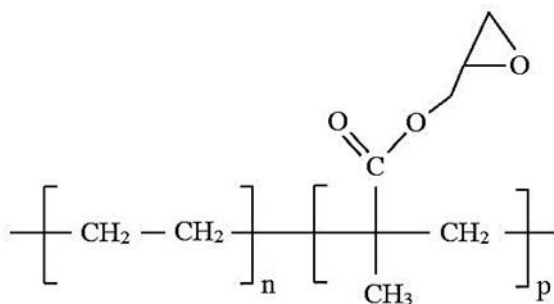


Figure 3.2 Chemical structure of Lotader® AX8840

The chemical structure of Lotader® 2210 and its properties are given in Table 3.3 and Figure 3.3, respectively.

Table 3.3 Properties of the impact modifier Lotader® 2210 (E-BA-MAH) [123]

Property	Unit	Value
MAH Content	% wt.	2.6
BA Content	% wt.	8
Melt Index	g/10 min	3
Melting Point	°C	107
Tensile Strength	MPa	12
Elongation at Break	%	600
Hardness	Shore D	46

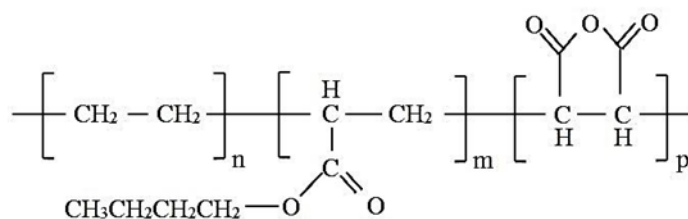


Figure 3.3 Chemical structure of Lotader® 2210

3.1.3 Fillers

Two different filler types were used in this study: organically modified clays and expanded graphite.

3.1.3.1 Organoclays

Five different natural montmorillonites: Cloisites®15A (C15A), 25A (C25A) and 30B (C30B), and Nanofils®5 and Nanofils®8 (N5 and N8) modified with various quaternary ammonium salts were purchased from Southern Clay Products, TX. They are natural off-white montmorillonites modified with quaternary ammonium salts and they were used as additives for improving various physical properties like reinforcement, heat distortion temperature and barrier effects.

Cloisites®

Three different types of Cloisites® were used in this study. Organic modifier of Cloisite®15A contains dimethyl, dihydrogenated tallow, quaternary ammonium cation with chloride anion where hydrogenated tallow is predominantly composed of chains with 18 carbons (~65 %), to a lesser degree chains with 16 carbons (~30 %) and 14 carbons (~5 %). The chemical structure of the organic modifier can be seen in Figure 3.4.

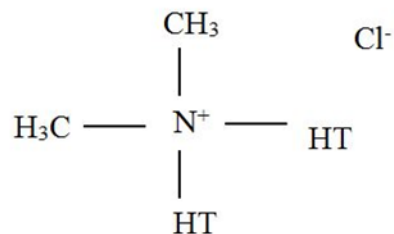


Figure 3.4 Chemical structure of organic modifier of Cloisite®15A

Dimethyl, dehydrogenated tallow, 2-ethylhexyl quaternary ammonium cation (2MHTL8) with methyl sulfate anion constitutes the chemical structure of the organic modifier of Cloisite®25A, where hydrogenated tallow contains chains mostly with 18 carbons (~65%), to a lesser degree chains with 16 carbons (~30%) and 14 carbons (~5%). Chemical structure of the organic modifier of Cloisite® 25A can be seen from Figure 3.5.

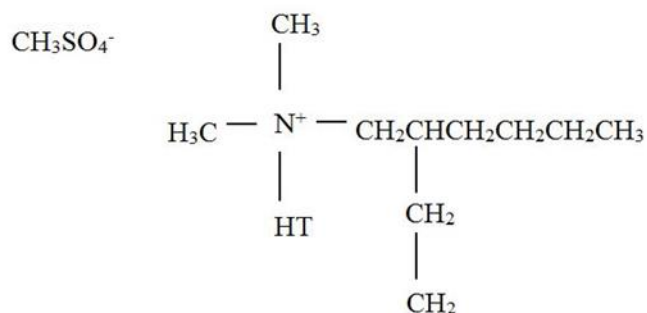


Figure 3.5 Chemical structure of organic modifier of Cloisite®25A

Quaternary ammonium salt cation and anion of the organic modifier of Cloisite®30B are methyl, tallow, bis-2-hydroxyethyl quaternary ammonium (MT2EtOH) and chloride, respectively. Almost 65% of the carbon chains have 18 carbons, 30% has 16 carbons and 5% has 14 carbons in the tallow structure.

Chemical structure of the organic modifier of Cloisite®30B can be seen from Figure 3.6. Properties of Cloisites® are summarized in Table 3.4.

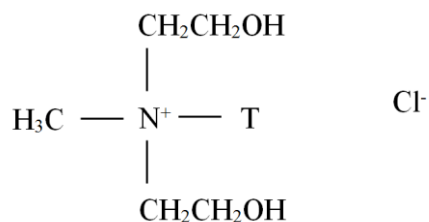


Figure 3.6 Chemical structure of organic modifier of Cloisite®30B

Table 3.4 Properties of Cloisites® [124]

Property	Cloisite®15A	Cloisite®25A	Cloisite®30B
Modifier concentration (CEC meq/100g clay)	125	95	90
Moisture (%)	<2	<2	<2
Weight loss by ignition (%)	43	34	30
d-spacing (Å)	31.5	18.6	18.5
Color	Off white	Off white	Off white
Specific gravity (g/cc)	1.66	1.87	1.98
Loose bulk density (Ibs/ft ³)	10.79	12.08	14.25
Packed bulk density (Ibs/ft ³)	18.64	20.48	22.71
Dry particle size (μ, by volume)	10% < 2 50% < 6 90% < 13	10% < 2 50% < 6 90% < 13	10% < 2 50% < 6 90% < 13

Nanofil®

Two different types of Nanofil® were used in this study. Properties of Nanofil® 5 and Nanofil®8 are given in Table 3.5. Chemical structures of the organic modifiers of these bentonite based clays are typically the same as Cloisite®15A. The main difference between Nanofil®5 and Nanofil®8 are the modifier contents and d-spacing values.

Table 3.5 Properties of Nanofil® [124]

Property	Nanofil®5	Nanofil®8
Modifier concentration (CEC meq/100g clay)	93	125
Moisture (%)	1.3	1.6
Weight loss by ignition (%)	38	43
d-spacing (Å)	28	35
Bulk density (g/l)	270	270
Dry particle size (μ , by volume), 50%	8	5

3.1.3.2 Expanded Graphite

Graphite was provided by TIMCAL with the trade name of Timrex® C-Therm 001. It is a type of expanded graphite (EG), but the manufacturer classifies it as confidential, therefore there is not much data about the properties of this specific product. It is reported to impart superior effects on thermal and electrical properties of the composite. Properties provided by the supplier are shown in Table 3.6.

Table 3.6 Properties of Timrex® C-Therm 001 [125]

Property	Unit	Value
Ash Content	% wt.	0.3
Scott Density (bulk density)	g/cm^3	0.15

3.2. Nanocomposite Preparation

In this study, PLA composites containing organically modified clays as fillers were prepared by melt compounding method only. For the composites containing expanded graphite as filler, two different production methods were compared, which are melt compounding and solution mixing. Solution mixing can also be referred as solvent assisted ultrasonication. Before each method, all raw materials were dried overnight under vacuum (0.2 bar) at 80-85°C.

3.2.1. Melt Compounding

PLA based nanocomposites were prepared by melt blending in a co-rotating, intermeshing Thermoprism TSE 16 TC twin screw extruder (L = 384 mm, D = 16 mm). Figure 3.7 shows a picture of the extruder used in this study. Regardless of the filler type, the feed rate was kept at 25 g/min and the temperature profile in the barrel was set to 150-170-170-170-170°C from the main hopper to the die. For the composites containing organoclays, the screw speed was 250 rpm, whereas it was 100 rpm for the ones containing EG.



Figure 3.7 Thermoprism TSE 16 TC twin screw extruder

After the extrusion step, the extrudate was cooled on a specially designed cooling band with a length of 120 cm which is carrying the extrudate with the help of a frequency control drive. Cooling process was accelerated using a compressor blowing air on to the band. Cooled strips of polymer composites were pelletized in a grinder. The pellets obtained at the end of the process were stored in polyethylene bags in desiccators. Before all molding and/or characterization processes, the composites were dried overnight under vacuum at 80-85°C. Schematic representation of melt compounding from the first drying step up to characterizations can be seen in Figure 3.8.

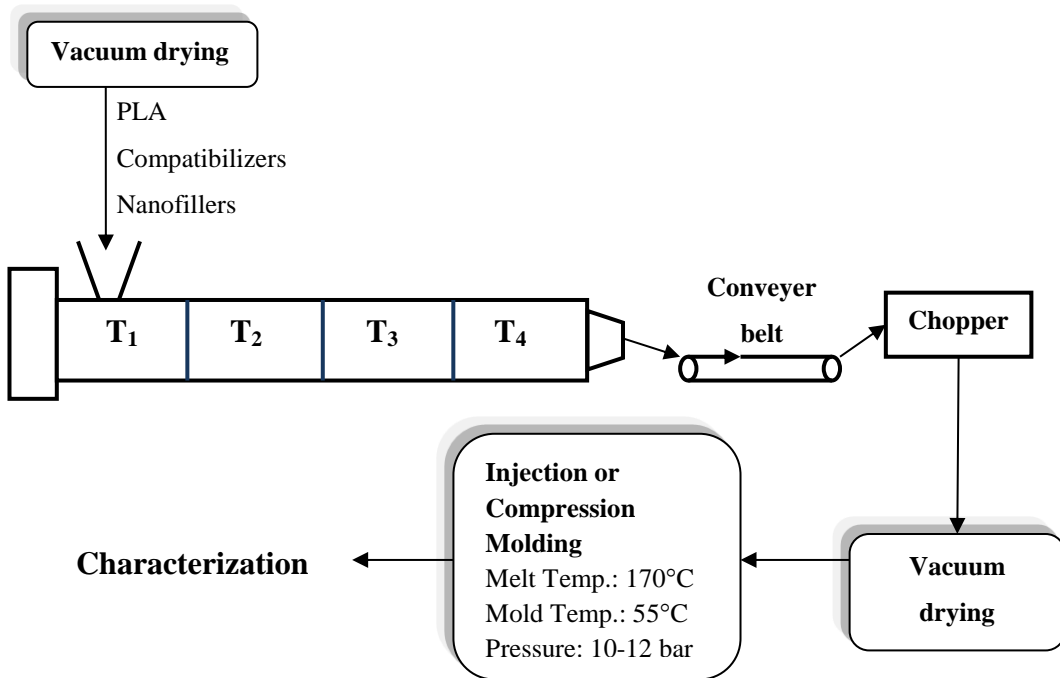


Figure 3.8 Preparation of nanocomposites through melt blending method

3.2.2. Solution Mixing

Solution mixing method was used only for the samples containing EG as filler. This process can also be referred to as “solvent assisted ultrasonication”. In this process, PLA was dissolved in xylene (0.2 g/ml) in a glass reactor with the help of a mechanical stirrer at 800 rpm and 95°C. Total dissolving took 3 hours. In the

meantime, EG was dissolved in xylene (0.01 g/ml) with the help of ultrasonication at 45°C for one and a half hour. At the end of the third hour of PLA dissolution, the sonicated EG/xylene solution was added dropwise into the PLA/xylene solution and this mixture was also mechanically mixed for one hour. Then the mixture is transferred to the ultrasonic water bath and the whole solution was further mechanically mixed for 3 hours assisted by sonication at 80°C. In some of the experiments, compatibilizer was also added to the solution. In that case, the compatibilizer (0.1 g/ml in Xylene) ultrasonicated for one hour at 80°C was added to the reactor just before the transfer of the reactor to the ultrasonic bath. At the end of the solution mixing process, the jelly mixture was poured on aluminum trays and left for drying under the hood at least for 7-8 days. Before further processing, the solution mixed nanocomposites were further dried in vacuum oven for 2-3 days. A simple schematic representation of nanocomposite preparation with solution mixing method can be seen in Figure 3.9.

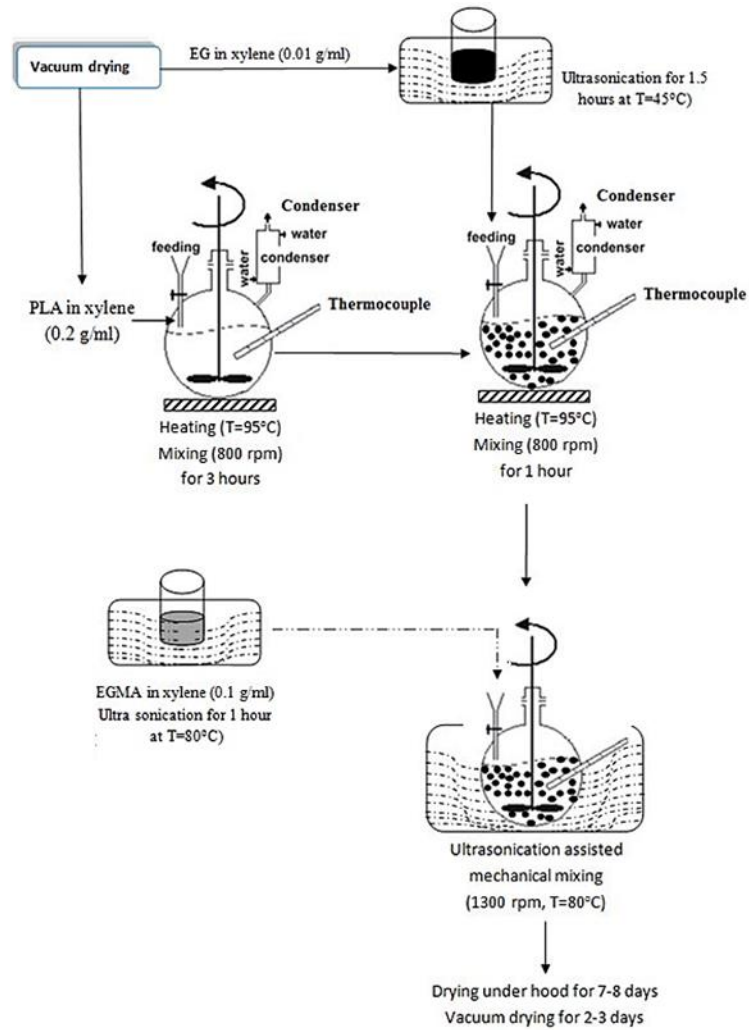


Figure 3.9 Preparation of PLA nanocomposites through solution mixing method

3.2.3. Composite Compositions

The experiments conducted throughout this study are based on PLA as the polymer matrix but they can be basically divided into two sections. A flowchart of the study can be seen in Figure 3.10.

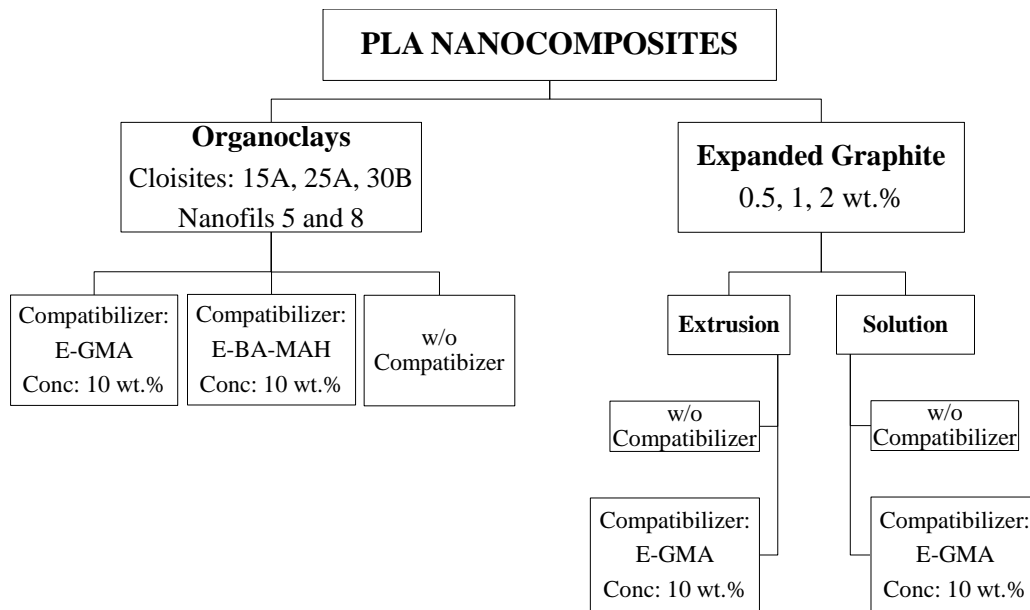


Figure 3.10 Flowchart of the study

The compositions and codes of the experiments done to investigate the effects of compatibilizer and organoclay types on PLA matrix are shown in Table 3.7. Not only ternary nanocomposites of PLA/compatibilizer/organoclay, but also binary nanocomposites of PLA/organoclay and PLA/compatibilizer blends were prepared with the same process conditions in order to compare their properties with the properties of the ternary nanocomposites. Except for the PLA analyzed as received, all compositions were prepared via melt blending at 170°C with 250 rpm screw speed.

Table 3.7 Sample compositions prepared to investigate the effects of organoclays and compatibilizers

Code	Method	Composition	PLA (wt.%)	Compatibilizer (wt.%)	Filler (wt.%)
A-00	AR*	PLA	100	-	-
A-01	Extrusion	PLA	100	-	-
A-02	Extrusion	PLA/E-GMA	90	10	-
A-03	Extrusion	PLA/E-BA-MAH	90	10	-
A-1	Extrusion	PLA/E-GMA/C15A	88	10	2
A-2	Extrusion	PLA/E-GMA/C25A	88	10	2
A-3	Extrusion	PLA/E-GMA/C30B	88	10	2
A-4	Extrusion	PLA/E-GMA/N5	88	10	2
A-5	Extrusion	PLA/E-GMA/N8	88	10	2
B-1	Extrusion	PLA/E-BA-MAH/C15A	88	10	2
B-2	Extrusion	PLA/E-BA-MAH/C25A	88	10	2
B-3	Extrusion	PLA/E-BA-MAH/C30B	88	10	2
B-4	Extrusion	PLA/E-BA-MAH/N5	88	10	2
B-5	Extrusion	PLA/E-BA-MAH/N8	88	10	2
C-1	Extrusion	PLA/C15A	98	0	2
C-2	Extrusion	PLA/C25A	98	0	2
C-3	Extrusion	PLA/C30B	98	0	2
C-4	Extrusion	PLA/N5	98	0	2
C-5	Extrusion	PLA/N8	98	0	2

*AR= As received

In the second part of the study, the filler used to modify properties of PLA was expanded graphite. Apart from the former experiments conducted with organoclays, two different production methods were applied to PLA/EG composites. In this part of the study, only one compatibilizer which resulted in promising results with organoclays was used, which is E-GMA. The codes and compositions of the experiments conducted with EG are tabulated in Table 3.8, below. For the

compositions prepared via extrusion, the temperature was 170°C and the screw speed was 100 rpm.

Table 3.8 Sample compositions prepared to investigate the effects of different production methods for PLA/EG composites

Code	Method	Composition	PLA (wt.%)	Compatibilizer (wt.%)	EG (wt.%)
E-0	Extrusion	PLA	100	-	-
E-1	Extrusion	PLA/EG	99.5	-	0.5
E-2	Extrusion	PLA/EG	99	-	1
E-3	Extrusion	PLA/EG	98	-	2
E-4	Extrusion	PLA/E-GMA	90	10	-
E-5	Extrusion	PLA/E-GMA/EG	89.5	10	0.5
E-6	Extrusion	PLA/E-GMA/EG	89	10	1
E-7	Extrusion	PLA/E-GMA/EG	88	10	2
S-1	Solution	PLA/EG	99.5	-	0.5
S-2	Solution	PLA/EG	99	-	1
S-3	Solution	PLA/EG	98	-	2
S-4	Solution	PLA/E-GMA	90	10	-
S-5	Solution	PLA/E-GMA/EG	89.5	10	0.5
S-6	Solution	PLA/E-GMA/EG	89	10	1
S-7	Solution	PLA/E-GMA/EG	88	10	2

3.2.4. Sample Preparation

For most of the characterization studies such as mechanical, thermal and morphological analyses, injection molded samples were used. For rheological analyses, compression molded samples were used.

3.2.4.1 Injection Molding

The injection molded samples were prepared using a laboratory scale injection-molding machine, DSM Micro 10 cc Injection Molding Machine, shown in Figure 3.11. During molding; barrel and mold temperatures were 170°C and 55°C, respectively. The maximum pressure achieved during sample preparation was 12 bars.



Figure 3.11 A photograph of injection molding device

Before molding the samples, the pellets were put into the barrel cylinder with the help of a funnel. After waiting for five minutes for the material to melt, the melt was injected into the mold. In each molding operation, two specimens were obtained, one of which had the shape of a dog-bone, whereas the other one was the sample of the impact test with rectangular shape.

3.2.4.2 Compression Molding

A laboratory size compression molding device which can be seen in Figure 3.12 was used to prepare samples for rheological analyses. Processing temperature was adjusted as 180°C. During compression molding the challenge was to eliminate the bubbles in the samples. To achieve samples without any bubbles, the mold was filled with samples and preheated for 5 minutes without any pressure. After that a small amount of pellets was added on to the molten material to provide positive pressure which would push the small amount of air or moisture trapped in the material. After

waiting for another 5 minutes to ensure that all the material in the mold was totally molten, the pressure was increased gradually to 2500 psi and kept there for 5 minutes. Compression molded samples were cooled down to room temperature before removing from the mold.



Figure 3.12 A photograph of the compression molding device

3.3. Characterization of Nanocomposites

In order to investigate the effects of the compatibilizers and fillers on the final properties of polymer matrix morphological, chemical, thermal, mechanical and rheological analyses were conducted on the samples. Morphology of the nanocomposites was investigated by XRD, SEM and TEM analyses. To investigate the reactive groups of polymer matrix and compatibilizers FTIR was done. Melting point and crystallinity of the nanocomposites were studied with DSC analysis. Mechanical behavior of the nanocomposites was evaluated by measuring tensile properties (tensile strength, Young's modulus, elongation at break). Impact toughness values of the samples were measured with Charpy impact test.

Rheological properties of the nanocomposites were investigated using oscillatory rheometer.

3.3.1. Analysis of Morphology

3.3.1.1 X-Ray Diffraction

X-ray diffraction (XRD) patterns of organoclays and nanocomposites were obtained by using Rigaku Ultima-IV X-Ray diffractometer (METU Central Laboratories) that generates a voltage of 40 kV and current 40 mA from Cu K α radiation source ($\lambda = 1.5418$). The diffraction angle 2θ was scanned from 1° to 10° with scanning rate of $1^\circ/\text{min}$ and a step size of 0.01° for PLA/organoclay nanocomposites. For PLA/EG compositions the scanned diffraction angle range was 1° to 40° and the scanning rate and step size were $1^\circ/\text{min}$ and 0.02° , respectively. To calculate the distance between the filler layers Bragg's equation was used as indicated in (2.5 in the previous chapter of this dissertation. X-Ray analysis of organoclays and graphite were done in powder form whereas injection molded tensile bars were used for nanocomposites.

3.3.1.2 Scanning Electron Microscopy

Scanning electron microscopy (SEM) analysis was performed with QUANTA 400F Field Emission SEM (METU Central Laboratories). In order to examine the failure mechanism and elastomer dispersion, the impact fracture surface of the nanocomposites were scanned. The elastomeric phase in binary blends and ternary nanocomposites was dissolved by using n-heptane as the solvent. The etching process was achieved at 60°C in an ultrasonic bath. The surfaces of the samples were kept in n-Heptane until deterioration occurred. SEM photographs of the impact-fractured surfaces were taken at x500 and x3000 magnifications.

3.3.1.3 Transmission Electron Microscopy

For TEM analysis ultra-thin sections of 120 nm in thickness were cryogenically cut with a diamond polymer knife at a temperature of -80°C for PLA/organoclay binary and PLA/elastomer/organoclay ternary nanocomposites and at -120°C for the PLA/EG binary and PLA/elastomer/EG nanocomposites. These samples were examined by a high-resolution transmission electron microscopy (FEI, Tecnai G2 F30) at an acceleration rate of 300 kV in UNAM Laboratories at Bilkent University. All samples were trimmed perpendicular to the molding direction.

3.3.2 Spectroscopic Analysis

3.3.2.1 Fourier Transform Infrared Spectroscopy

FTIR which stands for Fourier Transform InfraRed spectroscopy was used to investigate PLA-compatibilizer interactions. FTIR analyses of the nanocomposites were performed in METU Chemical Engineering Department on attenuated total reflectance (ATR) mode. No preliminary treatments were done on the samples cut from injection molded samples.

3.3.3 Thermal Analysis

3.3.3.1 Differential Scanning Calorimetry

Differential scanning calorimetry analysis was performed by using a differential scanning calorimeter DSC-60 Shimadzu in METU-Chemical Engineering Department. Measurements were carried out in the temperature range of 30°C to 200°C with a heating rate of 10°C/min under nitrogen atmosphere. Cold crystallization and melting points of the samples and the degree of crystallinity were determined with these analyses. ΔH_m^o value of 100% crystal PLA structure was taken as 93 J/g [97] in the calculations.

For the elastomers used as compatibilizer DSC 8000 in METU-Central Laboratory was used since lower temperatures should be scanned.

3.3.4 Mechanical Tests

Tensile and impact tests were conducted at room temperature and the properties were obtained on at least five samples to calculate the standard deviation.

3.3.4.1 Tensile Test

Tensile tests were performed at room temperature according to ISO 527 with Shimadzu AG-IS 100 kN test machine at METU-Chemical Engineering Department (Figure 3.13). Crosshead speed and strain rate were 3 mm/min and 0.1 min⁻¹, respectively.



Figure 3.13 A photograph of the tensile testing machine

Dog-bone type injection molded samples were used for tensile testing. The shape of the specimen was shown in Figure 2.25 and its dimensions can be seen in Table 3.9, below.

Table 3.9 Tensile test specimen dimensions according to ISO 527-2 Standards

Type of Specimen	5A
Overall length, minimum, l_2	≥ 75
Width at ends, b_2	12.5 ± 1
Length of narrow parallel sided portion, l_1	25 ± 1
Width of narrow parallel sided portion, b_1	4 ± 0.1
Small radius, r_1	8 ± 0.5
Large radius, r_2	12.5 ± 1
Initial distance between the grips, L	50 ± 2
Gauge length, L_0	20 ± 0.5
Thickness, h	≥ 2

3.3.4.2 Impact Test

Ceast Resil Impactor was used to perform the un-notched charpy impact test on samples with dimensions of 80x10x4 mm according to ISO 179. Its configuration is shown in Figure 3.14. All of the tests were performed at room temperature and the results are the averages of five tests carried out for all the compositions.



Figure 3.14 A photograph of the impact testing machine

3.3.5 Rheological Analysis (UMass-Lowell)

Linear viscoelastic behavior of PLA nanocomposites were analyzed by a dynamic oscillatory rheometer in the melt state as a function of time, strain and frequency. The Ares G2 Rheometer (Figure 3.15) was used in conjunction with 25 mm parallel disk fixtures for the small-amplitude oscillatory shear experiments.

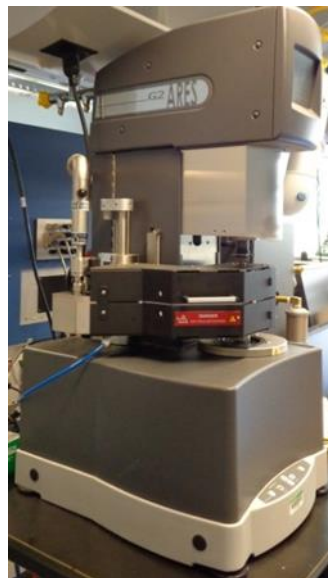


Figure 3.15 A photograph of Ares G2 Rheometer

All measurements were performed at 170°C and 10 rad/s. The gap height was set at 1.5 mm. For the selected representative samples, analyses were started with time sweep to determine the melt stability of the samples. Then an amplitude sweep between 0.1-100% strain at 10 rad/s was done to determine the linear viscoelastic region. After that frequency sweep was done between 0.1-500 rad/s at 5% strain to ensure that the experiments were conducted in the linear viscoelastic region.

As a result of the experiments, elastic moduli (G'), loss moduli (G'') and complex viscosity (η^*) were obtained. G' is called as the elastic (storage) modulus and represents the stored elastic energy. G'' is called as the loss modulus and represents the amount of energy irreversibly given off by the substance to the environment.

All rheological analyses and sample preparations for these analyses were done in University of Massachusetts Lowell.

CHAPTER 4

RESULTS AND DISCUSSION

This dissertation is based on production of PLA nanocomposites with improved mechanical properties compared to brittle neat PLA. Two different road maps were followed to achieve this aim. In the first one, organically modified clays were utilized together with thermoplastic elastomers as compatibilizers. Conventional twin-screw extrusion was used as the production method. In the second roadmap, as an alternative to the organically modified clays, expanded graphite was used as the nanofiller. The effects of different production methods on the dispersion of expanded graphite (EG) in the polymer matrix were investigated via extrusion and solution mixing techniques. Results of these two different parts of the study will be presented in different sections.

4.1. PLA/Layered Silicate Nanocomposites

The main idea behind this part of the study is to increase the potential applications of PLA by incorporating epoxy or maleic anhydride functionalities together with nanoclays to improve toughness. Mostly, the properties of the polymer nanocomposites are sensitive to small changes in the polymer structure. Even very low filler loadings can change the total mechanical, thermal and viscoelastic behavior, and morphology of the system. In this context, five different organically modified commercial nanoclays were used as nanofillers. In addition to that,

presence of an elastomeric phase which acts as a compatibilizer was investigated. For this purpose, two different commercial elastomers with different functional groups (E-GMA and E-BA-MAH) were selected. Both the clay and the compatibilizer contents were kept constant in order to observe the changes in the properties of the nanocomposites with changes in the structures of the additives.

4.1.1 Determination of Processing Parameters

PLA/clay nanocomposites were prepared via extrusion method. Suitable melt temperatures and screw speeds were scanned before production of the nanocomposites. Temperature and screw speed of the extruder are two important parameters for PLA processing, since PLA is susceptible to degradation at high temperature and shear. For this purpose, the most commonly used organically modified clay type in literature, C30B, was used as the filler. Dispersion of this clay was investigated by XRD and the changes in the mechanical properties with varying processing conditions were observed.

4.1.1.1 Dispersion of Clay

PLA/E-GMA/C30B nanocomposites were produced at three different temperatures (160-170-180°C) and screw speeds (150-250-350 rpm) at pre-determined concentrations of 88/10/2, respectively. Residence time of the polymer melt in the extruder and the shear applied by the screws depend on the screw speed applied in composite preparation. Processing temperature affects mainly the viscosity of the polymer melt. Low processing temperatures might result in poor fusion preventing uniform fluidity. High temperatures, on the other hand, decreases the melt viscosity, and the shear needed to force polymer chains to penetrate into the layers of silicates might not be sufficient. However, considering the XRD patterns, the clay dispersibility was not affected either by the screw speed or the melt temperature in the investigated ranges (Figure 4.1). For all processing conditions, the single peak observed for pure C30B ($2\theta \approx 5.1^\circ$) showing a basal spacing of 17.3 Å turned into two peaks, one of which was shifted towards a lower angle ($2\theta \approx 2.7^\circ$) indicating

intercalation with a gallery spacing of about 32.7 Å. This was accompanied with a second peak ($2\theta \approx 5.5^\circ$) which might be the reflection from the second layer (32.0 Å) or due to some unintercalated and/or agglomerated clay (16.0 Å). Similar results were obtained in the literature with the same clay type [99, 105].

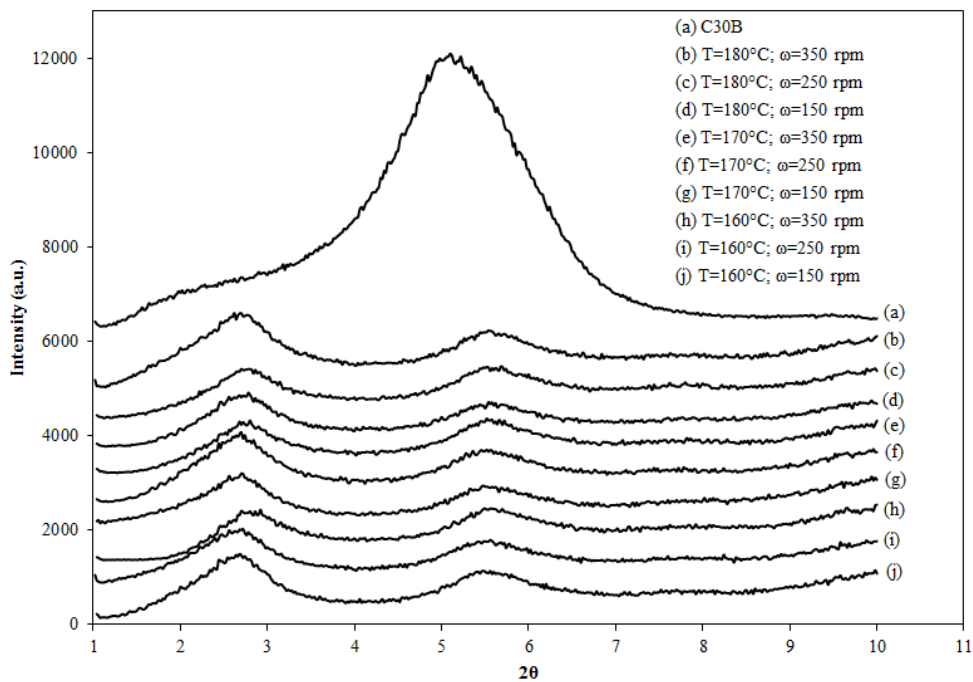


Figure 4.1 XRD patterns at different processing conditions

4.1.1.2 Mechanical Properties

Besides clay dispersibility, changes in mechanical properties of the selected nanocomposite type with respect to changing processing conditions were investigated. As mentioned before, PLA is susceptible to both temperature and shear. Harsh processing conditions and moisture may cause chain scission or degradation. Thus, properties of the final product might be significantly affected from the processing parameters.

In the scanned ranges, none of the mechanical properties showed a certain pattern with temperature and screw speed as can be seen in Table 4.1. In fact, tensile

strength and elongation at break values showed fluctuations independent of the processing parameters. Young's modulus, on the other hand, remained almost the same for all the sets reaching its maximum value as 1296 MPa for T=170°C and $\omega=250$ rpm. Impact strength of the nanocomposites decreased slightly as the temperature and screw speed increase.

It was decided to use the mean values of the scanned range in further investigations (T=170°C and $\omega=250$ rpm). This is not a naive selection, since the mechanical properties of the nanocomposites for these processing parameters are considerably above the mean values obtained in the scanned range. At first sight, tensile strength, Young's modulus and elongation at break values of this set might be considered as outliers among the nanocomposites produced at the same temperature but it should be noted that these properties were determined by testing at least 5 different specimens from the same batch.

Table 4.1 Mechanical properties of PLA/E-GMA/C30B (88/10/2) nanocomposites at different processing conditions

Temperature	Screw Speed	Tensile Strength (MPa)	Young's Modulus (MPa)	Elongation at Break (%)	Impact Strength (kJ/m ²)
160°C	150 rpm	45.1±0.9	1284±15	23.8±4.3	18.8±0.4
	250 rpm	45.5±1.8	1258±17	16.6±3.2	18.6±0.5
	350 rpm	29.9±1.9	1230±12	24.2±1.5	18.7±0.7
170°C	150 rpm	28.7±1.8	1224±18	14.5±2.6	19.3±0.9
	250 rpm	44.9±0.7	1296±10	21.8±7.0	18.5±0.9
	350 rpm	36.7±2.5	1269±9	17.1±2.9	17.7±0.8
180°C	150 rpm	33.3±2.6	1208±13	11.4±1.7	17.2±0.7
	250 rpm	33.7±1.7	1273±12	12.2±1.7	17.0±0.8
	350 rpm	33.2±0.6	1251±17	14.3±2.4	16.2±0.9

4.1.2 Effects of Clay Type and Compatibilizer Structure

4.1.2.1 Morphological Analyses

X-Ray Diffraction

X-ray diffraction patterns of the nanocomposites in the range of $2\theta = 1-10^\circ$ show the interlayer spacing (d) between the silicate layers of organoclays. Interlayer spacing is calculated using Bragg's law Equation (2.5). A shift in the peak to the left is indicative of an increase in the interlayer spacing of the silicate layers whereas disappearance of the characteristic peak indicates exfoliated structure [4].

Figure 4.2 to Figure 4.6 show the XRD patterns of binary and ternary nanocomposites together with neat PLA and the organoclay used in that particular set. Neat PLA does not show any reflection peaks in the scanned range. The basal spacing values of the organoclay powders are 33.1 Å, 18.3 Å, 18.1 Å, 34.2 Å, and 36.1 Å for C15A, C25A, C30B, N5 and N8, respectively. Under the same processing conditions, each type of nanoclay resulted in different degrees of layer expansion. It is known that the chemical compatibility between the polymer matrix and the nanoclay is the most important parameter determining the final morphology [126]. In this study, peak shifts are more apparent for the nanocomposites prepared with C25A (Figure 4.3) and C30B (Figure 4.4). Affinities of C25A and C30B to PLA were previously compared in the literature [100, 127], and C30B had shown to have more affinity to this polymer matrix. Changes in d -spacing values calculated from the XRD patterns obtained in this study are in accordance with the findings in the literature. PLA/C30B reached 37.1 Å gallery height, whereas it is 18.1 Å for pure C30B powder and PLA/C25A reached 31.9 Å, whereas C25A itself has a gallery height of 18.3 Å. Addition of the compatibilizer also resulted in changes in the peak positions especially when E-GMA was used. To illustrate, the peak showing basal spacing of 18.3 Å is shifted to 40.3 Å, and a second peak showing a basal spacing of 17.4 Å due to unintercalated clay appeared for PLA/E-GMA/C25A. On the other hand, the shift in the interlamellar space of PLA/E-BA-MAH/C25A is smaller (33.5 Å). Interestingly, the nanocomposites without a compatibilizer reached almost the

same interlamellar distances with the ones containing E-BA-MAH. This is probably due to better polarity matching between GMA as a functional group and the organic modifiers of C30B and C25A. Among the Cloisites®, C30B has the lowest hydrophobicity. C15A has the highest hydrophobicity which results in the lowest degree of intercalation according to the XRD patterns. In addition, XRD patterns of the nanocomposites containing C15A, N5 and N8 shown in Figure 4.2, Figure 4.5 and Figure 4.6 follow similar trends to each other. These three nanoclays contain modifiers of similar chemical structures and the changes in the gallery height of the nanocomposites containing either of these clay types are lower than the other two.

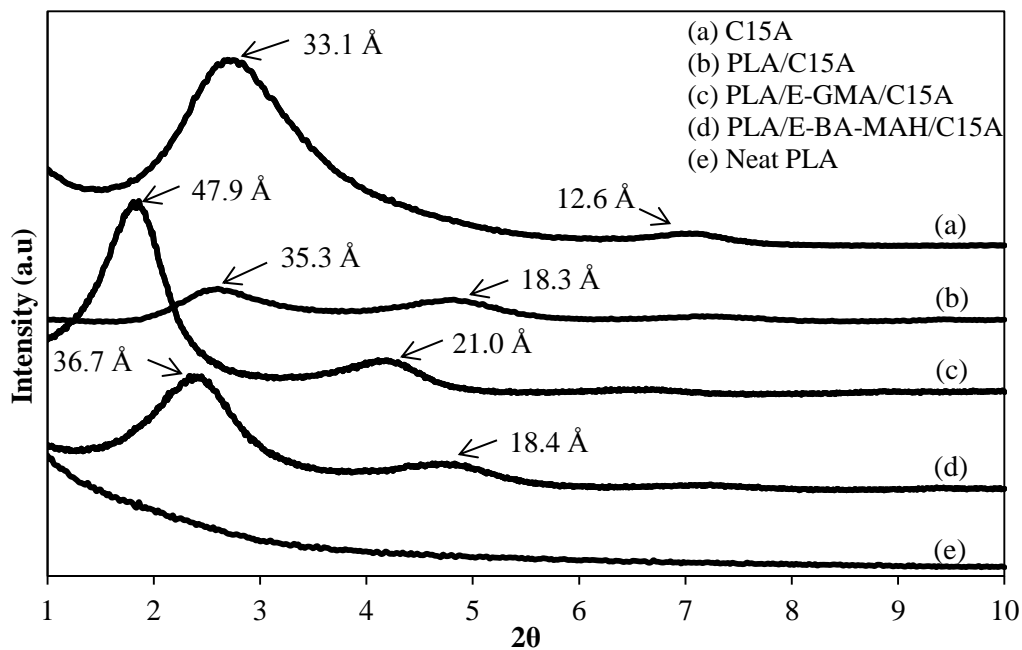


Figure 4.2 XRD patterns of neat PLA, C15A and PLA/C15A nanocomposites

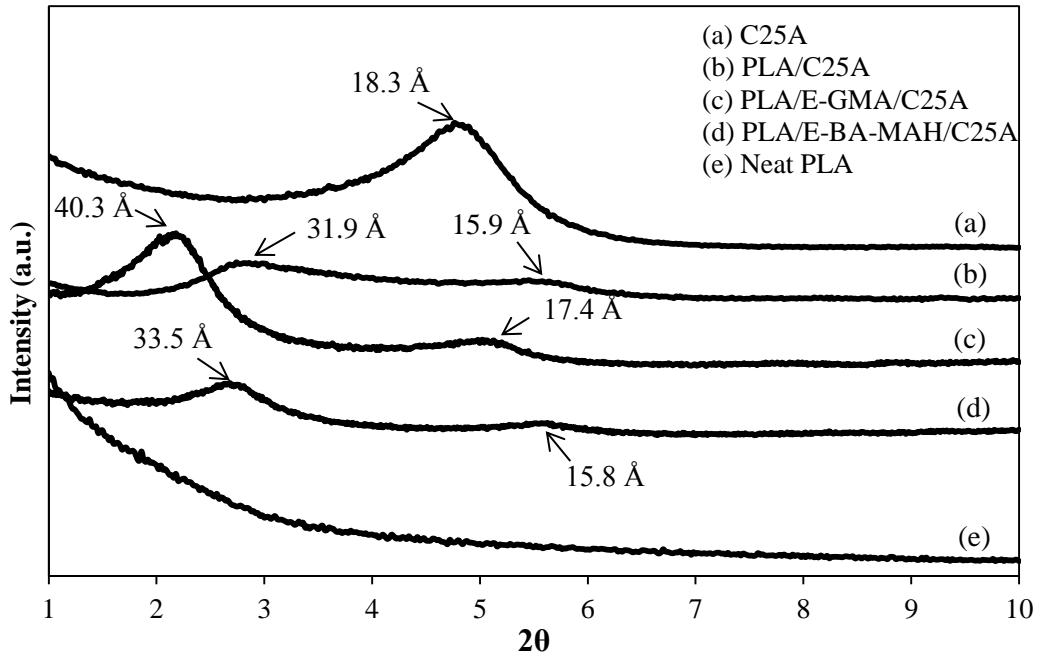


Figure 4.3 XRD patterns of neat PLA, C25A and PLA/C25A nanocomposites

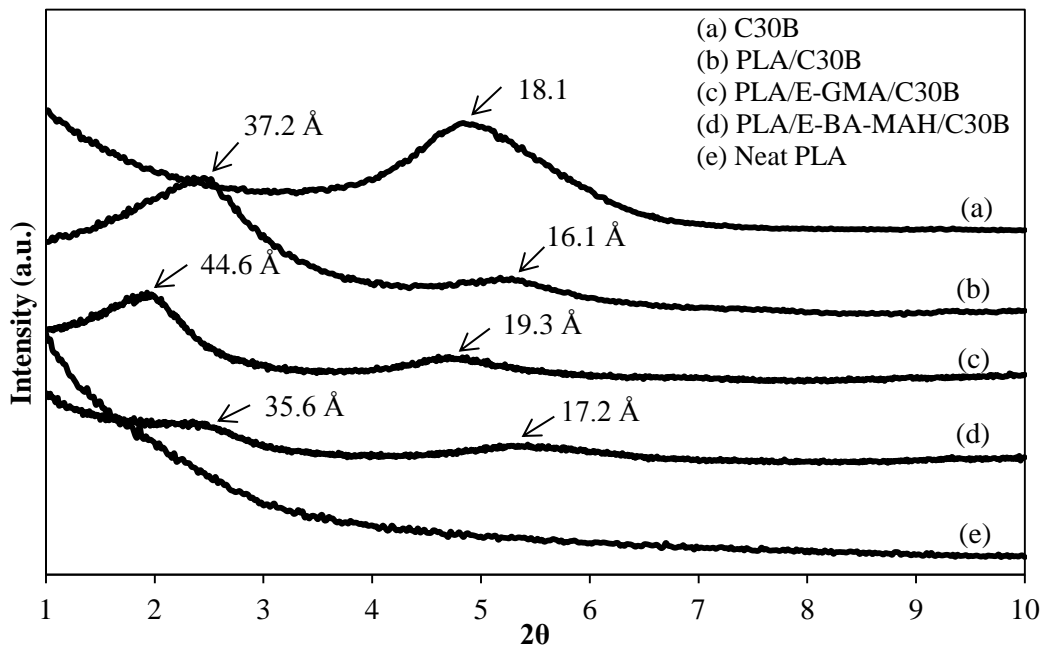


Figure 4.4 XRD patterns of neat PLA, C30B and PLA/C30B nanocomposites

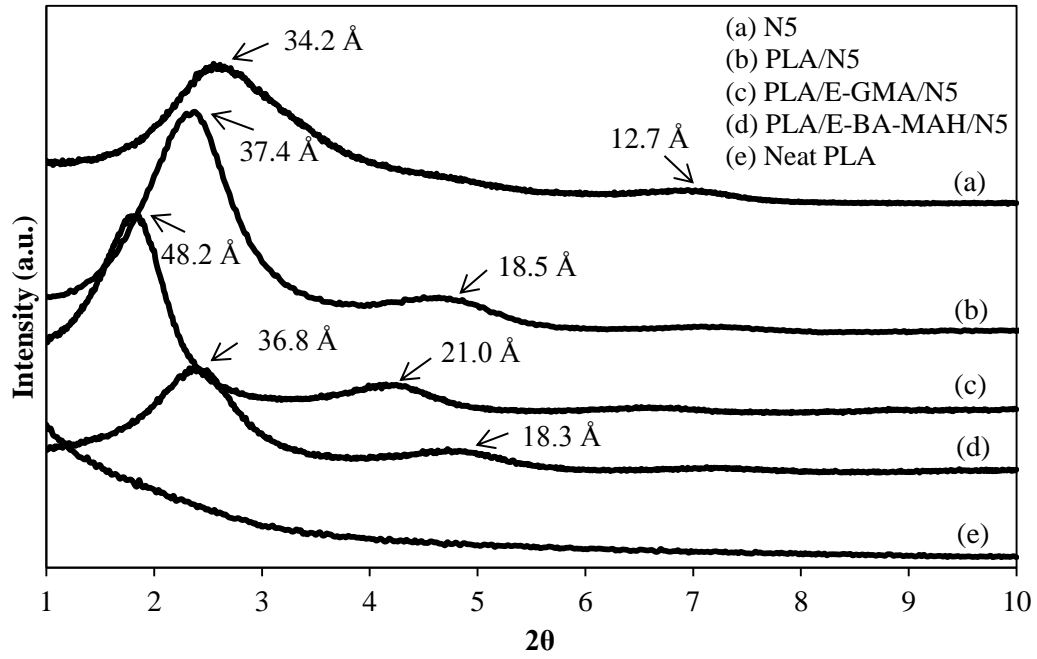


Figure 4.5 XRD patterns of neat PLA, N5 and PLA/N5 nanocomposites

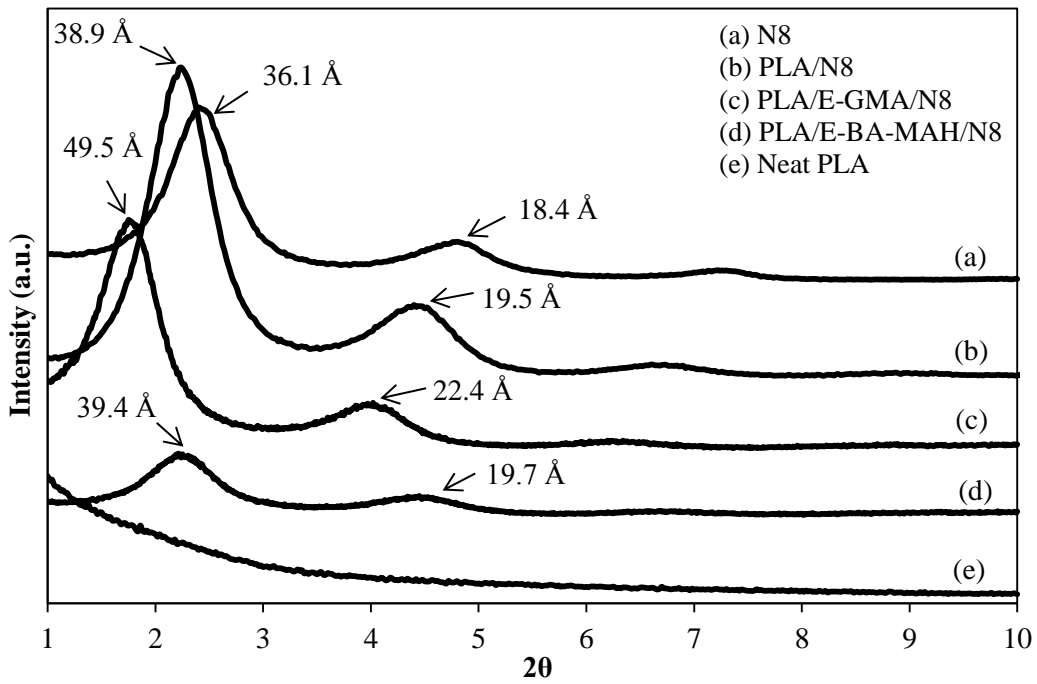


Figure 4.6 XRD patterns of neat PLA, N8 and PLA/N8 nanocomposites

For some nanocomposites, i.e., PLA/C15A, PLA/C25A and PLA/E-GMA/C25A, intensities of characteristic peaks are considerably low compared to neat clay, but in none of the nanocomposites there is an obvious disappearance of the basal reflection peak. This decrease can be attributed to the presence of mostly exfoliated structures since in general delamination of the silicate layers prevents diffraction of X-ray from the layers resulting in the disappearance of the diffraction peaks [34]. However, diffraction peaks of some of the samples gave higher intensities than the pure clay powder (i.e., pure N8 and PLA/N8 nanocomposite). It was expected to obtain lower intensities from the nanocomposites, because they contain only 2 wt. % clay, but it should be noted that the nanocomposites were analyzed as injection molded articles, whereas pure clays were in powder form. The nature of the sample affects the XRD patterns. Preferred orientation of crystallites in solid samples, particularly in injection molded samples, might be disappeared in powder form [128]. Alternatively in some samples clay layers are intercalated but still retain an ordered structure. Although XRD is a good method to determine the changes in the interlayer spacing of the silicate layers, it does not provide enough information about the spatial distribution of clay nano-particles and possible structural non-homogeneities in nanocomposites [34, 129]. Therefore, high resolution transmission electron microscopy was used to understand these discrepancies and the interactions between the polymer-compatibilizer-nanoclay.

Scanning Electron Microscopy

Blending with a rubbery polymer is one of the widely used methods to improve the toughness of a brittle polymeric material. The enhancement is mainly related with the dispersion of the rubbery phase in the polymer matrix. SEM is a useful tool to observe the dispersion on a fracture surface and the sizes of the rubbery phases. Besides, failure mechanism of the final product can be investigated through SEM images.

In this dissertation, impact fractured surfaces of the specimens were imaged, and the images at x500 and x3000 magnifications were taken for each specimen. For the

nanocomposites without a rubbery phase, SEM images are used to investigate the fracture mechanism. For the nanocomposites containing a rubbery phase, the fractured surfaces of the samples were etched with n-heptane at 60°C in a constant temperature water bath in the presence of ultrasonication. Etching was applied to remove the elastomeric phase on the surface so that the domain size analyses would be easier. The average size of the dispersed phase was analyzed by using Image J software program at least for 1000 different rubber domains. At least three images with a magnification of x3000 were analyzed. The area of each hole in the samples was determined by using the image analysis software by transforming these black holes into ellipsoids and calculating the area of these ellipsoids. Then, the average domain size (average diameter) was calculated statistically with the box plot method. Details of this procedure can be found in Appendix E.

First of all, the fracture surface of neat PLA was investigated (Figure 4.7). The main limitation in PLA applications is its inherent brittleness. As expected in a brittle polymer, the impact fracture surface of PLA exhibits straight crack propagation lines. These straight lines enhance further growth and make it easier to fracture the specimen with a small amount of energy [130].

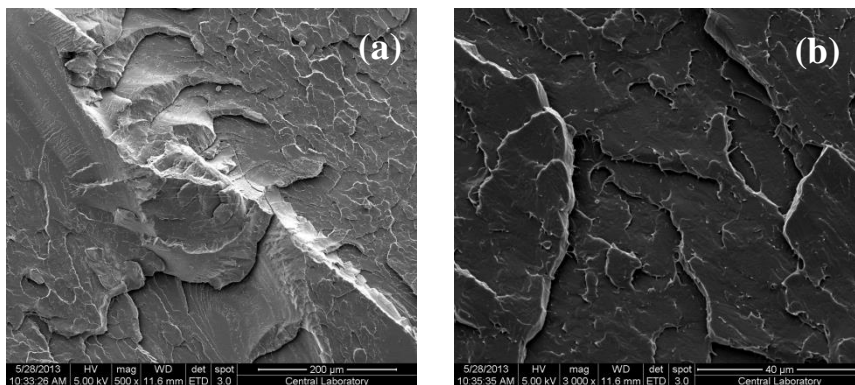


Figure 4.7 SEM micrographs of neat PLA with (a) x500 and (b) x3000 magnifications

PLA/organoclay nanocomposites have similar fracture surfaces to neat PLA (Figure 4.8 – Figure 4.12). Most of the crack propagation lines are distinct and long. However, in nanocomposites, crazing which is commonly observed in thermoplastic glassy polymers upon shearing can be observed more clearly. Surfaces of the nanocomposites are rougher compared to those of neat PLA. There are smaller cracks developed in different directions due to the presence of organoclays. The results of mechanical property investigations will be discussed in the forthcoming sections, but it can be stated here that addition of nanofillers did not result in a considerable enhancement in impact toughness compared to the impact toughness of neat PLA. This means, addition of organoclays deflected the cracks and increased their path to some extent, but they did not act as barriers to stop crack propagation.

Fibril structures formed during the impact test can be seen in almost all the images. Compared to the nanocomposites, short fibrils bridging the cracks are more apparent on neat PLA surface (Figure 4.7). Additionally, clay in the samples seems to be homogeneously dispersed in the nanocomposites. There are no big agglomerated stacks seen in the samples at these magnifications.

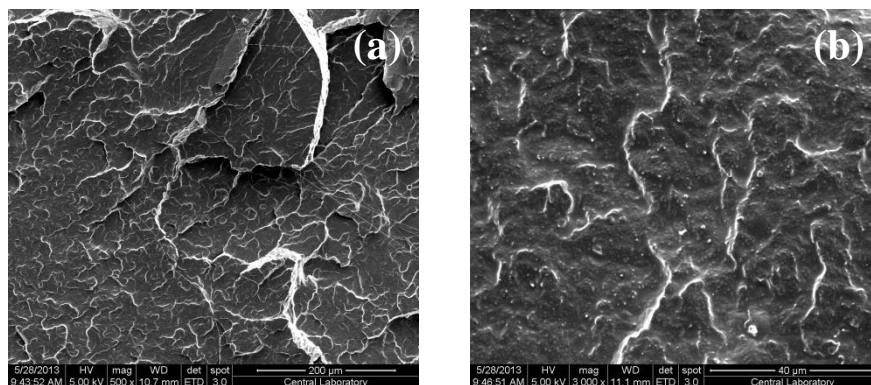


Figure 4.8 SEM micrographs of PLA/C15A nanocomposite with (a) x500 and (b) x3000 magnifications

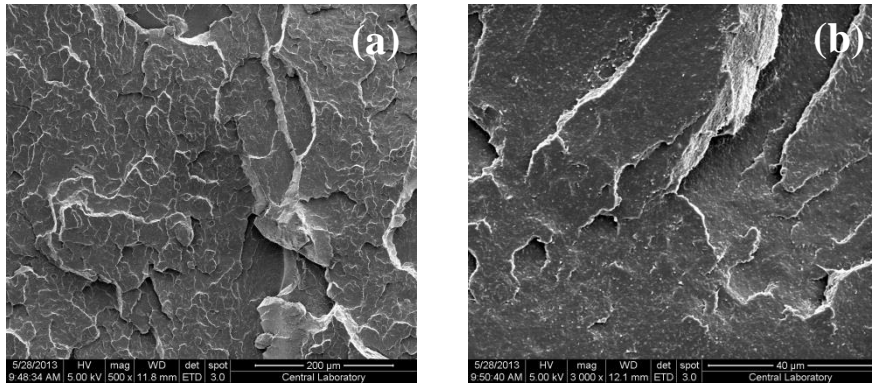


Figure 4.9 SEM micrographs of PLA/C25A nanocomposite with (a) x500 and (b) x3000 magnifications

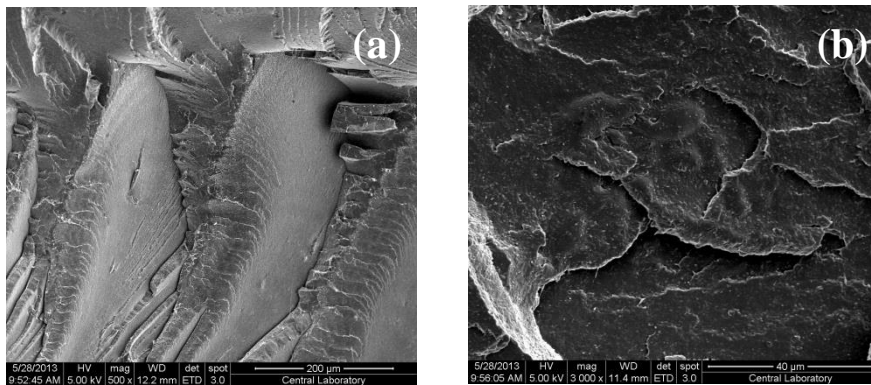


Figure 4.10 SEM micrographs of PLA/C30B nanocomposite with (a) x500 and (b) x3000 magnifications

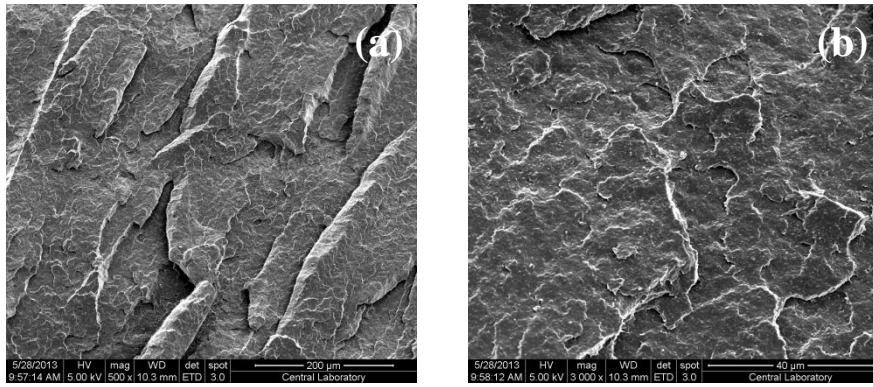


Figure 4.11 SEM micrographs of PLA/N5 nanocomposite with (a) x500 and (b) x3000 magnifications

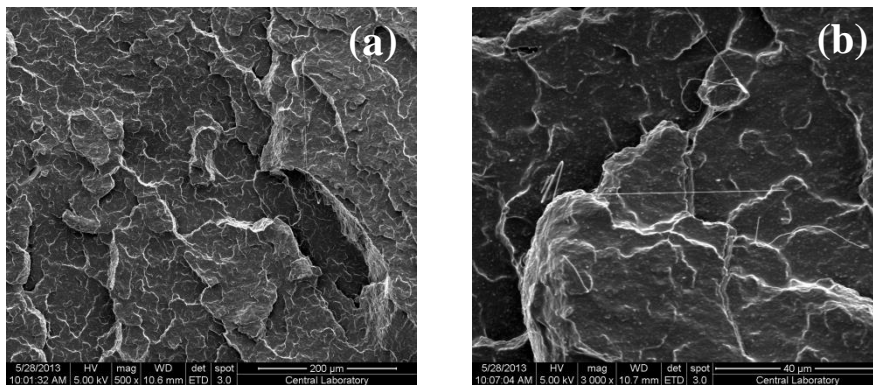


Figure 4.12 SEM micrographs of PLA/N8 nanocomposite with (a) x500 and (b) x3000 magnifications

Blending PLA with compatibilizers resulted in phase separated morphologies for both E-GMA and E-BA-MAH. However, sizes of the rubbery domains of these two blends are considerably different. Just by considering the images of these blends at x3000 magnification (Figure 4.13-b and Figure 4.14-b) bigger rubber droplets in PLA/E-BA-MAH blend are seen. The average domain sizes of PLA/E-GMA and PLA/E-BA-MAH blends are 714 and 1023 nm, respectively. Namely, average droplet size of E-BA-MAH is 1.4-fold larger than E-GMA droplets, blended at the identical conditions with PLA. In addition to the chemical interactions between the

polymer matrix and the rubbers, the viscosities of different rubbers might result in different coalescence mechanisms. For example, the viscosity of E-BA-MAH is slightly higher than the viscosity of E-GMA. Increased viscosity of the blend results in increase in the shear stress applied on the platelets during extrusion. However, increasing viscosity also prevents the elastomeric phase to disperse into small droplets, because the shear stress that is applied on to the material becomes insufficient. So the coalescence rate increases.

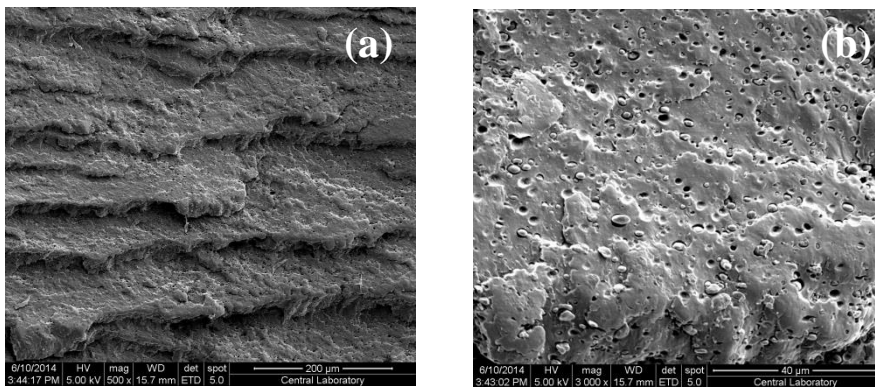


Figure 4.13 SEM micrographs of PLA/E-GMA blend with (a) x500 and (b) x3000 magnifications

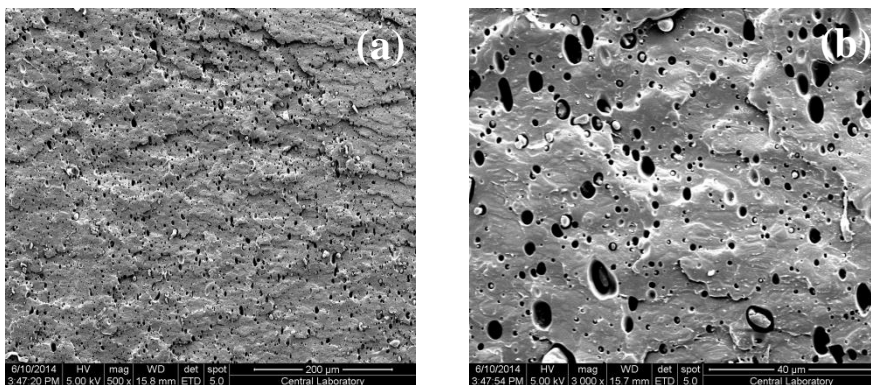


Figure 4.14 SEM micrographs of PLA/E-BA-MAH blend with (a) x500 and (b) x3000 magnifications

Morphologies of the ternary nanocomposites are different than the morphologies of the binary nanocomposites and blends. Since the fracture surfaces are etched and etching procedure annihilates the crack propagation lines, fracture mechanisms cannot be elaborated. However, the phase separation between the polymer matrix and the compatibilizer and the dispersion of the rubbery phase in the matrix can be seen obviously. SEM micrographs of PLA nanocomposites containing E-GMA can be seen in Figure 4.15 – Figure 4.19.

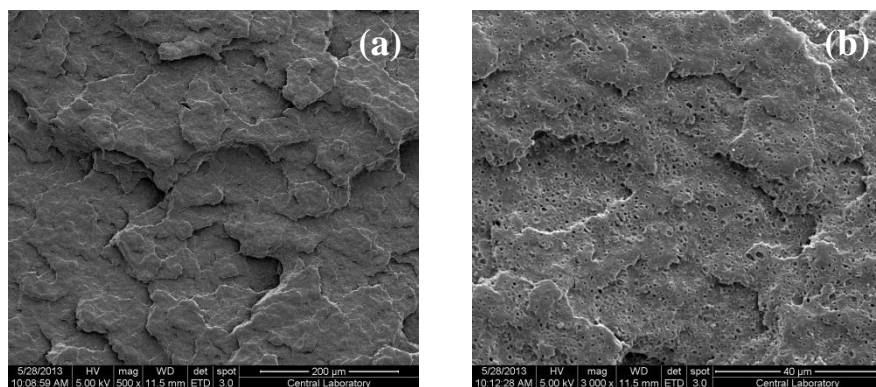


Figure 4.15 SEM micrographs of PLA/E-GMA/C15A nanocomposite with (a) x500 and (b) x3000 magnifications

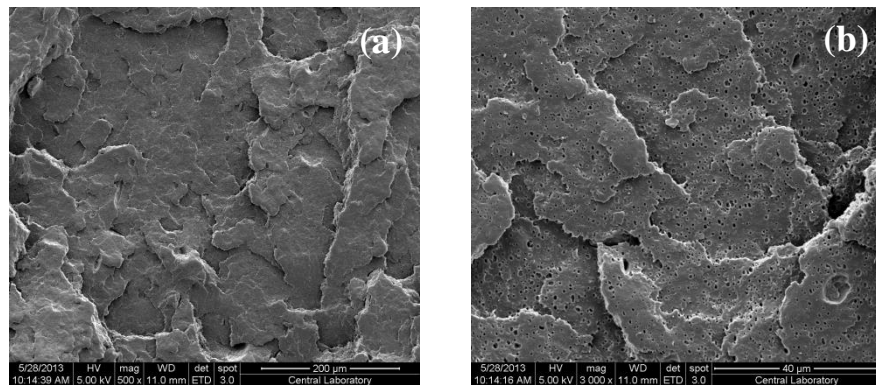


Figure 4.16 SEM micrographs of PLA/E-GMA/C25A nanocomposite with (a) x500 and (b) x3000 magnifications

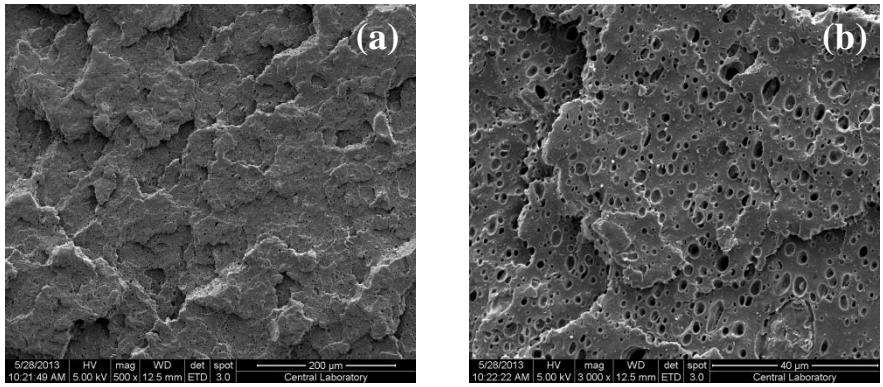


Figure 4.17 SEM micrographs of PLA/E-GMA/C30B nanocomposite with (a) x500 and (b) x3000 magnifications

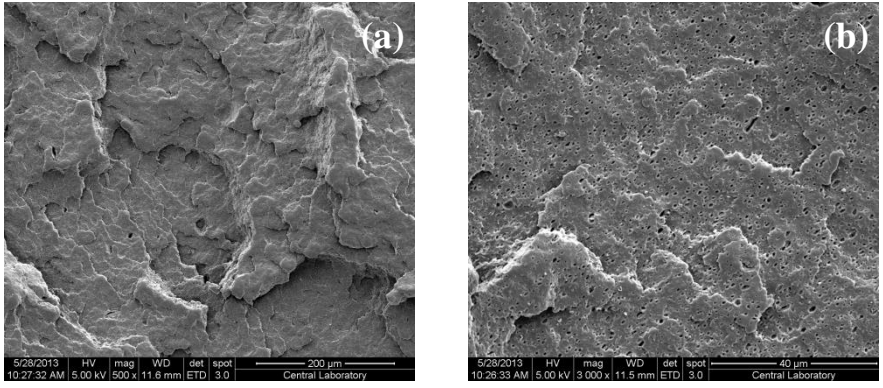


Figure 4.18 SEM micrographs of PLA/E-GMA/N5 nanocomposite with (a) x500 and (b) x3000 magnifications

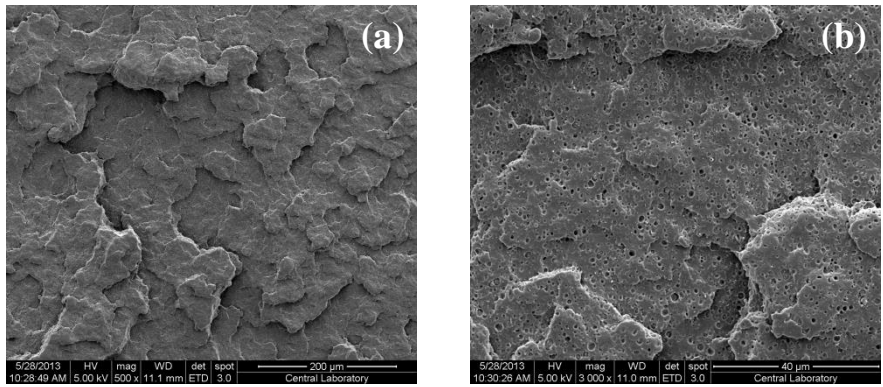


Figure 4.19 SEM micrographs of PLA/E-GMA/N8 nanocomposite with (a) x500 and (b) x3000 magnifications

In Figure 4.15 to Figure 4.19, etched fracture surfaces of the ternary nanocomposites in which E-GMA is used as compatibilizer can be seen. Size and shape of spherical vacuoles that remained after etching reveal the distribution of the domains, which is an indication of the stability of the system. Domain sizes should be optimum since both too small and too large domains can affect the final mechanical properties adversely. For example, if the two phases are highly compatible, ultra-fine domains could be formed. Finely distributed tiny domains might result in lower impact strength values since they cannot act as barriers on the cracks, and the cracks can propagate without touching the rubbery phases. On the other hand, too large domains can form large cavities when they are deformed [131]. As mentioned before, domain sizes of blends and nanocomposites were determined using Image J software and the results are summarized in Table 4.2. In the samples containing E-GMA, narrow size distribution of dispersed phase with sub-micron sizes could be attributed to the compatibility of the phases with low interfacial tension and the achievement of efficient reactive blending. The reactivity of epoxide group towards the functional end groups of PLA (hydroxyl and carboxyl groups) results in good compatibilization effect. These interactions between epoxide groups and PLA were proved in the literature by FTIR analyses [132, 133]. FTIR spectra of the nanocomposites, which will be given in the following sections, also support the presence of reactive blending.

Increased domain sizes in the nanocomposites containing C25A and C30B could be attributed to the positions of the clay nanoplatelets in the nanocomposite. If the organoclay particles were dispersed in the PLA matrix, the clay platelets would suppress the agglomeration of the elastomeric domains and cause a barrier effect that hinders the recombination of elastomeric domains [134]. However, for C25A and C30B, the average domain sizes increase with organoclay addition, no matter if they are well dispersed or not, because the clay particles reside at the interphase between the PLA and elastomeric material. Thus, the interfacial tension is reduced and the domain sizes are enlarged. However, ternary nanocomposites of C15A, N5 and N8 with E-GMA as the rubber resulted in smaller domain sizes compared to those of PLA/E-GMA binary blend. This indicates that these clay types are probably not

compatible with E-GMA. Thus, they are dispersed in the PLA matrix, suppressing the rubber droplets.

Table 4.2 Average domain sizes of all samples

Sample	Compatibilizer Type	Clay Type	d_{av} (nm)
A-02	E-GMA	-	714
A-03	E-BA-MAH	-	1023
A-1	E-GMA	C15A	547
A-2	E-GMA	C25A	732
A-3	E-GMA	C30B	792
A-4	E-GMA	N5	540
A-5	E-GMA	N8	573
B-2	E-BA-MAH	C25A	1255
B-4	E-BA-MAH	N5	1146

Shapes of the vacuoles remained after etching are ellipsoids rather than spherical droplets. This also indicates that there is a good interaction between the dispersed phase and the matrix such that the impact load is shared between the phases. The copolymer formed at the interface of the two phases acts a bridge which transfers the load and increases the toughness [129, 135].

For the samples with E-BA-MAH, SEM images were taken only for C25A and N5 containing nanocomposites (Figure 4.20 and Figure 4.21). Similar to the difference in binary blends, E-BA-MAH containing nanocomposites contain larger rubber droplets than their equivalent samples prepared with E-GMA. In the ternary nanocomposites containing E-GMA, increase in domain size was attributed to the higher compatibility of the particular clay types with both polymer matrix and the

compatibilizer, which in result decreased the surface tension between the phases. However, this is probably not the case in E-BA-MAH containing nanocomposites. As discussed previously, large droplets might be a result of increased coalescence rate due to increased viscosity in extrusion or weaker compatibility of maleic anhydride functional group to PLA, compared to epoxide functional group. Changing morphologies of E-GMA and E-BA-MAH containing nanocomposites are reflected in both mechanical and rheological properties, which will be discussed later in this dissertation.

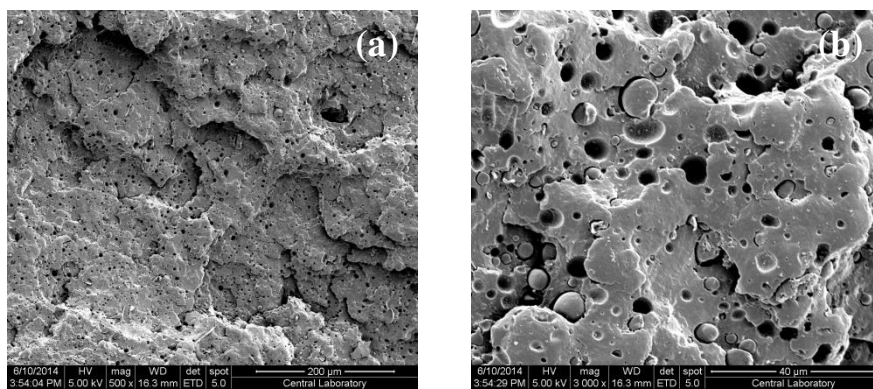


Figure 4.20 SEM micrographs of PLA/E-BA-MAH/C25A nanocomposite with (a) x500 and (b) x3000 magnifications

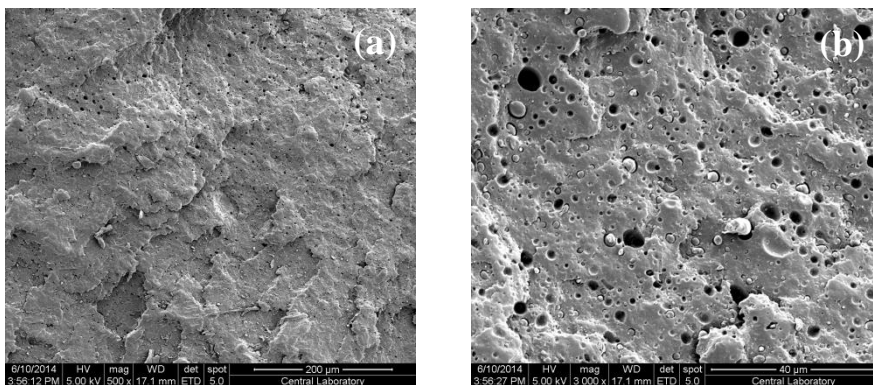


Figure 4.21 SEM micrographs of PLA/E-BA-MAH/N5 nanocomposite with (a) x500 and (b) x3000 magnifications

Transmission Electron Microscopy

TEM provides information about the spatial distribution of clay nano-particles. Four selected samples, which are nanocomposites of C25A and N5 were imaged, but the samples containing E-BA-MAH as the rubbery phase were not considered. The selection was mainly based on the XRD patterns of the nanocomposites which were discussed previously. As mentioned before, the interlayer spacings in the presence of E-BA-MAH were not increased. Furthermore, both mechanical and rheological properties, which will be discussed in the following sections, were not enhanced with the addition of E-BA-MAH to the nanocomposites.

Low magnification bright field TEM image of binary PLA/C25A nanocomposite can be seen in Figure 4.22. Even though there are a number of large tactoids, most of the clay particles are dispersed homogeneously.

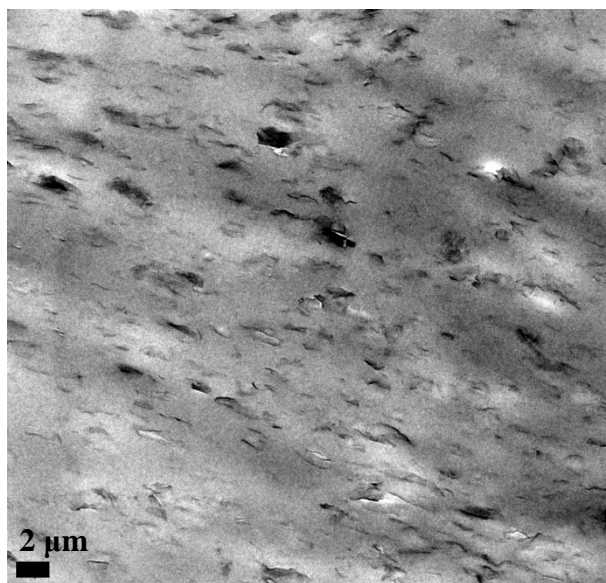


Figure 4.22 Low magnification TEM micrograph of PLA/C25A nanocomposite

At higher magnifications, it is possible to see three different dispersion states of the clay nanoplatelets (Figure 4.23). Tactoids are clearly seen at all magnifications.

Interlayer spacing between the intercalated layers are measured using Image J and they are in accordance with the XRD results (~ 3.2 nm).

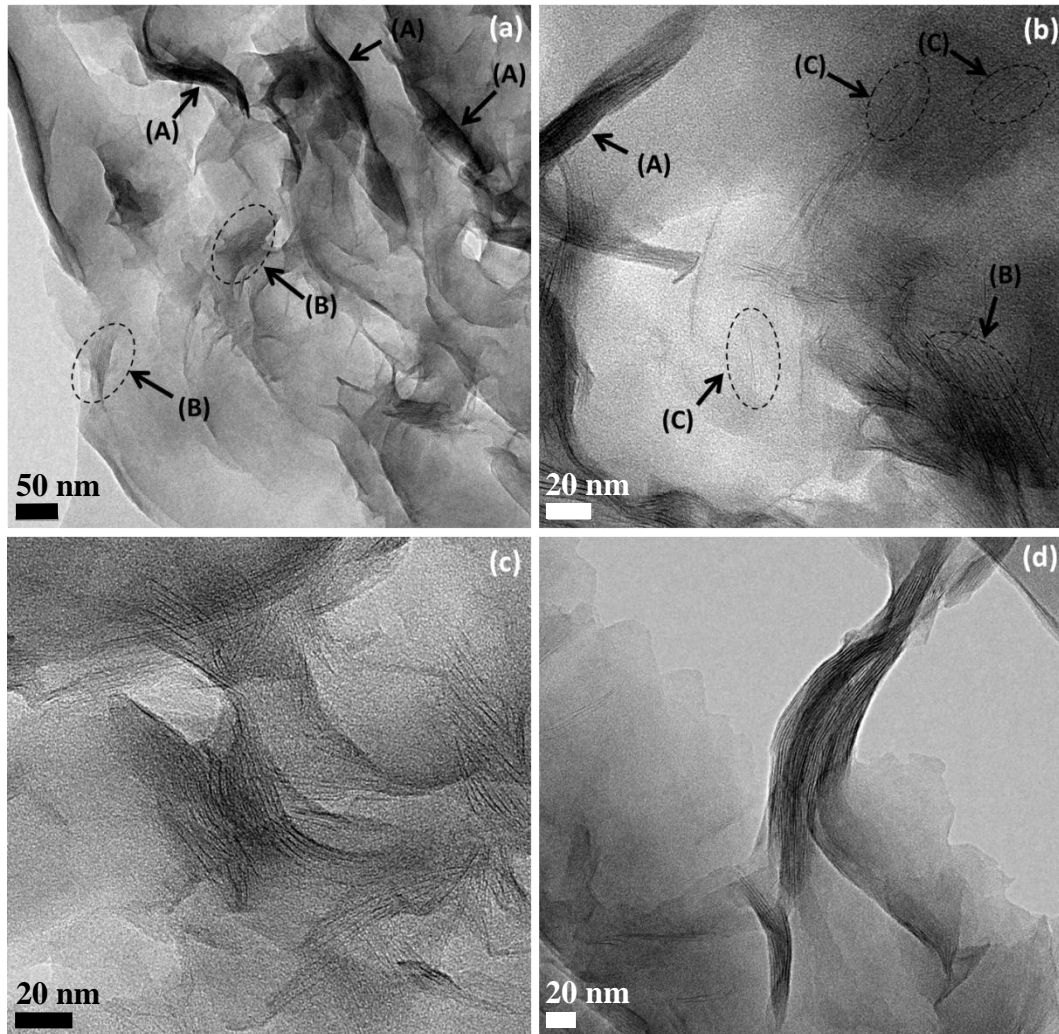


Figure 4.23 High magnification TEM micrographs of PLA/C25A: (A) tactoids, (B) intercalated and (C) exfoliated clay nanoplatelets

According to the XRD analyses, addition of E-GMA to the binary PLA/C25A nanocomposite resulted in increases in the interlayer spacing. TEM micrograph of this nanocomposite at low magnification shows the dispersion of clay nanoplatelets (Figure 4.24). Tactoids are rare in this micrograph where intercalated and orderly exfoliated silicate layers can be seen. Because of the low contrast difference between

the polymer matrix and the rubbery phase, positions of clay nanoplatelets cannot be exactly determined. They might be dispersed in the continuous phase, in the rubber phase or on the interface between the two phases. XRD patterns suggest that addition of E-GMA resulted in increases in interlayer spacings. Therefore, clay nanoplatelets are most probably embedded in the E-GMA phase or positioned on the interface. As discussed by Baouz et al. [19] some of the clay nano-particles could be located in the rubber phase, since its melting point is lower than that of PLA. During the extrusion process, the rubber is melted before PLA so that fillers might be encapsulated in the rubber before PLA melts. Increased domain sizes of ternary nanocomposites containing C25A and C30B, seen in SEM images, suggest that the clay platelets are also located at the interface of PLA and the rubber, decreasing the surface tension. Thus, none of the morphology analyses directly indicate the position of clay nanoplatelets, but they just show evidences supporting the possibilities of being located on the interface between the two phases or embedded in the rubber phase.

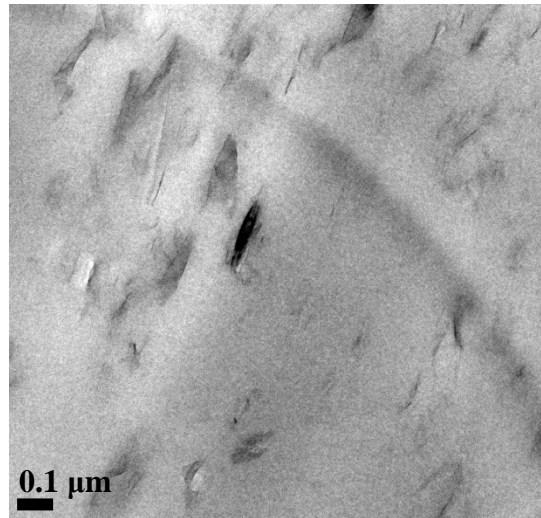


Figure 4.24 Low magnification TEM micrograph of PLA/E-GMA/C25A nanocomposite

At higher magnifications (Figure 4.25) clay tactoids and orderly exfoliated silicate layers can be seen in PLA/E-GMA/C25A nanocomposite. Compared to PLA/C25A nanocomposite, the tactoids are smaller. There are many orderly exfoliated layers close to the clay stacks.

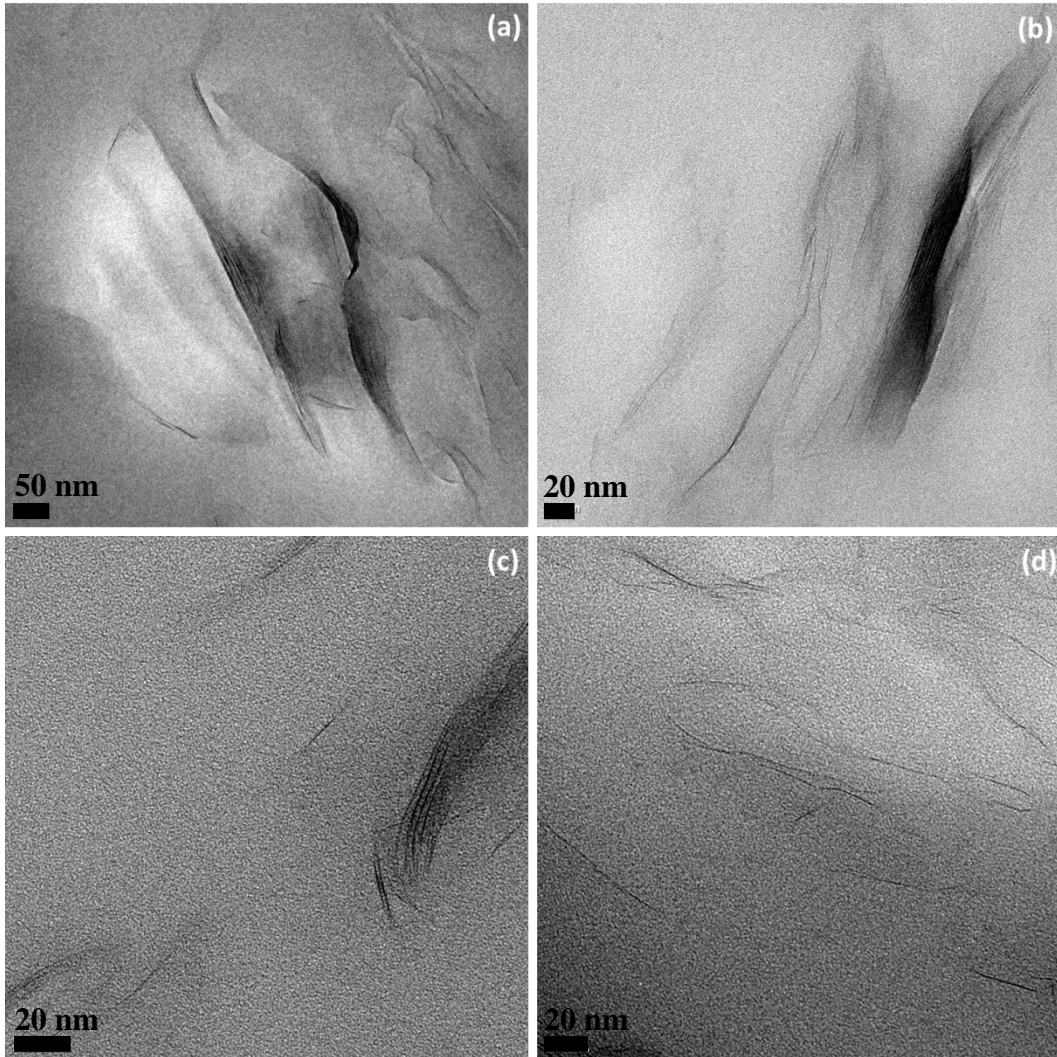


Figure 4.25 High magnification TEM micrograph of PLA/E-GMA/C25A nanocomposite

According to the XRD results, increases in interlayer spacing of C15A, N5 and N8 are smaller compared to those of C25A and C30B, in both binary and ternary nanocomposites. In order to represent these three clay types, N5 nanocomposites were imaged with TEM. Figure 4.26 shows low magnification TEM micrograph of PLA/N5 binary nanocomposite. The clay nanoplatelets are homogeneously dispersed in the polymer matrix with varying sizes of tactoids.

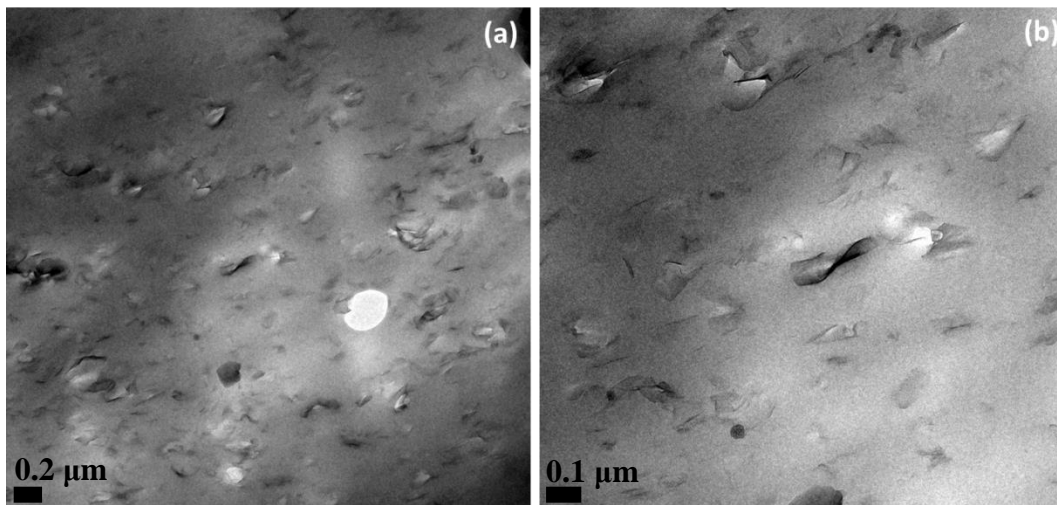


Figure 4.26 Low magnification TEM micrographs of PLA/N5 nanocomposite

At higher magnifications (Figure 4.27), different dispersion states can be seen as in the case of C25A binary nanocomposite. The layer spacings were analyzed with Image J software at the intercalated sections, and the results are consistent with the XRD analyses. Intercalated structures have interlayer spacing of about 3.7 nm according to the XRD analyses. In the high magnification micrographs, gallery heights varying between 3.5-4.0 nm were detected.

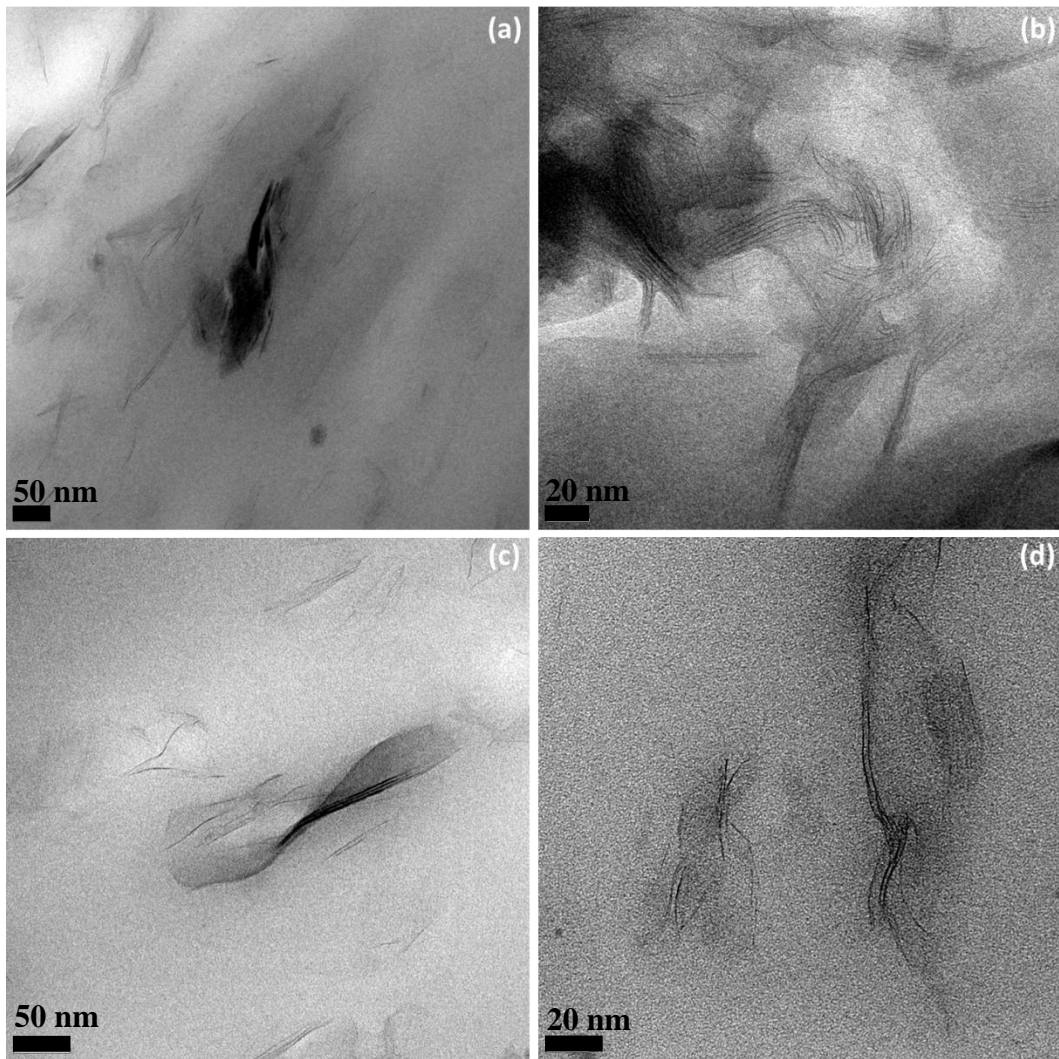


Figure 4.27 High magnification TEM micrographs of PLA/N5 nanocomposite

When E-GMA is added to the binary PLA/N5 nanocomposite, relatively larger tactoids were observed at low magnification images (Figure 4.28). However, at higher magnifications, as in the case of C25A, exfoliated and intercalated structures can be seen together with the tactoids (Figure 4.29).

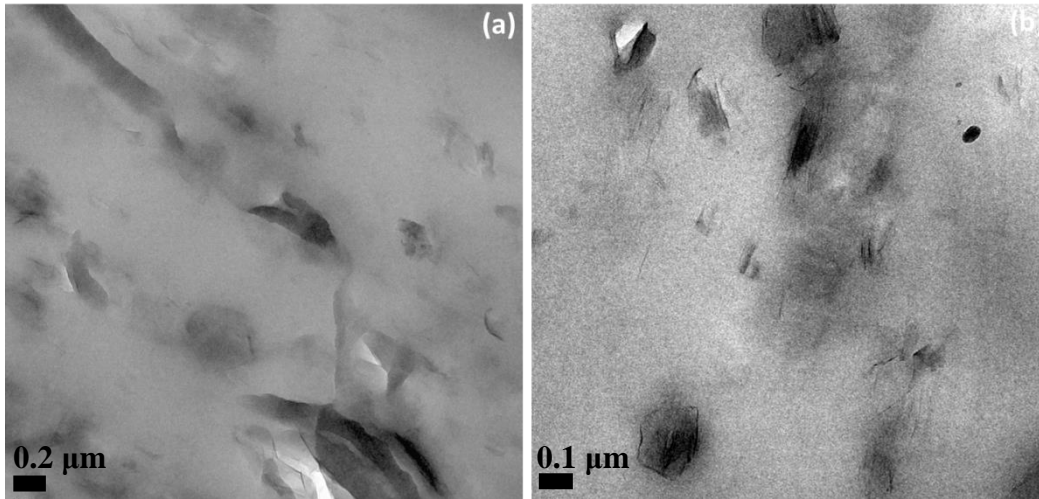


Figure 4.28 Low magnification TEM micrographs of PLA/E-GMA/N5 nanocomposite

Effects of clay dispersion on the mechanical and thermal properties of the nanocomposites will be discussed in the forthcoming sections. Apart from those inferences, only the spatial distributions of clay nanoparticles can be evaluated with TEM, and the gallery heights calculated from XRD patterns of these nanocomposites can be compared. In general, all of the nanocomposites imaged with TEM contain multiple clay dispersion types. In every sample, intercalated/exfoliated structures with tactoids of changing sizes are observed. Lengths of the tactoids in N5 nanocomposites are obviously shorter which can be attributed to the lower aspect ratio of the N5 nanoparticles.

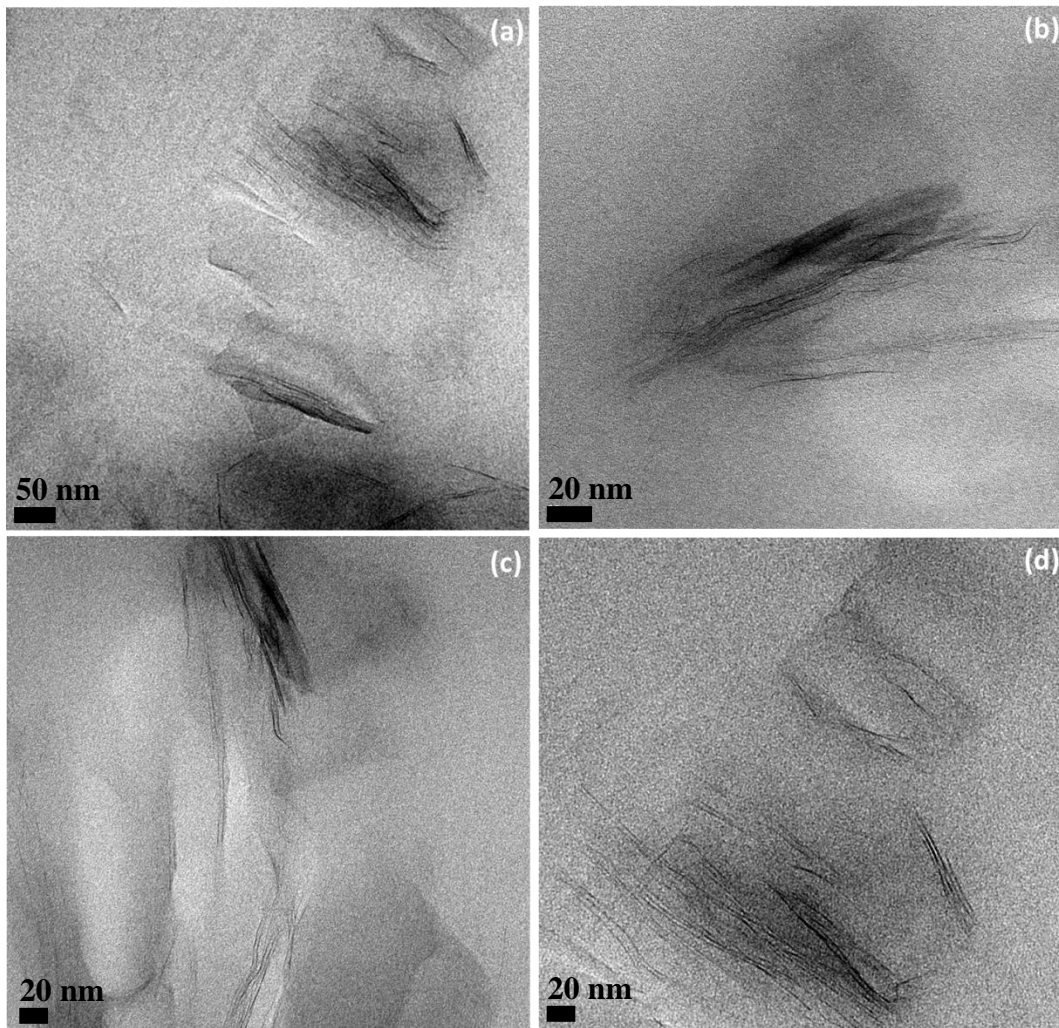


Figure 4.29 High magnification TEM micrographs of PLA/E-GMA/N5 nanocomposite

4.1.2.2 Spectroscopic Analyses

FTIR analyses were performed to find evidences of the interactions between the polymer matrix and the additives. The expected bands in the infrared spectra of PLA are given in the literature and listed in Table 4.3. These peaks are characterized also for the PLA used in this dissertation and shown Appendix A.

Table 4.3 Characteristic bands in IR spectrum of PLA [133, 136]

Bonding	Type	Characteristic Peak Positions (cm ⁻¹)
-C-C-	Stretching	868, 926
-OH	Bending	1047
-C-O-	Stretching	1093, 1130, 1194
-CH ₃	Bending	1456
-C=O-	Bending	1268
-C=O	Carbonyl stretching	1748
-CH-	Symmetric bending deformation	1382
	Asymmetric bending deformation	1365
-CH-	Symmetric bending	2950
	Asymmetric bending	2996

The interactions between the compatibilizers and the polymer matrix can be followed through the changes in FTIR spectra of the blends and nanocomposites. As an example, FTIR spectra of nanocomposites of C15A with and without compatibilizers, together with neat PLA, neat E-GMA and neat E-BA-MAH are shown in Figure 4.30. The reaction expected to occur between the end groups of PLA (-COOH and/or -OH) and the epoxide group of E-GMA can be detected from the decreasing intensity or disappearance of the epoxide peak seen at 910 cm⁻¹ in the FTIR spectra of neat E-GMA [133, 137]. Similarly, the possible reaction between PLA end groups and maleic anhydride functional group of E-BA-MAH can be observed from the decreasing intensity or disappearance of the maleic anhydride peak seen at 1785 cm⁻¹ [133, 138]. Both of the elastomers interacted with PLA during melt blending so that both epoxide and maleic anhydride peaks disappeared in the spectra of the corresponding nanocomposites. Similar results were obtained for other clay types and FTIR spectra of them can be seen in Appendix A.

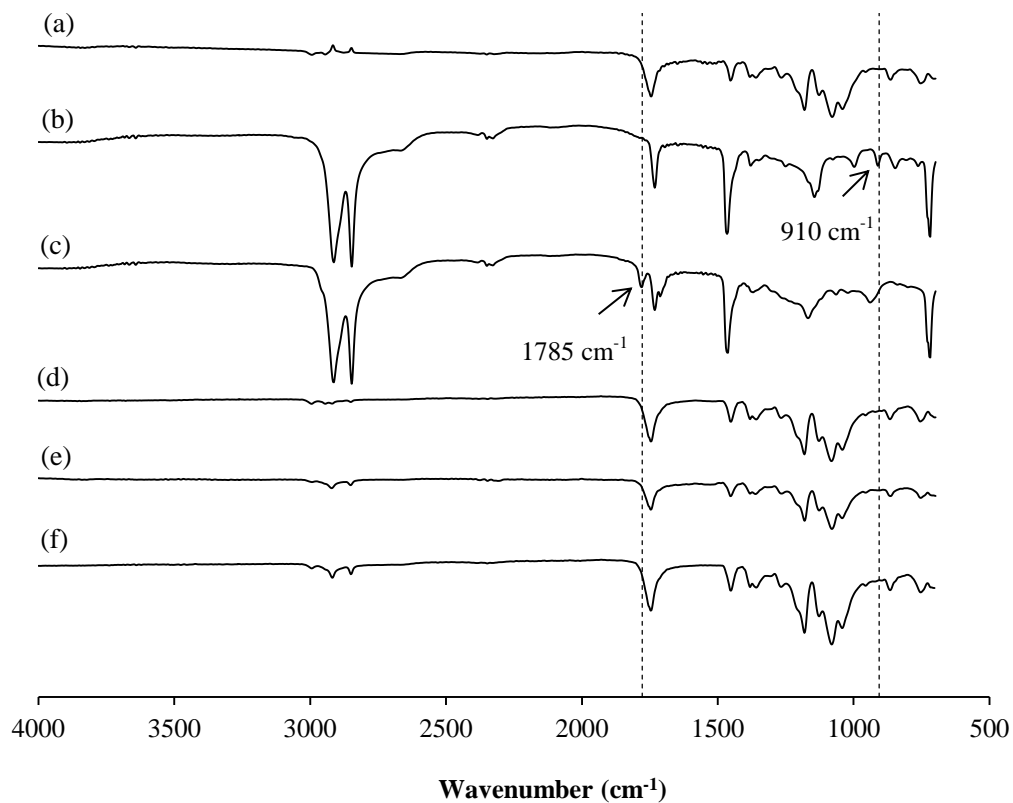


Figure 4.30 FTIR spectra of (a) PLA, (b) E-GMA, (c) E-BA-MAH, (d) PLA/C15A, (e) PLA/E-GMA/C15A, (f) PLA/E-BA-MAH/C15A

4.1.2.3 Mechanical Analyses

Tensile and impact tests were done on neat PLA, PLA/compatibilizer binary blends, PLA/organoclay binary nanocomposites and PLA/compatibilizer/organoclay ternary nanocomposites. For every set of samples, tensile strength, Young's modulus and elongation at break values were determined using the stress-strain curves, and the average values and standard deviation of the results are reported. Tabulated form of mechanical test results can be found in Appendix B.

The impact strength of PLA is comparable with polystyrene which is another relatively brittle polymer used extensively in industry. The tensile strength and elastic modulus of PLA are comparable to PET, but the elongation at break for PLA

is quite low, indicating low tensile toughness [139]. A typical stress-strain curve obtained with neat PLA used in this study can be seen in Figure 4.31.

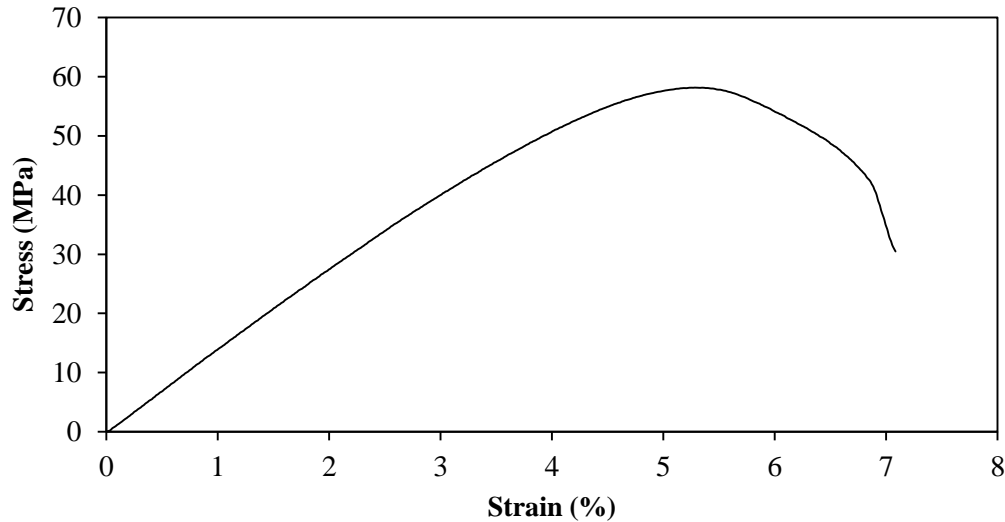


Figure 4.31 Typical stress-strain curve of neat PLA

As stated previously, in order to improve material properties of the PLA, organically modified clay nanoparticles were used as fillers. In order to improve toughness, two different elastomers were blended to these nanocomposites. These elastomers were also act as compatibilizers between the polymer matrix and the silicate layers. Usually, blends of brittle materials with flexible polymers are expected to show toughening, but this enhancement is accompanied by sacrifices in tensile strength and modulus. Addition of fillers, on the other hand, leads to reductions in elongation at break and impact strength while improving the tensile strength and modulus. The main parameter underlying these property changes is the interfacial interactions between the constituents of the nanocomposites. For example, the filler, which is supposed to be strong and stiff, bears most of the load or stress applied to the matrix while the polymer matrix, which has lower strength but higher toughness, effectively transmits the load to the filler only if the interfacial interactions are strong enough [140]. The mechanical properties of PLA/organoclay and

PLA/compatibilizer/organoclay nanocomposites discussed in this section reflect the importance of the interactions between the constituents. FTIR spectra of both binary PLA/compatibilizer blends and ternary PLA/compatibilizer/organoclay nanocomposites revealed that reactive blending was achieved during extrusion with both E-GMA and E-BA-MAH. However, morphologies of the nanocomposites showed that the dispersion of clay nanoplatelets and elastomeric phases differ from sample to sample. All nanocomposites were prepared at constant compatibilizer and/or filler content; i.e., for binary PLA/compatibilizer blends the ratio is 90/10 (w/w); for binary PLA/organoclay nanocomposites the ratio is 98/2 (w/w); and for ternary PLA/compatibilizer/organoclay nanocomposites the ratio is 88/10/2 (w/w/w). Furthermore, processing conditions are identical for all the nanocomposites. Therefore, the only reason that the material properties differ from each other could be the interactions between the constituents.

Consistent with the expectations, addition of the compatibilizers resulted in decreases in tensile strength and modulus values (Figure 4.32 and Figure 4.33). Both of the binary blends have the same tensile strength and comparable modulus values, both are lower than the neat PLA values. Surprisingly, PLA/organoclay nanocomposites resulted in reductions in tensile strength with the maximum reduction of 34% in PLA/N8 nanocomposite. In fact, addition of nanofillers is expected to result in an enhancement in tensile strength. The reason of the reductions obtained in this study might be weak spots in the matrix due to the clay agglomerates in the non-compatibilized samples. Compatibilization, on the other hand, resulted consistently with the general expectations of increasing tensile strength with addition of nanoclay. For example, drastically decreased strength of the PLA/E-GMA blend was improved with the addition of nanofillers up to 3.3-fold in PLA/E-GMA/N5 nanocomposite. Similar tensile strength reductions in binary nanocomposites and improvement in ternary nanocomposites were reported recently in the literature [129, 141]. Nanocomposites containing E-BA-MAH also showed tensile strength improvement with the addition of organoclay, but these enhancements are very low compared to E-GMA containing samples.

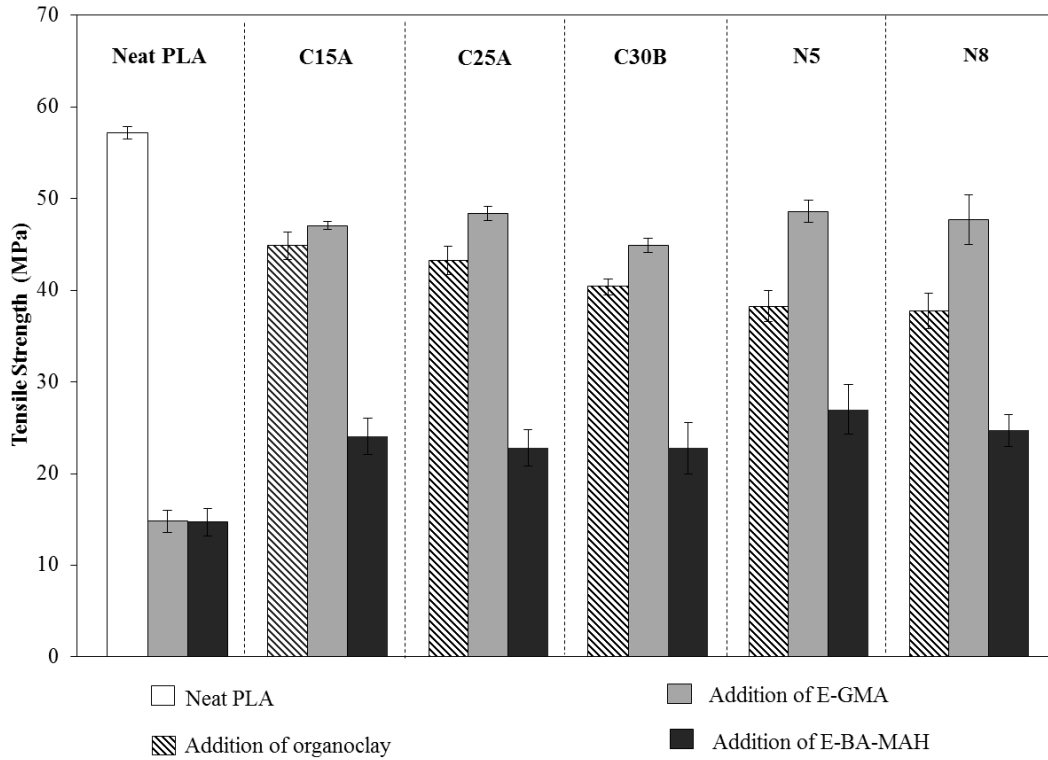


Figure 4.32 Effect of organoclay and compatibilizer types on tensile strength

Changes in Young's modulus of binary blends and, binary and ternary nanocomposites can be seen in Figure 4.33. Due to the elastomeric nature of the rubbers modulus values of blends are lower than that of neat PLA [129]. Blending with 10% E-GMA and E-BA-MAH caused 37% and 30% reductions in the tensile modulus. These reductions are a little higher than the similar studies published in the literature. For example, at 20 wt. % rubber content, the decrease is around 31% for PLA/E-GMA blend in a study of Oyama [97].

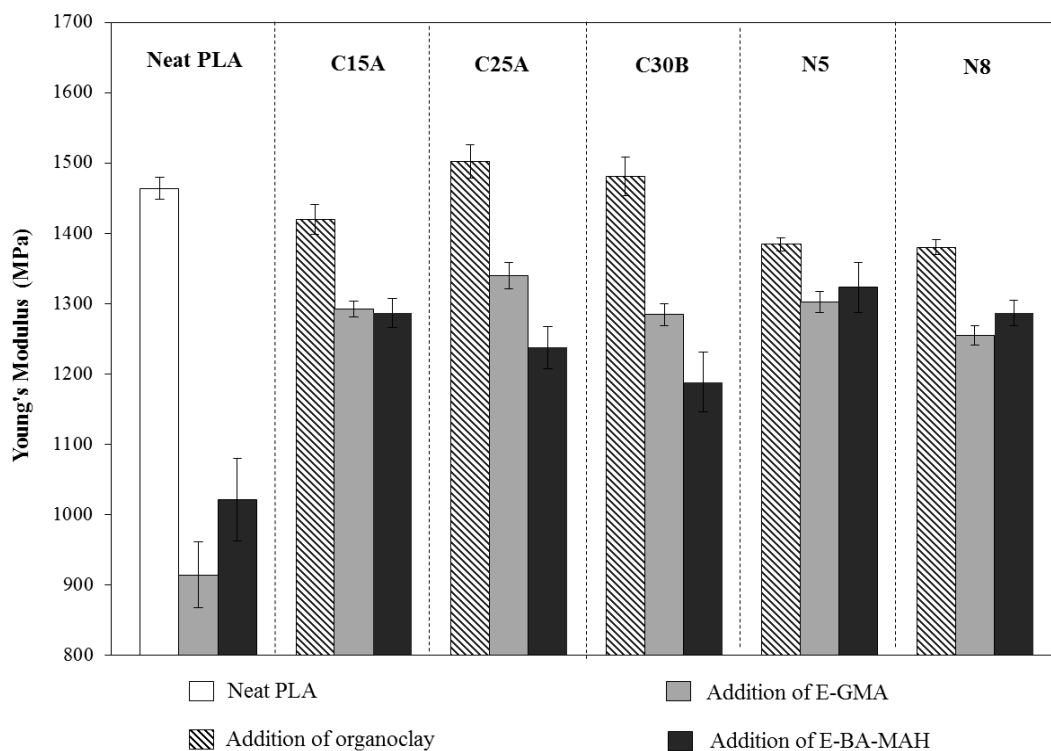


Figure 4.33 Effect of organoclay and compatibilizer types on Young's modulus

In binary nanocomposites, enhancement was seen only with C25A and C30B while the other clay types resulted in slight decreases. These two types of clays were previously used in literature with PLA as polymer matrix. Affinity of C30B has shown to be higher than that of C25A due to hydrogen-bonding between the carbonyl group in the PLA structure and the hydroxyl group in the organic modifier of 30B [100, 142, 143] even though modulus enhancement of C25A is slightly higher in this study. Furthermore, compared to C15A, C25A has also shown to have higher affinity to PLA [100]. According to the manufacturer, C15A, N5 and N8 involve similar organic modifiers and the main differences between them are the modifier contents and *d*-spacing values. Reminiscently, according to the XRD patterns, lower affinity of these clay types resulted also in lower degree of intercalation. Thus, dispersion of the filler and mechanical properties are highly affected by the intermolecular affinities of organic modifier with the polymer matrix even at low concentrations, i.e., 2 wt. %.

Positive effect of addition of nanofiller on the tensile modulus is clearer in ternary nanocomposites. Modulus reductions due to blending are highly compensated with addition of 2 wt. % organoclay for each sample. This is owing to the stiffening effect of the clay nanoplatelets which promotes chain immobilization [141, 144, 145, 146].

The most interesting results obtained from tensile tests are probably the elongation at break values. Neat PLA is known to elongate not more than 10% indicating that it is hard and brittle. Figure 4.34 shows the changes of elongations of binary blends and binary and ternary nanocomposites. Blending with E-GMA resulted almost 8-fold increase in elongation at break. However, blending with E-BA-MAH caused reduction in elongation. Ternary nanocomposites containing E-BA-MAH also failed at very low elongations, such that all of these nanocomposites failed at a lower percent elongation value compared to neat PLA. Petersson et al. [147] reported decreases in elongation at break of PLA/organically modified layered silicates with the addition of maleic anhydride grafted PLA (PLA-MA) to the nanocomposites. For example, elongation at break of PLA/bentonite nanocomposite with 5 wt. % clay decreased from 46% to 9% with the addition of PLA-MA. This decrease was from 70% to 32% for PLA/hectorite nanocomposite. Previously presented SEM images of PLA/E-BA-MAH binary blend and PLA/E-BA-MAH/organoclay nanocomposites involve considerably larger rubber droplets in their structure. Average droplet sizes of E-BA-MAH containing samples are almost 1.4-fold larger than the ones containing E-GMA. The change in morphology might be the reason of these drastic decreases in elongation at break values.

It is well known that the addition of stiff reinforcements can reduce the elongation at break of the matrix, because the reinforcements will cause stress concentrations. However, this is not the case in PLA/organoclay nanocomposites produced in this study. Contrarily, all clay types increased the percent elongations even at higher level than blending with E-GMA. For PLA/organoclay nanocomposites, increases in elongation values are also reported in literature. For example, Chang et al [148] claimed that the elongation at breaks of PLA increased with the introduction of an organoclay and with increasing organoclay content. However, 3 wt. % of organoclay loading corresponds to a maximum value, giving a 36 – 49 % increase in the

elongation at break. Thus, it was concluded that in a certain organoclay content range, the introduction of organoclay will lead to both strengthening and toughening of the PLA matrix. This may be regarded as a feature of nanocomposites. A further increase in the organoclay content leads to a decrease in the elongation at break. In that study [148], elongation at break started to decrease after 4 wt. % clay loading. Until a certain loading, both the small clay tactoids and the exfoliated/intercalated structures can be aligned during injection molding and also during tensile testing. This alignment in the direction of extension may also help distribution and transfer of load between the matrix and the filler, resulting in an increase in elongation. However, at higher filler contents, mobility of the constituents might decrease, causing a reduction in elongation at break.

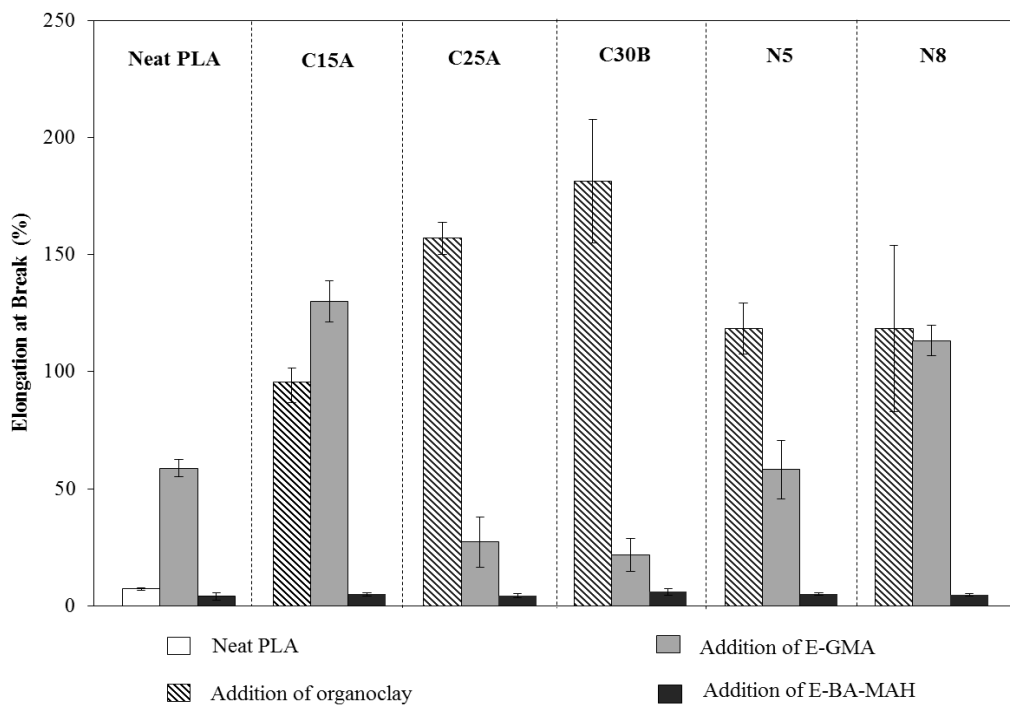


Figure 4.34 Effect of organoclay and compatibilizer types on percent elongation at break

For the samples in which E-GMA is used as the rubbery phase, the elongations of samples containing C15A, N5 and N8 are significantly higher than the elongations of other clays. XRD patterns of E-GMA containing ternary nanocomposites showed that C25A and C30B reached higher degrees of intercalation. Additionally, SEM micrographs of these nanocomposites suggest that in these nanocomposites clay nanoplatelets are more probably located at the interface between the matrix and the rubber droplets. These situations might prevent the alignment of silicate layers in the direction of extension, lowering the final strain at break.

Unnotched Charpy impact strength of neat PLA, PLA binary blends and PLA nanocomposites are shown in Figure 4.35. The unnotched impact strength is a measure of the energy to initiate and propagate a crack, in other words resistance to crack initiation and propagation [149]. Incorporation of 2 wt. % clay into the polymer matrix caused a minor decrease in the impact strength, independent of the type of clay. SEM images of the binary nanocomposites involved smaller cracks compared to that of neat PLA surface. However, as discussed before, deflection of the cracks obviously did not act as barriers to stop crack propagation and did not increase the energy absorbed.

The binary blends reached the highest impact strength values such that blending with E-GMA and E-BA-MAH resulted in increases of 1.5 and 1.4-fold compared to neat PLA. The mechanical properties and the morphological studies revealed that the interaction between different compatibilizers and PLA resulted in different structures and properties such that the clay dispersions, droplet sizes and tensile properties are very distinct in the presence of different rubbers. Although, they resulted in different structures; the reactive interaction between both rubbers and the polymer matrix was proven by FTIR results. The copolymer formed at the interface of the two phases, as a result of the reaction that occurred during extrusion, acts a bridge which transfers the load and increases the toughness [129, 135]. Furthermore, ellipsoidal shape of the vacuoles that remained on the fracture surface (presented in Section 4.1.2.1) indicates that there is good interaction between the dispersed phase and the matrix such that the impact load is shared between the phases. Otherwise, the droplets would probably have spherical shapes.

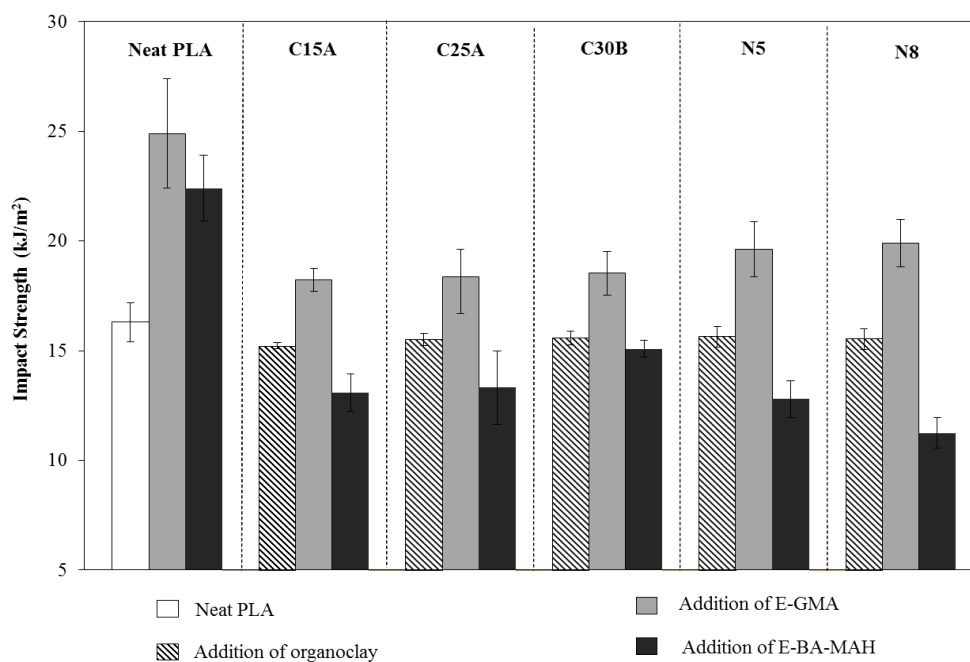


Figure 4.35 Effect of organoclay and compatibilizer types on impact strength

Impact strength values of ternary nanocomposites containing E-GMA are all higher than that of neat PLA, but lower than that of the binary PLA/E-GMA blend. The trends of E-BA-MAH containing nanocomposites are similar, but all of these samples resulted in a reduction compared to that of neat PLA. The improvement of impact strength by blending with block copolymers is directly related to the size of the dispersed elastomeric domains in the polymer matrix. Usually, as the domain size increases the impact strength increases owing to lower stress concentration effect of the domains. However, the domain size should not be too high to obtain high toughness, because large domains form large cavities that cannot stop the crack propagation. Image analyses of SEM micrographs showed that the droplet sizes of E-GMA and E-BA-MAH are significantly different than each other. Namely, E-BA-MAH droplets are almost twice the E-GMA droplets, both in binary blends and ternary nanocomposites. This difference in rubber domain sizes and the incompatibility of E-BA-MAH, which is observed in almost all material properties, are the main reasons of reduced impact strength values.

4.1.2.4 Rheological Analyses

Time Sweep Measurements

The melt stability of the nanocomposites can be determined via time sweep measurements at constant frequency and strain amplitude. Figure 4.36 shows the change of the storage modulus curves of processed neat PLA and its blends with respect to time. Decreases in storage modulus values after 15 minutes of testing are 16, 6 and 12% for PLA, PLA/E-GMA and PLA/E-BA-MAH, respectively, indicating that blending affects thermal stability positively. Additionally, decreases in storage modulus of PLA and PLA blends can be said to be reasonable when no thermal stabilizers were used [150, 151]. Although not shown here, the decreases in storage modulus curves of layered silicate filled nanocomposites are observed to be smaller owing to the increased thermal stability of polymer-layered silicate nanocomposites [5, 2]. As a result, in order to be sure that the samples have a stable viscoelastic response, the frequency sweep tests that were carried on later were limited to 10 minutes.

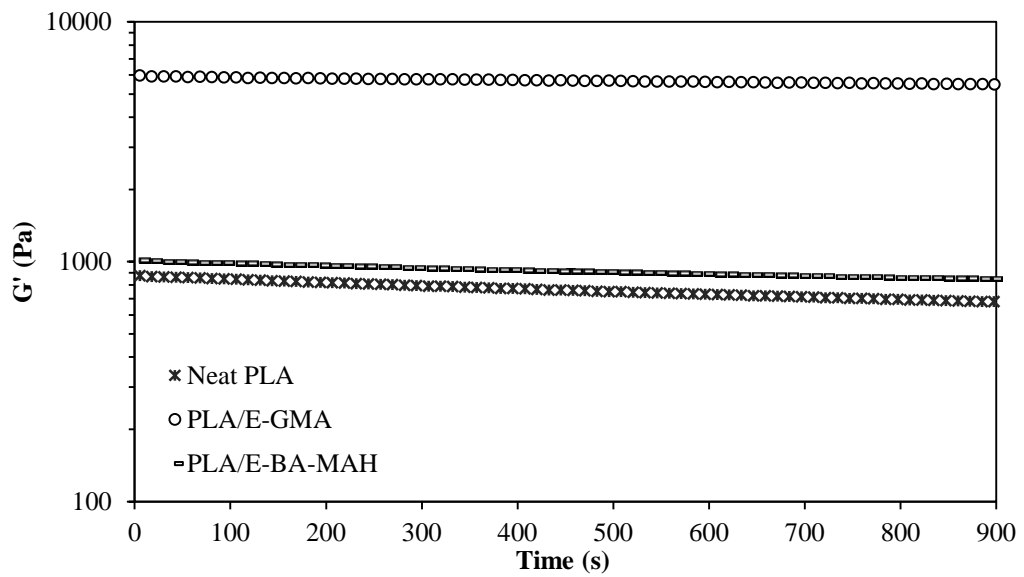


Figure 4.36 Time sweep curves of processed neat PLA, and PLA/E-GMA and PLA/E-BA-MAH blends at 170°C, at 5% strain amplitude and 10 rad/s

Strain Sweep Measurements

Strain sweep test is important to determine the Linear Viscoelastic Range (LVR) of materials. Frequency sweep tests should be conducted in the LVR. Figure 4.37 shows strain sweep curves of neat PLA and its binary and ternary nanocomposites for only one organoclay type, C25A, as an example. Even though actual values are different, trends for all clay types are quite similar.

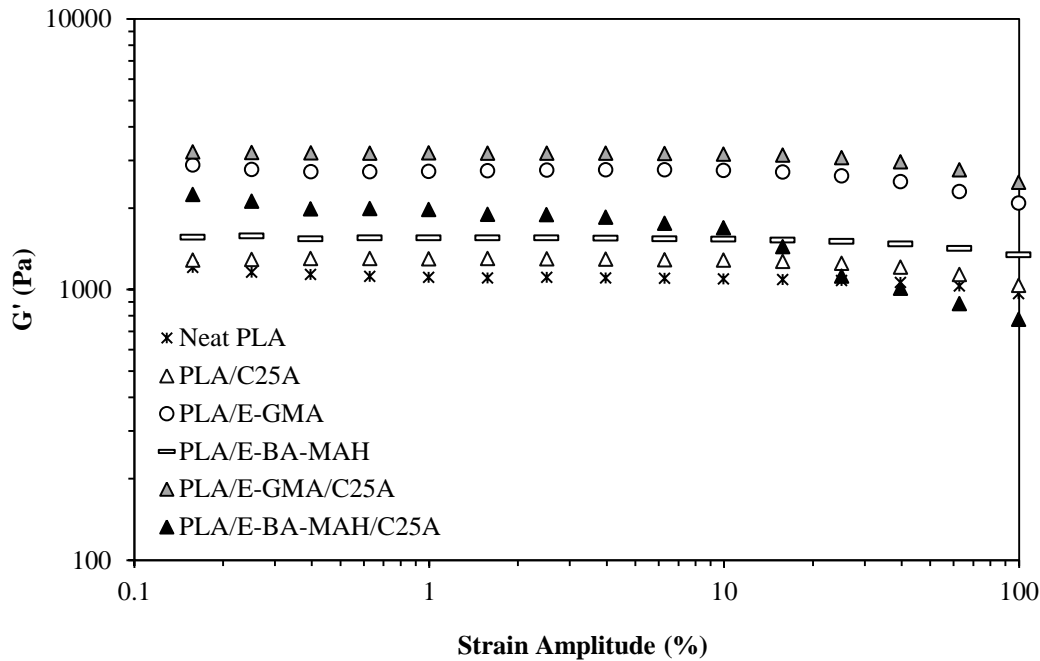


Figure 4.37 Strain sweep curves of processed neat PLA, PLA blends and, binary and ternary nanocomposites produced with C25A

Since the filler loading is relatively low, a critical strain value at which a pronounced nonlinear behavior starts could not be clearly observed, but there is a slight decrease in storage modulus at higher strain amplitudes. Such behavior can be considered as a characteristic of polymer-layered silicate nanocomposites, and it is prominent at high loadings [2, 152]. In the linear range, applied strain is not enough to disturb the microstructure, but as the strain increases layered silicates start to align in the direction of shear, paving the way of polymer chains to flow. Blends and ternary nanocomposites have higher storage modulus values than that of the simple nanocomposites, but the nonlinear behavior is observed more clearly in the blends and ternary nanocomposites. Especially PLA/E-BA-MAH/C25A showed an abrupt change in the limit of non-linearity compared to its binary combinations. Nanocomposites with different types of organoclays were investigated similarly. In terms of the limit of linearity, all nanocomposites resulted in a similar trend but with different orders of magnitudes of rheological properties due to the varying polymer matrix-compatibilizer-modifier interactions in the microstructure.

Frequency Sweep Measurements

Frequency sweep measurements were performed at a common strain amplitude (5%) at which all of the nanocomposites are within their LVR. Figure 4.38 and Figure 4.39 show G' and G'' data of PLA nanocomposites containing different organically modified clay types. Even though all the nanocomposites show the same trend, small differences provide evidences about the modifier-matrix interactions. There are no obvious changes in the slopes of the curves, either in low or high frequencies, compared to those of processed neat PLA. In fact, drastic increases in solid-like behavior can be seen at elevated filler loadings due to the formation of a network structure. At the current filler loading, storage modulus of nanocomposites containing C25A and C30B are only slightly higher than that of the neat PLA. Compatibility of these clays with the polymer matrix was also supported by the XRD patterns obtained in this study and the previous studies reported in the literature [100, 142]. Therefore, these clay types are more likely to form network structures resulting in enhancement in solid-like behavior. Nanocomposite containing N5 attained almost the same modulus values as neat PLA did, whereas in the presence of C15A and N8 modulus values are lower than that of the neat polymer at all frequencies. Since the rheological behaviors of nanocomposites are influenced by the intercalation of the polymer and formation of interconnected structures, enhancements in dynamic modulus values are expected for C25A and C30B.

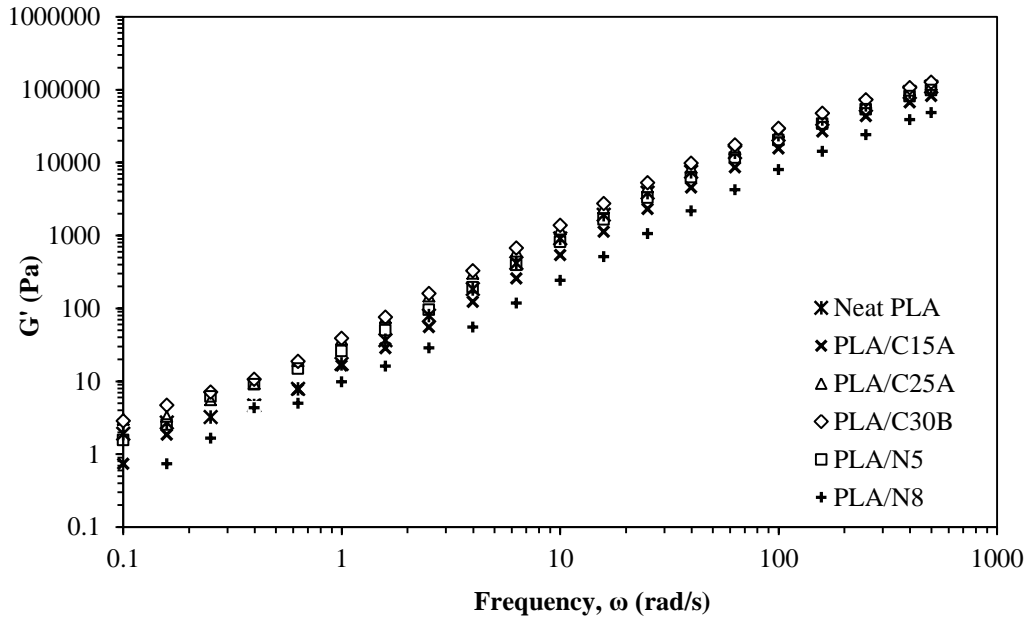


Figure 4.38 Storage modulus as a function of frequency for PLA/organoclay nanocomposites produced with different clay types

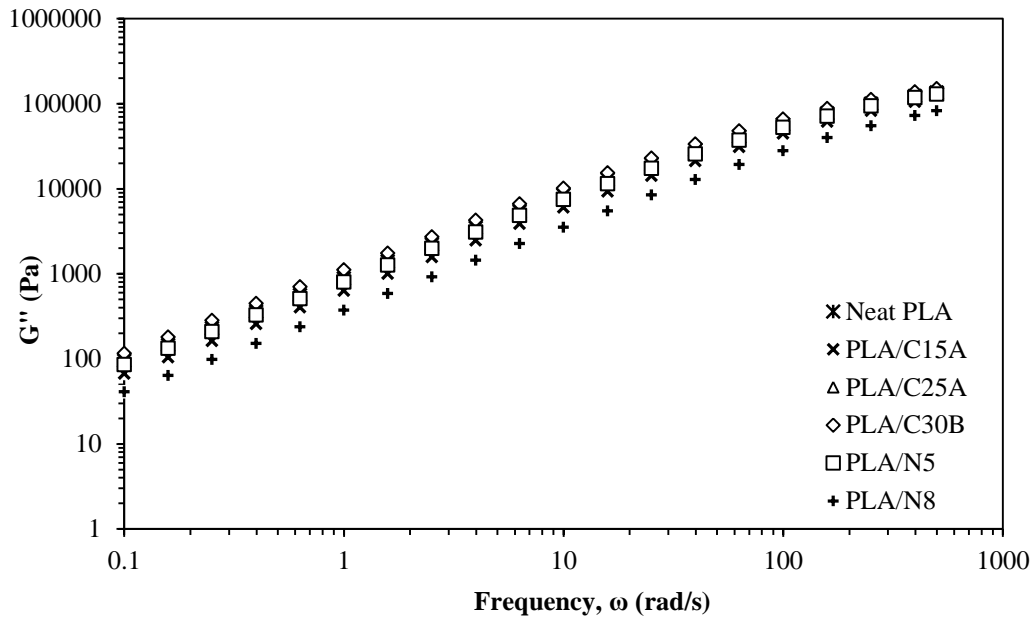


Figure 4.39 Loss modulus as a function of frequency for PLA/organoclay nanocomposites produced with different clay types

Changes in G'' are less pronounced, but the complex viscosity reveals the alterations more evidently (Figure 4.40). Usually, the consequence of adding fillers on rheological properties is an increase in the melt viscosity. However, in this study, 2 wt. % clay loadings resulted in lower complex viscosity for some clay types. It is not a coincidence that these reductions are encountered with C15A, N5 and N8 containing nanocomposites. Similar modifier structures with different modification levels and hallow tail contents of these three clay types resulted in viscosity reductions at different levels. Additionally, such decreases in viscosities of nanocomposites were seen in literature at low clay loadings [152].

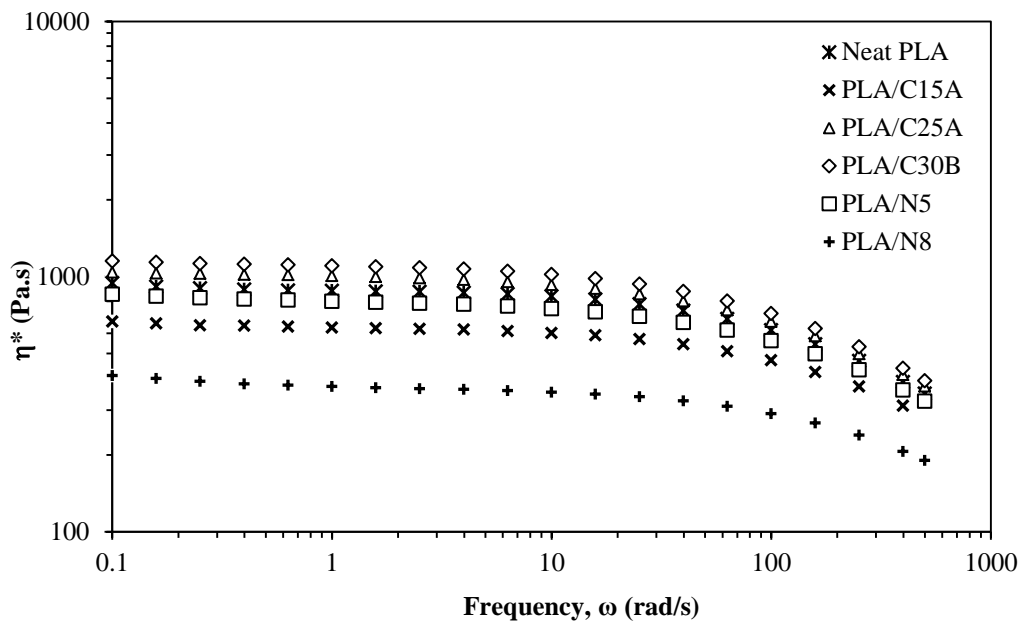


Figure 4.40 Complex viscosity as a function of frequency for PLA/organoclay nanocomposites produced with different clay types

Based on the binary nanocomposites' rheological behavior, clay types can be classified under two groups. C25A and C30B resulted in higher interaction with the polymer matrix reaching higher degrees of intercalation and improved dynamic modulus and viscosity values. However, C15A, N5 and N8, with their similar modifier structures, resulted in lower degree of intercalation and reductions in the

complex viscosity. The reason for the latter case may be the incompatibility of the modifier-matrix system resulting in stacks of silicate layers which could align easily even at low frequencies. This is, in fact supported by the low magnification TEM results where clay stacks of N5 are larger than C25A.

Addition of the ternary phase was carried out for both groups of clays. There are mainly two reasons for adding a rubbery phase to the nanocomposite system. First, it is expected to act as a compatibilizer between the clay surface and the polymer matrix. Secondly, in practical applications of the nanocomposites, if selected properly, the presence of a rubbery phase provides superior mechanical properties. Effects of adding two different types of rubbery compatibilizers were examined again for C25A and N5 nanocomposites. Figure 4.41 shows the storage modulus curves of nanocomposites with C25A. In order to follow the effect of addition of both filler and compatibilizer step by step, curves of neat PLA and its binary blends are also shown.

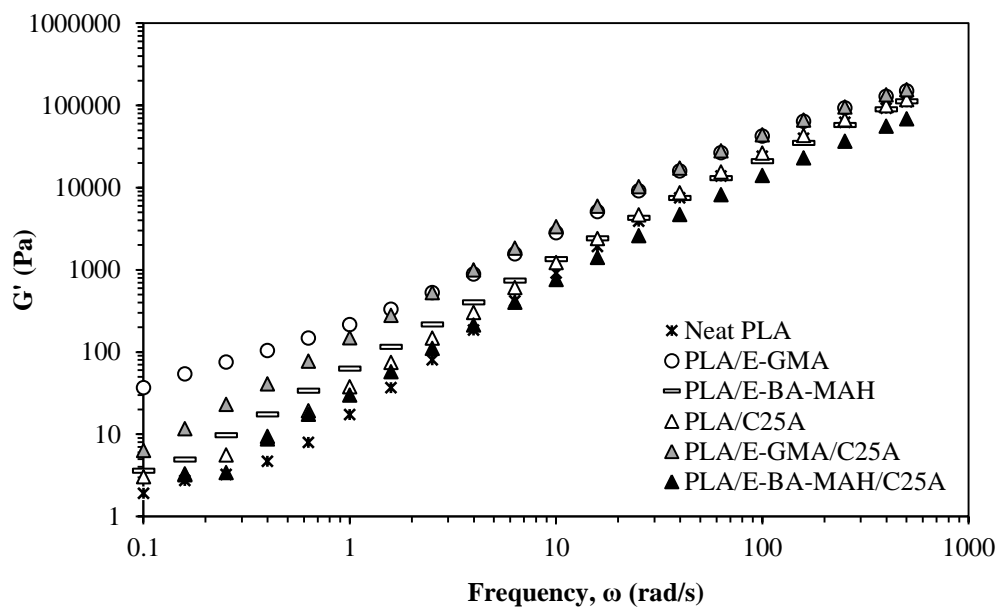


Figure 4.41 Storage modulus as a function of frequency for neat PLA, PLA blends and, binary and ternary nanocomposites produced with C25A

In the low frequency region, PLA/E-GMA blend and its nanocomposite resulted in considerably higher modulus values. Especially the slope of PLA/E-GMA blend changes significantly with an elevated elastic behavior. Addition of the nanoclay to PLA/E-GMA system reduced the solid-like behavior in the low frequency region. In the presence of organoclay, the reaction between PLA and compatibilizer could be limited due to the preferential placement of the silicate layers on the interface of the matrix polymer and the elastomeric phase. In PLA/E-BA-MAH blend, increase in solid-like behavior was not that high; it is even lower than that of PLA/E-GMA/C25A nanocomposite. This might be due to higher reactivity of the epoxide group of GMA towards the functional end groups of PLA (hydroxyl and carboxyl groups) in comparison to the MAH functional group. Decrease in G' in the low frequency region was also seen with the addition of C25A to PLA/E-BA-MAH blend. In the high frequency region, G' of all the nanocomposites were quite similar, indicating that the addition of nanoclay had no substantial influence on the short-range dynamics of the blend and the chain relaxation modes are almost independent of the presence of the silicate layers [152, 153]. G'' curves also exhibit comparable modulus values at higher frequencies, supporting the previous interpretation (Figure 4.42). Reflection of the changes in both dynamic moduli of nanocomposites to the complex viscosities can be seen in Figure 4.43. Interestingly, PLA/E-BA-MAH/C25A has the lowest viscosity values, whereas viscosity of the PLA/E-BA-MAH blend is almost unchanged compared to that of neat PLA. The reason might be the increased chain mobility and alignment of silicate layers easily due to weak interactions in the ternary system. On the contrary, PLA/E-GMA and its nanocomposite have high viscosity values through the whole frequency range which can be attributed to higher compatibility of E-GMA with PLA and successful reactive blending achieved in melt extrusion. Enhanced melt viscosity could be attributed to the flow restrictions due to the strong interaction between PLA-compatibilizer-organoclay system. Newtonian plateau in the low frequency range disappeared in the nanocomposites and it is followed by a shear thinning behavior.

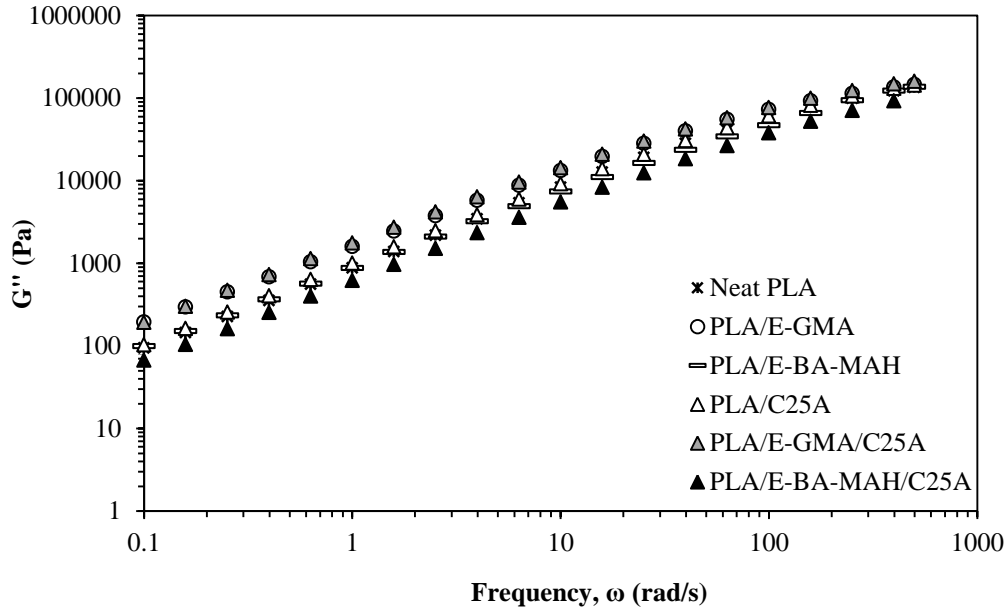


Figure 4.42 Loss modulus as a function of frequency for neat PLA, PLA blends and, binary and ternary nanocomposites produced with C25A

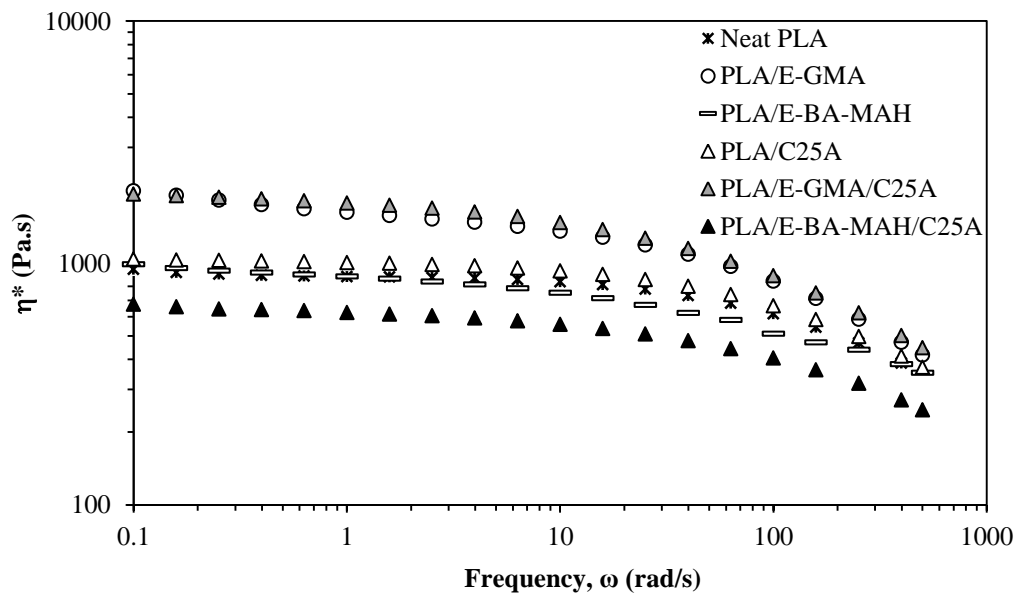


Figure 4.43 Complex viscosity as a function of frequency for neat PLA, PLA blends and, binary and ternary nanocomposites produced with C25A

Even though the degree of clay dispersion and binary nanocomposite rheological behaviors are different, N5 nanocomposites revealed very similar traces to C25A nanocomposites in terms of storage modulus (Figure 4.44). Solid-like behavior of PLA/E-GMA blend reduced with the addition of nanoclay and G' of all binary and ternary nanocomposites are below the PLA/E-GMA blend. Both dynamic moduli curves reach approximately the same values indicating that the chain relaxation nature of nanocomposites depends barely on the presence of layered silicates (Figure 4.44 and Figure 4.45).

Melt viscosity of N5 nanocomposites (Figure 4.46), on the other hand, exhibit the effect of compatibilizer structure. Independent of the presence of N5, addition of E-GMA resulted in enhanced melt viscosity values. Accordingly, effect of blending, when successful reactive blending is achieved, is to suppress the effect of the modifier compatibility at low filler contents.

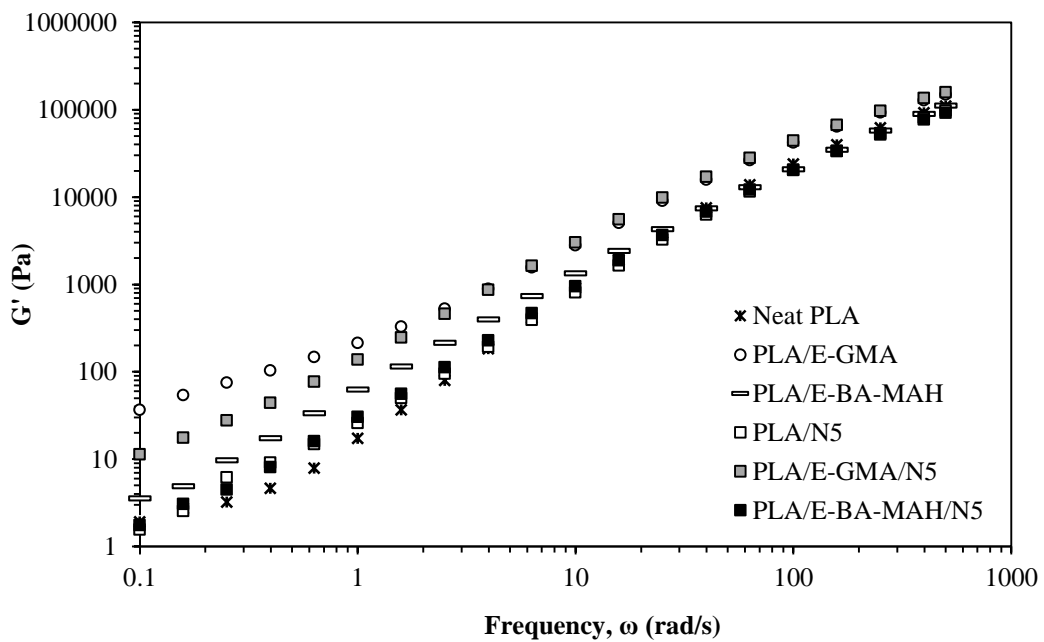


Figure 4.44 Storage modulus as a function of frequency for neat PLA, PLA blends and, binary and ternary nanocomposites produced with N5

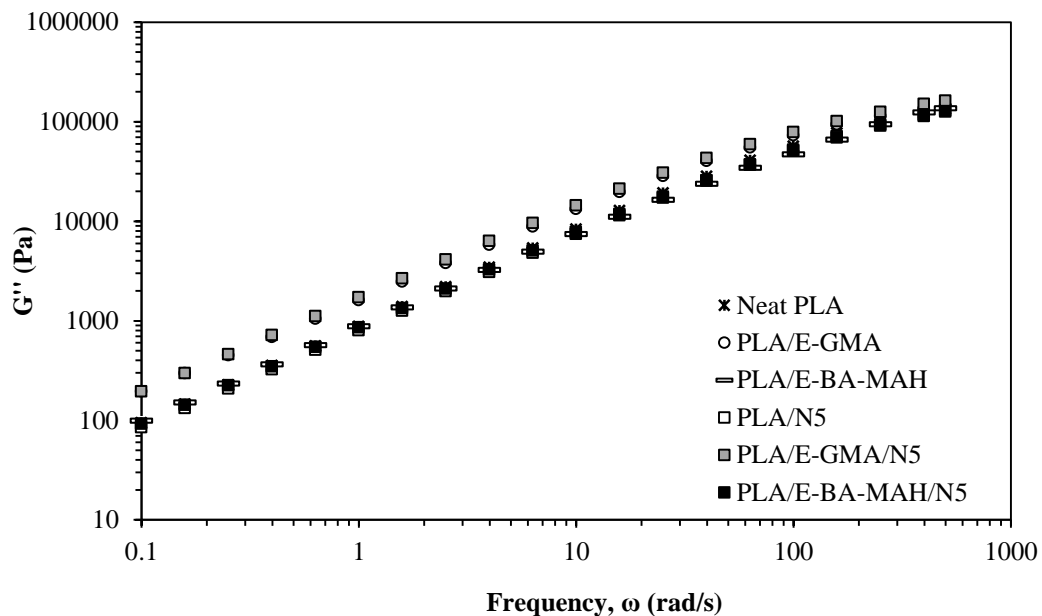


Figure 4.45 Loss modulus as a function of frequency for neat PLA, PLA blends and, binary and ternary nanocomposites produced with N5

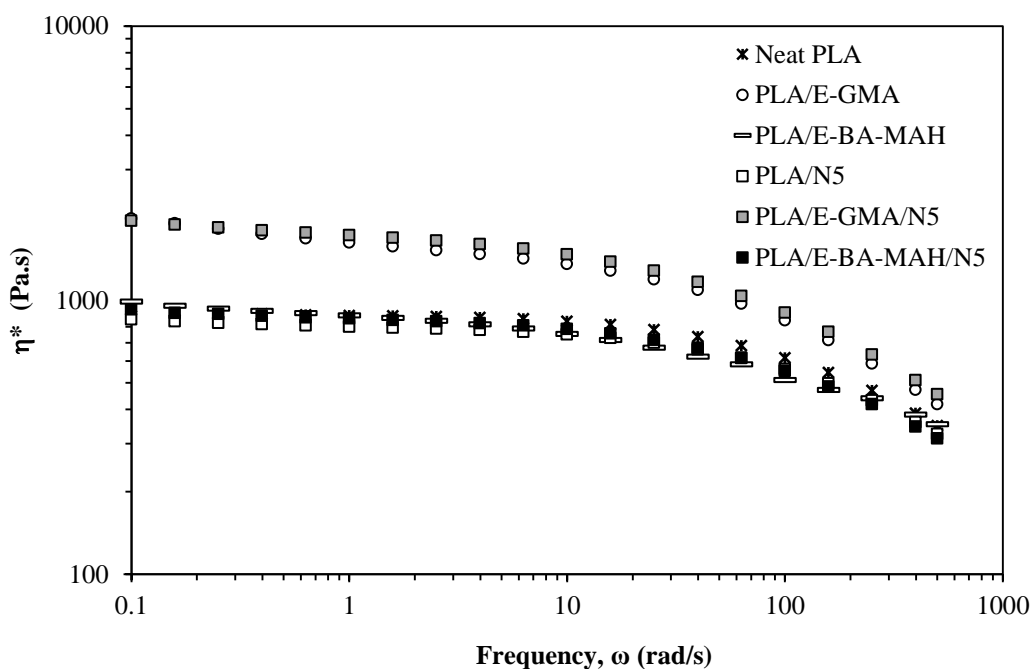


Figure 4.46 Complex viscosity as a function of frequency for neat PLA, PLA blends and, binary and ternary nanocomposites produced with N5

4.1.2.5 Thermal Analyses

Thermal properties of neat PLA, PLA/compatibilizer binary blends, PLA/organoclay and PLA/compatibilizer/organoclay nanocomposites were investigated using DSC. Thermal properties, especially the changes in glass transition temperature and degree of crystallinity, give information about the material properties. Changes in the glass transition, for instance, provide information about the toughness of the composites, while degree of crystallinity provides information about the molecular chain configuration and the possibility of nucleation effect of compatibilizers and the fillers in the final product at the applied processing conditions. Thermal properties of the PLA nanocomposites can be seen in Table 4.4 Percent crystallinities of the samples were calculated according to Equation (2.4) using DSC curves given in Appendix C.

It is known that twin-screw extrusion leads to degradation of the PLA with chain scissions. This degradation, generating smaller chains and higher chain mobility might result in an increase in degree of crystallinity. Hence, 7% increase in crystallinity of neat PLA by extrusion can be attributed to chain scission. Oyama reported that the dispersed E-GMA in PLA played the role of nucleating agent and promoted the crystallization of the matrix [97]. In this study, PLA/E-GMA/clay nanocomposites exhibited slightly higher crystallinities compared to those of binary nanocomposites; however, the difference is not that significant. Addition of E-BA-MAH to the nanocomposites resulted in the highest crystallinity values. Weaker compatibility of E-BA-MAH with the polymer matrix and the clay nanoparticles might result in easier alignment of polymer chains due to decreased restrictions.

Another point to be noted is that T_g values of PLA/organoclay nanocomposites are slightly lower than that of pristine PLA and its ternary nanocomposites. Similar decreases are also reported in the literature [154, 155] .

Table 4.4 Thermal properties of neat PLA, PLA/compatibilizer binary blends, PLA/organoclay and PLA/compatibilizer/organoclay nanocomposites determined by DSC

Code	Content	T _g (°C)	T _m (°C)	X _c (%)
A-00	Neat PLA (unext.)	62.1	148.0	3.3
A-01	Neat PLA (ext.)	60.4	147.2	10.0
C-1	PLA/C15A	57.9	147.0	6.3
C-2	PLA/C25A	58.2	146.5	6.7
C-3	PLA/C30B	58.1	146.7	6.7
C-4	PLA/N5	58.7	146.8	6.4
C-5	PLA/N8	58.6	145.8	7.0
A-1	PLA/E-GMA/C15A	61.1	148.4	6.4
A-2	PLA/E-GMA/C25A	60.5	147.0	6.7
A-3	PLA/E-GMA/C30B	60.9	146.0	7.6
A-4	PLA/E-GMA/N5	60.1	146.8	7.6
A-5	PLA/E-GMA/N8	60.4	148.1	7.2
B-1	PLA/E-BA-MAH/C15A	60.4	148.6	9.1
B-2	PLA/E-BA-MAH/C25A	60.0	148.4	8.4
B-3	PLA/E-BA-MAH/C30B	60.6	147.8	9.9
B-4	PLA/E-BA-MAH/N5	60.7	149.4	9.4
B-5	PLA/E-BA-MAH/N8	60.1	148.0	9.3

4.2. PLA/Expanded Graphite Nanocomposites

In this part of the study, expanded graphite was used as filler material where PLA was used again as the polymer matrix. In the literature, graphite and its derivatives were shown to be promising alternatives to nanoclays to produce nanocomposites, since they have low mass density compared to the conventional fillers. Additionally, their electrical and thermal conductivities are high owing to the sp² hybridized carbons in the graphene layers [10]. As in the case of all other nanofillers, the main difficulty in manufacturing polymer/graphite nanocomposites is the dispersion and

distribution of the fillers in the polymer matrix. In the literature, three conventional techniques are mainly employed to provide good dispersion and distribution. These are in situ polymerization, solution compounding and melt blending, which are explained in detail in Chapter 2 of this dissertation. To see the effects of different production methods on the dispersion problem of expanded graphite (EG) in the polymer matrix, extrusion and solution mixing techniques were compared. In the meantime, effect of EG content in the composites and addition of E-GMA as impact modifier were investigated. To the best of our knowledge, addition of a ternary elastomeric polymer was tried for the first time in this study.

Since the expanded graphite used in this study was provided from the manufacturer as a confidential product, the technical data about it is limited. Therefore, EG studies started with the characterization of EG itself. Then, the PLA/EG composites and PLA/E-GMA/EG composites were produced and characterized.

4.2.1 Characterization of Expanded Graphite

4.2.1.1 Energy-Dispersive X-Ray Spectroscopy

EDX is an analytical technique used for the elemental analysis or chemical characterization of a sample. The methods followed by the producer to expand the graphene layers in the EG structure such as acid intercalation or alkali metal treatment might result in some impurities in the structure of EG. Only carbon and oxygen could be detected in the elemental analysis and no metal contaminants exist in the structure as shown in Figure 4.47. This indicates the formation of graphite oxide (GO) during the EG fabrication. In EDX analysis it is known that elements in low abundance will generate X-ray peaks that may not be resolvable from the background radiation [156]. This might indicate that GO formation is in very small amounts since the oxygen peak is at very low intensity compared to carbon peak.

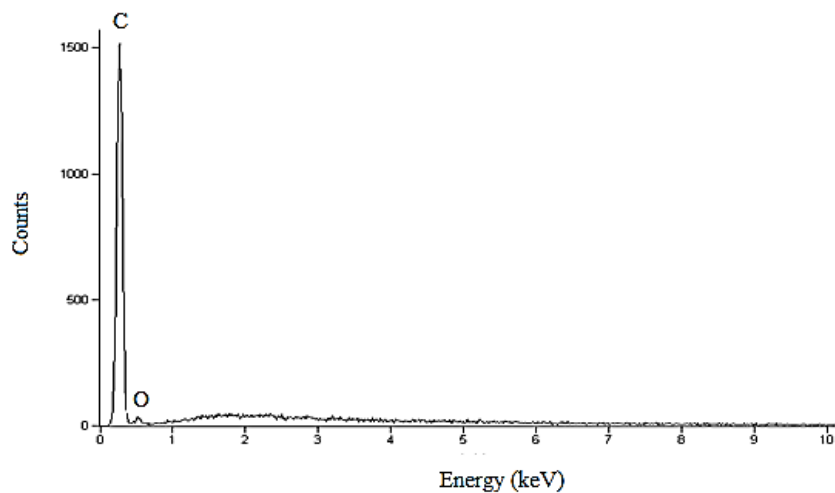


Figure 4.47 EDX spectrum of EG (Timrex® C-Therm 001)

4.2.1.2 Brunauer–Emmett–Teller (BET) Surface Area Analyses

Surface area of the filler is an important parameter, the higher the surface area the higher the polymer-filler interaction. The BET surface area analysis on Timrex® C-Therm 001 exhibited a surface area of 23.9 m²/g. This surface area is comparable to the other commercially produced products of the same manufacturer [119, 157].

4.2.1.3 X-Ray Diffraction

XRD analyses provide information about the interlayer spacing between graphene sheets comprising the graphite structure. XRD pattern of EG shows an intense peak at a 2θ value of approximately 26.5°, which is assigned to the stacking of single graphene layers at a distance of 0.335 nm (Figure 4.48). This interlayer spacing is consistent with the values reported in the literature [119, 157].

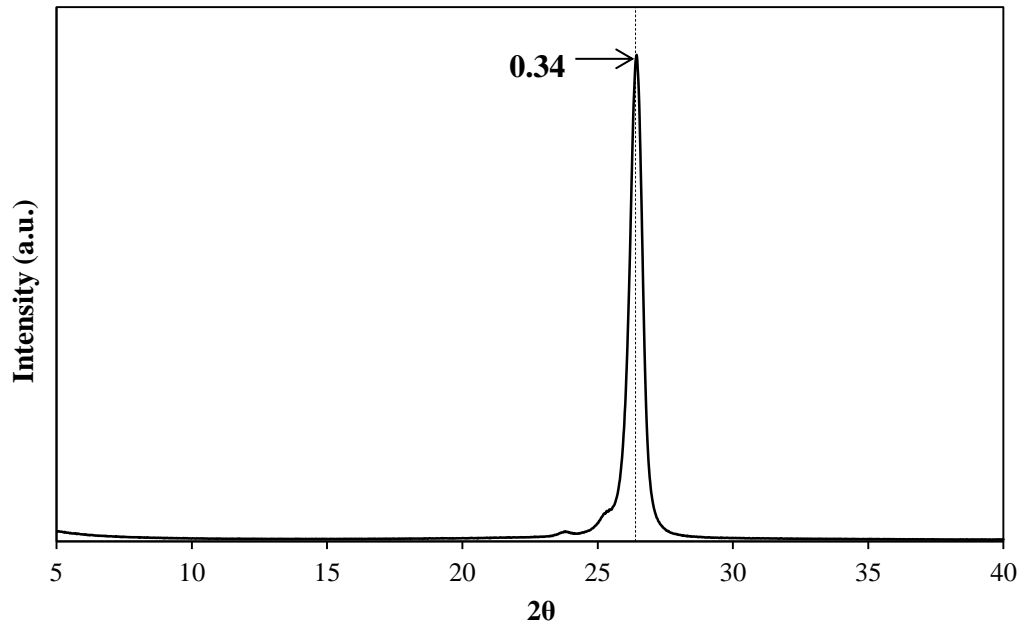


Figure 4.48 XRD pattern of pure EG (Timrex® C-Therm 001)

4.2.2 Characterization of PLA/Expanded Graphite Composites

4.2.2.1 Morphological Analyses

X-Ray Diffraction

XRD patterns are important since they provide information about the structure of polymer-filler interaction. However, in terms of quality of EG dispersion, the term ‘complete exfoliation’ has no exact meaning like in the case of OMLS. Accordingly, it was revealed that using different procedures of premixing and various processing conditions, EG mostly yields partially exfoliated graphite, because the carbon nanosheets in the structure remain interlinked with each other [158].

XRD patterns of composites are given in Figure 4.49 and Figure 4.50, showing samples produced via melt blending and solution mixing, respectively.

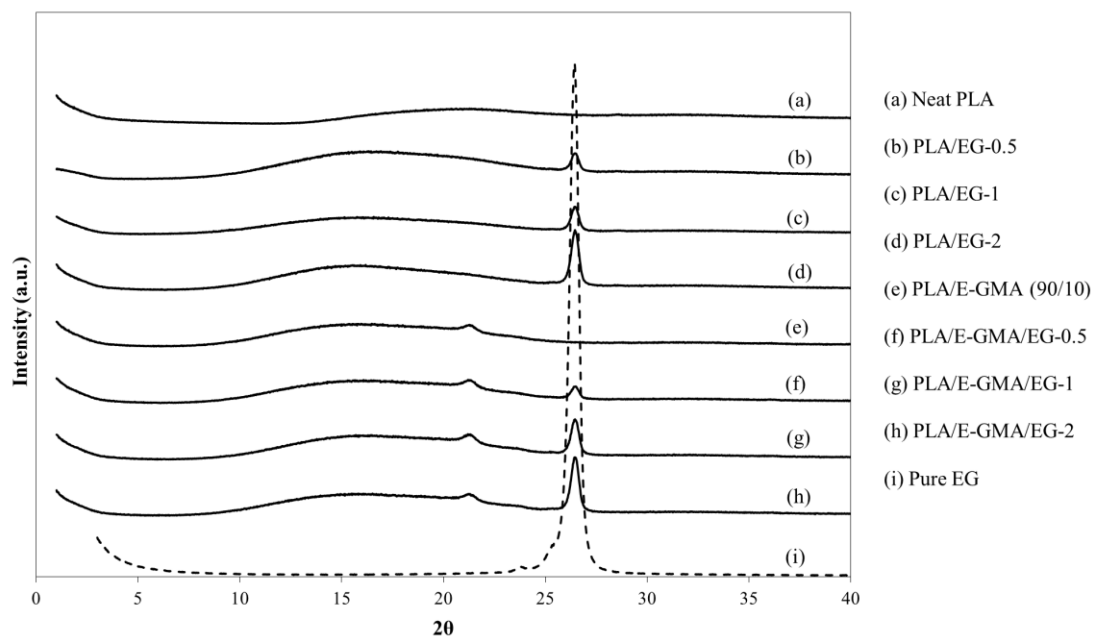


Figure 4.49 XRD patterns of PLA/EG nanocomposites prepared by extrusion

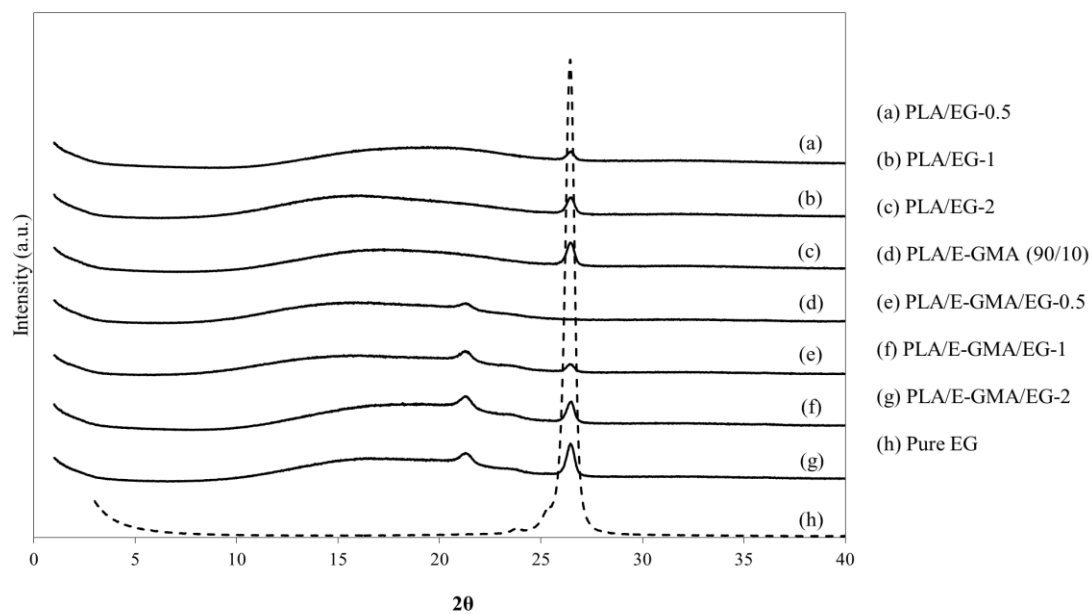


Figure 4.50 XRD patterns of PLA/EG nanocomposites prepared by solution mixing

The presence of the sharp peak at 26.5° confirms not only the presence of pure graphite based on stacks of parallel graphene sheets, but also the fact that both melt blending and solution mixing applied in this study are not able to exfoliate or completely separate the graphene layers, and some sheets still exist in aggregate form. Since EG is fragile and breaks down during blending with different polymers it is generally assumed that in polymer/EG composites it is difficult to completely delaminate the nano-filler, and even in advanced mixing conditions a dense stacking of single graphene layers still exists [157].

Reduced intensity of the peaks as the EG concentration is attributed to lower number of aggregates and graphite layers. In other words, the increased intensity recorded at higher EG content is probably due to the higher number of graphene layers organized in stacks. In short, XRD patterns confirm that with both production methods the graphite platelets remain organized at least partially in multilayers and thus, maintain their original *d*-spacing.

Addition of E-GMA has no effect on layer spacing of EG structure. In this part of the study, addition of the rubber just improves the mechanical properties of the final product. In this study, EG is used without making any modifications on the surface. This probably resulted in lack of wetting of the EG surface. E-GMA might act as a compatibilizer if the EG structure is chemically modified and better polarity matching between the filler and the rubber is achieved. In the literature, two different methods were employed for this purpose: 1- oxidative plasma treatments to populate the graphite surface with carboxyl and hydroxyl groups; 2- bonding of epoxy oligomers to the nano-reinforcements using reactive coupling agents. Both of these approaches have proven to be successful with graphite structures [159]. Modification of EG surface could be considered as a suggestion for the continuation of this study.

Scanning Electron Microscopy

As mentioned in the previous part, blending with a rubbery polymer is one of the mostly used methods to improve the toughness of a brittle polymeric material. The enhancement is mainly related to the dispersion of the rubbery phase in the polymer

matrix. In order to investigate the fracture surface and the dispersion of the rubbery phases SEM is used.

Impact fractured surfaces of the specimens were imaged, and the images at x500 and x3000 magnifications were taken for each specimen. The average size of the dispersed phase was analyzed by using Image J software program. At least two images with a magnification of x3000 were analyzed. The area of each hole in the samples was determined by using the image analysis software by transforming these holes into ellipsoids and calculating the area of these ellipsoids. Then, the average domain size (average diameter) was calculated statistically with the box plot method.

Figure 4.51 shows the dispersion of EG in the PLA matrix at the lowest concentration (0.5 wt. %) when melt blending was employed as the preparation method. At the lowest magnification (Figure 4.51–a) stacks of EG can clearly be seen. At the lowest EG concentration, PLA/EG composites mostly exhibit straight crack propagation lines. These straight lines enhance further growth and make it easier to fracture the specimen with a small amount of energy [130]. However, especially around the large stacks, small short cracks extending to different directions can be seen. The stacks seen in higher magnification images are different in size, but all are in micron scale in two directions. Therefore, it would be appropriate to consider these final products as “composites” rather than “nanocomposites”. Again in Figure 4.51, graphene sheets forming the graphite structure can be seen. There is no evidence of polymer penetration into the graphene layers supporting the XRD results.

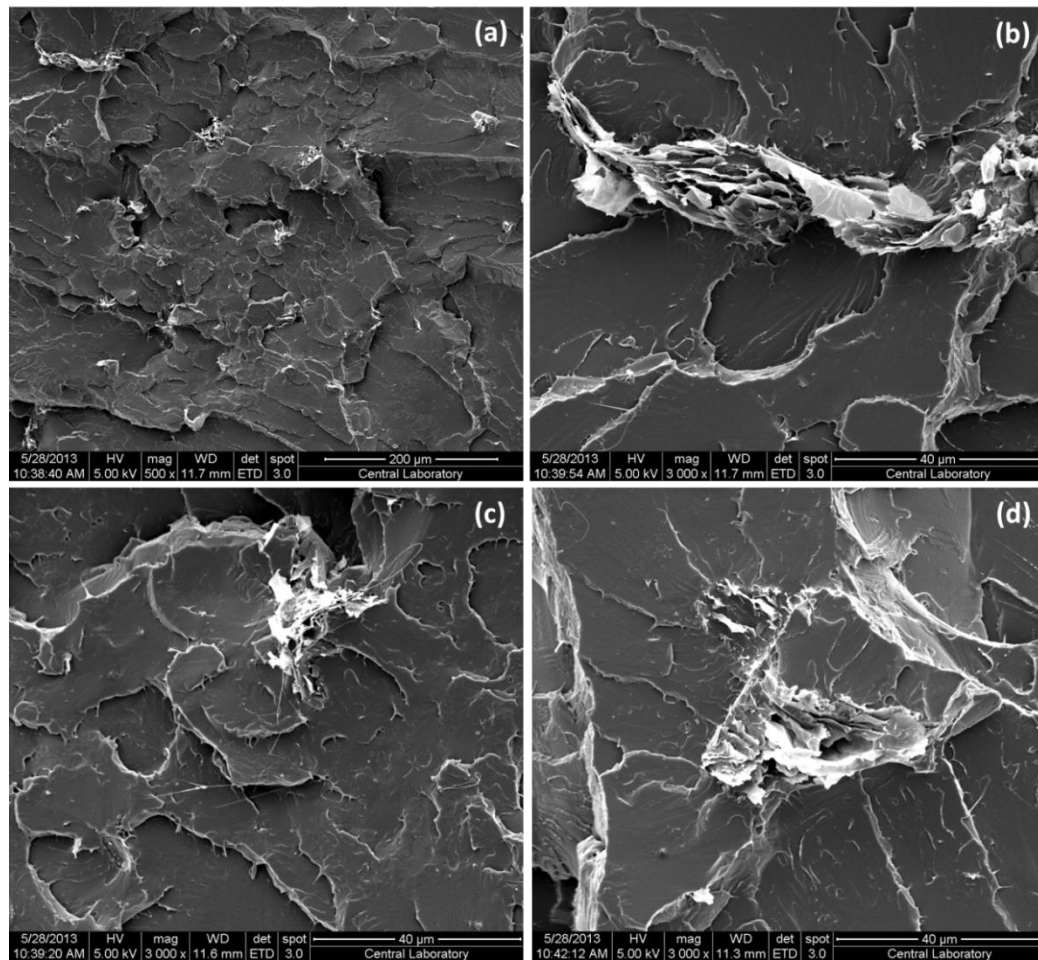


Figure 4.51 SEM micrographs of PLA/EG-0.5 prepared via extrusion at (a) x500 and (b), (c) and (d) x3000 magnifications

Figure 4.52 shows the SEM micrographs when the EG concentration is increased 4-fold. At low concentrations, it is difficult to elaborate on the EG dispersion, but at higher concentrations it is clearly seen that the EG stacks are distributed homogeneously in the polymer matrix, but the polymer chains still could not penetrate into the graphene sheets. However, the sizes of the stacks are varying as expected since EG is fragile and breaks down during blending [157]. Furthermore, the crack propagation lines are not distinct as seen in neat PLA (Figure 4.7) and in PLA/EG-0.5 binary composite (Figure 4.51). Many short cracks are seen around the stacks. The results of mechanical property investigations will be discussed in the

following sections, but beforehand it should be stated that addition of EG did not result in drastic enhancement in impact toughness compared to that of neat PLA. This means, addition of EG deflected the cracks and increased their path to some extent, but they did not act as barriers to stop crack propagation. Conversely, presence of large EG agglomerates might create weak spots due to lack of wetting of the filler surface, namely due to weak interface interactions.

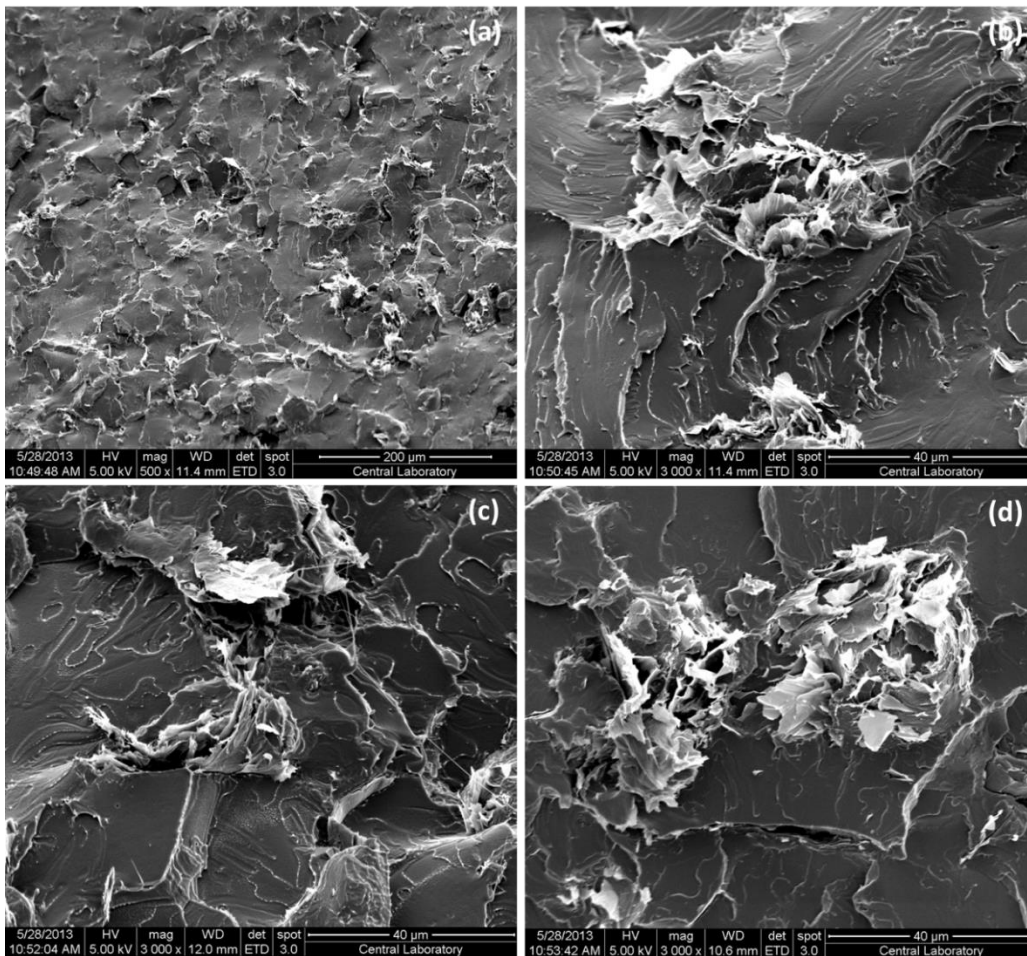


Figure 4.52 SEM micrographs of PLA/EG-2 prepared via extrusion at (a) x500 and (b), (c) and (d) x3000 magnifications

At the same processing conditions with the PLA/EG composites, PLA/E-GMA (90/10) binary blend was also produced and imaged (Figure 4.53). Etching was not applied to the samples containing E-GMA in the structure. Nevertheless, the phase separation between the PLA matrix and elastomer E-GMA can apparently be seen in samples produced by extrusion.

Phase separation between PLA and E-GMA occurs such that E-GMA forms droplets in the polymer matrix. Droplet matrix morphologies are expected to increase the toughness of the blend, but the final properties depend upon the average domain size and inter-domain distances. Small inter-particle distance suppresses craze or crack growth and facilitate the overlap of the stress fields around the adjacent rubber articles. By this way, local shear yielding is promoted and high impact energies are absorbed [160]. However, the size of the domain should be neither too small nor too big. When there is high adhesion owing to good compatibilization, ultra-fine domains of elastomers can be formed, and this structure results in low impact strength values, because crack propagation lines progress without touching the elastomer domains. Larger elastomeric domains also influence the toughness negatively, since they form large regions that could not stop the crack propagation. In this case, SEM micrograph of this blend shows evenly distributed rubbery phases with the crack propagation lines that are denser and shorter. This indicates toughening of the blend and the results of the mechanical property investigation studies will be discussed later. The radius of the distributed rubber phase is determined as 837 nm for PLA/E-GMA blend. Furthermore, shapes of the vacuoles on the fracture surface are all ellipsoidal which indicates that there is a good interaction between the dispersed phase and the matrix so that the load is successfully shared between the phases.

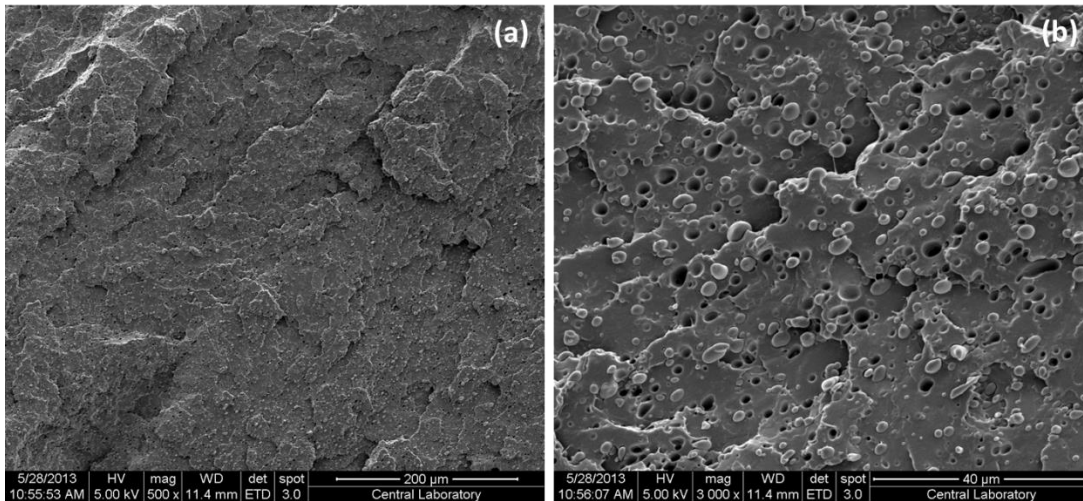


Figure 4.53 SEM micrographs of PLA/EG (90/10) binary blend prepared via extrusion at (a) x500 and (b) x3000 magnifications

Addition of 0.5 wt. % EG to the binary blend has the effects is shown in Figure 4.54. Distribution of EG seems homogeneous. However, graphite structures seen at higher magnifications are not different than in the samples in which E-GMA was not present. In this respect, SEM images support XRD results where there are no changes in the characteristic peak of EG with the addition E-GMA. Moreover, the EG agglomerations are still in micron sizes and the average radius of E-GMA droplets are 668 nm, which is 20% smaller than the droplets observed in PLA/E-GMA binary blend. Presence of large EG tactoids in the polymer matrix might suppress the rubber droplets, although the EG loading is very low.

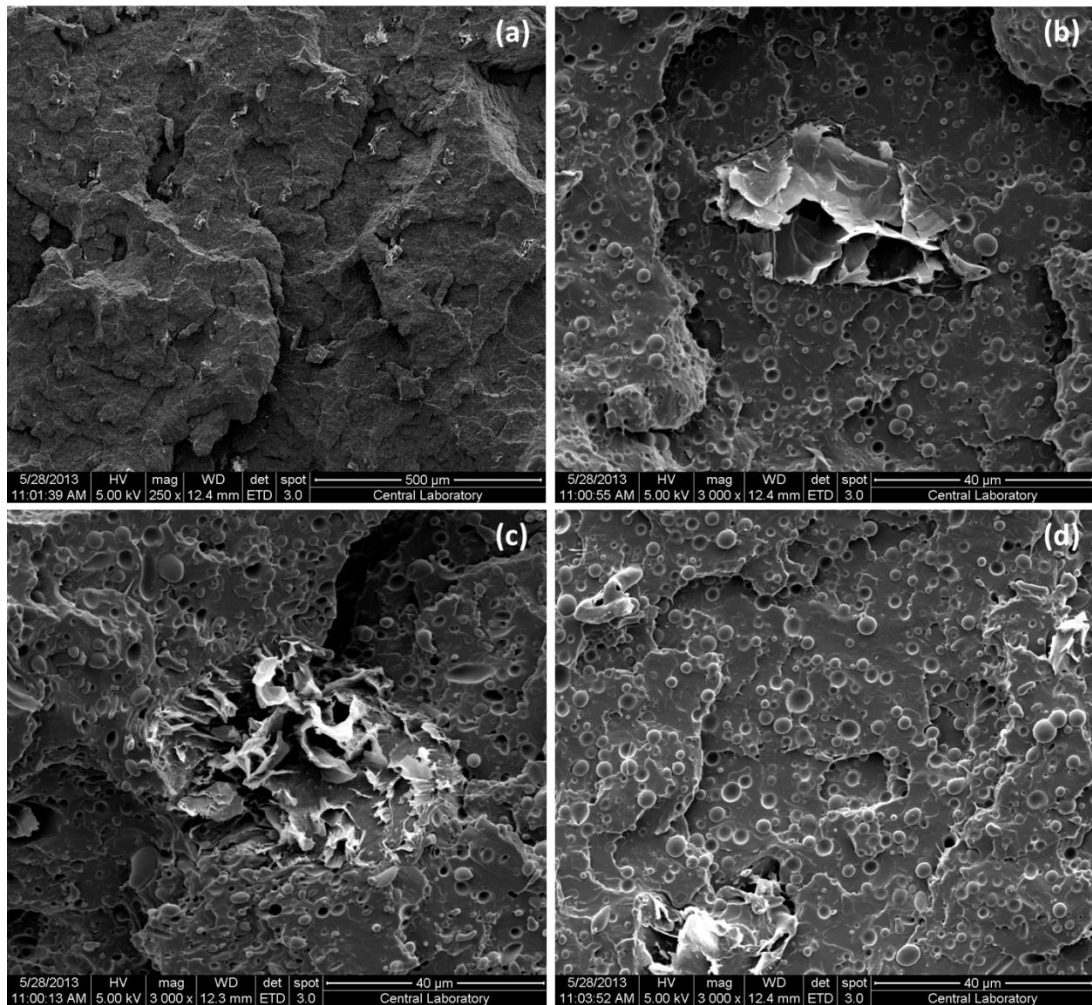


Figure 4.54 SEM micrographs of PLA/E-GMA/EG-0.5 prepared via extrusion at (a) x250 and (b), (c) and (d) x3000 magnifications

As an alternative to the melt blending method, polymer matrix, PLA, and the filler, EG, was also mixed in solution. During mixing, ultrasound was applied to the mixture as well as to the EG solution before mixing in order to enhance EG dispersion. However, XRD analyses revealed that the interlayer spacing of the EG structure was identical to the one obtained in melt blending. SEM images of the samples prepared via solution mixing are given below.

In Figure 4.55-a agglomerates of the filler can be seen. The crack propagation lines are distinct and straight. However, there are also shorter cracks especially around the agglomerates. Even though the XRD patterns of solution mixed samples are almost

identical to the complementary composites prepared by extrusion, in Figure 4.55-c and Figure 4.55-d exfoliated graphite structures are detected at low EG content. Improved mechanical properties of solution mixed samples, which will be discussed later, could be attributed to these rare but exfoliated EG structures. Fiber structures formed during shearing are seen at higher magnifications.

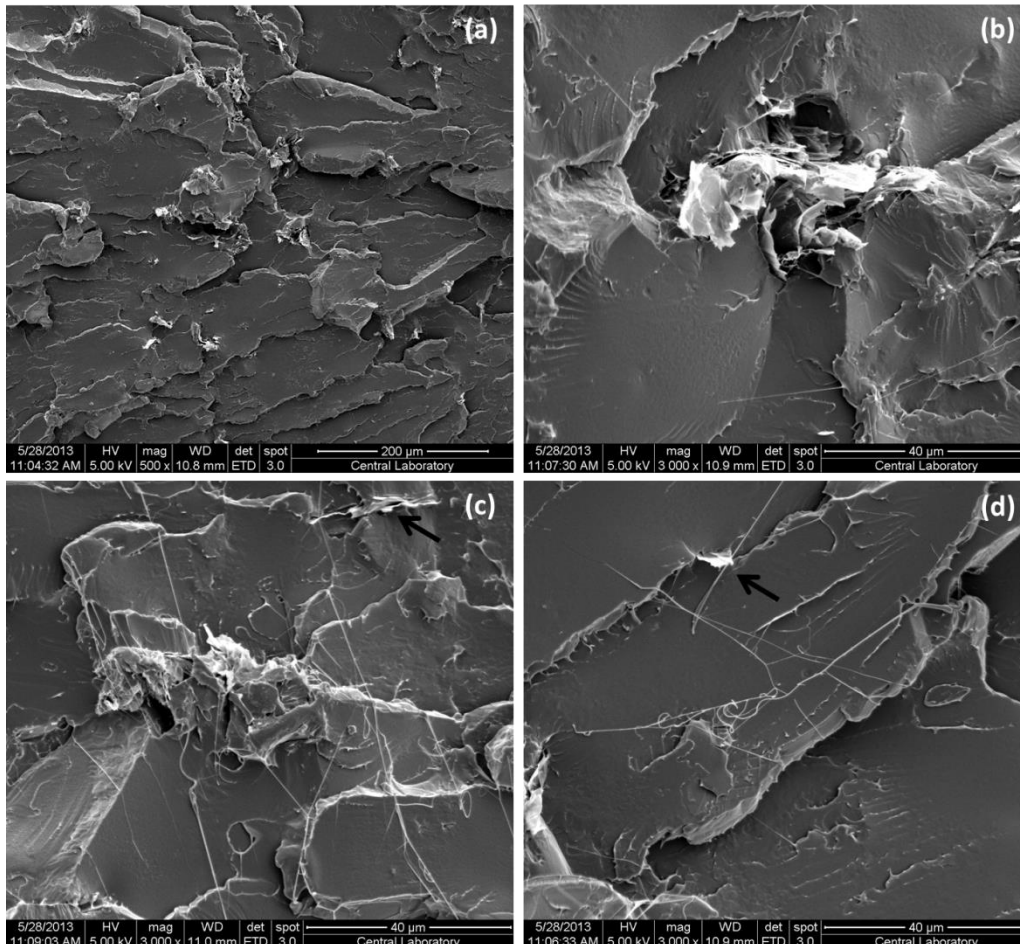


Figure 4.55 SEM micrographs of PLA/EG-0.5 prepared via solution mixing at (a) x500 and (b), (c) and (d) x3000 magnifications

When the EG concentration was increased 4-fold, similar to the extruded composites, crazing on the fracture surface becomes more obvious (Figure 4.56). Stacks of EG show similar structures both in extruded and solution mixed samples. However, in the solution mixed samples some graphite structures with lower number of graphene layers compared to the agglomerates are observed. This structure indicates that solution mixing method used in this study is partially successful to separate carbon layers in the graphite structure, but it is still not enough to totally disperse them in the polymer matrix.

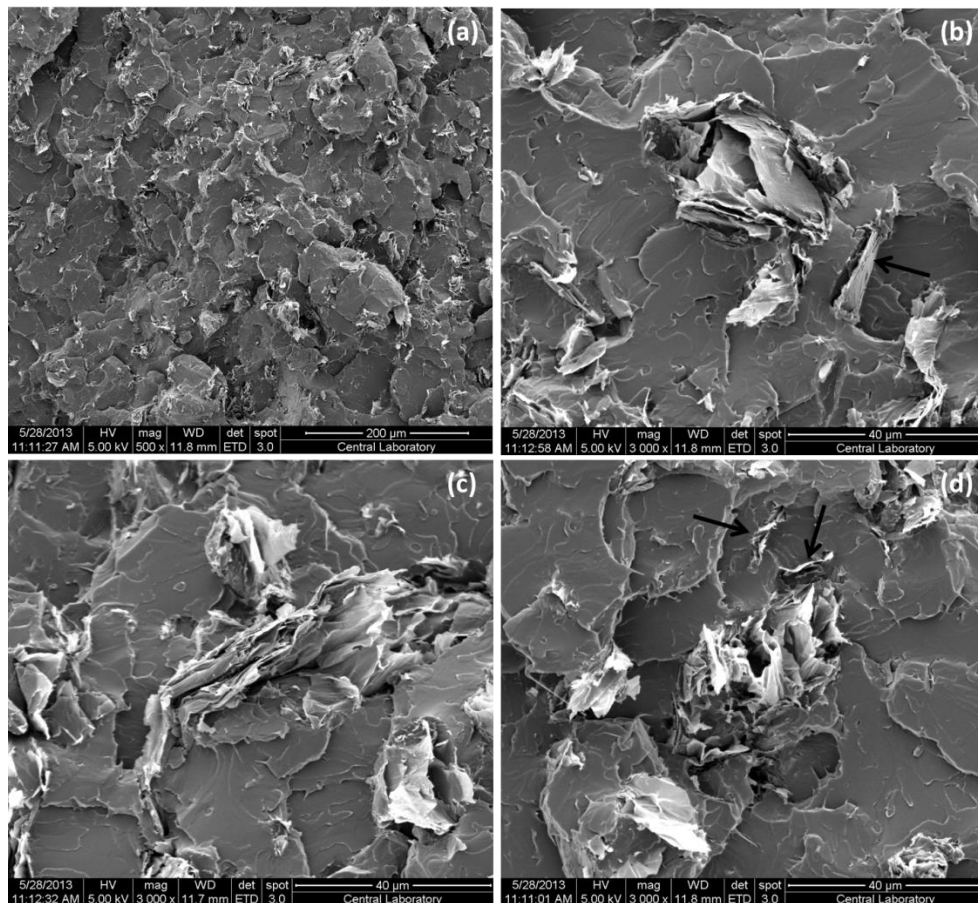


Figure 4.56 SEM micrographs of PLA/EG-2 prepared via solution mixing at (a) x500 and (b), (c) and (d) x3000 magnifications

Mixing PLA and E-GMA in a solution results in a very different morphology compared to the one obtained with melt blending. In melt blending, the rubbery phase E-GMA forms droplets in the polymer matrix. As shown in Figure 4.57 the same blend prepared via solution mixing show a continuous morphology with no visible interface between the phases. As indicated before, etching procedure was not applied to these samples. However, in the melt blended PLA/E-GMA, phase separation between the matrix and the rubber was apparent though etching was not applied.

It is generally difficult to predict the mechanical properties of a mixture, and understanding the effects of mixing is necessary. One should know the conditions under which polymers would form either a homogeneous phase or a two-phase structure. It is obvious that the thermodynamics of mixing in extrusion and solution mixing are different. The factors that affect the miscibility of two polymeric materials are: interacting surface areas, coil dimensions as a function of temperature, molar mass and concentration, molar mass distribution and free volume [161]. Each of these factors changes in different production methods. Furthermore, in melt blending, though high magnitudes of shear are applied and there is continuous mixing throughout the extruder, the polymeric materials can interact only at the interface of the coalesced droplets. In solution mixing, the possibility of interaction between the polymer matrix chains and the elastomer chains is higher. Thus, the final morphologies are different.

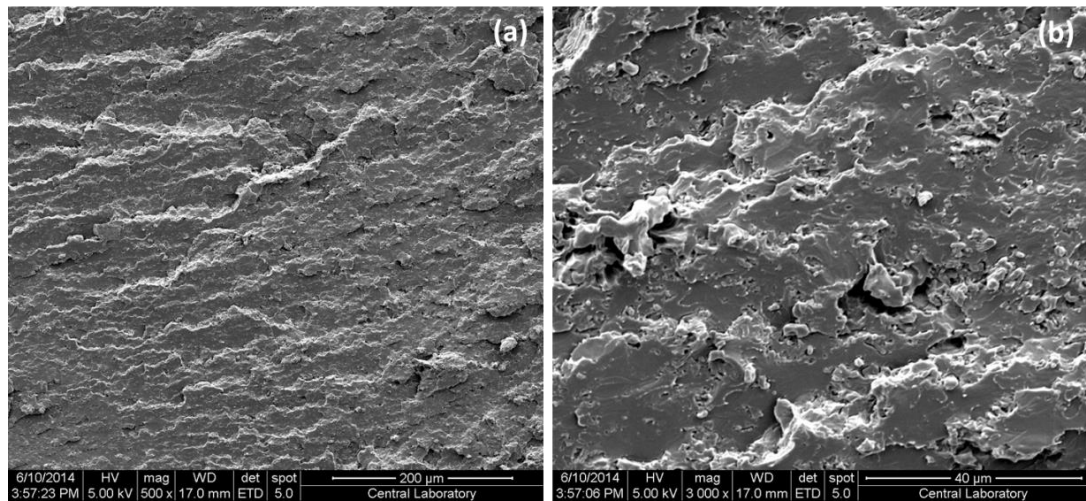


Figure 4.57 SEM micrographs of PLA/E-GMA (90/10) binary blend prepared via solution mixing at (a) x500 and (b) x3000 magnifications

Addition of EG to the PLA/E-GMA blend prepared by solution mixing did not also show any phase separation morphology (Figure 4.58). EG stacks are still in micron sizes with no evidence of polymer or rubber intercalation between the carbon layers. The single phase obtained with solution blending of PLA and E-GMA resulted in rough fracture surface indicating high energy absorbance during impact. However, compared to PLA/EG-0.5 nanocomposite prepared via solution mixing (Figure 4.55), the crack propagation lines are superficial and some small holes are observed which might cause decreases in energy absorbed in the case of an impact load.

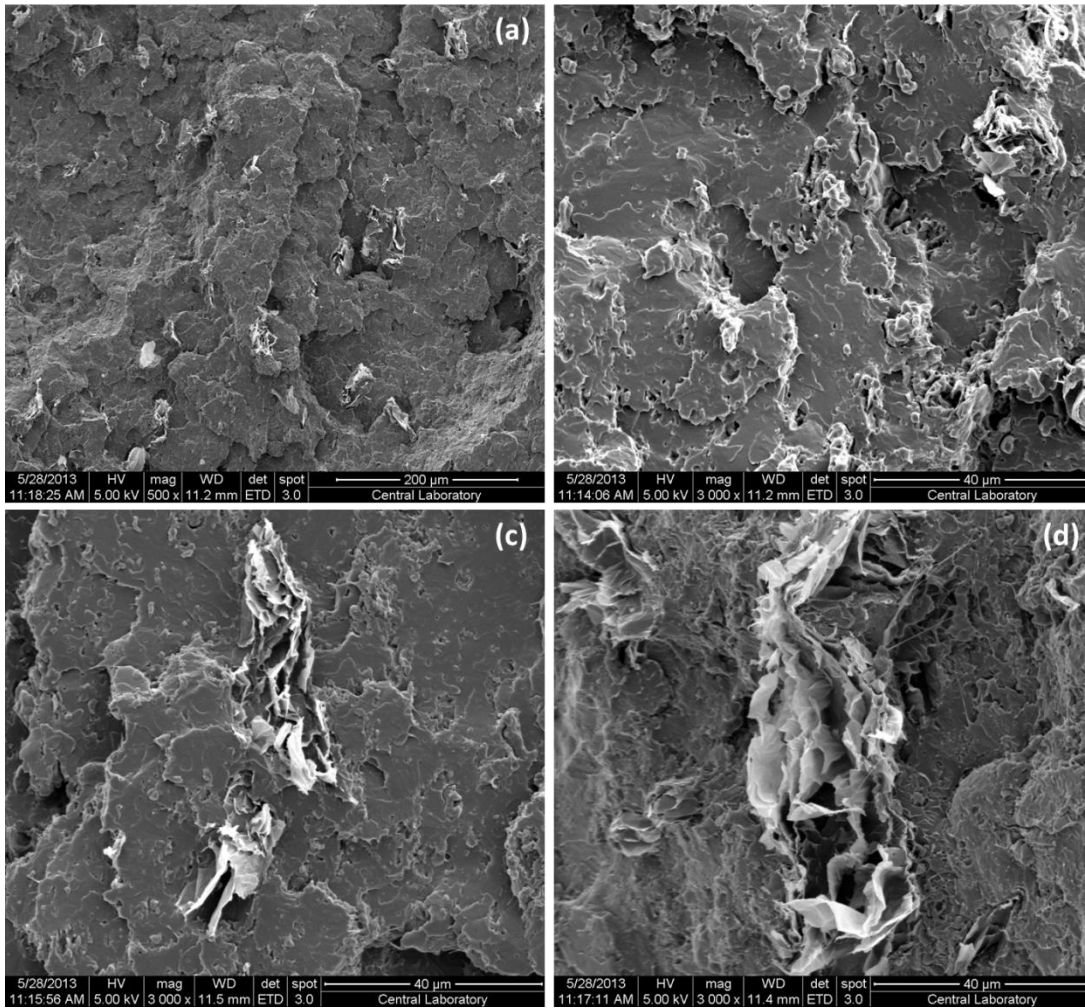


Figure 4.58 SEM micrographs of PLA/E-GMA/EG-0.5 prepared via solution at (a) x250 and (b), (c) and (d) x3000 magnifications

Transmission Electron Microscopy

PLA/EG-2 and PLA/E-GMA/EG-2 samples were selected to obtain more information on the structure using TEM. In fact, the presence of large agglomerates can be seen in SEM images presented in the previous section. Almost all of the agglomerates seen in SEM images are in micron sizes. In TEM micrographs, smaller EG structures can be seen. Figure 4.59 shows TEM micrographs of PLA/EG-2 at different magnifications. At low magnification (Figure 4.59-a) a large tactoid is observed. At higher magnifications, especially in Figure 4.59-c together with a

tactoid in sub-micron size, some single EG layers or smaller assemblies with a few number of graphene sheets can be observed.

Addition of E-GMA to PLA/EG-2 composite has no significant effect on layer separation. Similar to PLA/EG-2, both tactoids and intercalated assemblies are observed. However, for both samples prepared via melt blending, the shear applied during extrusion is not enough to totally separate the graphene layers, although a number of well dispersed single layers are observed. In both PLA/EG-2 and PLA/E-GMA/EG-2, most of the EG in the structure is still in the form of tactoids with a large number of graphene sheets positioned on one another. These sheets are obviously seen in Figure 4.59-f and Figure 4.60-f, respectively. These structures are fully consistent with the strong peak observed at 26.5° in XRD patterns.

Most of the studies on polymer nanocomposites prepared with graphite derivatives reported that direct melt mixing is not sufficient for a good dispersion of the filler material in the matrix polymer [10, 119, 157]. In literature, observation of unexpected single layer dispersions in TEM has been associated with the presence of hydroxyl, carboxyl and/or carbonyl functional groups on graphite structure that remained from the acid or high temperature treatment. These functional groups could promote hydrogen bonding between PLA and graphite [119]. In fact, this approach could be valid since presence of some oxygen in the EG structure was previously proven with EDX analyses.

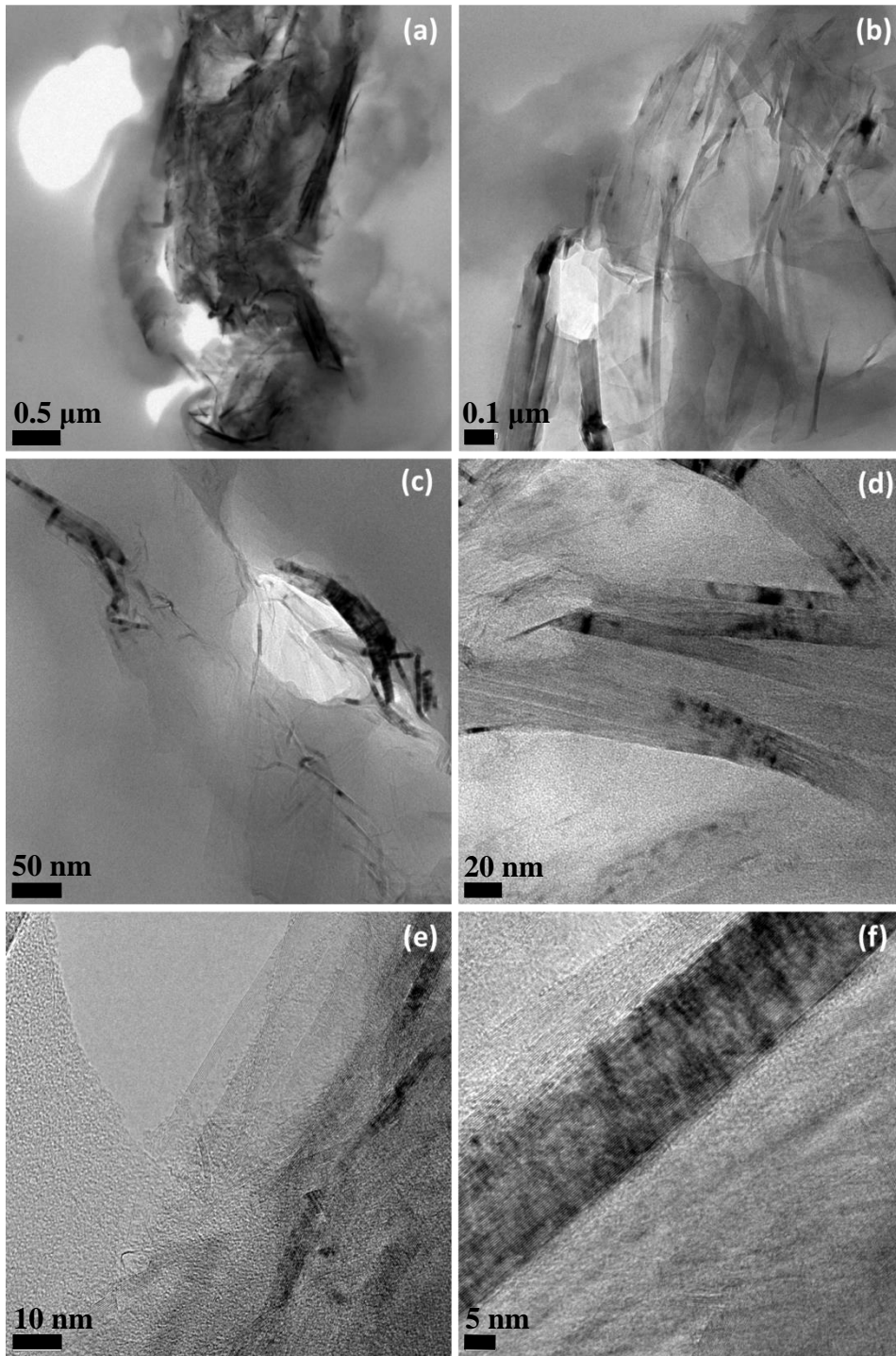


Figure 4.59 TEM micrographs of PLA/EG-2 produced via melt blending at different magnifications

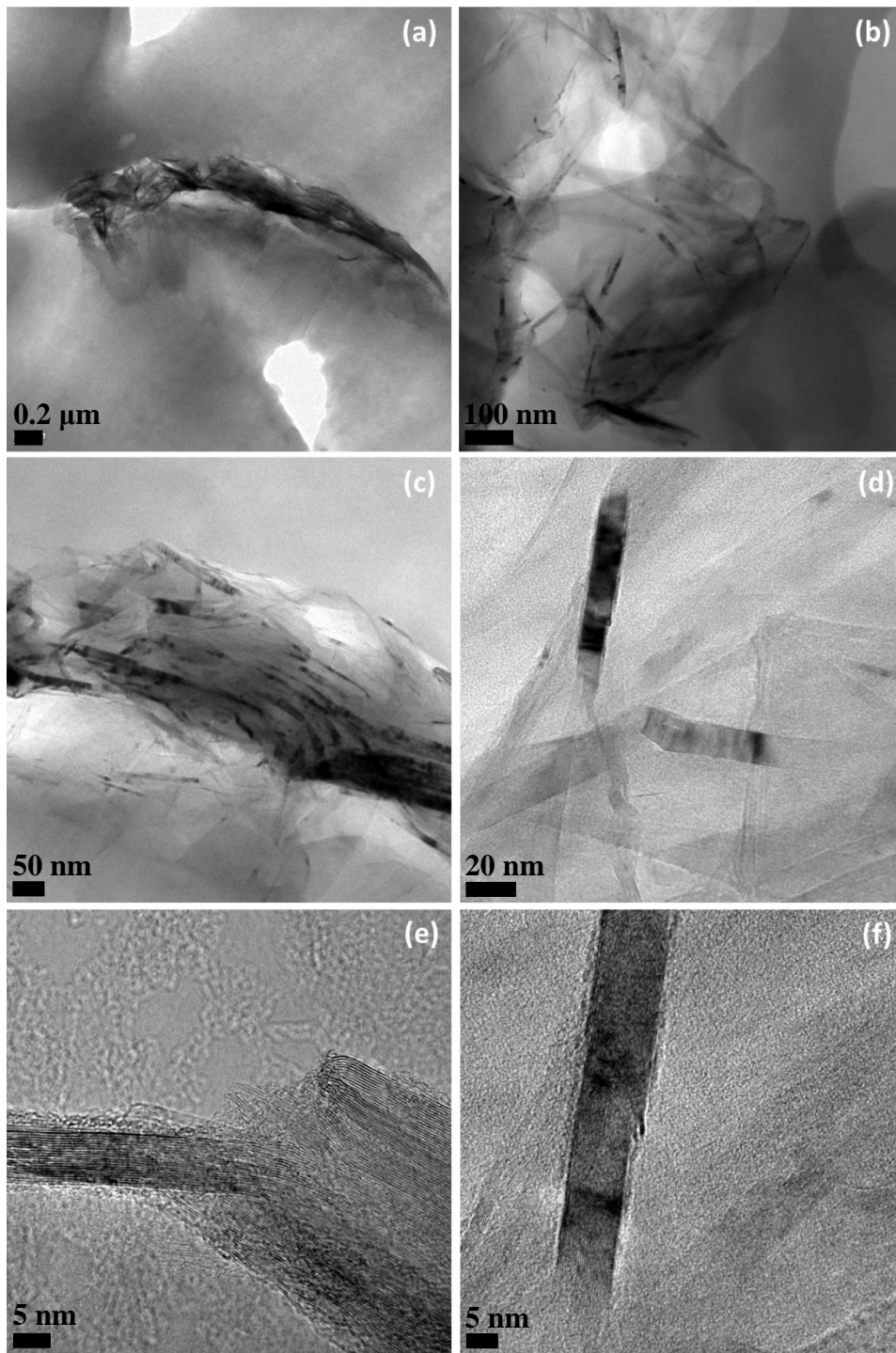


Figure 4.60 TEM micrographs of PLA/E-GMA/EG-2 produced via melt blending at different magnifications

PLA/EG-2 and PLA/E-GMA/EG-2 composites produced via solution mixing were also investigated with TEM. Figure 4.61 shows the binary composite micrographs at different magnifications. Large EG tactoids are still present as can be seen in Figure 4.61-a. However, smaller tactoids, intercalated assemblies and dispersed single graphene layers in polymer matrix are seen more frequently (Figure 4.61-b and Figure 4.61-c). Addition of E-GMA to the binary composite did not change the fact that mixed EG structures are seen in the composite (Figure 4.62). Even though presence of exfoliated graphene layers are detected more frequently in solution mixed samples compared to the melt blended ones (Figure 4.62-d and e), presence of EG agglomerates with high number of graphene layers organized in stacks explains the single peak seen in XRD patterns, which is identical to the ones seen in samples prepared via extrusion.

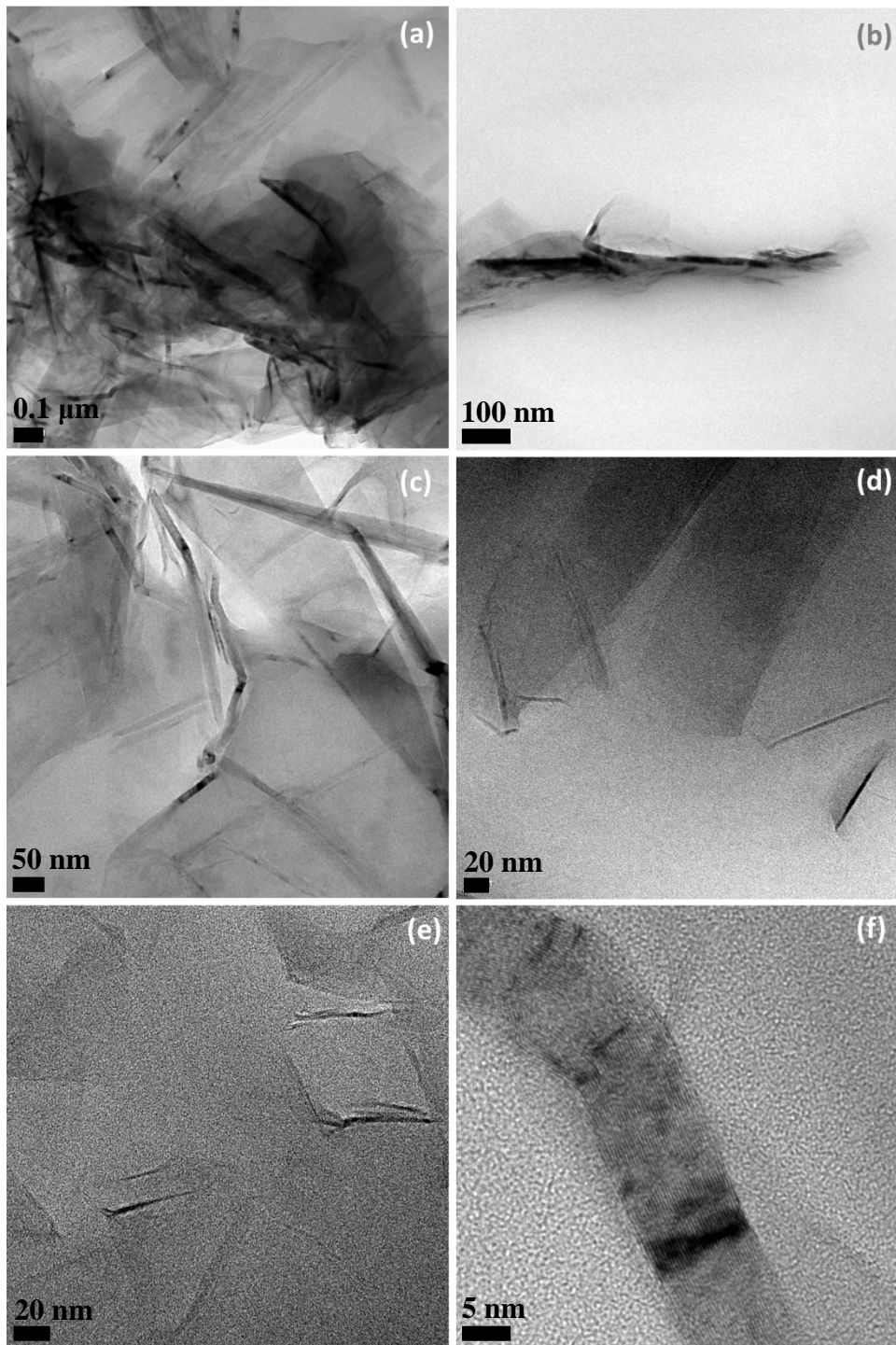


Figure 4.61 TEM micrographs of PLA/EG-2 produced via solution mixing at different magnifications

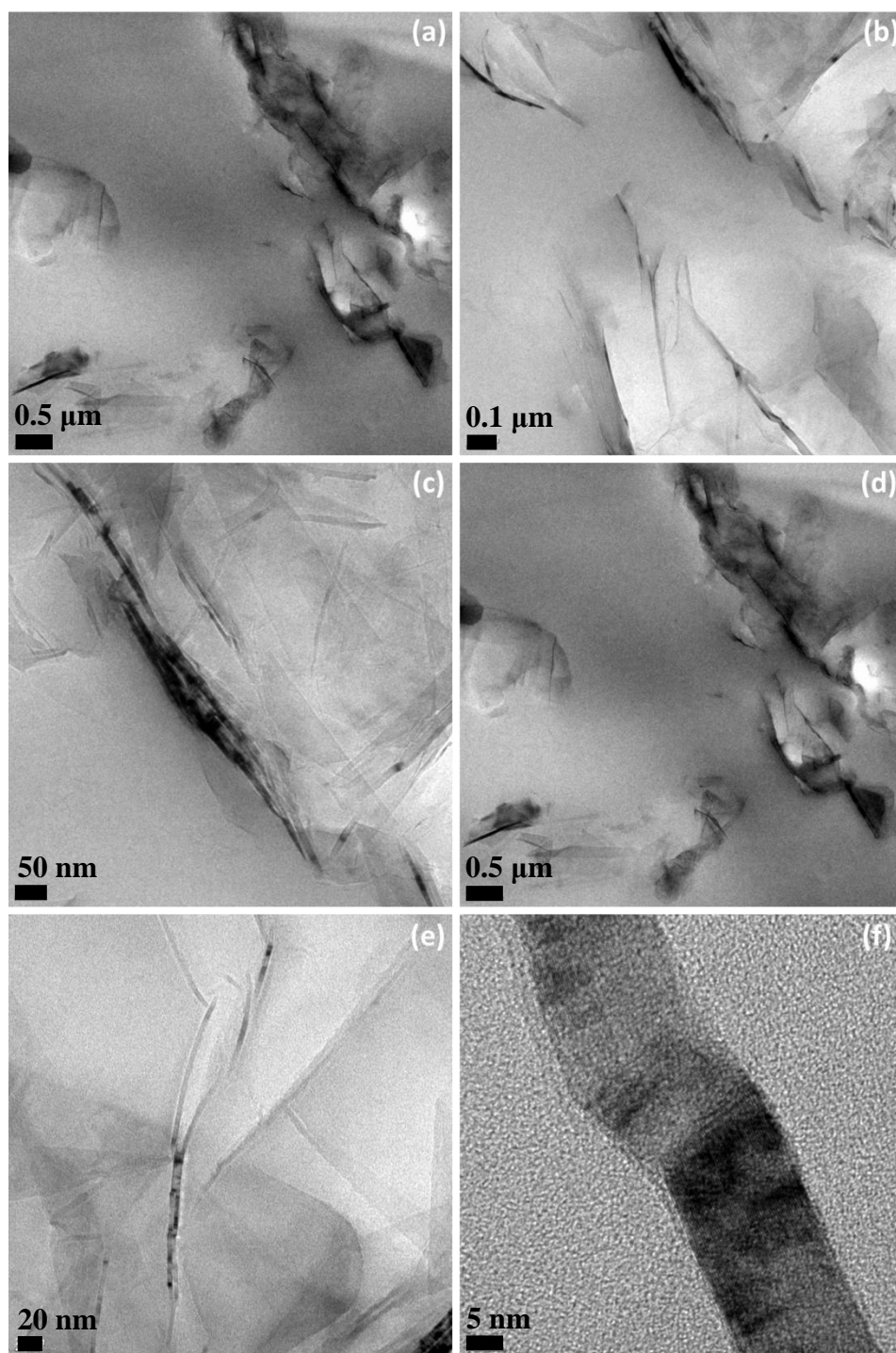


Figure 4.62 TEM micrographs of PLA/E-GMA/EG-2 produced via solution mixing at different magnifications

4.2.2.2 Spectroscopic Analyses

FTIR analyses were performed to find evidences of the interactions between the polymer matrix, PLA, and the rubber, E-GMA. The characteristic peaks of PLA and E-GMA structures were shown previously in Section 4.1.2.2. A similar approach was followed: the reaction expected to occur between the end groups of PLA (COOH and/or OH) and the epoxide group of E-GMA can be detected from the decreasing intensity or disappearance of the epoxide peak seen at 910 cm^{-1} in the FTIR spectra of neat E-GMA [133, 137]. For this purpose, FTIR spectra of four selected samples were compared (Figure 4.63).

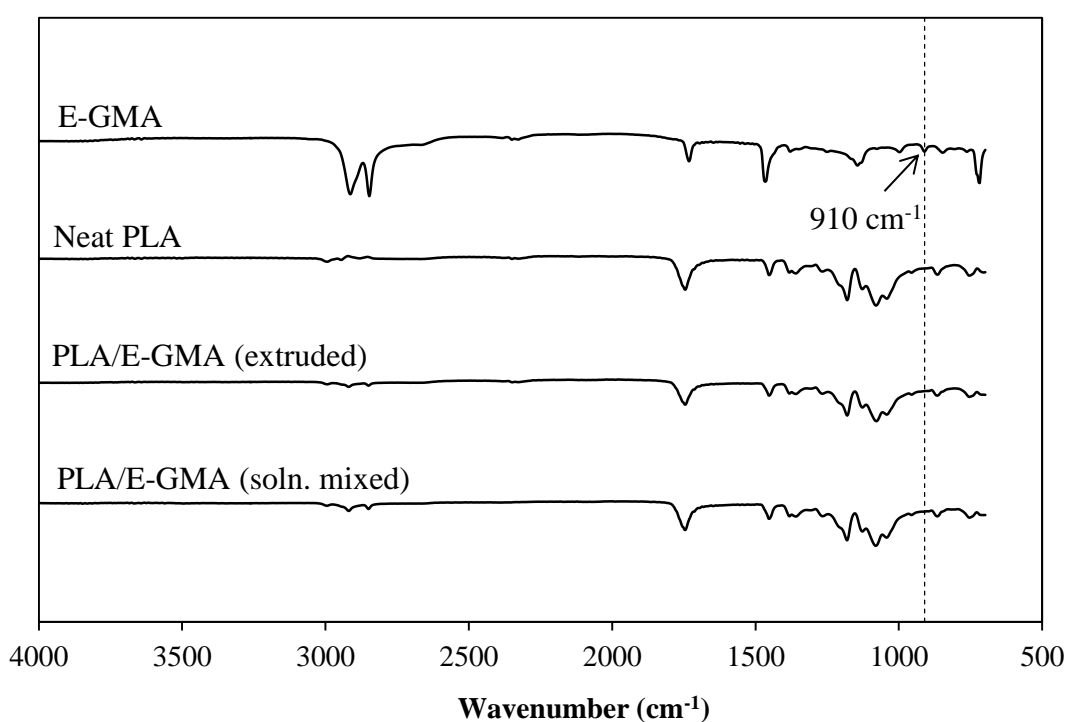


Figure 4.63 FTIR spectra of E-GMA, PLA and their binary blends prepared via melt blending or solution mixing

FTIR spectra of blends prepared with different methods are identical which means that in both methods, PLA is reactively blended with E-GMA. As shown in previous section concerning the morphologies of the samples prepared by different methods,

binary blends of PLA/E-GMA resulted in totally distinct structures. However, FTIR spectra of these blends revealed that chemical interactions between the matrix and the rubber are not affected by the production method.

4.2.2.3 Mechanical Analyses

Mechanical properties of the nanocomposites are very important to pursue and evaluate the effects of different procedures applied in production processes and the changes in the material contents. These results should be discussed in accordance with the morphological structures of the samples.

First, mechanical properties of different production methods will be presented separately to show the effects of different compositions. Then the analogous compositions will be compared for different production techniques. Tabulated form of mechanical test results can be found in Appendix B.

Effect of Composition in Melt Blending

Figure 4.64 shows changes in tensile strength of neat PLA and ternary nanocomposites prepared by melt blending as EG concentration is increased. Blending PLA with a rubber caused 32% decrease in tensile strength. This is an expected reduction owing to the elastomeric nature of E-GMA.

Addition EG does not significantly affect the tensile strength so that all PLA/EG binary composites, independent of the EG content, have a tensile strength value in the same order of magnitude of neat PLA. Similar results were obtained in a study of Fukushima et al. [119] where PLA/EG binary composites were prepared in a Brabender internal mixer in a range of 3-9 wt. % EG content. They reported that for all binary nanocomposites, tensile strength remains practically constant as compared to neat PLA. In fact, addition of exfoliated graphite structures resulted in three different reinforcing behaviors reported in the literature: strength might descend with increasing loading or strength goes up with increasing loading or finally strength goes up to a peak value at a critical concentration, and then goes down with further

loading, which is considered as the unsuccessful dispersion at higher loading of the filler, causing more stress concentration sites [10].

Usually, addition of a nanofiller is expected to increase tensile strength. Although this is not observed in PLA/EG binary composites, increasing EG concentration caused a gradual increase in tensile strength of ternary nanocomposites. In other words, decreasing strength of brittle polymer due to blending with an elastomer is compensated with addition of stiff filler to a certain extent. However, this compensation is not enough to totally recover to neat PLA strength in the EG range used in this study.

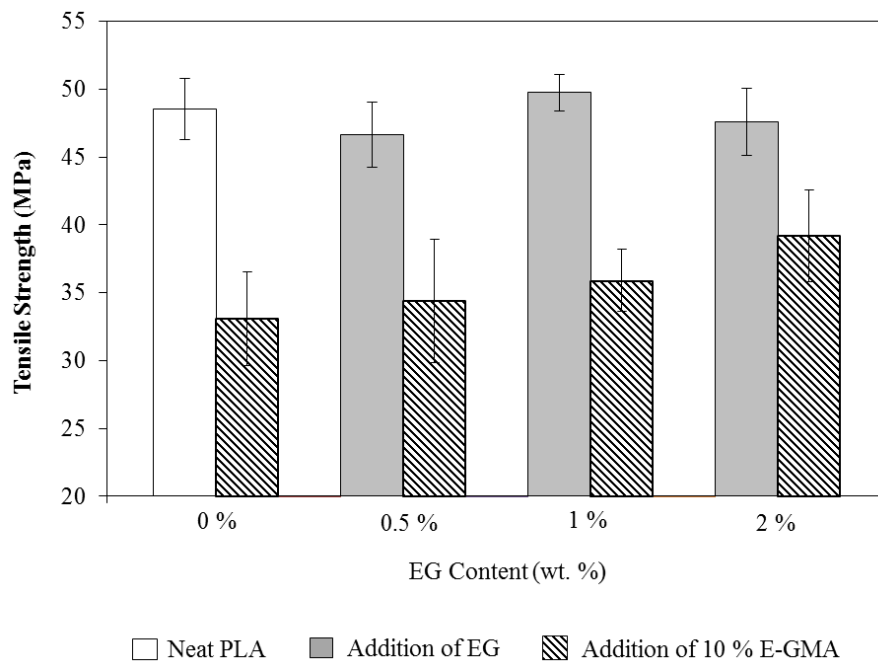


Figure 4.64 Tensile strength of neat PLA, PLA/E-GMA binary blend and PLA/E-GMA/EG ternary composites prepared via melt blending

Tensile modulus values are also not affected noticeably from addition of EG to the polymer matrix (Figure 4.65). The main parameter affecting the modulus is the addition of the rubbery phase. Consistently with the expectations, Young's modulus of PLA/E-GMA is 16% lower than that of neat PLA. However, contrary to the

tensile strength, modulus values are not recovered at a considerable extent with the addition of EG. The effect of EG concentration on Young's modulus was also reported in the literature, however, the results are not consistent with this study. For example, in a study PLA/EG nanocomposites were prepared in an internal mixer with EG concentrations varying between 3 to 9 wt. %. Addition of 6% and 9% EG into PLA led to increases of Young's modulus of about 30% and 50%, respectively, compared to that of neat PLA [119]. In another study, PLA/EG composites were prepared in a twin-screw extruder with EG contents in between 0.1-7 wt. %. In that study, Young's modulus of PLA/EG nanocomposites increased noticeably with the increase of EG content, which was more pronounced at filler concentrations less than 2 wt. % [162].

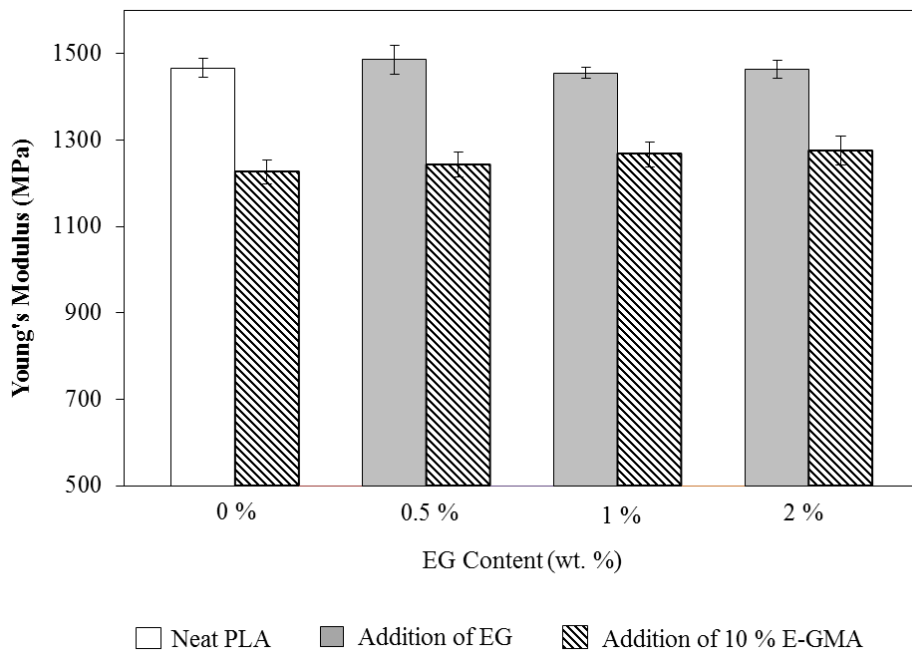


Figure 4.65 Young's modulus of neat PLA, PLA/E-GMA binary blend and PLA/E-GMA/EG ternary composites prepared via melt blending

Figure 4.66 represents percent strain at break under the applied tension. Elongation of the material is an indication of toughness and blending with the rubber caused a

drastic increase in elongation. On the other hand, increasing EG concentration made the PLA matrix more brittle. At the highest EG concentration (2 wt. %), PLA/EG binary nanocomposite has the lowest strain at break.

In ternary nanocomposites, elongations at break do not follow a pattern with increasing or decreasing EG concentration. However, all PLA/E-GMA/EG nanocomposites failed at a strain lower than the PLA/E-GMA blend and higher than neat PLA and/or PLA/EG binary composites.

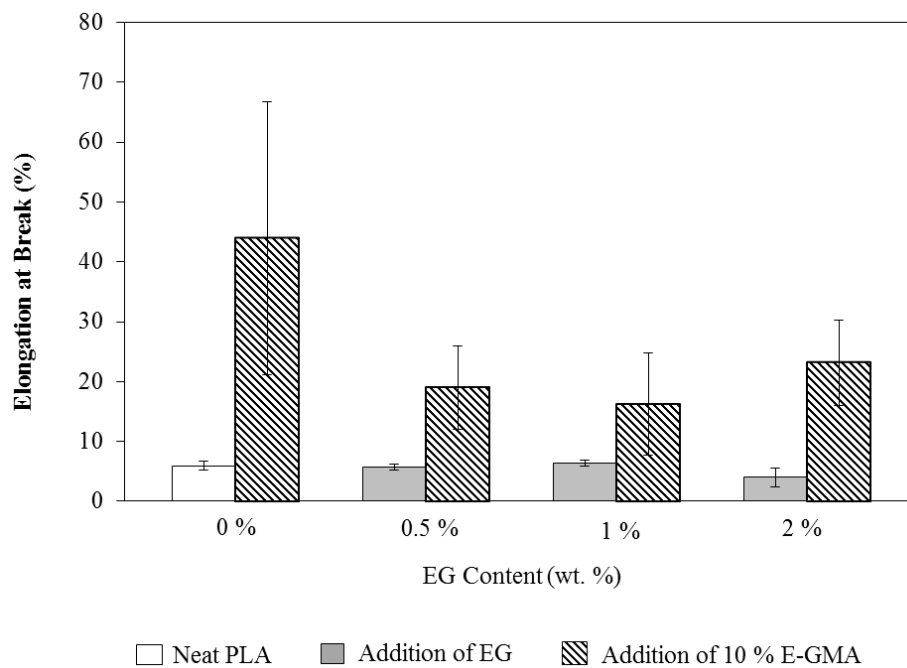


Figure 4.66 Elongations at break of neat PLA, PLA/E-GMA binary blend and PLA/E-GMA/EG ternary composites prepared via melt blending

Another indication of toughness is the impact strength of the composite material. In the literature, there are a few studies that succeeded in improving the impact toughness of polymer/expanded graphite nanocomposites. For example, Wang et al. [162] reported that impact strength of HDPE/EG system increases with EG loading less than 2 wt. %, but decreases markedly with EG loading over 4 wt. % as

compared with that of neat HDPE. It is claimed that when the EG content is low, the nanosheets that are successfully dispersed in the matrix absorb part of the impact energy, but as the loading is increased, the movement of polymer molecular chains is intensively restricted. In another study, it is reported that addition of exfoliated graphite nanoplatelets in PLA matrix improves the impact energy with the largest increase in the impact strength observed for filler contents of 8 and 10 wt. %. However, in most of the studies, elevated EG loadings result in sacrifices in impact strength [44, 163, 164].

Figure 4.67 shows the changes in absorbed energies of unnotched samples in Charpy impact test. In PLA/EG binary nanocomposites, effect of EG loading on impact strength is about $\pm 3\%$, which is in the experimental error range. Therefore, it can be said that EG loadings employed in this study did not affect the impact strength significantly. As discussed in detail on SEM micrographs of PLA/EG binary composites, PLA/EG composites mostly exhibit straight crack propagation lines on their fracture surfaces. These lines usually enhance further growth and make it easier to fracture the specimen with a small amount of energy. However, short cracks extending to different directions were also seen around the large stacks. This crazing effect around the EG stacks might compensate the stiffening effect of the filler and the impact strength remains in the same order of magnitude.

The main influence on impact strength is obtained by addition of E-GMA to the composite system. Blending E-GMA with neat PLA yields almost 50% increase in impact toughness. In the ternary systems, a synergistic effect of E-GMA and EG can be seen at the lowest EG loading. As the EG content increases, impact strength starts descending but it does not go down to the impact strength of neat PLA. This decrease of the impact strength in ternary nanocomposites is most probably due to the insufficient dispersion of the filler.

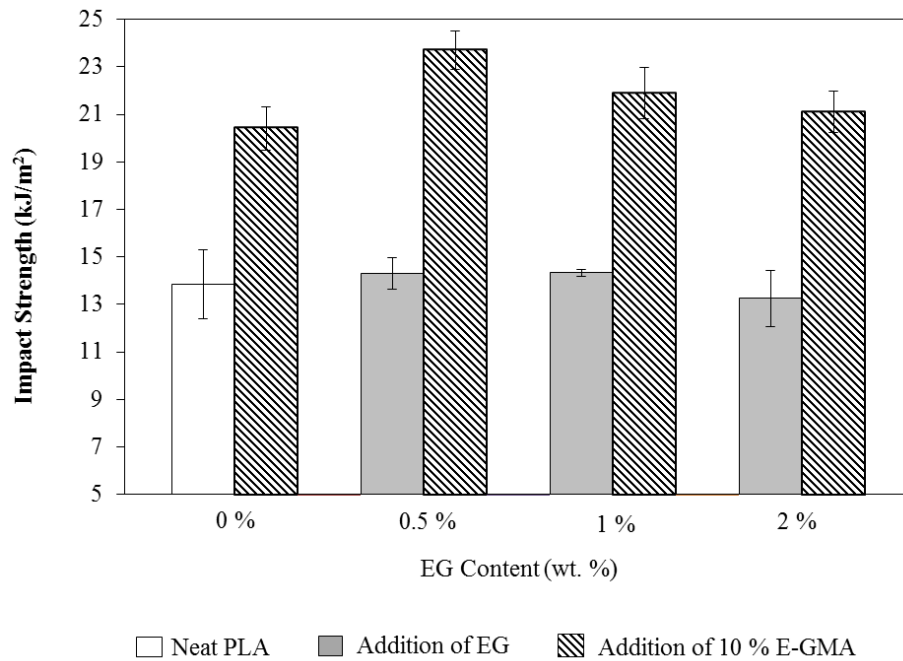


Figure 4.67 Impact strength of neat PLA, PLA/E-GMA binary blend and PLA/E-GMA/EG ternary composites prepared via melt blending

Effect of Composition in Solution Mixing

Compared to neat PLA, both tensile strength and modulus decreased significantly by blending with E-GMA as can be seen in Figure 4.68 and Figure 4.69, respectively. The reductions are 59% and 35%, respectively, for strength and modulus. The elastomeric nature of E-GMA is the main reason of these reductions. In addition, tensile strength of PLA/EG binary nanocomposites prepared via solution mixing showed a decreasing trend with increasing EG loading. In fact, addition of a nanofiller is expected to increase the tensile strength, but there are some studies reporting a number of polymer/EG nanocomposites with lower strength caused by increasing loading [165, 166]. Young's modulus values of binary nanocomposites are not affected from the EG loading, and regardless of the filler content all binary nanocomposites have approximately the same modulus values. PLA/E-GMA/EG nanocomposites show a synergistic effect where reduction modulus is compensated with the presence of a rigid filler to certain extent.

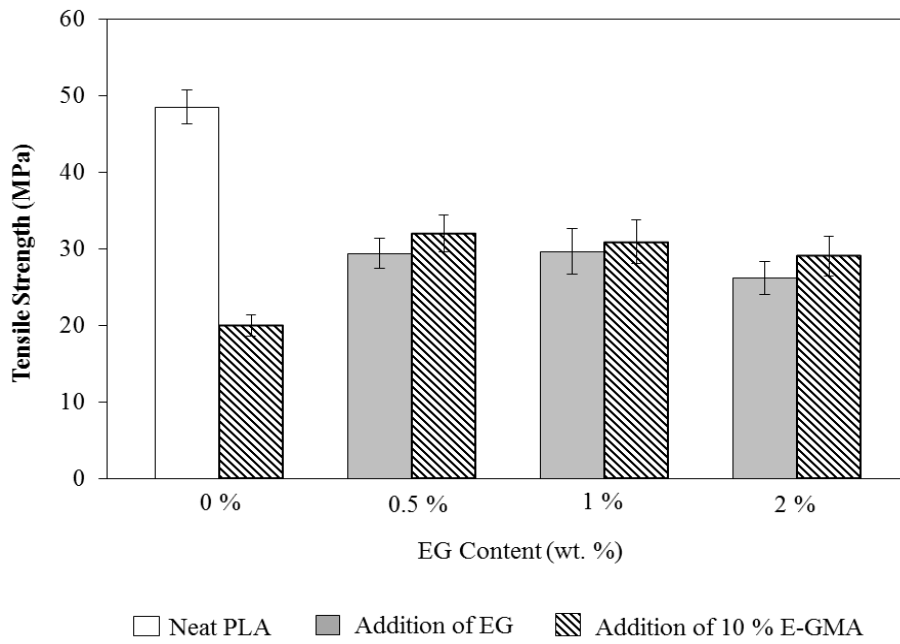


Figure 4.68 Tensile strength of neat PLA, PLA/E-GMA binary blend and PLA/E-GMA/EG ternary composites prepared via solution mixing

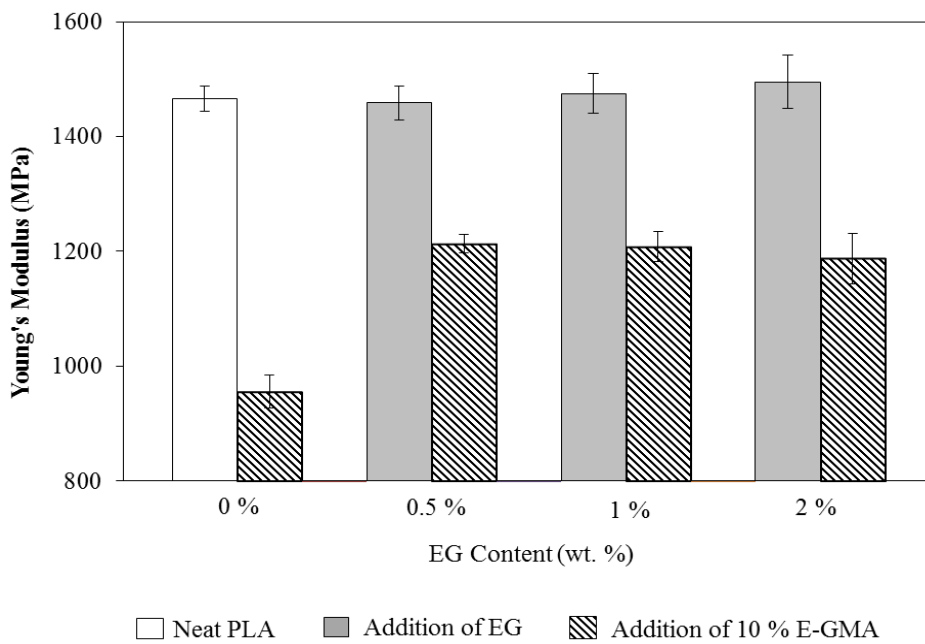


Figure 4.69 Young's modulus of neat PLA, PLA/E-GMA binary blend and PLA/E-GMA/EG ternary composites prepared via solution mixing

Another important information obtained from tensile test is the strain at break, which is an indicator of tensile toughness. The lowest EG loading (0.5 wt. %) increased the elongation at break of the binary nanocomposite for about 50% compared to that of the neat PLA (Figure 4.69). However, as the EG loading increased to 2 to 4-fold, elongations decreased to lower values than that of the neat PLA. As discussed in Section 4.2.2.1 considering the TEM micrographs, there are smaller tactoids well dispersed in polymer matrix of solution mixed samples, and intercalated assemblies and dispersed single graphene layers are seen frequently. At the lowest EG loading, these well dispersed mixed EG structures might align in the direction of extension, providing good transfer of the load and therefore increase the toughness. At higher loadings, this effect might be suppressed due the presence of larger tactoids.

The main enhancement in tensile toughness is obtained in the presence of E-GMA. Just by blending PLA with E-GMA via solution mixing method yields 8-fold increase in strain at break. The increase in elongation at break reaches its highest value for PLA/E-GMA/EG-0.5 nanocomposite 169%. Increased EG loading caused a gradual decrease in elongations, but still the nanocomposites containing E-GMA and prepared via solution mixing can be considered as super-toughened compared to neat PLA. SEM micrographs of solution mixed binary PLA/E-GMA blend and ternary nanocomposites showed no phase separation behavior.

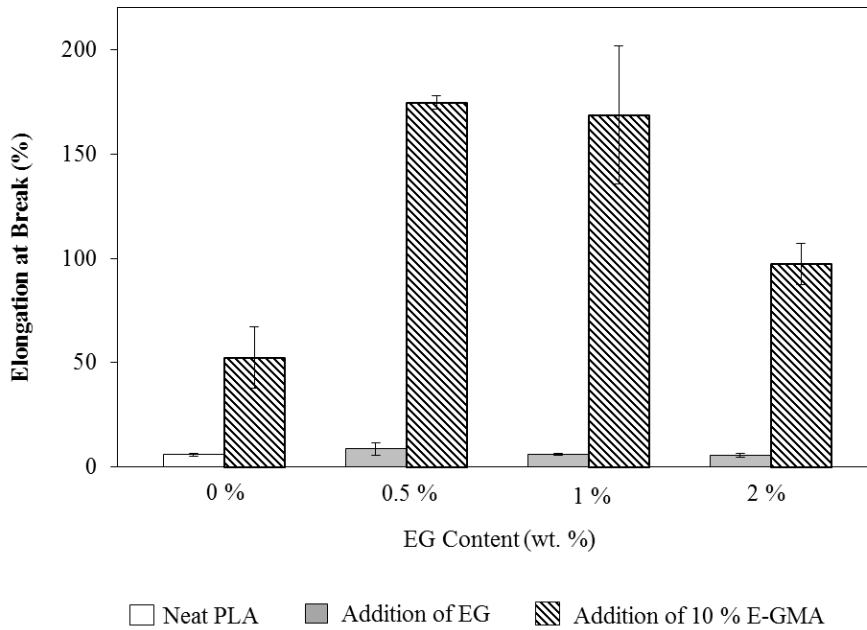


Figure 4.70 Elongations at break of neat PLA, PLA/E-GMA binary blend and PLA/E-GMA/EG ternary composites prepared via solution mixing

Changes in impact toughness of nanocomposites prepared via solution mixing are very different than tensile toughness. Blending with E-GMA without adding the nanofiller resulted in 2-fold improvement, however, as the filler is added to this binary blend, impact strength decreased systematically with increasing filler loading. Interestingly, among all nanocomposites prepared via solution mixing, the maximum impact strength was achieved at the lowest EG loading without addition of E-GMA. As the filler content increases, impact strength also decreases. At every filler concentration, PLA/EG binary nanocomposites exhibited slightly higher impact strength compared to those of PLA/E-GMA/EG nanocomposites. According to the SEM micrographs, PLA and E-GMA constitute a continuous phase when mixed in solution, but addition of a stiff filler like EG might cause weaker points in the structure. Furthermore, as mentioned previously in Section 4.2.2.1, the crack propagation lines seen on the fracture surface images of PLA/E-GMA/EG-0.5 nanocomposite prepared via solution mixing are more superficial compared to the binary nanocomposite (PLA/EG-0.5) with the same loading of EG without E-GMA.

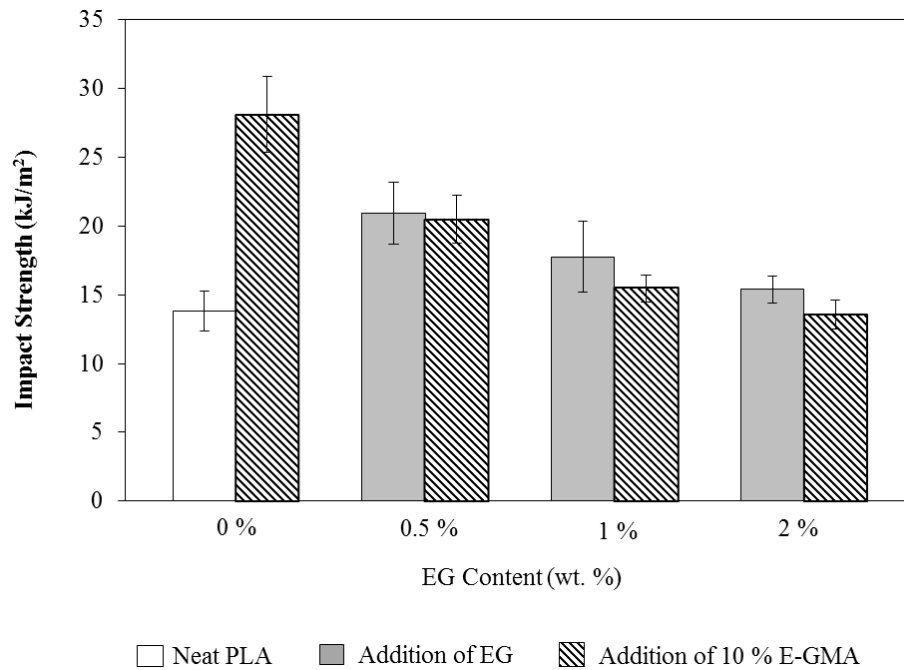


Figure 4.71 Impact strength of neat PLA, PLA/E-GMA binary blend and PLA/E-GMA/EG ternary composites prepared via solution mixing

Comparison of Production Methods

Mechanical properties such as strength, modulus, and toughness of a polymer nanocomposite depend extremely on the dispersion quality and interface bonding between polymer matrix and nanofillers. A uniform dispersion and strong interface bonding can assist the load transfer within the composites. However, in composites of graphite derivatives, there are stress concentrations due to the multiple filler structures (heterogeneous microstructures) which are harmful to the mechanical performance [10]. According to the results published in the literature, two conventional methods used in this study (melt blending and solution mixing) to produce PLA/EG nanocomposites result in different dispersion states and probably different interface interactions. From industrial point of view, melt blending is the preferred compounding technique for the preparation of composites since it is a direct, cost effective and environmental friendly process. No solvents are involved during melt blending. Traditional mixing equipment such as extruder, internal mixer,

and two-roll mill can be implemented for the melt blending operations and are usually available in most compounding units [40]. There are no published studies directly comparing the material properties obtained with these two methods but it is well known that melt blending is usually not successful in dispersing EG in various polymer matrices. Better dispersion obtained via solution mixing is accompanied with the requirement of high amounts of solvent usage in order to dissolve both the polymer matrix and the filler. In this study, the comparison between melt blending and solution mixing is done at low EG loadings to decrease solvent usage. In fact, improvement with low filler loading with low amount of solvent usage is one of the main objectives.

Figure 4.72 shows tensile strength values of PLA/EG binary composites prepared via melt blending and solution mixing methods. Filler loading range (0.5-2 wt. %) has no significant effect on the samples prepared with the same method, i.e.; 4-fold increase in EG (from 0.5 to 2 wt. %) caused only 2% increase in melt blended samples. Tensile strength of samples mixed in solution also did not vary among themselves. However, solution mixed composites have significantly lower strength compared to melt blended samples. Usually, a decrease in tensile strength is evaluated as poor dispersion of the filler and poor interaction between the filler and the matrix. There are some studies on different polymer matrices and fillers in which higher tensile strength values with melt blending were obtained compared to solution mixing. For instance, sisal fibers in PP matrix are reported to be exposed to breakage during melt blending which was claimed to result in effective mixing and orientation in comparison to that of solution mixed samples [167].

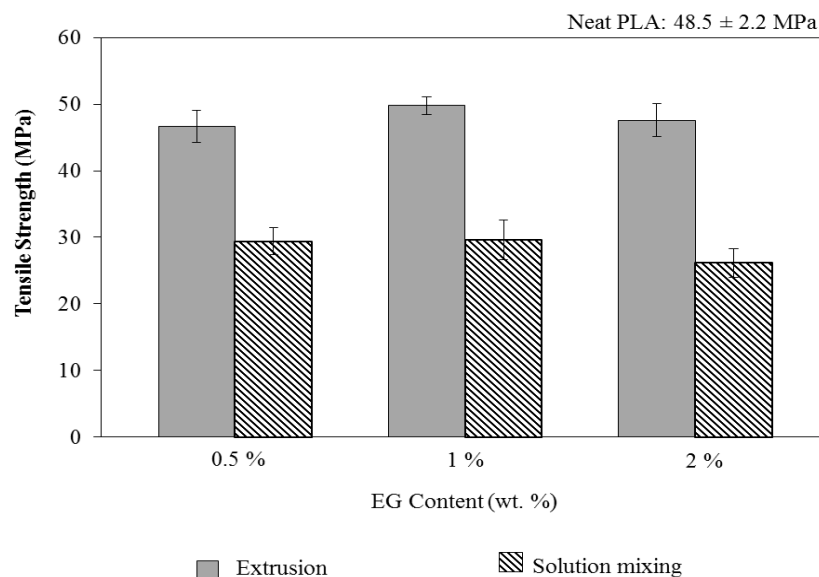


Figure 4.72 Comparison of tensile strength values of PLA/EG binary composites prepared via extrusion and solution mixing

In this study, XRD patterns of the samples suggest that there are no differences between the two production methods in terms of final interlayer distances. This is valid for both binary and ternary composites. TEM micrographs also suggest that smaller tactoids together with some intercalated assemblies and dispersed single graphene layers in polymer matrix can be observed in solution mixed composites. Thus, morphology analyses suggest that solution mixed samples should compete with melt blended samples or even show better tensile performance. The decrease in tensile strength could be attributed to the possible changes in physical properties of PLA such as reduction in molecular weight. Detailed studies on glassy polymers revealed that M_w has significant effect on tensile properties [168, 169, 170]. For example, tensile strength of PS was found to increase sharply with the molecular weight of the material through the range 50000 to 200000 reaching a value of more than ten times the value at low molecular weights.

Comparison of tensile strength values of binary blends and ternary nanocomposites produced with the addition of elastomeric E-GMA is shown in Figure 4.73. The extent of the decrease in tensile strength is more apparent in the PLA/E-GMA blend

prepared via solution mixing. As aforementioned, the morphologies of the blends are also substantially different such that spherical droplet shaped phase separation was observed in melt blended sample, whereas solution mixed sample resulted in a continuous structure.

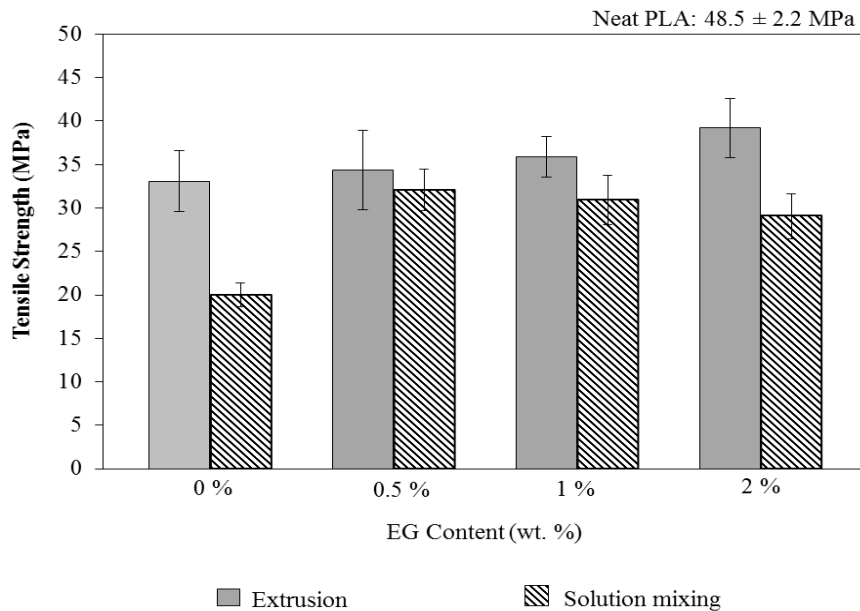


Figure 4.73 Comparison of tensile strength values of PLA/E-GMA/EG ternary composites prepared via extrusion and solution mixing

As in the case of PLA/EG composites, melt blended ternary composites exhibited higher tensile strength values compared to those of solution mixed samples. However, the difference between these two methods is considerably lower than the difference observed in binary composites (Figure 4.72). Additionally, the drastic decrease in strength of binary blend produced via solution mixing was compensated to some extent with the addition of filler. This recovery is at its maximum at the lowest filler content due to the better dispersion and filler-matrix interactions obtained at lower concentrations. The rubber obviously acts as compatibilizer between the matrix and filler, but with increasing EG loading, slight decrease in strength was observed. However, samples prepared via melt mixing show incremental increase as EG content is increased.

The changes in modulus of the binary composites are shown in Figure 4.74. Regardless of the filler loading and production method, binary composites attained modulus values in the same order of magnitude, which are also comparable to that of the neat PLA. Enhancements in rigidity with addition of EG to different polymer matrices were reported in literature at relatively higher loadings (*ca.* 3 wt. %) [119, 171, 172].

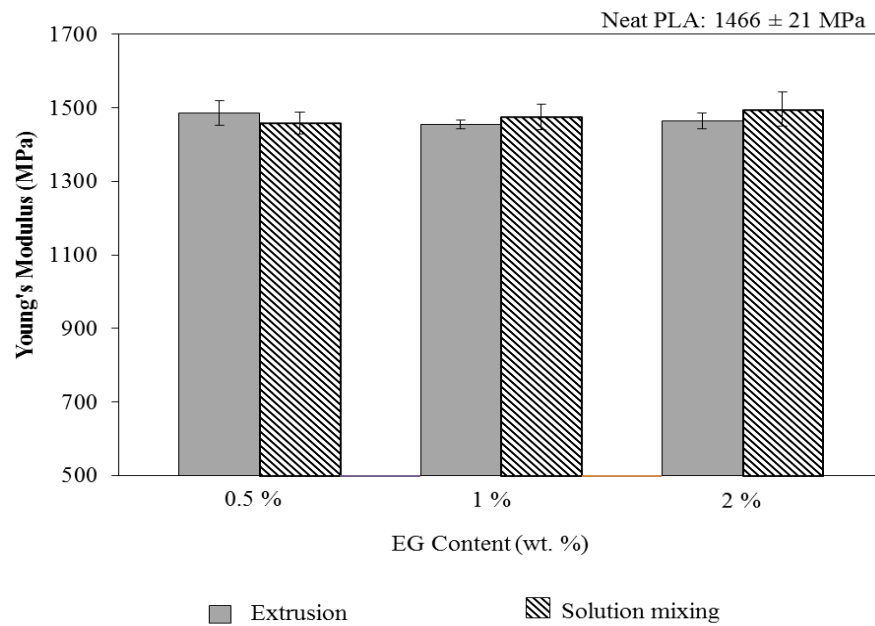


Figure 4.74 Comparison of Young's modulus values of PLA/EG binary composites prepared via extrusion and solution mixing

When the binary blends are considered, it is obvious that both methods result in decreases in rigidity (Figure 4.75). Blending with an elastomeric copolymer was expected to result as such. The reduction in elastic modulus is more apparent in the binary blend prepared via solution mixing. Addition of EG to solution mixed PLA/E-GMA binary blend successfully recovers the lost rigidity. In melt blended samples, there is a gradual increase in modulus with increasing filler content, however, the recovery is not as explicit as in solution mixing.

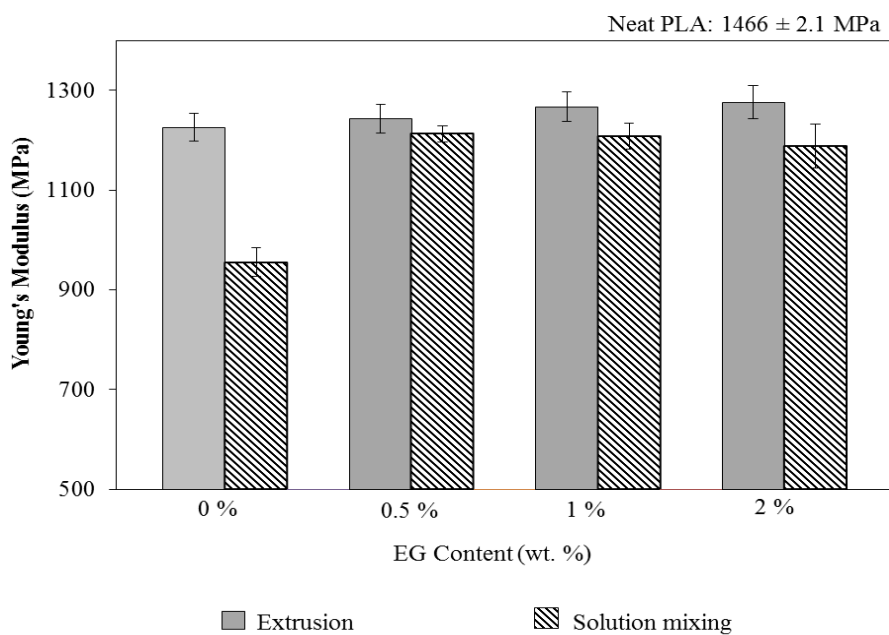


Figure 4.75 Comparison of Young's modulus values of PLA/E-GMA/EG ternary composites prepared via extrusion and solution mixing

Tensile strength and rigidity of samples mixed in solution obviously remained below those of melt blended nanocomposites. However, changes in elongation at break, which is an indication of tensile toughness, are significantly different. As shown in Figure 4.76, binary composites still have low toughness. Only the solution mixed composite with the lowest EG loading show considerable increase, but still all binary composites show brittle behavior. The main enhancement in tensile toughness was achieved when E-GMA is added to the nanocomposites (Figure 4.77). Elongations of binary PLA/E-GMA blends are also considerably higher compared to that of neat PLA. To illustrate, melt blended PLA/E-GMA sample reached 7-times higher elongation at break (~44%) in comparison to neat PLA. Addition of EG to this blend caused a drastic decrease to almost half of the value of the blends. Contrarily, in solution mixed composites, addition of EG to the binary blend with the lowest loading resulted in the highest strain at break. Then, as EG content increases, elongation starts decreasing.

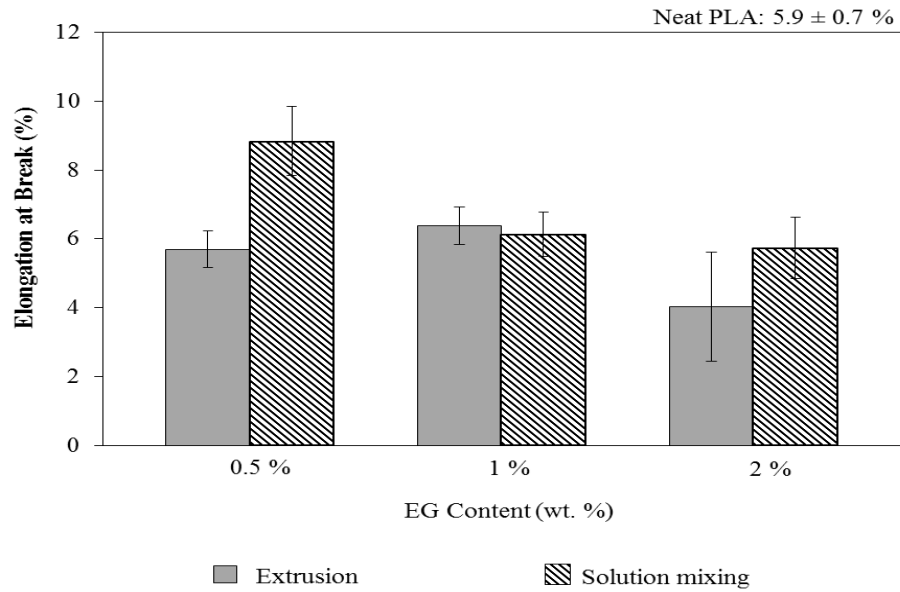


Figure 4.76 Comparison of elongation at break of PLA/EG binary composites prepared via extrusion and solution mixing

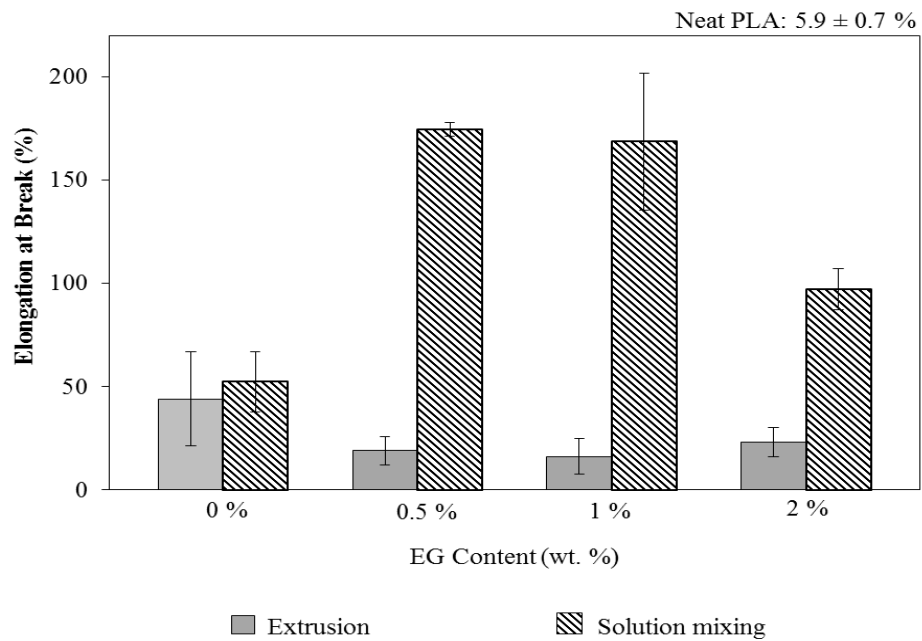


Figure 4.77 Comparison of elongation at break of PLA/E-GMA/EG ternary composites prepared via extrusion and solution mixing

Considering all the tensile test results, it is obvious that the extent of intermolecular interactions changes significantly with the production method. Previously mentioned FTIR spectra of E-GMA containing samples showed that both production methods resulted in successful reactive blending. SEM analyses, on the other hand, revealed that morphology of solution mixed blends and composites have no phase separation behavior when E-GMA is added. This final continuous structure loses its strength and rigidity more than the phase separated structures. However, compensation of these reductions with the presence of rigid filler is more apparent. Furthermore, graphite is known for its self-lubricating behaviour, which arises from the weak binding between the graphene sheets kept together only by weak Van der Waals forces. These weak interactions allow for the interlamellar sliding [157]. This self-lubricating effect might result in easier sliding of both EG layers and polymer chains interacting with the filler surface. Increased chain mobility might result in decreasing ultimate tensile strength and elastic modulus, but increased strain without failure.

Besides the tensile test, unnotched Charpy impact test provides information about the toughness of the final product. Figure 4.78 and Figure 4.79 show the comparison of impact energies of the samples with and without elastomer addition, respectively. PLA/EG nanocomposites prepared via melt blending reached almost the impact strength of neat PLA. Short cracks around EG stacks seen in SEM images of these samples obviously were not enough to increase the energy absorbed during the impact load. Analogous compositions prepared via solution mixing, on the other hand, exhibited higher impact strength values. Interestingly, addition of E-GMA to the composites resulted in opposite behavior. Even though solution mixing of PLA with E-GMA imparts significantly higher energy absorbance compared to both neat PLA and PLA/E-GMA blend prepared via melt blending, ternary nanocomposites behaved quite the opposite manner. Melt blended ternary nanocomposites reached higher impact strength values at all EG loadings. As aforementioned in the morphology analyses part, the E-GMA droplets are ellipsoidal in shape rather than being smooth spheres. This is an indication of sharing of the impact load between the dispersed phase and the matrix. The continuous phase formed in PLA/E-GMA/EG

nanocomposites and the small hole-like structures seen on fracture surface might result in easier failure of the samples.

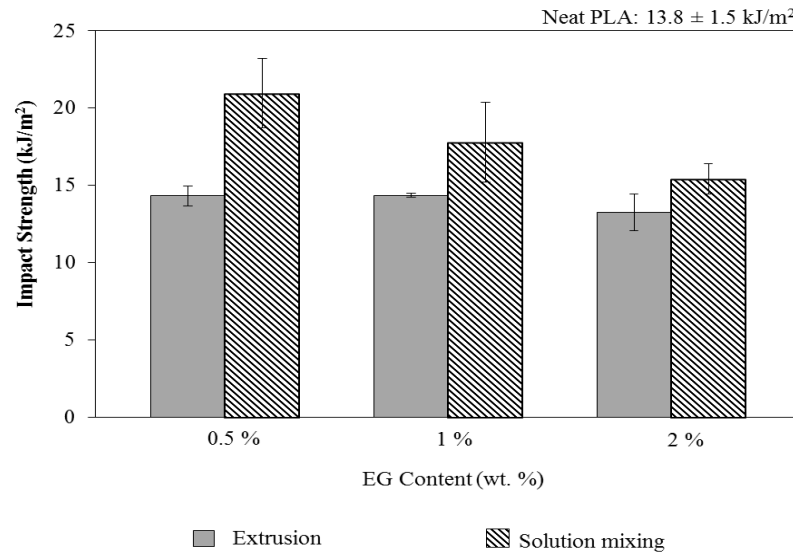


Figure 4.78 Comparison of impact strength values of PLA/EG binary composites prepared via extrusion and solution mixing

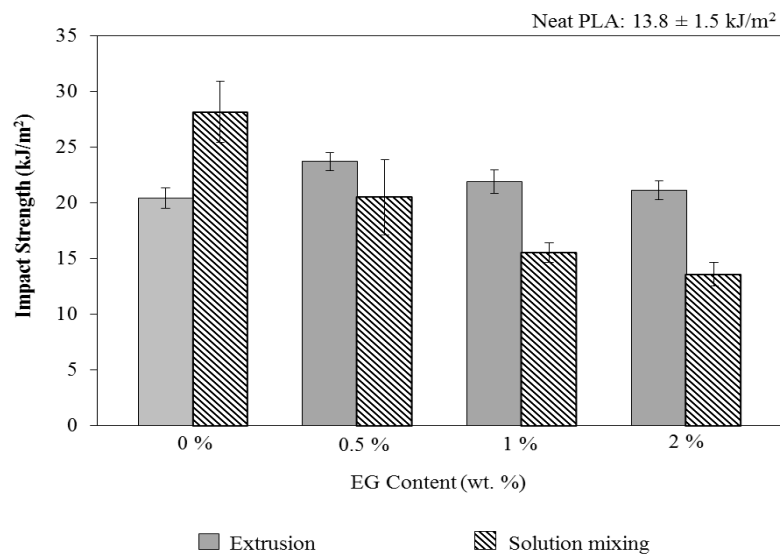


Figure 4.79 Comparison of impact strength of PLA/E-GMA/EG ternary composites prepared via extrusion and solution mixing

4.2.2.4 Rheological Analyses

Time Sweep Measurements

Stability of the nanocomposites in the melt state can be investigated through time sweep measurements at constant frequency and strain amplitude. Figure 4.80 shows the change of the storage modulus curves of processed neat PLA and its blends with respect to time. Decreases in storage modulus values after 15 minutes of testing are 25, 11 and 4% for neat PLA and PLA/E-GMA blends prepared via extrusion and solution mixing, respectively. These results revealed that thermal stability is significantly enhanced after blending. Addition of EG to PLA (not shown here) further increased the thermal stability, i.e., storage modulus of PLA/EG-2 decreased 16% after 10 minutes of time sweep, which was 25% for extruded neat PLA. Enhanced thermal stability of polymer/graphite nanocomposites were also reported in the literature for PLA [119, 118] and other polymer matrices [173, 174, 175]. Kim and Macosko [176] also reported the increase in thermal stability during time sweep measurements for polycarbonate/graphite composites e.g. G' of PC containing 1 and 3 wt. % of graphite remained nearly unchanged over 8000–11000 s. Considering that both filler loading and blending improve thermal stability of the final product, no thermal stabilizers were used. In order to be sure that the samples have a stable viscoelastic response, the frequency sweep tests that were carried on later were limited to 10 minutes.

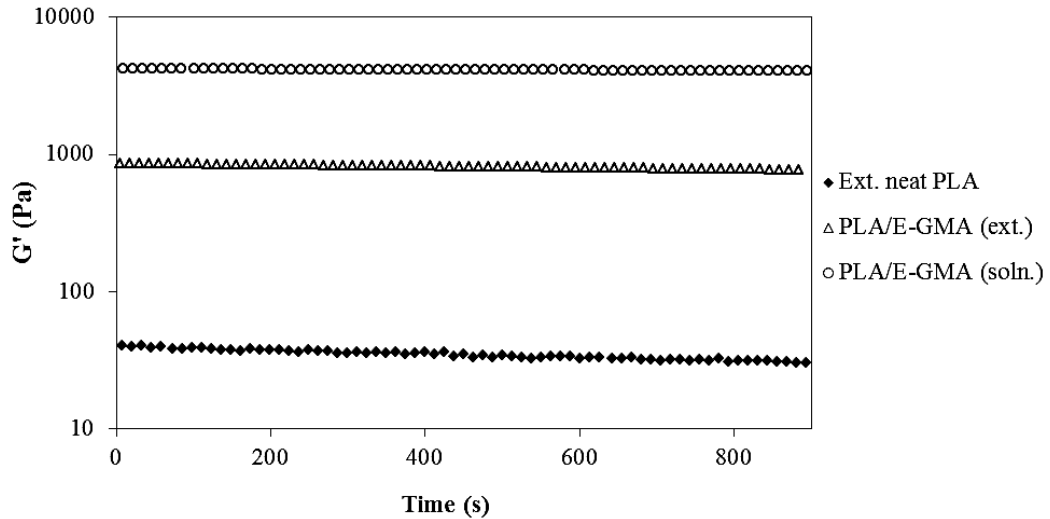


Figure 4.80 Time sweep curves obtained at 170°C, at 5% strain amplitude and 10 rad/s for processed neat PLA, and PLA/E-GMA blends prepared via extrusion and solution mixing

Strain Sweep Measurements

In order to determine LVR of the blends and composites, strain amplitudes between 0.1-100% were swept at 10 rad/s frequency. For PLA/EG nanocomposites, amplitude sweep should be discussed from two different views: filler content and production method. In terms of filler concentration in melt blended samples, slight decreases in G' was observed at high amplitudes but these are not detectable on the logarithmic scale for PLA/EG binary composites since relatively low loadings were used. In fact, the limit of linearity slightly decreases with increasing filler content. This decrease is more apparent for the ternary composites. Results of strain amplitude measurements of melt blended samples are shown in Figure 4.81. Strain amplitude curves of solution mixed samples are similar to the melt blended ones (Figure 4.82). In this set, the shear thinning behavior at high amplitudes are more prominent for the highest EG loading. Since the storage modulus (G') is a more sensitive rheological function than the loss modulus (G'') to the structural changes of the nanocomposites, only the storage modulus curves are given for the strain sweep tests [177].

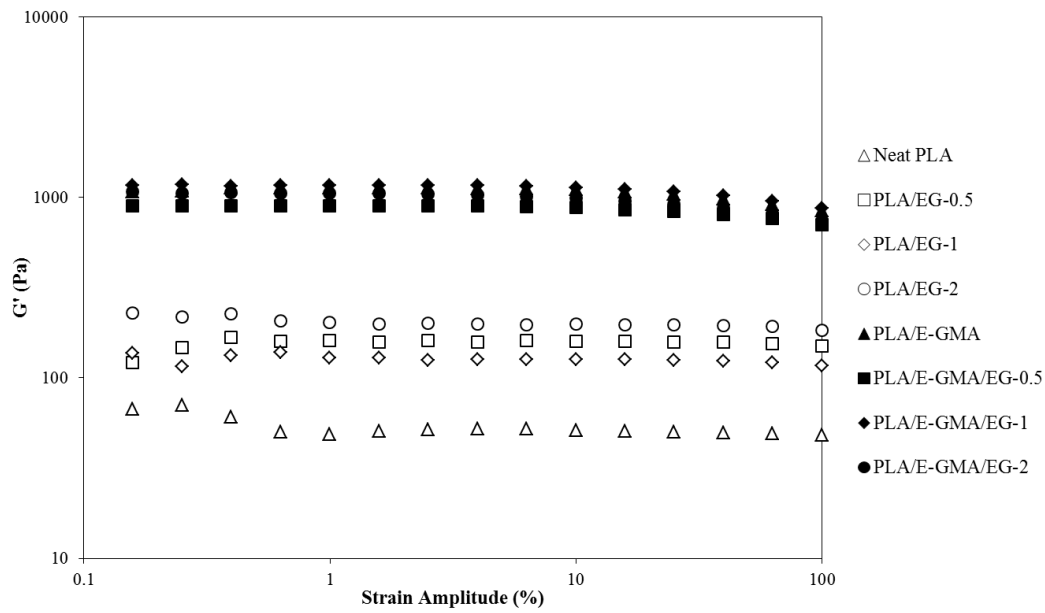


Figure 4.81 Strain sweep curves of processed neat PLA, PLA/E-GMA binary blend, PLA/EG binary composites and PLA/E-GMA/EG ternary composites prepared via melt blending

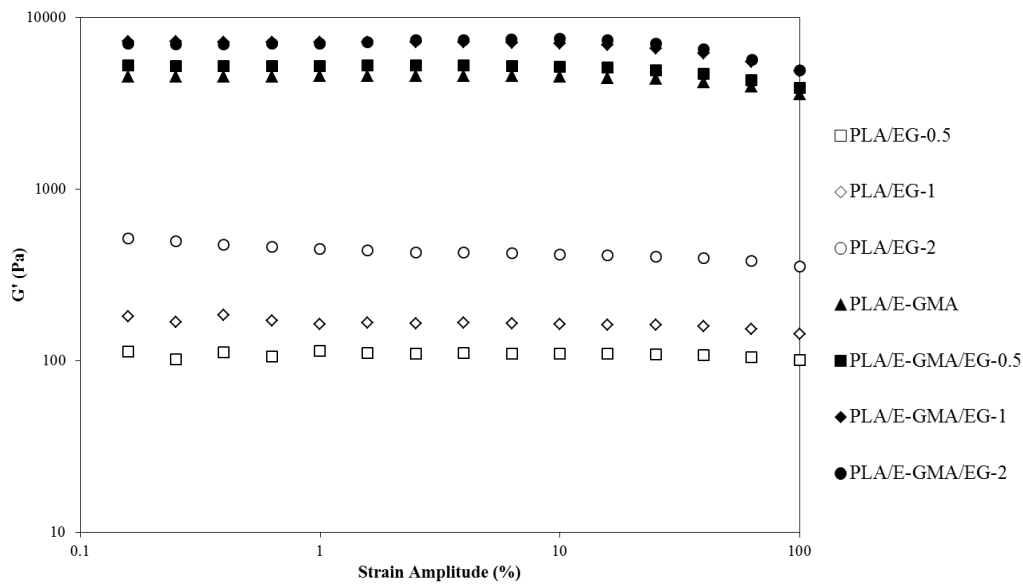


Figure 4.82 Strain sweep curves of processed neat PLA, PLA/E-GMA binary blend, PLA/EG binary composites and PLA/E-GMA/EG ternary composites prepared via solution mixing

The rheological measurements, which would provide the main information about the melt behavior of the final product, should be performed in the LVR, since in this region the microstructure of the material would not be affected by shear alignment during the experiment. Blends and ternary nanocomposites have higher storage modulus values than that of the simple nanocomposites, but the nonlinear behavior is observed more clearly and at lower amplitudes for the blends and ternary nanocomposites in both production methods. Therefore, considering the two amplitude sweep graphs presented above (Figure 4.81 and Figure 4.82) the subsequent frequency sweep measurements are decided to be performed at a constant strain amplitude (5 %) for all the batches in order to have comparable results.

Frequency Sweep Measurements

Rheological behavior of PLA/EG composites produced in this part of the study will be evaluated again from the point of different production methods, and at the same time, effects of EG loading and E-GMA addition will be elaborated. Then, the effects of production methods on the viscoelastic behavior of composite materials will be compared based on a single loading.

Figure 4.83, Figure 4.84 and Figure 4.85 show G' , G'' and η^* of the nanocomposites produced via melt compounding. There is a substantial increase in storage modulus with increasing EG loading, especially at low frequencies. This increase in G' , together with a decrease in the slope of the curve, indicates increase in solid-like behavior, or elastic nature of the nanocomposites, at higher filler contents, probably due to the formation of a network structure. Usually, interconnected network structures of anisometric fillers like layered silicates and graphite derivatives lead to noticeable qualitative changes in the dynamic moduli and viscosity. Similar observations were reported also in literature [152, 176]. Effect of filler content in ternary nanocomposites, on the other hand, is suppressed by the presence of the rubber. The PLA/E-GMA blend showed higher storage modulus as compared to all the nanocomposites at all frequencies.

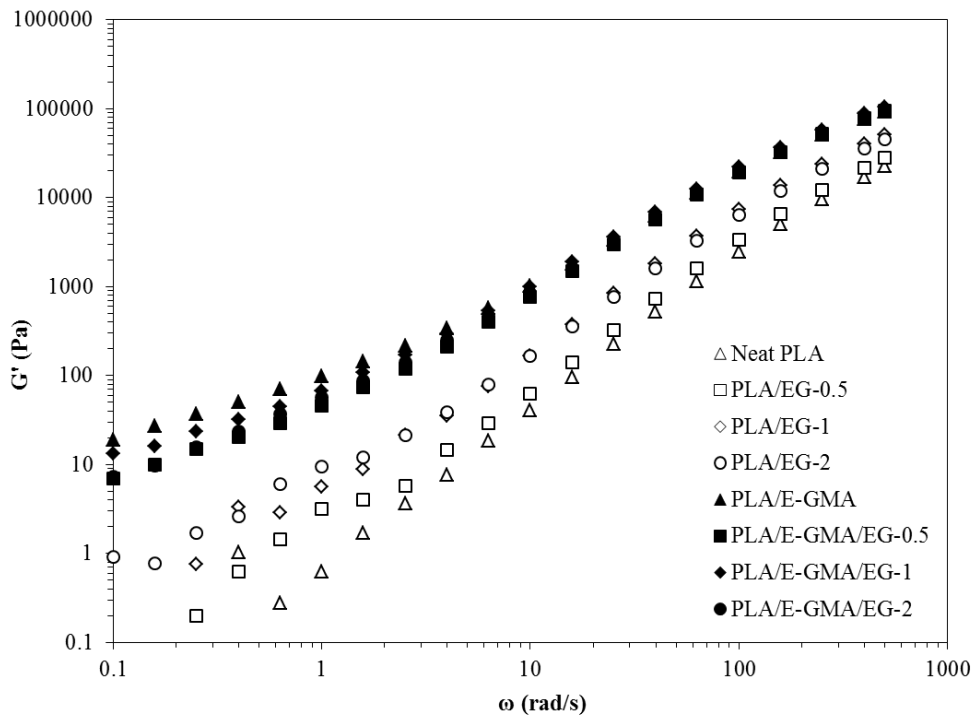


Figure 4.83 Storage modulus as a function of frequency for PLA, PLA/E-GMA binary blend, PLA/EG binary composites and PLA/E-GMA/EG ternary composites prepared produced via melt blending method

Similarly, G'' of the PLA/E-GMA blend and all binary and ternary composites are higher than that of neat PLA as can be seen in Figure 4.84. G'' is a viscoelastic parameter that indicates the viscous or liquid-like behavior of the material, and it gives information mainly on the viscous or energy dissipation during flow [178]. Loss modulus of all samples increased monotonically over the whole frequency range investigated. At high frequency region, the anisotropic EG sheets or stacks probably get aligned in the direction of the flow, therefore, less increase in G'' is observed. In fact, this interpretation of limited contribution at high frequencies is observed for both dynamic moduli for all the nanocomposites.

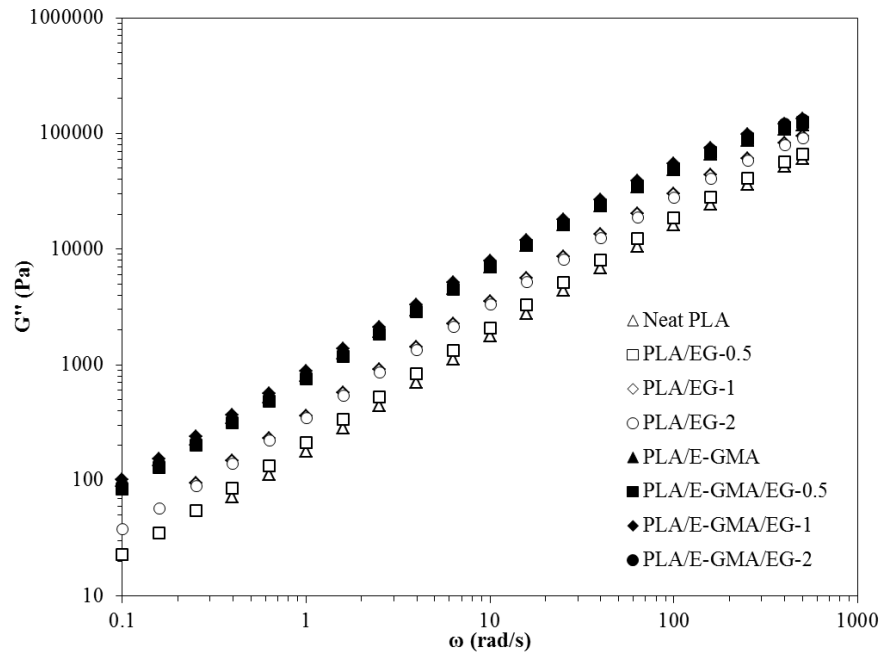


Figure 4.84 Loss modulus as a function of frequency for PLA, PLA/E-GMA binary blend, PLA/EG binary composites and PLA/E-GMA/EG ternary composites prepared produced via melt blending method

The complex viscosity behavior of all samples are similar, such that the Newtonian plateau seen in the low frequency range disappeared in the nanocomposites accompanied with a shear-thinning behavior. The disappearance is clearer in the ternary nanocomposites which also showed significant increase in elastic behavior at low frequencies as G' values suggest. There is a slight increase in the viscosity of PLA/EG-0.5 compared to that of pristine PLA. Thus, addition of 0.5 wt. % EG is obviously not enough for an enhancement compared to pristine PLA. However, the overall enhanced viscosity with increased EG loading in binary PLA/EG nanocomposites could be attributed to the flow restrictions caused by the relatively large stacks. The shear thinning behavior starting at lower frequencies for 1 and 2 wt. % PLA/EG composites could be due to the inherent lubricating nature of graphite containing graphene sheets resulting from the weak Van der Waals forces.

Similar to the storage modulus results, incorporation of E-GMA into the composites suppressed the effect of EG on viscosity in ternary nanocomposites. Dynamic

frequency test results of E-GMA can be seen in Appendix D. The viscosity of E-GMA in melt state is significantly higher than that of pristine PLA at low frequencies (almost 7 times larger) with no Newtonian behavior. At high frequency region, on the other hand, the complex viscosity of pure E-GMA becomes comparable to that of pure PLA. Incorporation of E-GMA to pristine PLA and PLA/EG nanocomposites through melt compounding showed considerable increases in complex viscosity with earlier disappearance of the Newtonian range. This indicates good interaction between the polymer matrix and the rubber with a dominant shear-thinning behavior at high frequencies.

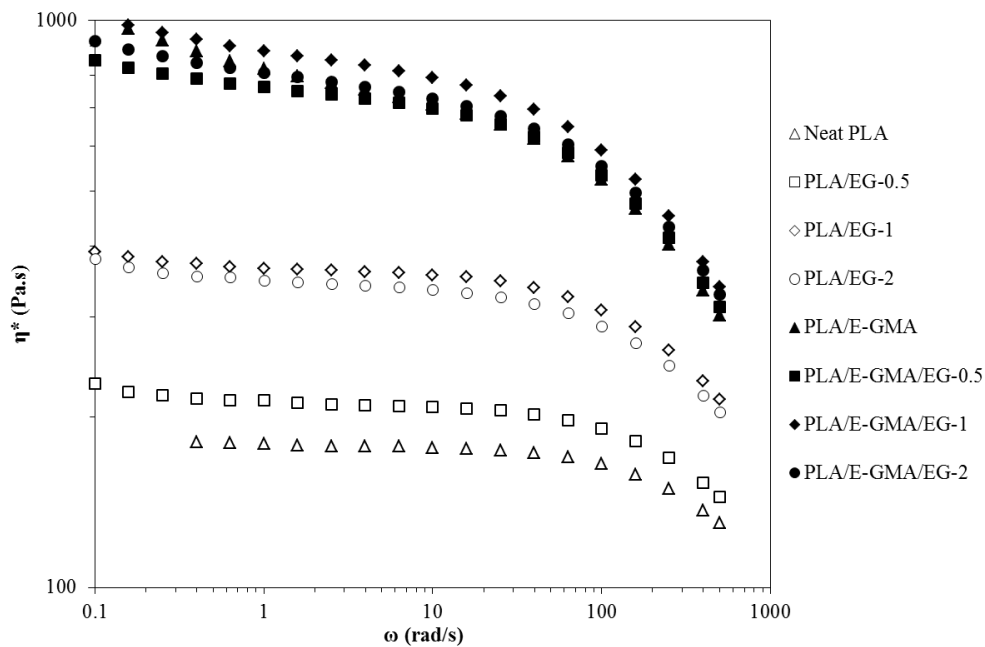


Figure 4.85 Complex viscosity as a function of frequency for PLA, PLA/E-GMA binary blend, PLA/EG binary composites and PLA/E-GMA/EG ternary composites prepared produced via melt blending method

The so-called modified Cole–Cole plots (the curve of $\log G'$ versus $\log G''$) are very sensitive to a variation in the morphological state of multicomponent or multiphase polymer systems such as immiscible polymer blends, micro phase-separated block copolymers and liquid crystalline polymers [179].

Figure 4.86 shows Cole-Cole plots for PLA nanocomposites prepared via melt compounding [86]. Pristine PLA is on the very right side of the equimoduli line indicating liquid-like behavior. The slope of PLA/E-GMA blend is considerably smaller than that of neat PLA. The blend becomes more elastic as it is compounded with E-GMA. The curve for pure E-GMA lies on the equimoduli line. It is indicated in literature that, according to the molecular theories, modified Cole-Cole plot gives a master curve whose slope is 2 for homogeneous polymer melts and solutions [180, 181, 182]. Slopes less than 2 suggest heterogeneous systems [182, 183]. The slope of the $\log G'$ versus $\log G''$ plot of neat PLA is 1.7, which is consistent with the value given in literature [183]. Slope of the blend and ternary composites are smaller than that for pure PLA (around 1.3 for blends). This suggests that all melt mixed PLA/E-GMA blends are immiscible forming a phase separated structure, confirming the result of SEM observations.

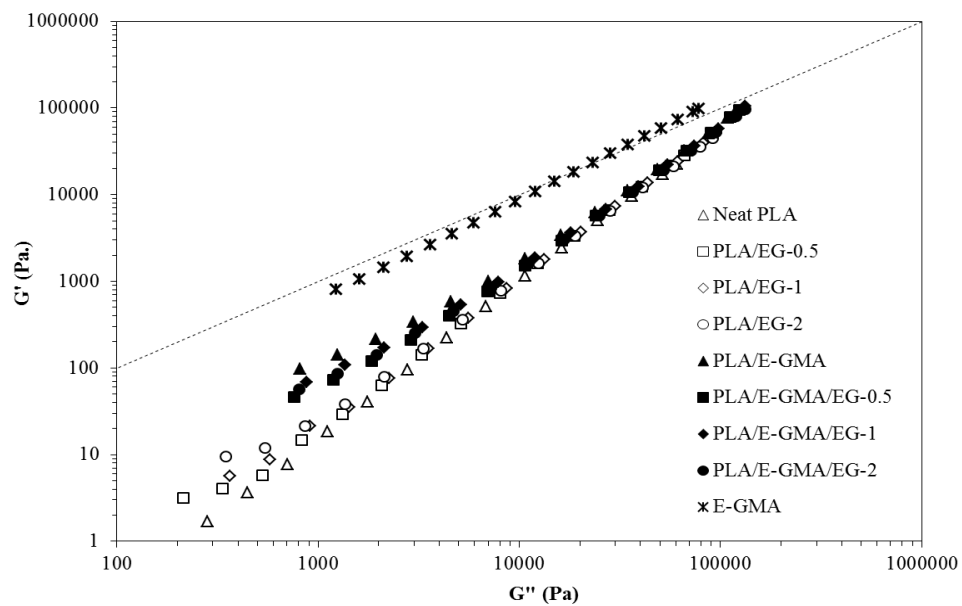


Figure 4.86 Storage modulus as a function of loss modulus for PLA, PLA/E-GMA binary blend, PLA/EG binary composites and PLA/E-GMA/EG ternary composites prepared produced via melt blending method

Previously presented properties of composites produced via solution mixing method revealed that both filler and the rubber interacted differently with the polymer matrix compared to melt compounded samples. There are also some differences between solution mixed composites and melt compounded samples in terms of rheological behavior. Figure 4.87, Figure 4.88 and Figure 4.89 show G' , G'' and η^* of the nanocomposites produced via solution mixing. The enhancements in storage modulus of PLA/EG binary nanocomposites are not very different than melt compounded analogous compositions in terms of order of magnitude. At low frequencies, the increase in G' with increasing EG loading in binary composites supports the TEM results where smaller tactoids, intercalated assemblies and dispersed single graphene layers in polymer matrix are seen more frequently compared to melt blended samples. The increase in the solid-like behavior at higher filler contents is attributed to the formation of a network structure. However, the incorporation of E-GMA in the solution mixed samples resulted in almost 100-fold increase compared to melt compounded samples at the low frequency region. This tremendous increase in solid-like behavior, in which storage modulus is almost independent of the frequency, is more clearly reflected on the modified Cole-Cole plot (Figure 4.90). Similar to the melt blended ternary nanocomposites, effect of filler content is suppressed by the presence of the rubber at low frequencies. However, different from the melt blended samples, at higher frequencies, the curves are separated and the highest EG loading reaches the highest storage modulus.

It is well known that the phase morphology is an important factor in the rheology of immiscible polymer blends. Most binary polymer blends are immiscible and usually the characteristics of these immiscible polymer blends are determined by the state of the interface between the components [184]. SEM micrographs revealed that melt blending results in phase separation while solution mixing forms a continuous morphology. Interactions between PLA and E-GMA chains probably occur only on the surfaces of the dispersed droplets in melt blending. However, in solution mixing, single polymer chains dissolved in the solvent have the chance to directly interact with each other. Therefore, in the melt blended samples the interaction is provided by the copolymer formed on the droplet surface, whereas it is probably in the form of

chain extension in solution mixed samples. Even though no molecular weight determination studies were performed on the samples produced in this study, it is assumed that reactive blending was achieved for both methods based on the FTIR results. The potential chain extension and decreased chain mobility in the overall system might result in the enhanced solid-like behavior. Incorporation of EG into the system further restricts the easy flow of the chains especially in the higher loadings resulted in higher storage modulus values at higher frequencies.

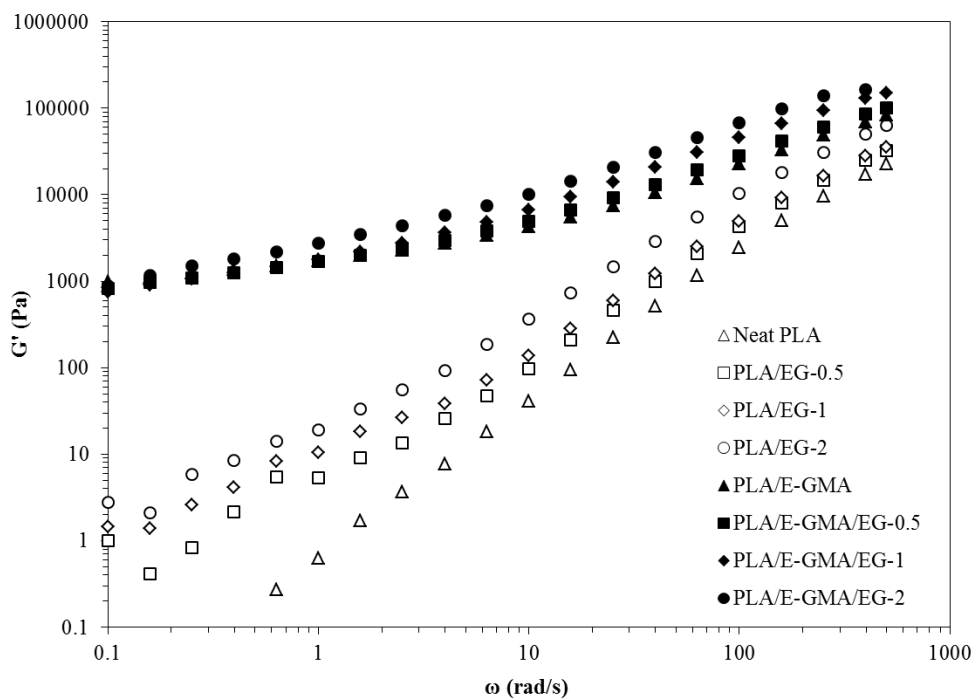


Figure 4.87 Storage modulus as a function of frequency for PLA, PLA/E-GMA binary blend, PLA/EG binary composites and PLA/E-GMA/EG ternary composites prepared produced via solution mixing method

Figure 4.88 shows the loss modulus of samples prepared via solution mixing. Similar to the storage modulus, G'' of the PLA/E-GMA blend and all binary and ternary composites showed increases. Loss modulus of all samples increased over the whole frequency range investigated, with a smaller slope at low frequencies indicating

lower frequency dependence. In the high frequency region, aligned EG stacks in the direction of the flow caused less increase in G'' similar to the melt blended analogues.

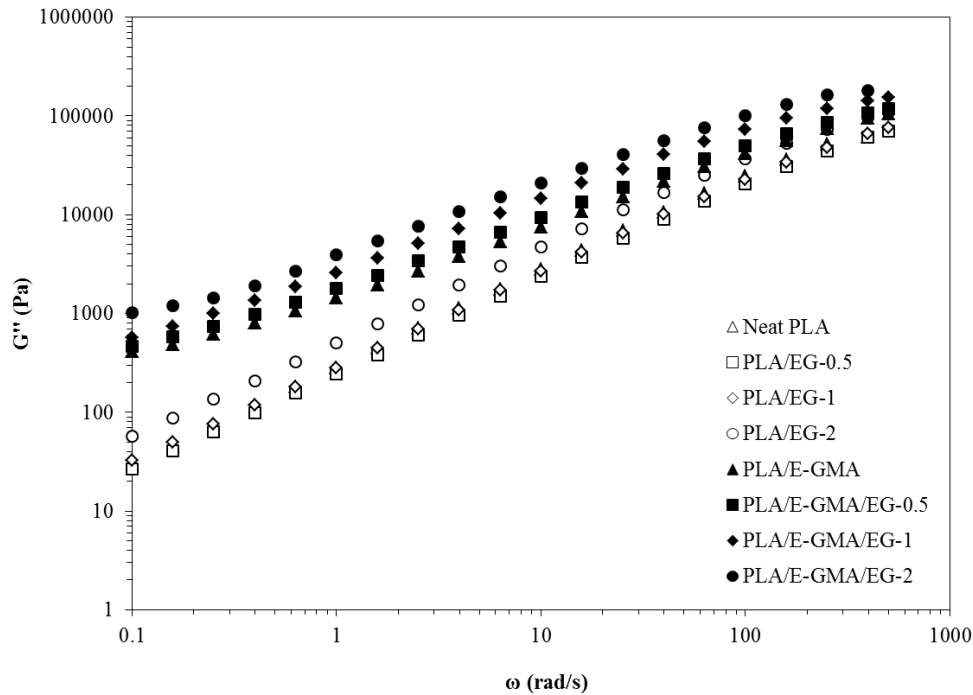


Figure 4.88 Loss modulus as a function of frequency for PLA, PLA/E-GMA binary blend, PLA/EG binary composites and PLA/E-GMA/EG ternary composites prepared produced via solution mixing method

Figure 4.89 shows the dependence of complex viscosities of solution mixed composites. PLA/EG composites, with a rise in viscosity together with the increasing EG loading, exhibited a Newtonian plateau followed by shear thinning at high frequencies. In the low filler loading levels used in this study, only slight changes in the inception of this shear thinning was observed, but this non-Newtonian behavior is of great importance in processing and fabrication of polymer composites. The decreased viscosity enables easier processing of the polymer melt [7]. As mentioned

before, melt compounded samples containing E-GMA showed shear–thinning at lower frequencies compared to the binary composites. Analogous samples prepared via solution mixing, on the other hand, showed no Newtonian behavior. All E-GMA containing samples exhibited high viscosities compared to pristine PLA and their binary composites at low frequencies. At higher frequencies, the viscosities became comparable.

The solid-like behavior observed in the rheology of polymer composites due to the formation of network-like structure in the suspension is now well-established. The effect of network-like structure is clearer at large time scales, namely at lower frequencies. This network structure may be governed by particle-particle and polymer-particle interactions which vary from one polymeric system to the other [183]. In this study, both mechanisms probably affect the behavior of the composites. The change in the matrix morphology restricts the alignment of filler material and the changes in network structure at low frequencies, resulting in a great increase in viscosity. This situation changes at high frequencies, and thus the effect of filler loading is observed clearly. In addition, the potential chain extension and decreased chain mobility in the overall system might result in increase in viscosity. In general, as molecular weight of the continuous phase increases, shear thinning of the complex and shear viscosity become more pronounced [185].

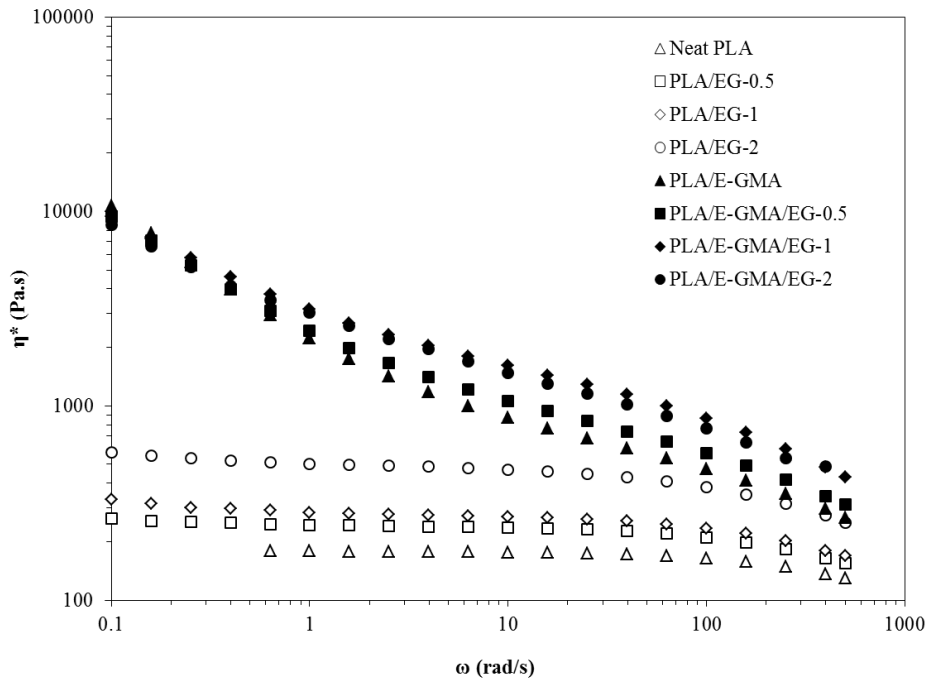


Figure 4.89 Complex viscosity as a function of frequency for PLA, PLA/E-GMA binary blend, PLA/EG binary composites and PLA/E-GMA/EG ternary composites prepared produced via solution mixing method

The drastic increase in solid-like behavior of E-GMA addition to PLA and PLA composites in solution mixing method is clearly reflected on the Cole-Cole plot (Figure 4.90). Pristine PLA curve is again on the very right side of the equimoduli line indicating liquid-like behavior. Slight increase in solid-like behavior in PLA/EG binary composites can be observed. The PLA/E-GMA binary blend and PLA/E-GMA/EG ternary nanocomposites, on the other hand, exhibit strong elastic behavior.

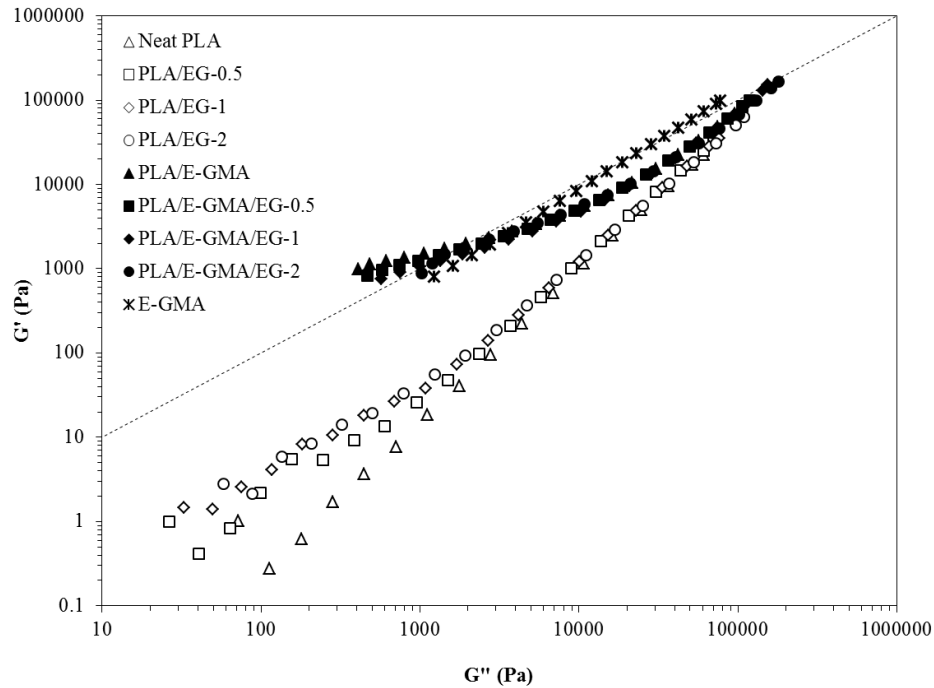


Figure 4.90 Storage modulus as a function of loss modulus for PLA, PLA/E-GMA binary blend, PLA/EG binary composites and PLA/E-GMA/EG ternary composites prepared produced via solution mixing method

Effects of production methods on rheological behavior of PLA and EG composites can be seen in the graphs presented below. In order to observe these results, single EG loading (1 wt. %) was selected and G' and η^* curves are shown on the same plot in Figure 4.91 and Figure 4.92, respectively. PLA/EG binary composites behaved similarly throughout the tested frequency range. This filler loading caused only a slight increase in elastic behavior in the low frequency range, but still G' depends on frequency. The main enhancement in G' is obtained with the addition of E-GMA to the composites. Drastic increase in G' of PLA/E-GMA/EG-1 composite at the low frequencies compared to all other samples indicates that the matrix-rubber-filler interactions were substantially improved in solution mixing method. These interactions in turn forms an interconnected structure which is not affected by the deformations on large time scales.

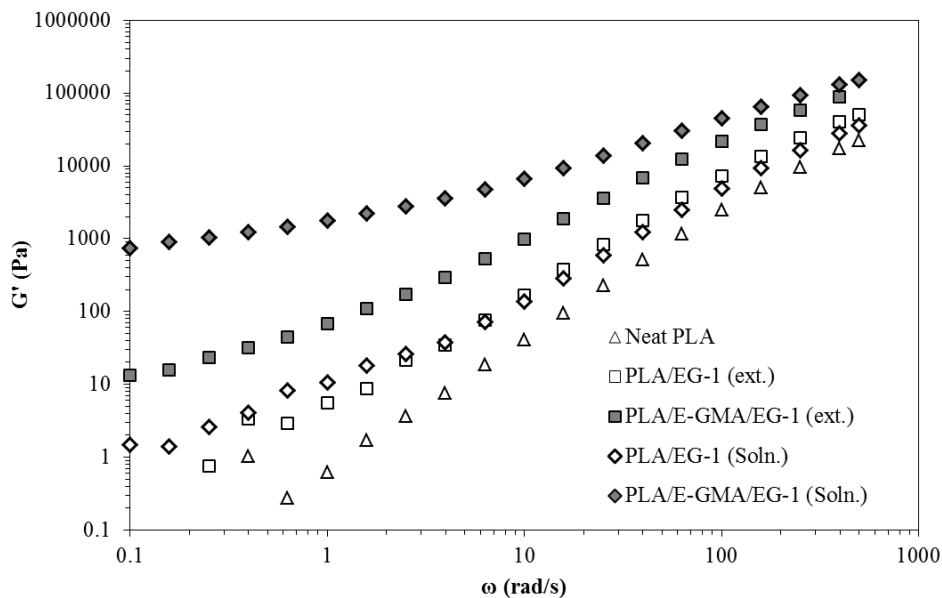


Figure 4.91 Comparison of storage modulus of binary and ternary nanocomposites with respect to the preparation methods

Similar to the storage modulus results, viscosity of the E-GMA containing composites are significantly higher than that of neat PLA and PLA/EG composites prepared via either production method. As discussed beforehand, effect of network-like structure, the obvious change in the matrix morphology, and the possible chain extension reactions between the polymer matrix and the rubber causing a decrease in chain mobility could be reasons of increases in viscosities.

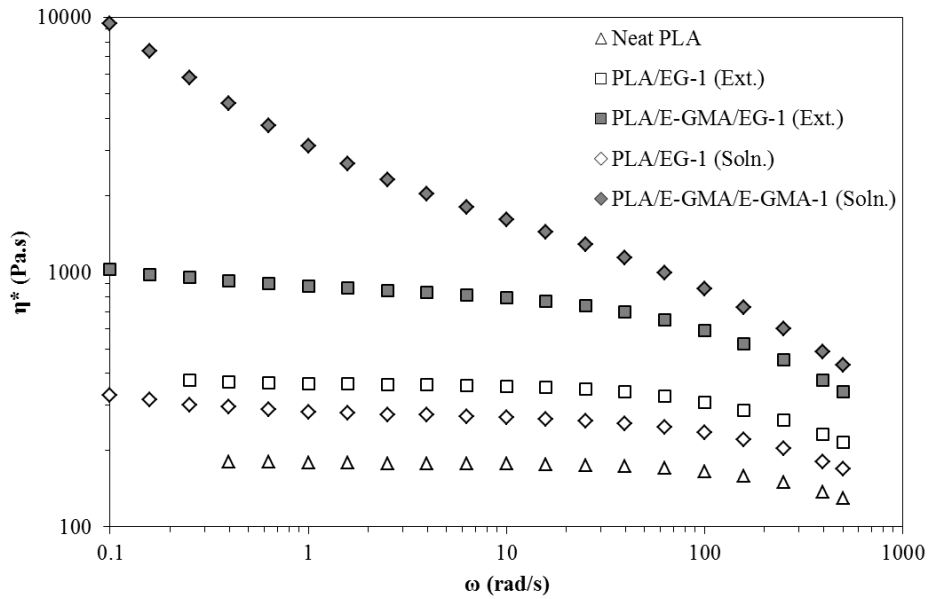


Figure 4.92 Comparison of complex viscosity of binary and ternary nanocomposites with respect to the preparation methods

4.2.2.5 Thermal Analyses

Thermal properties of neat PLA, PLA/E-GM binary blends, PLA/EG and PLA/E-GMA/EG nanocomposites were investigated using DSC, and the main results are tabulated in Table 4.5. In the analysis, only the first heating cycle was considered so that in both mechanical and thermal analysis, all the specimens have the same thermal history. There is no obvious change in melting temperatures of different compositions but crystallinity (X_c) values with respect to production method give clues about different structures. In the literature it is reported that graphite loading induces PLA crystallization [119]. Similar observations are also valid for this study. In both production methods, binary PLA/EG composites follow a pattern of increasing crystallinities with increasing EG loading compared to neat PLA. Except for the PLA/EG binary composites prepared via melt blending, the peaks of crystallization temperature (T_c) are at lower values compared to that of pristine PLA, which supports the nucleation effect of the nanofiller. The exception for PLA/EG

binary composites prepared via melt blending might be due to the weaker interactions of the polymer matrix and filler due to the insufficient dispersion in melt processing. It should be noted that addition of E-GMA to these samples also caused a decrease in T_c , suggesting improved nucleation effect in the presence of E-GMA.

Binary PLA/E-GMA blends have lower crystallinity values compared to the binary PLA/EG composites. This may be due the reactive blending achieved in both methods. Lower crystallinities of solution mixed samples are more pronounced. As discussed before, solution mixing method increased the chain-to-chain interactions between PLA and E-GMA, asserting the continuous morphology, increased elastic properties and decreased chain mobility, which in turn decreased the crystallinity of the materials analyzed.

Table 4.5 Thermal properties of PLA, PLA/E-GMA binary blend, PLA/EG binary composites and PLA/E-GMA/EG ternary composites determined by DSC

Code	Content	T_g (°C)	T_c (°C)	T_m (°C)	X_c (%)
E-0	Neat PLA (ext.)	57.9	119.2	148.4	9.4
E-1	PLA/EG-0.5	58.9	119.1	148.1	10.4
E-2	PLA/EG-1	57.8	119.2	148.3	11.1
E-3	PLA/EG-2	57.9	118.3	148.1	11.8
E-4	PLA/E-GMA (90/10)	57.7	112.6	148.2	9.6
E-5	PLA/E-GMA/EG-0.5	57.8	111.9	148.3	11.1
E-6	PLA/E-GMA/EG-1	57.3	114.2	149.1	9.7
E-7	PLA/E-GMA/EG-2	58.2	112.5	148.3	13.5
S-1	PLA/EG-0.5	54.2	112.9	147.8	9.0
S-2	PLA/EG-1	53.6	117.2	148.9	9.7
S-3	PLA/EG-2	52.6	112.9	148.0	10.2
S-4	PLA/E-GMA (90/10)	60.3	112.7	147.4	4.2
S-5	PLA/E-GMA/EG-0.5	56.3	112.2	149.0	6.3
S-6	PLA/E-GMA/EG-1	56.4	112.9	147.6	7.6
S-7	PLA/E-GMA/EG-2	57.3	112.1	147.7	7.9

CHAPTER 5

CONCLUSIONS

PLA nanocomposites containing different nano-size fillers and commercial elastomeric additives were produced in order to obtain improved properties compared to the pristine PLA. The attempts made in this study to obtain enhanced material properties can be divided into two parts: In the first one, by incorporating epoxy and maleic anhydride functionalities together with nanoclays, it was aimed to improve toughness. Five different organically modified commercial nanoclays were used as nanofillers and two different commercial elastomers with different functional groups (ethylene-glycidyl methacrylate and ethylene-butyl acrylate-maleic anhydride) were selected as the compatibilizers. Both the clay and the compatibilizer contents were kept constant in order to observe the changes in the nanocomposites with changes in the structure of the clay modifiers. Conventional twin-screw extrusion was used as the production method for the nanocomposites. In the second part, expanded graphite was used as nanofiller. The effects of different production methods on the dispersion of expanded graphite (EG) in the polymer matrix were investigated via extrusion and solution mixing techniques. Graphite loading (under 2 wt. %) was investigated together with the incorporation of a rubber. The following conclusions can be given for the separate sections of this dissertation:

PLA/Organoclay Nanocomposites:

- Among the five organoclays utilized, C25A and C30B have more affinity to the PLA polymer matrix. Addition of E-GMA resulted in an increased degree of

polymer intercalation into the galleries between silicate layers. But E-BA-MAH caused no significant change clay dispersion compared to PLA/clay binary nanocomposites.

- Phase separated morphologies were obtained by blending PLA with compatibilizers. Sizes of the rubbery domains of different rubbers are noticeably different. Average droplet size of E-BA-MAH is almost 1.4-fold larger than E-GMA droplets after blending at identical conditions.
- TEM analyses revealed that all nanocomposites were comprised of multiple clay dispersion states. In every sample, intercalated/exfoliated structures with tactoids of changing sizes are observed.
- According to the FTIR analyses, both E-GMA and E-BA-MAH interacted reactively with PLA.
- According to the tensile test results, binary blends have significantly lower tensile strength and modulus than the pristine PLA. These decreases were compensated with the incorporation of nanofillers to some extent, especially for E-GMA containing nanocomposites.
- Results of elongations at break, which are indicators of tensile toughness, were totally different than the expectations. Blending with E-GMA resulted almost 8-fold increase in elongation at break, but blending with E-BA-MAH caused reduction in elongation. All clay types increased the percent elongations even at higher level than blending with E-GMA.
- Impact strength values of ternary nanocomposites containing E-GMA are all higher than that of neat PLA, but lower than that of the binary PLA/E-GMA blend. However, E-BA-MAH containing nanocomposites resulted in a reduction compared to neat PLA. The difference in rubber domain sizes and the incompatibility of E-BA-MAH with PLA could be the reasons of reduced impact strength values.
- Although the contents of all nanocomposites are the same, effects of modifier structure and the compatibility of the dispersed phase were clearly reflected on

the rheological behavior. E-BA-MAH containing nanocomposites showed earlier nonlinear behavior in strain sweep measurements.

- Organoclays C25A and C30B, and the compatibilizer E-GMA came into focus in terms of increased melt viscosity and elastic behavior in the low frequency range. Addition of E-BA-MAH, on the other hand, resulted in no significant changes in solid-like behavior. In particular cases, both dynamic moduli and viscosity values of E-BA-MAH containing samples remained below that of the neat PLA, which is attributed to increased chain mobility and alignment of silicate layers easily due to weak interactions in these ternary systems. Enhanced melt viscosity in the samples containing E-GMA could be attributed to the high viscosity of E-GMA itself, and flow restrictions owing to the strong interaction between the polymer matrix and the compatibilizers.
- Extrusion caused 7% increase in global crystallinity of pristine PLA due to the chain scissions caused by extrusion.
- Due to the low filler loading, effect of organoclays on the thermal properties of nanocomposites compared to neat polymer cannot be evaluated efficiently but the effect of rubber addition can be seen in the case of E-BA-MAH. Addition of E-BA-MAH to the nanocomposites resulted in the highest crystallinity values due to the weaker compatibility of this rubber with the polymer matrix and the clay nanoparticles might result in easier alignment of polymer chains due to decreased restrictions.

To sum up this part of the dissertation, it was observed that even at low clay loadings the structure of modifier influences the nanocomposite properties. Clay dispersion in the PLA matrix is highly affected by the type of organic modifier of the clay. Even though nanocomposites exhibit both intercalated and some exfoliated layers with some remaining tactoids, the degree of intercalation is determined by the chemical compatibility between the polymer matrix and the modifier. Compatibilizer structure is another important parameter affecting the final morphology. Good polarity matching between the modifier structures of C25A and C30B and the compatibilizer E-GMA resulted in high degree of intercalation. This

phenomenon is coupled with the high reactivity of the epoxide group of GMA towards the end groups of PLA compared to the MAH functional group, and possibly resulted in network structures in the final product. Effects of the changes in microstructure were reflected in both mechanical and rheological properties. Both of the binary blends have lower tensile strength and modulus values, which are lower than that of the neat PLA, and tensile strength and modulus were compensated to a certain extent with the formation of ternary nanocomposites. Increases in both tensile and impact toughness were also observed with the addition of rubber and/or organoclay.

In the melt state, the most explicit shear-thinning behavior was observed for E-BA-MAH containing composites due to the weaker interactions. Addition of E-GMA, obviously changed the elastic behavior of the nanocomposites at low frequencies. Solid-like behavior of PLA/E-GMA blend was reduced with the addition of nanoclay which might be an indication of clay positioning in the ternary nanocomposites. All nanocomposites behaved similarly at high frequencies indicating that chain relaxation modes are not affected by the presence of layered silicates.

PLA/Expanded Graphite Nanocomposites:

- According to the XRD analyses, both melt blending and solution mixing were not able to exfoliate or completely separate the stacks of parallel graphene sheets. However, there are smaller tactoids, intercalated assemblies and dispersed single graphene layers as observed in TEM micrographs of solution mixed samples.
- SEM images of samples produced via both melt compounding and solution mixing consist of large EG stacks in micron sizes.
- Melt blended composites containing E-GMA have phase separated morphologies with ellipsoidal submicron size E-GMA droplets dispersed in the polymer matrix. Morphologies of analogous samples produced via solution mixing are totally different. Continuous, single phase morphology is observed in these samples.

- FTIR spectra of blends prepared with different methods are identical which means in both methods PLA is reactively blended with E-GMA.
- Mechanical properties of the composites change significantly with EG loading, rubber addition and preparation method. Blending PLA with E-GMA resulted in significant reductions in tensile strength and modulus for both production methods. This reduction is more pronounced for solution mixing, but the compensation of these reductions with the incorporation of filler is also clearer in solution mixed samples.
- Increases in tensile toughness are more apparent in samples prepared via solution mixing, especially in E-GMA containing ones.
- Effects of changing morphological structures obtained via different production methods were also seen in rheological behavior. Binary PLA/EG composites behaved similarly at all frequencies, but incorporation of E-GMA into these composites with different production methods were obviously different. Addition of E-GMA via solution mixing resulted in drastic increase in solid like behavior, especially at low frequencies.
- Complex viscosities of binary and ternary composites were also different. Increased EG loading in binary composites caused a gradual increase in complex viscosities. But E-GMA addition suppressed the effect of filler loading and at all EG concentrations ternary composites had higher viscosities with earlier disappearance of Newtonian behavior in melt blended samples. Samples prepared via solution mixing did not even show Newtonian behavior.
- Thermal analyses revealed that in both production methods, binary PLA/EG composites followed a pattern of increasing crystallinity with increasing EG loading compared to neat PLA. Additionally, lower crystallization temperature of composites compared to pristine PLA verifies nucleation effects of the nanofiller.

To sum up this second part of the study, it was observed that the production method determines the final properties of the product even though no significant differences

were observed in filler dispersion with morphological analyses. High magnitudes of shear is applied to the polymer melt during extrusion, and there is continuous mixing throughout the extruder, but the polymeric materials can interact only on the interface of the coalesced droplets. In solution mixing, there is the possibility of polymer chains and the elastomer chains to interact with each other, i.e., there is mixing at the molecular level. Thus, the final morphologies are different. Continuous morphology observed in samples prepared via solution mixing results in lower strength and rigidity than phase separated melt blended samples. However, compensation of these reductions with the presence of rigid filler is more apparent. The self-lubricating effect might result in easier sliding of both graphene sheets and polymer chains interacting with the filler surface. Increased chain mobility might result in decreasing ultimate tensile strength and elastic modulus but in increased strain without failure. The rheological behavior of solution mixed ternary nanocomposites suggest that the network-like structure, the obvious change in the matrix morphology, and the possible chain extension reactions between the polymer matrix and the rubber caused a decrease in chain mobility accompanied with increases in both dynamic moduli and viscosity.

Under the light of all the results obtained in this study, PLA nanocomposites with very low filler contents have shown to possess various mechanical, rheological, and thermal property enhancements, and these enhancements mainly depend on polymer-particle interactions and effective dispersion of the filler in the matrix. In the first part of the study, it was revealed that E-GMA is a better compatibilizer and impact modifier for PLA/organoclay nanocomposites. In the second part, solution mixing method to produce ternary nanocomposites was shown to provide better interactions between the elastomer and the polymer matrix and thus the filler. However, the enhancements and reductions in a particular property are usually accompanied with changes in another property. Thus, the type of filler material, the structure of the elastomer and the production method to be used for a specific product should be selected according to the desired final properties.

REFERENCES

- [1] R. M. Rasal, A. V. Janokar and D. E. Hirt, "Poly(lactic acid) Modifications," *Progress in Polymer Science*, vol. 35, pp. 338-356, 2010.
- [2] S. Sinha Ray and M. Bousmina, "Biodegradable Polymers and Their Layered Silicate Nanocomposites: In Greening The 21st Century Materials World," *Progress In Materials Science*, vol. 50, pp. 962-1079, 2005.
- [3] G. M. Bohlmann, "General Characteristics, Processibility, Industrial Applications an Market Evolution of Biodegradable Polymers," in *Handbook of Biodegradable Polymers*, Rapra Technology Limited, 2005.
- [4] H. Liu and J. Zhang, "Research Progress in Toughening Modification of Poly(lactic acid)," *Polymer Physics*, vol. 49, p. 1051–1083, 2011.
- [5] M. Alexandre and P. Dubois, "Polymer-Layered Silicate Nanocomposites: Preparation, Properties and Uses of a New Class of Materials," *Materials Science and Engineering*, vol. 28, pp. 1-63, 2000.
- [6] E. P. Giannelis, "Polymer-Layered Silicate Nanocomposites: Emerging Scientific and Commercial Opportunities," in *Proceedings of 57th SPE Annual Technical Conference (ANTEC)*, 1999.
- [7] M. Song and J. Jin, "Characterization of Rheological Properties of Polymer Nanocomposites," in *Characterization Techniques for Polymer Nanocomposites*, Singapore, Wiley, 2012, pp. 251-280.
- [8] Y. Kojima, A. Usuki, M. Kawasumi, A. Okada, Y. Fukushima, T. Kurauhi and O. Kamigaito, "Mechanical Properties of Nylon 6-Clay Hybrid," *Journal of Materials Research - Materials Research Society*, vol. 8, no. 5, pp. 1185-1189, 1993.

- [9] N. Ogata, G. Jimenez, H. Kawai and T. Ogihara, "Structure and Thermal/Mechanical Properties of Poly (l-lactide)-Clay Blend," *Journal of Polymer Science Part B: Polymer Physics*, vol. 35, pp. 389-396, 1997.
- [10] B. Li and W.-H. Zhong, "Review on Polymer/Graphite Nanoplatelet Nanocomposites," *Journal of Material Sciences*, no. 46, p. 5595–5614, 2011.
- [11] M. Tait, A. Pegoretti, A. Dorigato and K. Kalaitzidou, "The Effect of Filler Type and Content and The Manufacturing Process on The Performance of Multifunctional Carbon/Poly-Lactide Composites," *Carbon*, vol. 49, pp. 4280-4290, 2011.
- [12] D. Cho, S. Lee, G. Yang, H. Fukushima and L. T. Drzal, "Dynamic Mechanical and Thermal Properties of Phenylethynyl-Terminated Polyimide Composites Reinforced with Expanded Graphite Nanoplatelets," *Macromolecular Materials and Engineering*, vol. 290, no. 3, pp. 179-187, 2005.
- [13] F. Campbell, *Structural Composite Materials*, ASM International, 2010.
- [14] D. Hull, *An Introduction to Composite Materials*, Cambridge: Cambridge University Press, 1981.
- [15] A. Kaw, *Mechanics of Composite Materials*, Boca Raton: Taylor & Francis Group, 2006.
- [16] K. K. Chawla, *Composite Materials Science and Engineering*, New York: Springer Science & Business Media, 2013.
- [17] M. M. Schwartz, *Composite Materials: Properties, Nondestructive Testing and Repair*, New Jersey: Prentice-Hall, 1996.
- [18] L. C. Sawyer and D. T. Grubb, *Polymer Microscopy*, New York: Chapman and Hall, 1987.
- [19] S. L. Rosen , *Fundamental Principles of Polymeric Materials*, New York: John Wiley & Sons, 1993.
- [20] J. E. Mark, "Ceramic Reinforced Polymers and Polymer-Modified Ceramics," *Polymer Engineering and Science*, vol. 36, pp. 2905-2920, 1996.

- [21] E. Reynauld, C. Gauthier and J. Perez, "Nanophases in Polymers," *Revue De Metallurgie-cahiers D Informations Techniques*, vol. 96, pp. 169-176, 1999.
- [22] T. von Weme and T. E. Patten, "Preparation of Structurally Well Defined Polymer-Nanoparticle Hybrids with Controlled Living Radical Polymerization," *Journal of the American Chemical Society*, vol. 121, pp. 7409-7410, 1999.
- [23] N. Herron and D. L. Thorn, "Nanoparticles: Uses and Relationships to Molecular Clusters," *Advanced Materials*, vol. 10, pp. 1173-1184, 1998.
- [24] V. Favier, G. R. Canova, S. C. Shrivastava and J. Y. Cavaille, "Mechanical Percolation in Cellulose Whisker Nanocomposites," *Polymer Engineering and Science*, vol. 37, pp. 1732-1739, 1997.
- [25] H. F. Mark and J. I. Kroschwitz, *Encyclopedia of Polymer Science and Engineering*, N.J.: Wiley Interscience, 2003.
- [26] T. J. Pinnavaia and G. W. Beall, *Polymer-Clay Nanocomposites*, New York: John Wiley and Sons Ltd., 2000.
- [27] Q. H. Zeng, D. Z. Wang, A. B. Yu and G. Q. Lu, "Synthesis of Polymer-Montmorillonite Nanocomposites by In-situ Intercalative Polymerization," *Nanotechnology*, vol. 13, pp. 549-553, 2002.
- [28] D. M. Moore and D. M. Reynolds, *X-ray Diffraction and the Identification and Analysis of Clay Minerals*, Oxford: Oxford University Press, 1997.
- [29] M. Zanetti, S. Lomakin and G. Camino, "Polymer Layered Silicate Nanocomposites," *Macromolecular Materials and Engineering*, vol. 279, pp. 1-9, 2000.
- [30] E. P. Giannelis, R. Krishnamoorti and E. Manias, "Polymer-Silicate Nanocomposites: Model Systems for Confined Polymers and Polymer Brushes," *Advances in Polymer Science*, vol. 138, pp. 193-227, 1999.
- [31] P. C. LeBaron, Z. Wang and T. J. Pinnavaia, "Polymer-Layered Silicate Nanocomposites: An Overview," *Applied Clay Science*, vol. 15, pp. 11-29,

- 1999.
- [32] F. Işık-Coşkunes, "Ternary Nanocomposites of Low Density, High Density and Thesis: Linear Low Density Polyethylenes with The Compatibilizers E-MA-GMA and E-BA-MAH," Middle East Technical University, 2001.
- [33] R. A. Vaia and E. P. Giannelis, "Lattice Model of Polymer Melt Intercalation in Organically-Modified Layered Silicates," *Macromolecules*, vol. 30, pp. 7990-7999, 1997.
- [34] S. Sinha Ray and M. Okamoto, "Polymer/Layered Silicate Nanocomposites: A Review from Preparation to Processing," *Prog. Polym. Sci.*, vol. 28, pp. 1539-1641, 2003.
- [35] X. Kornmann, "Synthesis and Characterisation of Thermoset Nanocomposites," Lulea University of Technology, Lulea, 2001.
- [36] H. R. Dennis, D. L. Hunter, D. Chang, S. Kim, J. L. White, Cho J. W. and D. R. Paul, "Effect of Melt Processing Conditions on the Extent of Exfoliation in Organoclay-Based Nanocomposites," *Polymer*, vol. 42, pp. 9513-9522, 2001.
- [37] H. O. Pierson, Handbook of Carbon, Graphite, Diamond, and Fullerenes, Park Ridge, N.J., U.S.A.: Noyes Publications, 1993.
- [38] D. Chung, "Graphite," *Journal of Materials Science*, no. 37, pp. 1475-1489, 2002.
- [39] "TutorVista," 2005. [Online]. Available: <http://chemistry.tutorvista.com/-organic-chemistry/carbon-compounds.html#>. [Accessed 7 1 2014].
- [40] R. Sengupta, . M. Bhattacharyaa, S. Bandyopadhyayb and A. K. Bhowmicka, "A Review on the Mechanical and Electrical Properties of Graphite and Modified Graphite Reinforced Polymer Composites," *Progress in Polymer Science*, no. 36, pp. 638-670, 2011.
- [41] G.-H. Chen, D.-J. Wu, W.-G. Weng, B. He and W. Yan, "Preparation of Polystyrene-Graphite Conducting Nanocomposites via Intercalation Polymerization," *Polymer International*, vol. 50, pp. 980-985, 2001.

- [42] A. Geim and K. S. Novoselov, "The Rise of Graphene," *Nature Materials*, vol. 6, pp. 183-191, 2007.
- [43] K. Kalaitzidou, H. Fukushima and L. Drzal, "A New Compounding Method for Exfoliated Graphite–Polypropylene Nanocomposites with Enhanced Flexural Properties and Lower Percolation Threshold," *Composites Science and Technology*, vol. 67, no. 10, pp. 2045-2051, 2007.
- [44] K. Wakabayashi, C. Pierre, D. Dikin, R. Ruoff, T. Ramanathan, L. Brinson and J. Torkelson, "Polymer-Graphite Nanocomposites: Effective Dispersion and Major Property Enhancement via Solid-State Shear Pulverization," *Macromolecules*, no. 41, pp. 1905-1908, 2008.
- [45] M. Jamshidian, E. A. Tehrany, M. Imran, M. Jacquot and S. Desobry, "Poly-Lactic Acid: Production, Applications, Nanocomposites, and Release Studies," *Comprehensive Reviews in Food Science and Food Safety*, vol. 9, pp. 552-571, 2010.
- [46] C. Bastioli, "Properties and Applications of Mater-Bi Starch-Based Materials," *Polymer Degradation and Stability*, vol. 59, pp. 263-272, 1998.
- [47] M. Kutz, *Applied Plastics Engineering Handbook: Processing and Materials*, Elsevier, 2011.
- [48] E. T. Vink, K. R. Rabago, D. A. Glessner and P. R. Gruber, "Applications of life cycle assessment to NatureWorks™ polylactide (PLA) production," *Polymer Degradation and Stability*, vol. 80, pp. 403-419, 2003.
- [49] K. M. Nampoothiri, N. R. Nair and R. P. John, "An Overview of the Recent Developments in Polylactide (PLA) Research," *Bioresource Technology*, vol. 101, pp. 8493-8501, 2010.
- [50] R. E. Drumright, P. R. Gruber and D. E. Henton, "Polylactic Acid Technology," *Advanced Materials*, vol. 12, no. 23, pp. 1841-1845, 2000.
- [51] D. E. Henton, P. Gruber, J. Lunt and J. Randall, "Polylactic Acid Technology," in *Natural Fibers, Biopolymers, and Biocomposites*, CRC Press, 2005, pp. 527-578.

- [52] R. Franchini, R. Plessu, J. R. Sarasua and R. E. Prudhome, "Cracking in Polylactide Spherulites," *Journal of Polymer Science Part B: Polymer Physics*, vol. 43, pp. 3308-3315, 2005.
- [53] J. R. Dorgan, H. J. Lehermier, L. I. Palade and J. Cicero, "Polylactides: Properties and Prospects of an Environmentally Benign Plastic from Renewable Resources," *Macromolecular Symposia*, vol. 175, pp. 55-66, 2001.
- [54] A. V. Janokar, A. T. Metters and D. E. Hirt, "Modification of Poly(lactic acid) Films: Enhanced Wettability from Surface-Confined Photografting and Increased Degradation Rate Due to an Artifact of the Photografting Process," *Macromolecules*, vol. 37, pp. 9151-9159, 2004.
- [55] R. O. Ebewele, *Polymer Science and Technology*, Boca Raton: CRC Press, 2000.
- [56] J. R. Fried, *Polymer Science and Technology*, New Jersey: Prentice Hall, 2003.
- [57] A. Shah and M. Gupta, "Comparison of the Flow in Co-rotating and Counter-rotating Twin-Screw Extruders," in *ANTEC® - The Plastics Conference*, 2004.
- [58] Z. Tadmor and C. G. Gogos, *Principles of Polymer Processing*, New Jersey: John Wiley & Sons, 2006.
- [59] S. Yeşil, *Processing and Characterization of Carbon Nanotube Based Conductive Polymer Composites*, Ankara: Thesis, METU, 2010.
- [60] J. S. Colton, *Injection Molding - Process Description*, Georgia Institute of Technology- Lecture notes of Manufacturing Processes and Engineering.
- [61] S. Middleman, *Fundamentals of Polymer Processing*, McGraw-Hill, 1977.
- [62] R. Aluru, M. Keefe and S. Advani, "Simulation of Injection Molding into Rapid-Prototyped Molds," *Rapid Prototyping Journal*, vol. 7, no. 1, pp. 42-51, 2001.
- [63] V. Ahluwalia and A. Mishra, *Polymer Science - A textbook*, New Delhi:

CRC Press, 2008.

- [64] *ISO 527-2 Determination of Tensile Properties*, International Organization for Standardization, 1993.
- [65] J. J. Yue, "Virginia Tech Materials Science and Engineering," 4 5 1997. [Online]. Available: http://www.sv.vt.edu/classes/MSE2094_NoteBook-/97ClassProj/anal/yue/energy.html. [Accessed 24 4 2014].
- [66] D. Campbell, R. A. Pethrick and J. R. White, *Polymer Characterization: Physical Techniques*, Cheltenham: Chapman and Hall, 2000.
- [67] R. R. Hegde, M. G. Kamath and A. Dahiya, "Polymer Crystallinity," [Online]. Available: <http://www.engr.utk.edu/mse/pages/Textiles/PolymerCrystallinity.htm>. [Accessed 2014].
- [68] *ISO 11357-2: Plastics - Differential Scanning Calorimetry (DSC) - Part 2: Determination of The Glass Transition Temperature*, International Organization for Standardization, 1999.
- [69] "X-Ray Diffraction - Bruker D8 Discover," Ku Leuven, [Online]. Available: <https://fys.kuleuven.be/iks/nvsf/experimental-facilities/x-ray-diffraction-2013-bruker-d8-discover>. [Accessed 2014].
- [70] *Introduction to X-Ray Diffraction (XRD)*, Creative Commons Attribution-Noncommercial-Share Alike 2.5 License.
- [71] M. Birkholz, "Principles of X-ray Diffraction," in *Thin Film Analysis by X-Ray Scattering*, Weinheim, Wiley, 2006.
- [72] D. Henry, E. Nelson, J. Goodge and D. Mogk, "X-Ray reflection in Accordance with Bragg's Law," *Geochemical Instrumentation and Analyses*-Carlton University, [Online]. Available: http://serc.carleton.edu/research_education/geochemsheets/BraggsLaw.html. [Accessed 2014].
- [73] R. B. Seymour, *Polymer Chemistry: An Introduction*, New York: Marrel Dekker, 1996.
- [74] "Scanning Electron Microscopy," *Materials Evaluation and Engineering, Inc.*, [Online]. Available: <http://www.mee-inc.com/sem.html>. [Accessed

- 2014].
- [75] I. Tiginyanu, S. Langa, H. Foell and V. Ursachi, Porous III-V Semiconductors, www.porous-35.com, 2009.
- [76] "Transmission and Scanning Electron Microscopy," [Online]. Available: www.expertsmind.com/topic/looking-at-microbes/transmission-and-scanning-electron-microscopy-92282.aspx. [Accessed 2014].
- [77] "The Transmission Electron Microscopy," Nobel Prize, [Online]. Available: <http://www.nobelprize.org/educational/physics/microscopes/tem/>. [Accessed 2014].
- [78] "Electron Microscopy," Swiss Federal Institute of Technology Zurich, [Online]. Available: <http://www.microscopy.ethz.ch/TEM-structure.htm>. [Accessed 2014].
- [79] Y.-T. Lu and A. R. Barron, "Transmission Electron Microscopy: An Overview," [Online]. Available: <http://cnx.org/content/m34523/latest/?collection=col10699/latest>. [Accessed 26 04 2014].
- [80] C. R. Brundle, C. A. Evans and S. Wilson, Encyclopedia of Material Characterization, Stoneham: Butterworth-Heinemann, 1992.
- [81] G. Swann and S. Patwardhan, "Application of Fourier Transform Infrared Spectroscopy (FTIR) for Assessing Biogenic Silica Sample Purity in Geochemical Analyses and Palaeoenvironmental Research," vol. 7, pp. 65-74, 2011.
- [82] E. Laboratories, "FTIR," [Online]. Available: <http://www.etslabs.com/analysis.aspx?id=%23JJUICPRF>. [Accessed 05 05 2014].
- [83] R. F. Gibson, Principles of Composite Material Mechanics, New York: McGraw-Hill, Inc., 1994.
- [84] TA Instruments, "ARES G2 Rheometer - Application of Rheology of Polymers," [Online]. Available: <http://www.tainstruments.com/product.aspx?id=31&n=1&siteid=11>. [Accessed 26 4 2014].
- [85] D. Weitz, H. Wyss and R. Larsen, "Oscillatory Rheology: Measuring the

Viscoelastic Behaviour of Soft Materials," *G.I.T. Laboratory Journal*, Vols. 3-4, pp. 68-70, 2007.

- [86] T. Seyidođlu, *PhD Thesis: Purification and Modification of Bentonite and Its Use In Polypropylene and Linear Low Density Polyethylene Matrix Nanocomposites*, Ankara: Middle East Technical University, 2010.
- [87] R. G. Sinclair, "The Case for Polylactic Acid as a Commodity Packaging Plastic," *Journal of Macromolecular Science, Part A: Pure and Applied Chemistry*, vol. A33, pp. 585-597, 1996.
- [88] S. Jacobsen and H. G. Fritz, "Plasticizing Polylactide - the Effect of Different Plasticizers on the Mechanical Properties," *Polymer and Engineering Science*, vol. 39, no. 7, pp. 1303-1310, 1999.
- [89] O. Martin and L. Averous, "Poly(lactic acid): Plasticization and Properties of Biodegradable Multiphase Systems," *Polymer*, vol. 42, pp. 6209-6219, 2001.
- [90] I. Noda, M. M. Satkowski, A. E. Dowrey and C. Marcott, "Polymer Alloys of Nodax Copolymers and Poly(lactic Acid)," *Macromolecular Bioscience*, vol. 4, pp. 269-275, 2004.
- [91] L. Wang, W. Ma, R. A. Gross and S. P. McCarthy, "Reactive Compatibilization of Biodegradable Blends of Poly(lactic acid) and Poly(ϵ -caprolactone)," *Polymer Degradation and Stability*, vol. 59, pp. 161-168, 1998.
- [92] T. Semba, K. Kitagawa, U. S. Ishiaku and H. Hamada, "The Effect of Crosslinking on the Mechanical Properties of Polylactic Acid/Polycaprolactone Blends," *Journal of Applied Polymer Science*, vol. 101, pp. 1816-1825, 2006.
- [93] T. Takayama and M. Todo, "Improvement of Impact Fracture Properties of PLA/PCL Polymer Blend due to LTI Addition," *Journal of Materials Science*, vol. 41, pp. 4989-4992, 2006.
- [94] M. Harada, T. Ohya, K. Iida, H. Hayashi, K. Hirano and H. Fukuda, "Increased Impact Strength of Biodegradable Poly(lactic acid)/Poly(butylene

- succinate) Blend Composites by Using Isocyanate as a Reactive Processing Agent," *Journal of Applied Polymer Science*, vol. 106, pp. 1813-1820, 2007.
- [95] Y. Li and H. Shimizu, "Toughening of Polylactide by Melt Blending with a Biodegradable Poly(ether)urethane Elastomer," *Macromolecular Bioscience*, vol. 7, no. 7, pp. 921-928, 2007.
- [96] K. S. Anderson, S. H. Lim and M. A. Hilmmyer, "Toughening of Polylactide by Melt Blending with Linear Low-Density Polyethylene," *Journal of Applied Polymer Science*, vol. 89, no. 14, pp. 3757-3786, 2003.
- [97] H. T. Oyama, "Super-tough Poly(lactic acid) Materials: Reactive Blending with Ethylene Copolymer," *Polymer*, vol. 50, pp. 747-751, 2009.
- [98] K. Hashima, S. Nishitsuji and T. Inoue, "Structure-properties of Super-tough PLA Alloy with Excellent Heat Resistance," *Polymer*, vol. 51, pp. 3934-3939, 2010.
- [99] M. Pluta, A. Galeski, M. Alexandre, M.-A. Paul and P. Dubois, "Polylactide/Montmorillonite Nanocomposites and Microcomposites Prepared by Melt Blending: Structure and Some Physical Properties and Some Physical Properties," *Journal of Applied Polymer Science*, vol. 86, pp. 1497-1506, 2002.
- [100] V. Krikorian and D. J. Pochan, "Poly (L-Lactic Acid)/Layered Silicate Nanocomposite: Fabrication, Characterization, and Properties," *Chemistry of Materials*, vol. 15, pp. 4317-4324, 2003.
- [101] M. A. Paul, C. Delcourt, M. Alexandre, P. Degee, F. Monteverde and P. Dubois, "Polylactide/Montmorillonite Nanocomposites: Study of the Hydrolytic Degradation, Polymer Degradation and Stability," *Polymer Degradation and Stability*, vol. 87, pp. 535-542, 2005.
- [102] S. S. Ray, K. Yamada, M. Okamoto and K. Ueda, "Polylactide-Layered Silicat Nanocomposit: A Novel Biodegradable Material," *Nano Letters*, vol. 2, pp. 1093-1096, 2002.
- [103] G. Ozkoc and S. Kemaloglu, "Morphology, Biodegradability, Mechanical,

- and Thermal Properties of Nanocomposite Films Based on PLA and Plasticized PLA," *Journal of Applied Polymer Science*, vol. 114, pp. 2481-2487, 2009.
- [104] G. X. Chen, H. S. Kim, E. S. Kim and J. S. Yoon, "Compatibilization-like Effect of Reactive Organoclay on the Poly(L-lactide)/Poly(butylene succinate) Blends," *Polymer*, vol. 46, no. 25, pp. 11829-11836, 2005.
- [105] T. Li, L. S. Turng, S. Gong and K. Erlacher, "Polylactide, Nanoclay, and Core-shell Rubber Composites," *Polymer Engineering & Science*, vol. 46, no. 10, pp. 1419-1427, 2006.
- [106] L. Jiang, B. Liu and J. Zhang, "Properties of Poly(lactic acid)/Poly(butylene adipate-co-terephthalate)/Nanoparticle Ternary Composites," *Industrial & Engineering Chemistry Research*, vol. 48, no. 16, pp. 7594-7602, 2009.
- [107] V. P. Martino, A. Jimenez, R. A. Rueckaiter and L. Averous, "Structure and Properties of Clay Nano-biocomposites Based on Poly(lactic acid) Plasticized with Polyadipates," *Polymers for Advanced Technologies*, vol. 22, pp. 2206-2213, 2010.
- [108] S. C. Tjong, *Polymer Nanocomposites with Carbonaceous Nanofillers*, Singapore: Wiley-VCH, 2012.
- [109] K. P. Pramoda, H. Hussain, H. Koh, H. Tan and C. He, "Covalent Bonded Polymer-Graphene Nanocomposites," *Journal of Polymer Science Part A: Polymer Chemistry*, no. 48, p. 4262-4267, 2010.
- [110] X. Du, M. Xiao, Y. Z. Meng and A. Hay, "Facile Synthesis of Exfoliated and Highly Conductive Poly(arylene disulfide)/Graphite Nanocomposites," *Polym. Adv. Technol.*, no. 15, p. 320-323, 2004.
- [111] J. Lu, L. Drzal, R. Worden and I. Lee, "Simple Fabrication of a High Sensitive Glucose Biosensor Using Enzymes Immobilized in Exfoliated Graphite Nanoplatelets Nafion Membrane," *Chemistry of Materials*, vol. 19, no. 25, pp. 6240-6246, 2007.
- [112] L. Chen, L. Lu, D. Wu and G. Chen, "Silicone Rubber/Graphite Nanosheet

- Electrically Conducting Nanocomposite with a Low Percolation Threshold," *Polymer Composites*, vol. 28, no. 4, pp. 493-498, 2007.
- [113] S. Gupta, P. Mantena and A. Al-Ostaz, "Dynamic Mechanical and Impact Property Correlation of Nanoclay and Graphite Platelet Reinforced Vinyl Ester Nanocomposites," *Journal of Reinforced Plastics & Composites*, vol. 29, no. 13, pp. 2037-2047, 2009.
- [114] G. Chen, X. Chen, H. Wang and D. Wu, "Dispersion of Graphite Nanosheets in Polymer Resins via Masterbatch Technique," *Journal of Applied Polymer Science*, no. 103, pp. 3470-3475, 2007.
- [115] E. Planes, J. Duchet, A. Maazouz and J.-F. Gerard, "Characterization of New Formulations for the Rotational Molding Based on Rthylene-propylene Copolymer/Graphite Nanocomposites," *Polymer Engineering and Science*, vol. 48, no. 4, pp. 723-731, 2008.
- [116] A. Katbab, A. Hrymak and K. Kasmadjian, "Preparation of Interfacially Compatibilized PP-EPDM Thermoplastic Vulcanizate/Graphite Nanocomposites: Effects of Graphite Microstructure upon Morphology, Electrical Conductivity, and Melt Rheology," *Journal of Applied Polymer Science*, no. 107, p. 3425-3433, 2007.
- [117] X. Du, M. Xiao, Y. Meng and A. Hay, "Novel Synthesis of Conductive Poly(arylene disulfide)/Graphite Nanocomposite," *Synthetic Metals*, vol. 143, no. 1, pp. 129-132, 2004.
- [118] I.-H. Kim and Y. G. Jeong, "Polylactide/Exfoliated Graphite Nanocomposites with Enhanced Thermal Stability, Mechanical Modulus, and Electrical Conductivity," *Journal of Polymer Science*, vol. 48, pp. 850-858, 2010.
- [119] K. Fukushima, M. Murariu, G. Camino and P. Dubois, "Effect of Expanded Graphite/Layered-silicate Clay on Thermal, Mechanical and Fire Retardant Properties of Poly(lactic acid)," *Polymer Degradation and Stability*, vol. 95, pp. 1063-1076, 2010.
- [120] H. Zhu, Q. Zhu, J. Li, K. Tao, L. Xue and Q. Yan, "Synergistic Effect

Between Expandable Graphite and Ammonium Polyphosphate on Flame Retarded Polylactide," *Polymer Degradation and Stability*, vol. 96, pp. 183-189, 2011.

- [121] S. O. Han, M. Karevan, M. A. Bhuiyan, J. H. Park and K. Kalaitzidou, "Effect of Exfoliated Graphite Nanoplatelets on The Mechanical and Viscoelastic Properties of Poly(Lactic Acid) Biocomposites Reinforced with Kenaf Fibers," *Journal of Material Science*, vol. 47, pp. 3535-3543, 2012.
- [122] NaturePlast, "NaturePlast Natural Evolution of Plastics," [Online]. Available: <http://www.natureplast.eu>. [Accessed 1 07 2014].
- [123] Arkema, "Lotader by Arkema," [Online]. Available: <http://www.lotader.com>. [Accessed 1 07 2014].
- [124] Southern Clay Products, "Rockwood Additives - Cloisite® Additives," [Online]. Available: <http://www.rockwoodadditives.com/nanoclay/>. [Accessed 1 07 2014].
- [125] Timcal Graphite&Carbon, "Timrex C-Therm Brochure," 3 11 2010. [Online]. Available: <http://www.timcal.com/scopi/group/timcal/timcal.nsf>. [Accessed 1 7 2014].
- [126] Z. I. Marras and I. Zuburtikudis, "Structure and Thermal Behavior of Poly(L-Lactic Acid) Clay Nanocomposites: Effect of Preparation Method as a Function of The Nanofiller Modification Level," *Journal of Applied Polymer Science*, vol. 124, no. 4, pp. 2999-3006, 2012.
- [127] M. Pluta, "Melt Compounding of Polylactide/Organoclay: Structure and Properties of Nanocomposites," *Journal of Polymer Science*, vol. 44, pp. 3392-3405, 2006.
- [128] A. B. Morgan and J. W. Gilman, "Characterization of Polymer-Layered Silicate (Clay) Nanocomposites by Transmission Electron Microscopy and X-Ray Diffraction: A Comparative Study," *Journal of Applied Polymer Science*, vol. 87, pp. 1329-1338, 2003.
- [129] T. Baouz, F. Rezgui and U. Yilmazer, "Ethylene-Methyl Acrylate-Glycidyl

- Methacrylate Toughened Poly(lactic acid) Nanocomposites," *Journal of Applied Polymer Science*, 2012.
- [130] L. E. Nielsen, *Mechanical Properties of Polymers*, New York: Reinhold, 1962.
- [131] C. E. Yeniova and U. Yilmazer, "Characteristics of Impact Modified Polystyrene/Organoclay Nanocomposites," *Polymer Composites*, vol. 31, no. 11, pp. 1853-1861, 2010.
- [132] Z. Su, Q. Li, Y. Liu, G.-H. Hu and C. Wu, "Compatibility and Phase Structure of Binary Blends of Poly(Lactic Acid) and Glycidyl Methacrylate Grafted Poly(Ethylene Octane)," *European Polymer Journal*, vol. 45, pp. 2428-2433, 2009.
- [133] S. K. Dogan, S. Gumus, A. Aytac and G. Ozkoc, "Properties of Modified Ethylene Terpolymer/Poly(Lactic Acid) Blends Based Films," *Fibers and Polymers*, vol. 14, no. 9, pp. 1422-1431, 2013.
- [134] M. Mert and U. Yilmazer, "Processing and Properties of Modified Polyamide 66-Organoclay Nanocomposites," *Journal of Applied Polymer Science*, vol. 108, pp. 3890-3900, 2008.
- [135] S. Sun, M. Zhang, H. Zhang and X. Zhang, "Polylactide Toughening with Epoxy-Functionalized Grafted Acrylonitrile-Butadiene-Styrene Particles," *Journall of Applied Polymer Science*, vol. 122, pp. 2992-2999, 2011.
- [136] R. Auras, L.-T. Lim, S. Selke and H. Tsuji, *Poly(lactic acid):Synthesis, Structures, Properties, Processing and Applications*, John Wiley & Sons, 2011.
- [137] H. Durgun and G. Bayram, "Improvement of Adhesion Between Poly(ethylene terephthalate) and Polyethylene," *Journal of Adhesion Science and Technology*, vol. 19, no. 6, pp. 407-425, 2012.
- [138] H.-T. Chiu and Y.-K. Hsiao, "Compatibilization of Poly(ethylene terephthalate)/Polypropylene Blends with Maleic Anhydride Grafted Polyethylene-Octene Elastomer," *Journal of Polymer Research*, vol. 13, pp.

153-160, 2006.

- [139] K. S. Anderson, K. M. Schreck and M. A. Hillmyer, "Toughening Polylactide," *Polymer Reviews*, vol. 48, no. 1, pp. 85-108, 2008.
- [140] A. V. Shenoy, *Rheology of Filled Polymer Systems*, Great Britain: Kluwer Academic Publishers, 1999.
- [141] Y. Y. Leu, Z. A. Mohd Ishak and W. S. Chow, "Mechanical, Thermal, and Morphological Properties of Injection Molded Poly(lactic acid)/SEBS-g-MAH/Organo-Montmorillonite Nanocomposites," *Journal of Applied Polymer Science*, vol. 124, pp. 1200-1207, 2012.
- [142] M. Pluta, M.-A. Paul, M. Alexandre and P. Dubois, "Plasticized Polylactide/Clay Nanocomposites. I. The Role of Filler Content and Its Surface Organo-Modification on the Physico-Chemical Properties," *Journal of Polymer Science: Part B: Polymer Physics*, vol. 44, pp. 299-311, 2005.
- [143] Y. Di, S. Iannace, E. Di Maio and L. Nicolais, "Poly(lactic acid)/Organoclay Nanocomposites: Thermal, Rheological Properties and Foam Processing," *Journal of Polymer Science: Part B: Polymer Physics*, vol. 43, pp. 689-698, 2005.
- [144] M. Kumar, S. Mohanty, S. K. Nayak and M. R. Parvaiz, "Effect of Glycidyl Methacrylate (GMA) on The Thermal, Mechanical and Morphological Property of Biodegradable PLA/PBAT Blend and Its Nanocomposites," *Bioresource Technology*, vol. 101, pp. 8406-8415, 2010.
- [145] Kusmono, Z. A. Mohd Ishak, W. S. Chow, T. Takeichi and Rochmadi, "Influence of SEBS-g-MA on Morphology, Mechanical, and Thermal Properties of PA6/PP/organoclay Nanocomposites," *European Polymer Journal*, vol. 44, pp. 1023-1039, 2008.
- [146] H. Balakrishnan, A. Hassan, M. U. Wahit, A. A. Yussuf and S. B. A. Razak, "Novel Toughened Polylactic Acid Nanocomposite: Mechanical, Thermal and Morphological Properties," *Materials and Design*, vol. 31, no. 7, pp. 3289-3298, 2010.

- [147] L. Petersson, K. Oksman and A. P. Mathew, "Using Maleic Anhydride Grafted Poly(lactic acid) as a Compatibilizer in Poly(lactic acid)/Layered-Silicate Nanocomposites," *Journal of Applied Polymer Science*, vol. 102, pp. 1852-1862, 2006.
- [148] J. -. H. Chang, Y. U. An, D. Cho and E. P. Giannelis, "Poly(lactic acid) Nanocomposites: Comparison of Their Properties with Montmorillonite and Synthetic Mica (II)," *Polymer*, vol. 44, pp. 3715-3720, 2003.
- [149] T. Baouz and S. Fellahi, "Interfacial Modification of High Density Polyethylene/Glass Fiber Reinforced and Non-reinforced Polyamide 66 Blends," *Journal of Applied Polymer Science*, vol. 98, no. 4, pp. 1748-1760, 2005.
- [150] L.-I. Palade, H. J. Lehermeier and J. R. Dorgan, "Melt Rheology of High L-Content Poly(lactic acid)," *Macromolecules*, vol. 34, pp. 1384-1390, 2001.
- [151] Y.-M. Corre, J. Duchet, J. Reignier and A. Maazouz, "Melt Rheology of High L-Content Poly(lactic acid) Through Reactive Extrusion With Epoxy-functionalized Chains," *Rheologica Acta*, vol. 50, pp. 613-629, 2011.
- [152] A. Bhatia, R. K. Gupta, S. N. Bhattacharya and H. J. Choi, "An Investigation of Melt Rheology and Thermal Stability of Poly(lactic acid)/ Poly(butylene succinate) Nanocomposites," *Journal of Applied Polymer Science*, pp. 2837–2847, 2009.
- [153] H. Zhao , Z. Cui , X. Wang, L.-S. Turng and X. Peng, "Processing and Characterization of Solid and Microcellular Poly(lactic acid)/Polyhydroxybutyrate-valerate (PLA/PHBV) Blends and PLA/PHBV/Clay Nanocomposites," *Composites :Part B*, vol. 51, pp. 79-91, 2013.
- [154] K. Fukushima, D. Tabuani and G. Camino, "Poly(lactic acid)/Clay Nanocomposites: Effect of Nature and Content of Clay on Morphology, Thermal and Thermo-mechanical Properties," *Materials Science and Engineering C*, vol. 32, pp. 1790-1795, 2012.
- [155] S. Sinha Ray, P. Maiti, M. Okamoto, K. Yamada and K. Ueda, "New

- Poly(lactide)/Layered Silicate Nanocomposites. 1. Preparation, Characterization, and Properties," *Macromolecules*, vol. 35, pp. 3104-3110, 2002.
- [156] J. Goodage, "SERC - Geochemical Instrumentation and Analysis," Science and Education Research Centre - Caletton College. [Online]. [Accessed 13 1 2013].
- [157] M. Murariu, A. Dechief, L. Bonnaud, Y. Paint, A. Gallos, G. Fontaine, S. Bourbigot and P. Dubois, "The Production and Properties of Poly(lactide) Composites Filled with Expanded Graphite," *Polymer Degradation and Stability*, pp. 889-900, 2010.
- [158] F. Hussain, M. Hojjati, M. Okamoto and R. Gorga, "Polymer-matrix Nanocomposites, Processing, Manufacturing, and Application: An Overview," *Journal of Composite Materials*, pp. 1511-75, 2006.
- [159] R. E. Allred, J.-M. Gosau and J. P. Barlow, "Surface Modification of Exfoliated Graphite Nano-Reinforcements," in *Proc. 38th SAMPE Tech. Conf.*, Dallas, TX, 2006.
- [160] S. Wu, "Phase Structure and Adhesion in Polymer Blends: A Criterion for Rubber Toughening," *Polymer*, vol. 26, pp. 1855-1863, 1985.
- [161] C. Vasile and A. K. Kulshreshtha, *Handbook of polymer Blends and Nanocomposites*, Shropshire: Rapra Technology Limited, 2003.
- [162] L. Wang, J. Hong and G. Chen, "Comparison Study of Graphite Nanosheets and Carbon Black as Fillers for High Density Polyethylene," *Polymer Engineering and Science*, vol. 50, no. 11, p. 2176, 2010.
- [163] Y. C. Li and G.-H. Chen, "HDPE/Expanded Graphite Nanocomposites Prepared via Masterbatch Process," *Polymer Engineering and Science*, vol. 49, no. 6, pp. 882-888, 2007.
- [164] S. Kim, I. Do and L. T. Drzal, "Multifunctional xGnP/LLDPE Nanocomposites Prepared by Solution Compounding Using Various Screw Rotating Systems," *Macromolecular Materials and Engineering*, vol. 294,

- no. 3, pp. 196-205, 2009.
- [165] J. Li, L. Vaisman, G. Marom and J. K. Kim, "Br Treated Graphite Nanoplatelets for Improved Electrical Conductivity of Polymer Composites," *Carbon*, vol. 45, pp. 744-750, 2007.
- [166] D. Chen, J. Yang and G. Chen, "The Physical Properties of Polyurethane/Graphite Nanosheets/Carbon Black Foaming Conducting Nanocomposites," *Composites: Part A*, vol. 41, pp. 1636-1638, 2010.
- [167] P. V. Joseph, K. Joseph and S. Thomas, "Effect of Processing Variables on the Mechanical Properties of Sisal Fiber-reinforced Polypropylene Composites," *Composites Science and Technology*, vol. 59, pp. 1625-1640, 1999.
- [168] H. W. McCormick, F. Brower and L. Kin, *Journal of Polymer Science*, vol. 39, p. 87, 1959.
- [169] P. Vincent, *Polymer*, vol. 41, p. 344, 1960.
- [170] A. N. Gent and A. G. Thomas, "Effect of Molecular Weight on the Tensile Strength of Glassy Plastics," *Journal of Polymer Science Part A-2: Polymer Physics*, vol. 10, no. 3, 1971 (online 2003).
- [171] J. George and A. K. Bhowmick, "Ethylene Vinyl Acetate/Expanded Graphite Nanocomposites by Solution Intercalation: Preparation, Characterization and Properties," *Journal of Materials Science*, vol. 43, pp. 702-708, 2008.
- [172] W. Zheng, X. Lu and S.-C. Wong, "Electrical and Mechanical Properties of Expanded Graphite-reinforced High Density Polyethylene," *Journal of Applied Polymer Science*, vol. 91, pp. 2781-2788, 2004.
- [173] W. Weng, G. Chen, D. Wu, X. Chen, J. Lu and P. Wang, "Fabrication and Characterization of Nylon 6/Foliated Graphite Electrically Conducting Nanocomposite," *Journal of Polymer Science Part B: Polymer Physics*, vol. 42, no. 15, pp. 2844-2856, 2004.
- [174] F. M. Uhl, Q. Yao and C. A. Wilkie, "Formation of Nanocomposites of Styrene and Its Copolymers Using Graphite as the Nanomaterial," *Polymers*

for Advanced Technologies, vol. 16, no. 7, pp. 533-540, 2005.

- [175] T. Ramanathan, S. Stankovich, D. A. Dikin, H. Liu, H. Shen, S. Nguyen and L. C. Brinson, "Graphitic Nanofillers in PMMA Nanocomposites — An Investigation of Particle Size and Dispersion and Their Influence on Nanocomposite Properties," *Journal of Polymer Science Part B: Polymer Physics*, vol. 45, no. 15, pp. 2097-2112, 2007.
- [176] H. Kim and C. W. Macosko, "Processing-property Relationships of Polycarbonate/Graphene Composites," *Polymer*, vol. 50, pp. 3797-3809, 2009.
- [177] A. Durmus, A. Kasgoz and Macosko, "Linear Low Density Polyethylene (LLDPE)/Clay Nanocomposites. Part I: Structural Characterization and Quantifying Clay Dispersion by Melt Rheology," *Polymer*, vol. 48, pp. 4492-4502, 2007.
- [178] J. P. Greene and J. O. Wilkes, "Steady-State and Dynamic Properties of Concentrated Fiber Filled Thermoplastics," *Polymer Engineering and Science*, vol. 35, no. 21, pp. 1670-1681, 1995.
- [179] C. D. Han and J. K. Kim, "On the Use of Time-Temperature Superposition in Multicomponent/Multiphase Polymer Systems," *Polymer*, vol. 34, no. 12, pp. 2533-2539, 1993.
- [180] H. Aoki, J. L. White and J. F. Fellers, "Rheological and Optical Properties Investigation of Aliphatic (Nylon 66, PgammaBLG) and Aromatic (Kevlar, Nomex) Polyamide Solutions," *Journal of Applied Polymer Science*, vol. 23, no. 8, pp. 2293-2314, 1979.
- [181] R. M. Ottenbrite, L. R. Utracki and S. Inoue, *Current Topic in Polymer Science*, Munich: Hanser Publishers, 1987.
- [182] Y. H. Cho, K. S. Dan and B. C. Kim, "Effects of Dissolution Temperature on the Rheological Properties of Polyvinyl Alcohol Solutions in Dimethyl Sulfoxide," *Korea-Australia Rheology Journal*, vol. 20, no. 2, pp. 73-77, 2008.

- [183] H. Eslami and M. R. Kamal, "Elongational Rheology of Biodegradable Poly(lactic acid)/Poly[(butylenesuccinate)-co-adipate] Binary Blends and Poly(lactic acid)/Poly[(butylenesuccinate)-co-adipate]/Clay Ternary Nanocomposites," *Journal of Applied Polymer Science*, vol. 129, no. 5, pp. 2290-2306, 2013.
- [184] O. Sadiku-Agboola, E. R. Sadiku, A. T. Adegbola and O. F. Biotidara, "Rheological Properties of Polymers: Structure and Morphology of Molten Polymer Blends," *Materials Sciences and Applications*, vol. 2, pp. 30-41, 2011.
- [185] D. W. Litchfield and D. G. Baird, "The Rheology of High Aspect Ratio Nano-particle Filled Liquids," *Rheology Reviews*, pp. 1-60, 2006.
- [186] D. C. Montgomery and G. C. Runger, *Applied Statistics and Probability for Engineers*, Hoboken, NJ: John Wiley & Sons Inc., 2003.

APPENDIX A

SPECTROSCOPIC ANALYSES

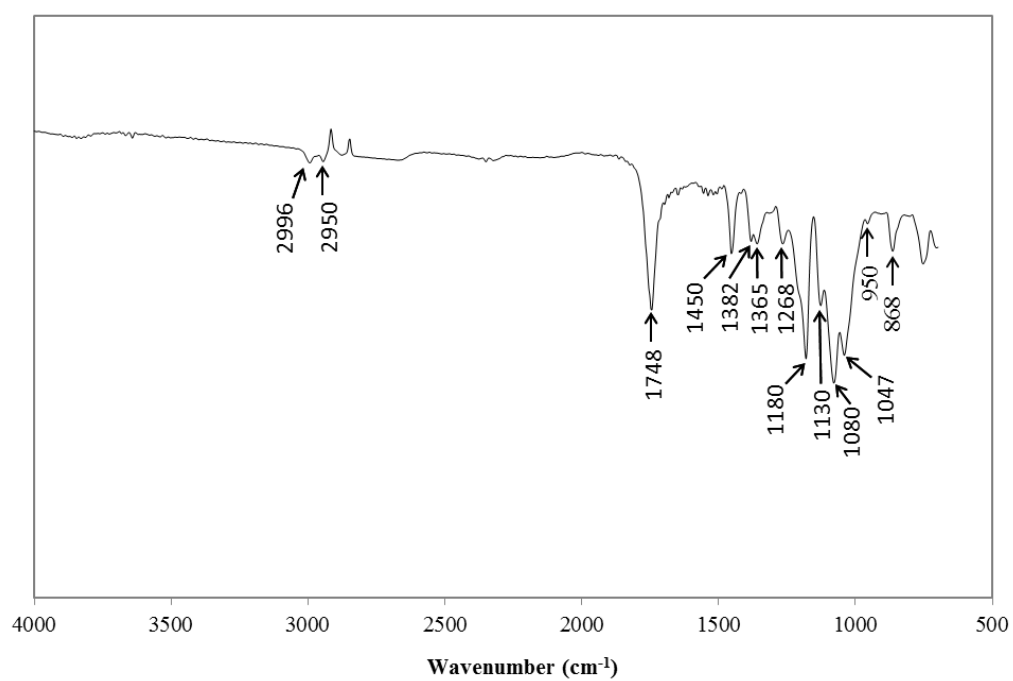


Figure A.1 The FTIR spectra of neat PLA

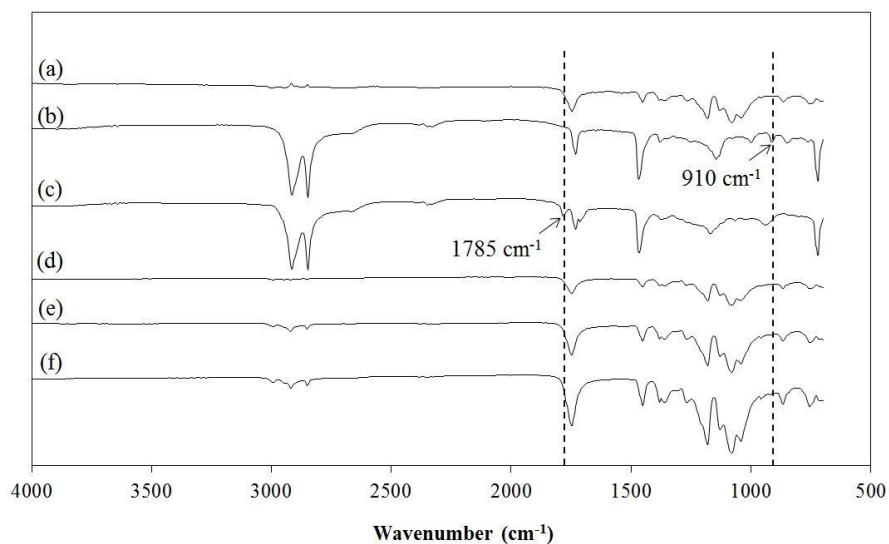


Figure A.2 FTIR spectra of (a) PLA, (b) E-GMA, (c) E-BA-MAH, (d) PLA/C25A, (e) PLA/E-GMA/C25A, (f) PLA/E-BA-MAH/C25A

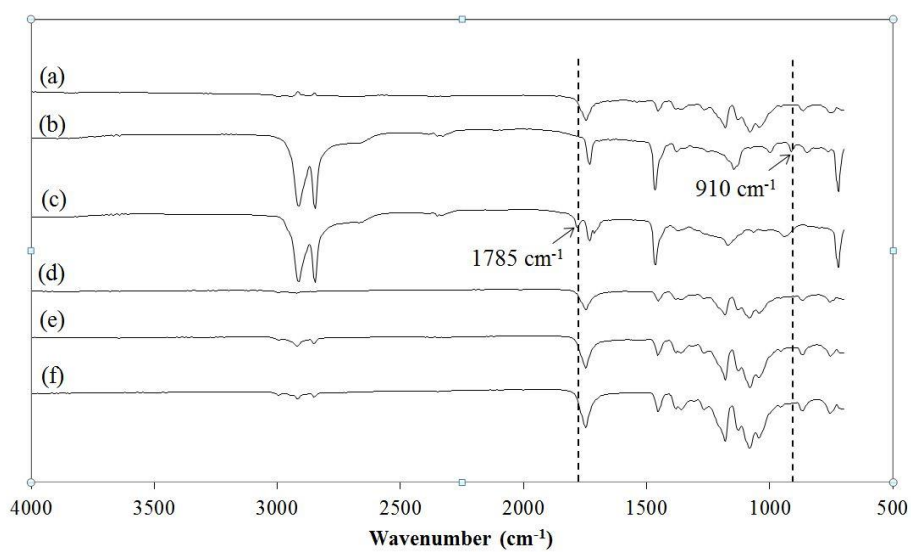


Figure A.3 FTIR spectra of (a) PLA, (b) E-GMA, (c) E-BA-MAH, (d) PLA/C30B, (e) PLA/E-GMA/ C30B, (f) PLA/E-BA-MAH/ C30B

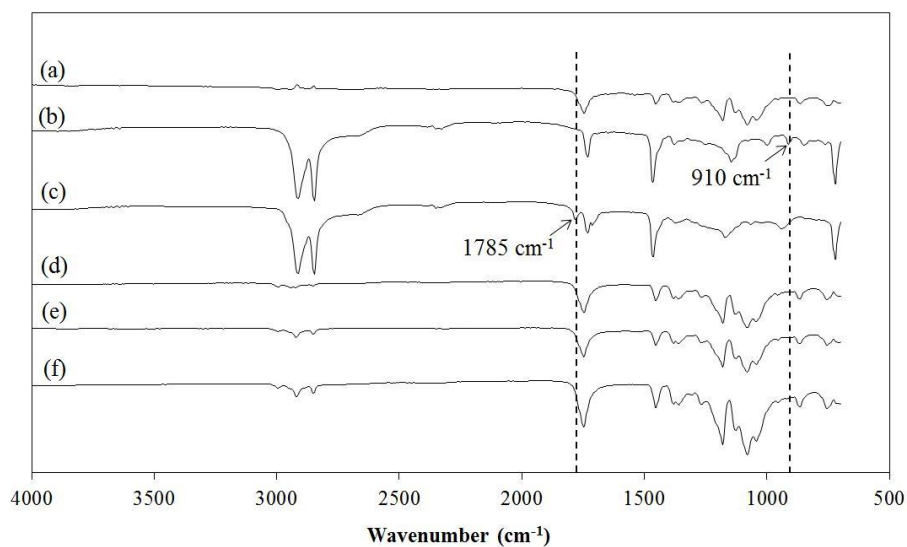


Figure A.4 FTIR spectra of (a) PLA, (b) E-GMA, (c) E-BA-MAH, (d) PLA/N5, (e) PLA/E-GMA/N5, (f) PLA/E-BA-MAH/N5

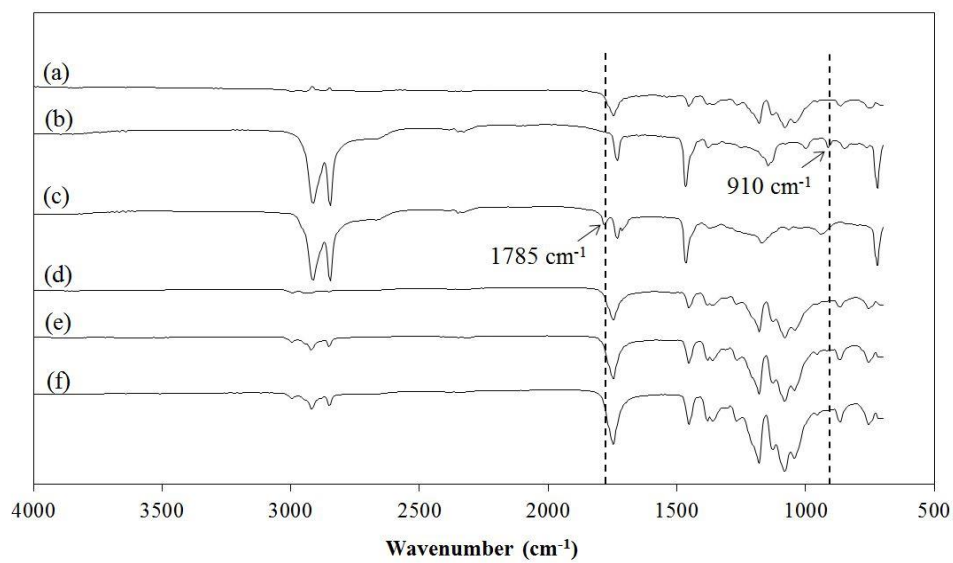


Figure A.5 FTIR spectra of (a) PLA, (b) E-GMA, (c) E-BA-MAH, (d) PLA/N8, (e) PLA/E-GMA/N8, (f) PLA/E-BA-MAH/N8

APPENDIX B

MECHANICAL ANALYSES

Table B.1 Tensile test results of neat PLA, PLA/compatibilizer binary blends, PLA/organoclay binary nanocomposites and PLA/compatibilizer/organoclay ternary nanocomposites

Code	Content	Tensile Strength (MPa)	Young's Modulus (MPa)	Elongation at Break (%)	Impact Strength (kJ/m ²)
A-00	Neat PLA (unext.)	57.1 ± 1.0	1372.9 ± 16	6.6 ± 0.6	17.3 ± 0.4
A-01	Neat PLA (ext.)	57.1 ± 0.7	1463.7 ± 16	7.3 ± 0.5	15.6 ± 0.9
A-02	PLA/E-GMA	14.8 ± 1.2	914 ± 46	58.8 ± 3.6	24.9 ± 2.5
A-03	PLA/E-BA/MAH	14.7 ± 1.5	1021 ± 58	4.1 ± 1.5	22.4 ± 1.5
C-1	PLA/C15A	44.9 ± 1.5	1477 ± 12	95.7 ± 5.9	15.2 ± 0.1
C-2	PLA/C25A	43.3 ± 1.6	1502 ± 23	156.9 ± 6.9	15.5 ± 0.3
C-3	PLA/C30B	40.4 ± 0.9	1426 ± 28	181.3 ± 26.5	15.6 ± 0.3
C-4	PLA/N5	38.3 ± 1.7	1384 ± 10	118.5 ± 11.0	15.6 ± 0.5
C-5	PLA/N8	37.7 ± 2.0	1380 ± 11	118.4 ± 35.5	15.5 ± 0.5
A-1	PLA/E-GMA/C15A	47.1 ± 0.5	1291 ± 11	130.0 ± 8.8	18.2 ± 0.5
A-2	PLA/E-GMA/C25A	48.4 ± 0.8	1339 ± 18	27.2 ± 10.6	18.4 ± 1.3
A-3	PLA/E-GMA/C30B	44.9 ± 0.7	1284 ± 16	21.8 ± 7.0	18.6 ± 1.0
A-4	PLA/E-GMA/N5	48.6 ± 1.2	1302 ± 15	58.2 ± 12.6	19.6 ± 1.3
A-5	PLA/E-GMA/N8	47.7 ± 2.7	1255 ± 14	113.3 ± 6.5	19.9 ± 1.1
B-1	PLA/E-BA-MAH/C15A	24.1 ± 2.0	1286 ± 20	5.0 ± 0.8	13.1 ± 0.8
B-2	PLA/E-BA-MAH/C25A	22.8 ± 2.0	1237 ± 30	4.5 ± 0.9	13.3 ± 1.7
B-3	PLA/E-BA-MAH/C30B	22.8 ± 2.8	1188 ± 43	6.0 ± 1.3	15.1 ± 0.4
B-4	PLA/E-BA-MAH/N5	27.0 ± 2.7	1323 ± 37	5.1 ± 0.6	12.8 ± 0.9
B-5	PLA/E-BA-MAH/N8	24.7 ± 1.7	1286 ± 18	4.7 ± 0.4	11.3 ± 0.7

Table B.2 Tensile test results of neat PLA, PLA/compatibilizer binary blends, PLA/EG binary nanocomposites and PLA/compatibilizer/EG ternary nanocomposites

Code	EG (wt.%)	E-GMA Content (wt.%)	Tensile Strength (MPa)	Young's Modulus (MPa)	Elongation at Break (%)	Impact Strength (kJ/m ²)
E-0	0	0	48.5 ± 2.3	1466 ± 22	5.9 ± 0.7	13.8 ± 1.5
E-1	0.5	0	46.7 ± 2.4	1486 ± 33	5.7 ± 0.5	14.3 ± 0.7
E-2	1	0	49.8 ± 1.3	1455 ± 13	6.4 ± 0.6	14.3 ± 0.1
E-3	2	0	47.6 ± 2.5	1464 ± 21	4.0 ± 1.6	13.3 ± 1.2
E-4	0	10	33.1 ± 3.5	1226 ± 27	128.0 ± 16.4	20.4 ± 1.0
E-5	0.5	10	34.4 ± 4.6	1243 ± 29	19.0 ± 7.0	23.7 ± 0.8
E-6	1	10	35.9 ± 2.3	1267 ± 29	9.7 ± 2.2	21.9 ± 1.1
E-7	2	10	39.2 ± 3.4	1312 ± 33	29.5 ± 13.8	21.1 ± 0.8
S-1	0.5	0	29.4 ± 2.0	1459 ± 30	8.8 ± 3.0	20.9 ± 2.2
S-2	1	0	29.6 ± 3.0	1475 ± 35	6.1 ± 0.6	17.8 ± 2.6
S-3	2	0	26.2 ± 2.2	1496 ± 47	5.8 ± 0.9	15.4 ± 1.0
S-4	0	10	20.0 ± 1.3	955 ± 28	52.4 ± 14.6	28.1 ± 2.7
S-5	0.5	10	32.0 ± 2.4	1213 ± 16	154.9 ± 34.2	20.5 ± 1.7
S-6	1	10	30.9 ± 2.8	1208 ± 26	168.6 ± 33.0	15.5 ± 0.9
S-7	2	10	29.1 ± 2.6	1189 ± 44	97.4 ± 10.0	13.6 ± 1.1

APPENDIX C

DSC ANALYSES

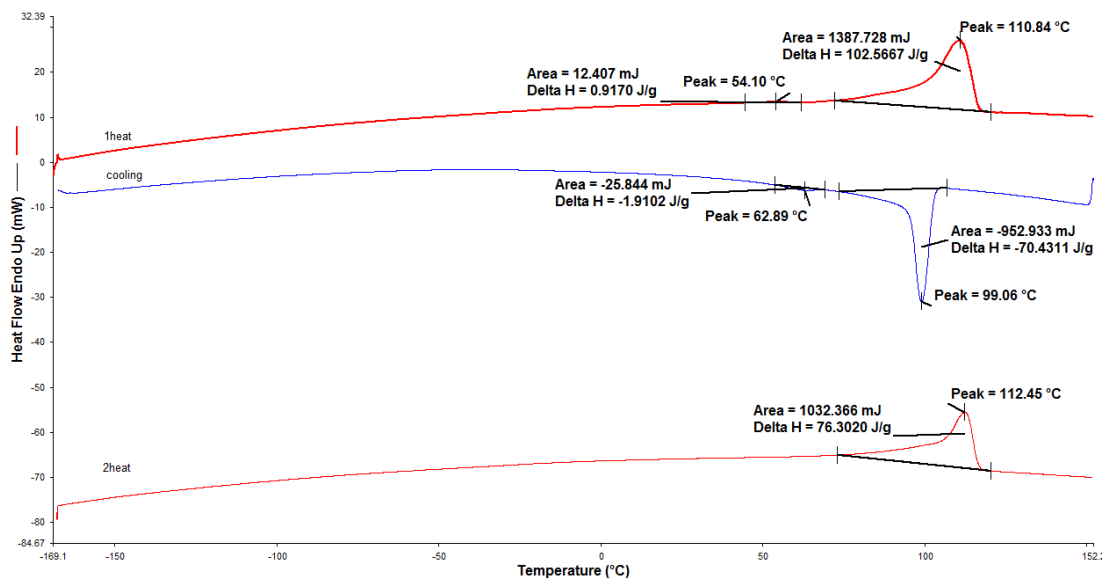


Figure C.1 DSC curve of E-GMA performed under He purge between -180°C and 150°C at an heating rate of 10°C/min

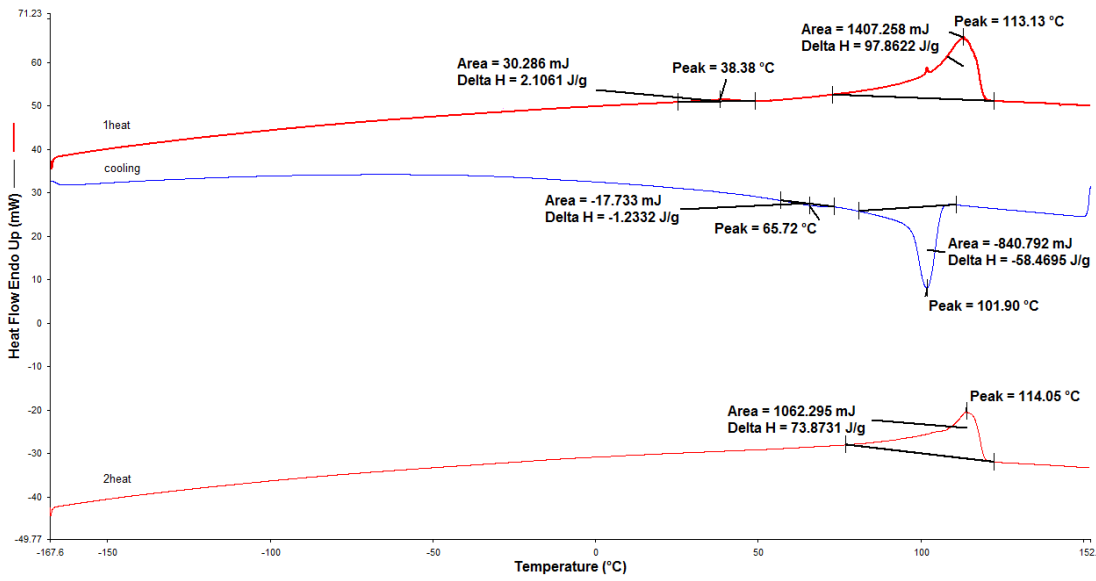


Figure C.2 DSC curve of E-BA-MAH performed under He purge between -180°C and 150°C at an heating rate of 10°C/min

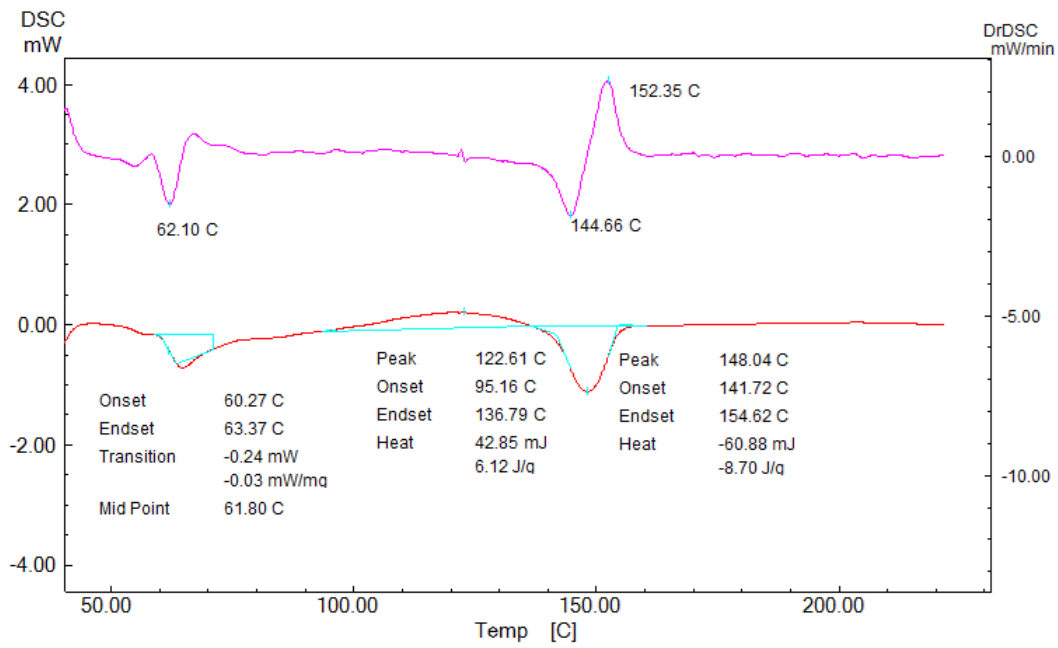


Figure C.3 DSC curve for A-00

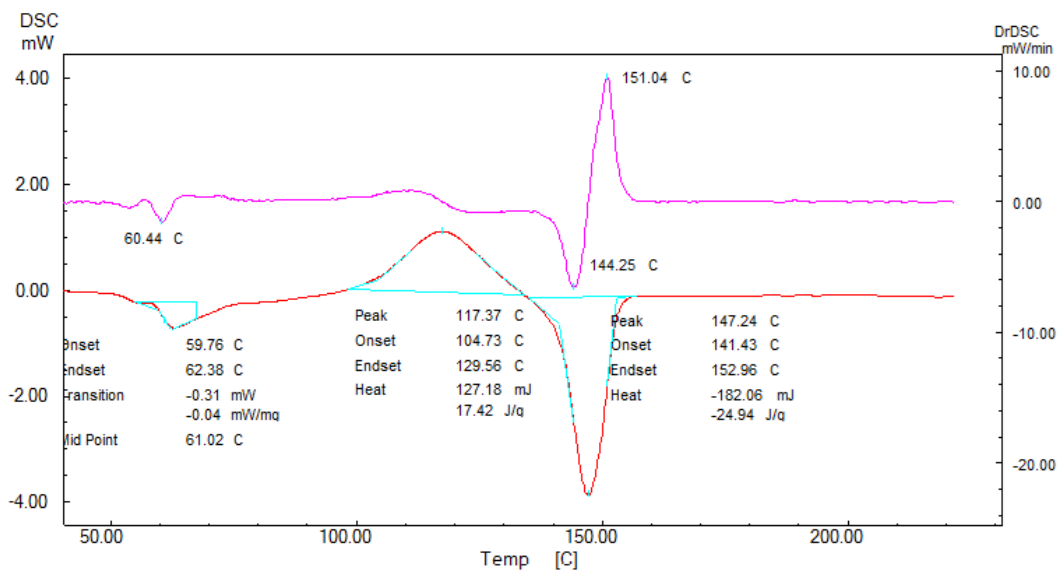


Figure C.4 DSC curve for A-01

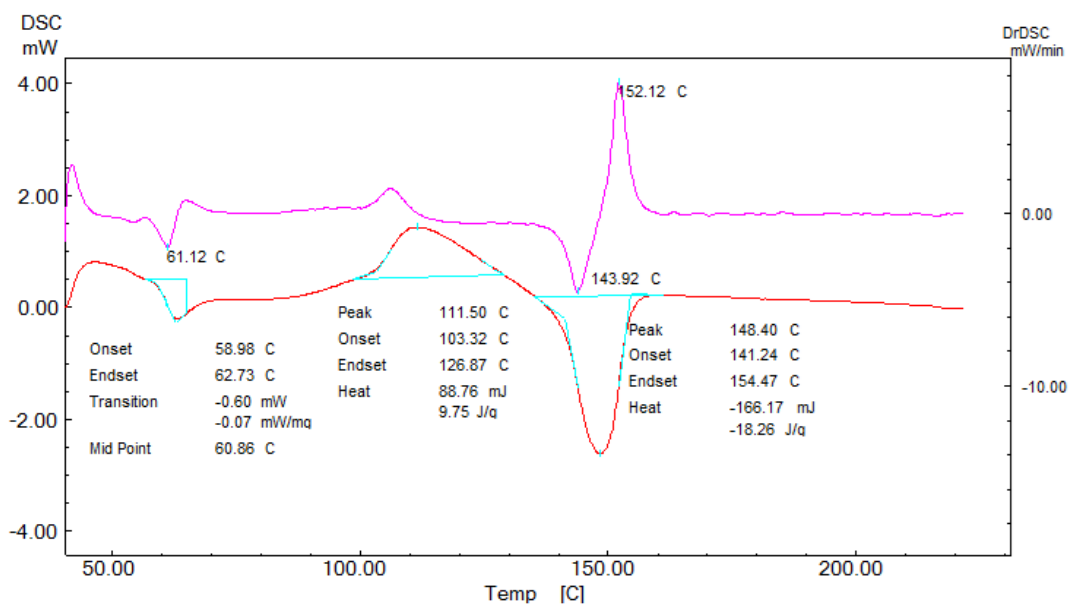


Figure C.5 DSC curve for A-1

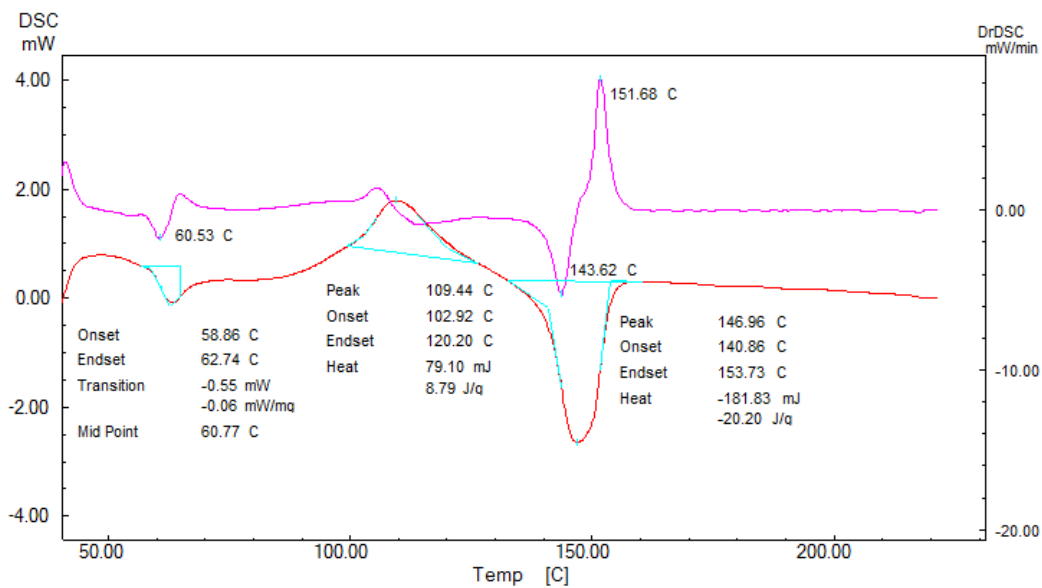


Figure C.6 DSC curve for A-2

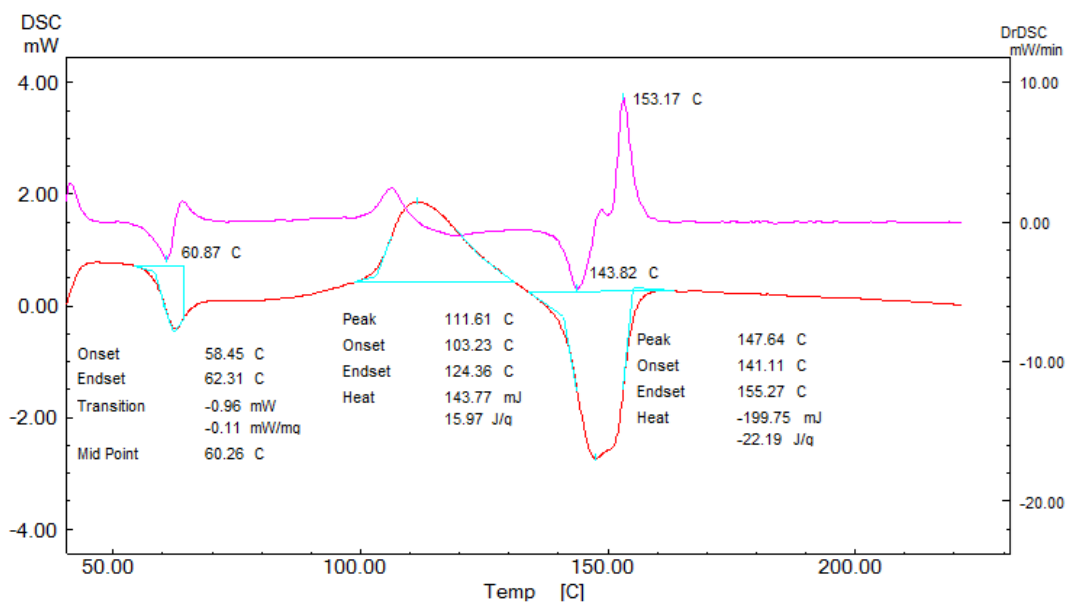


Figure C.7 DSC curve for A-3

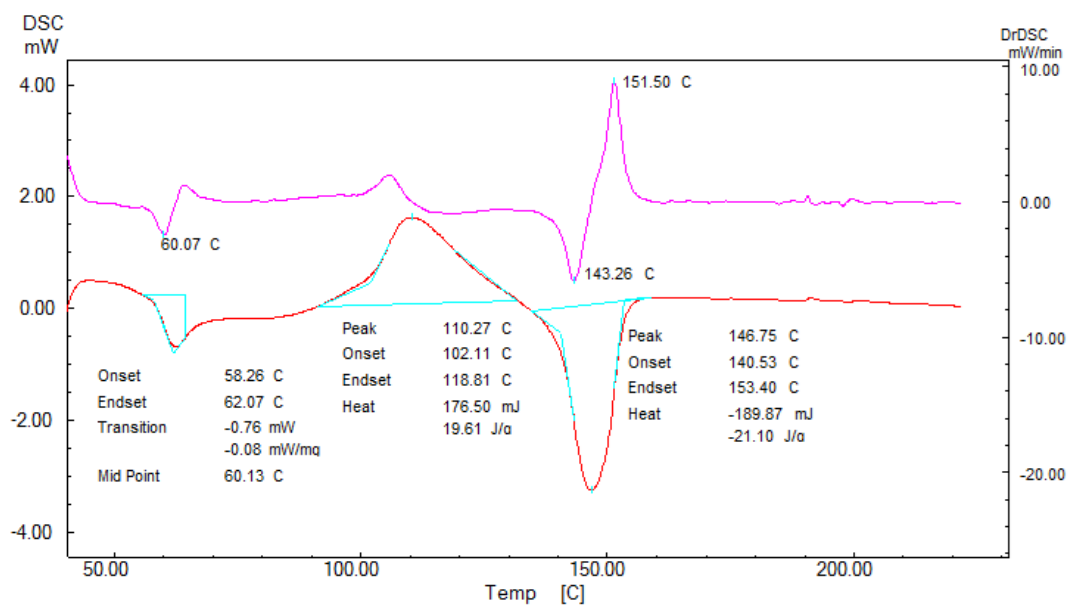


Figure C.8 DSC curve for A-4

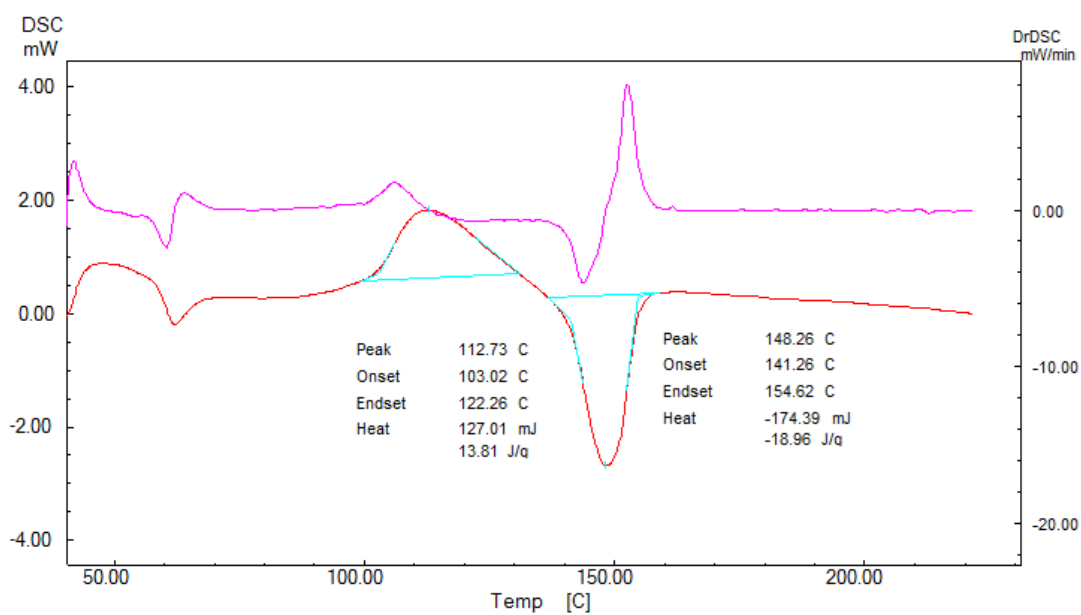


Figure C.9 DSC curve for A-5

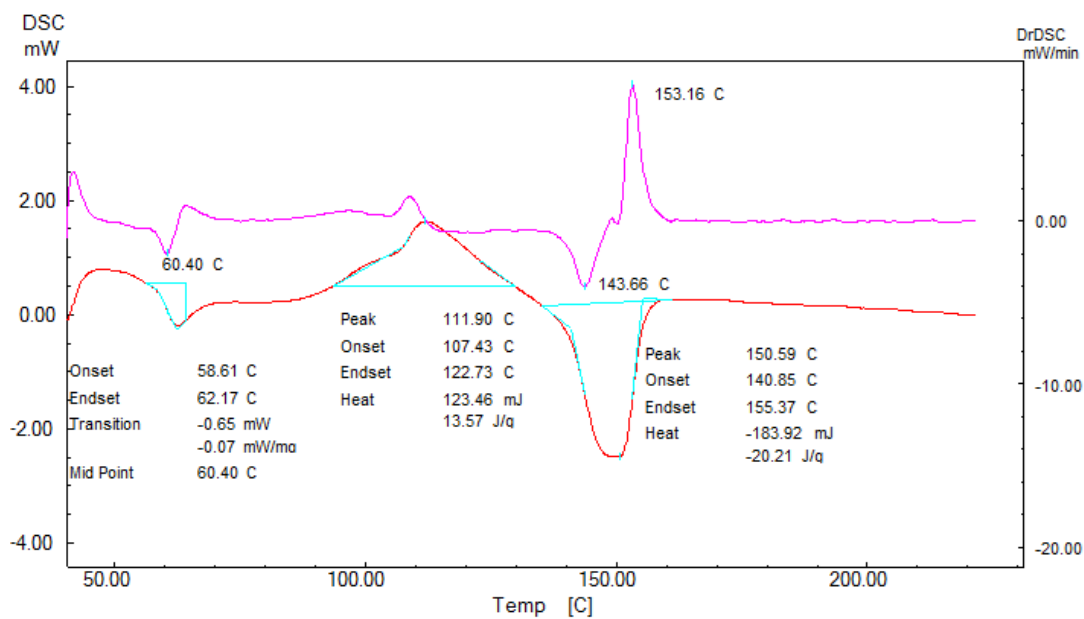


Figure C.10 DSC curve for B-1

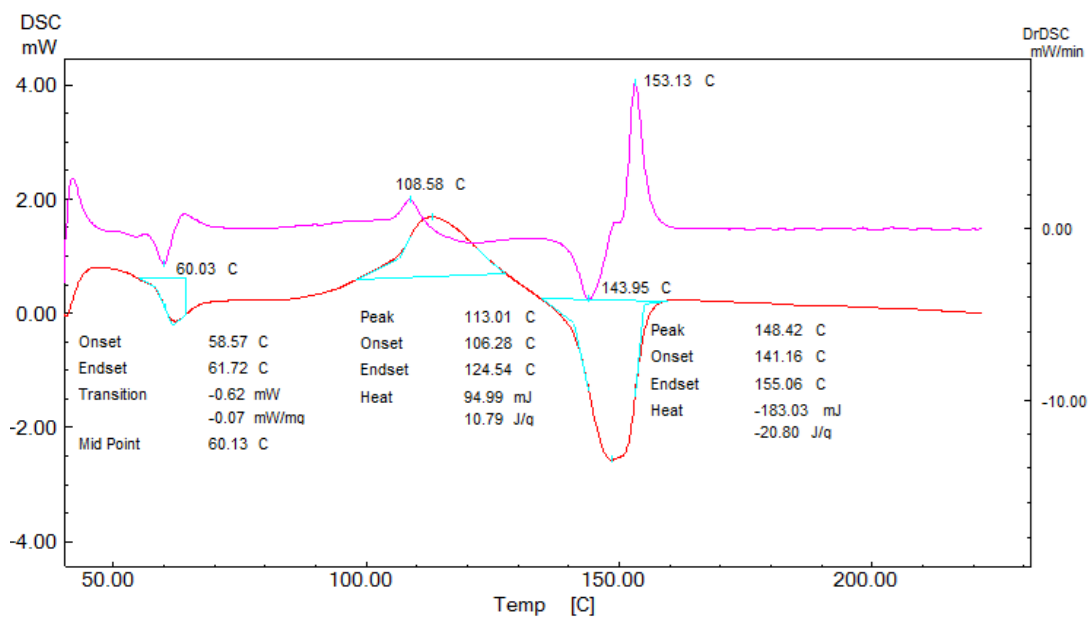


Figure C.11 DSC curve for B-2

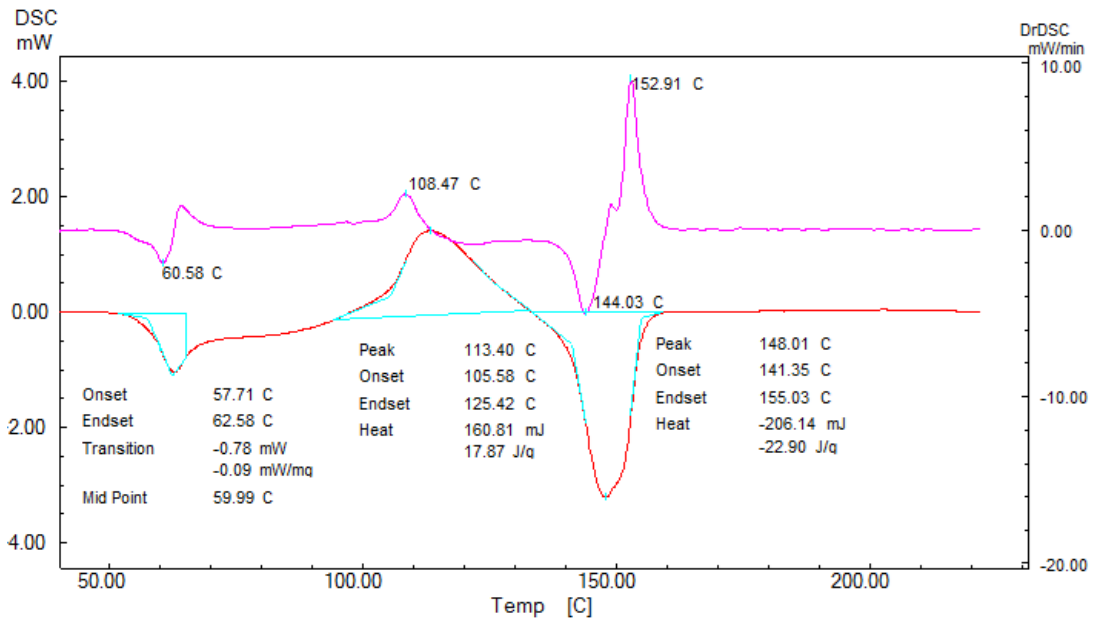


Figure C.12 DSC curve for B-3

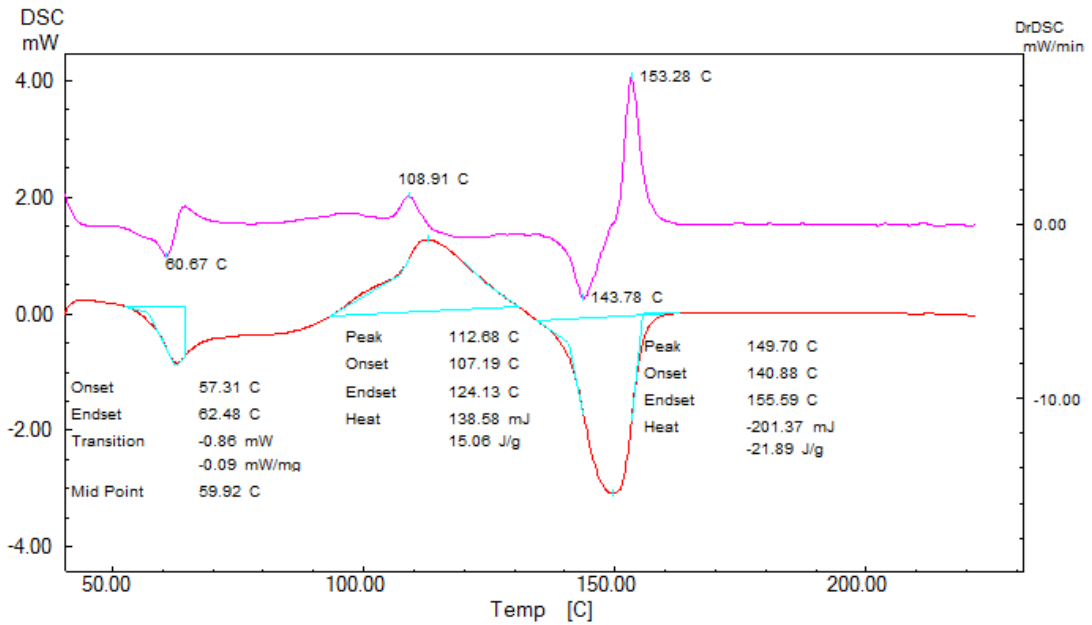


Figure C.13 DSC curve for B-4

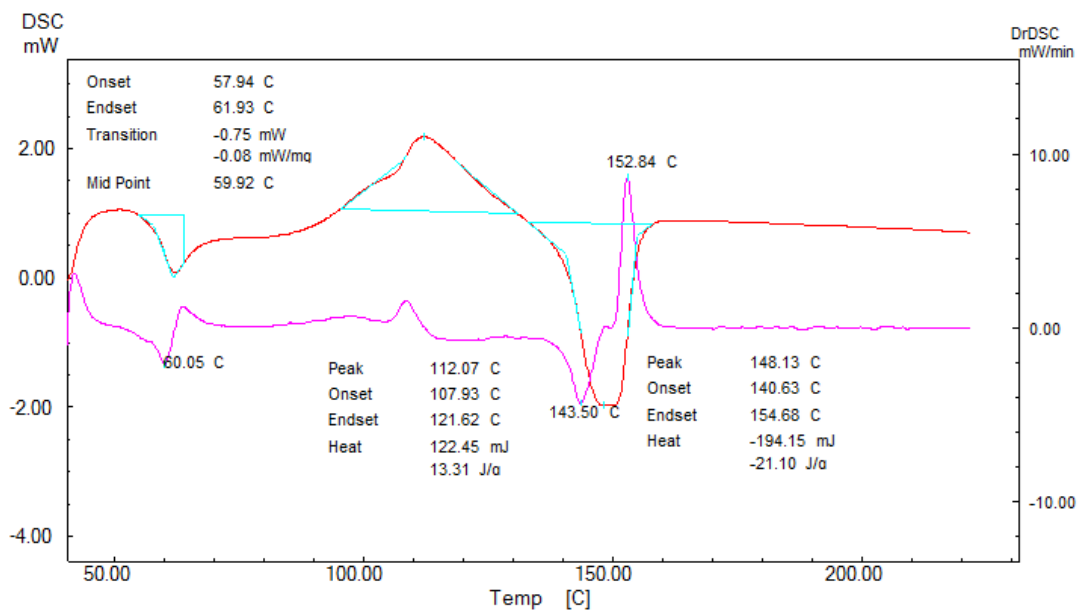


Figure C.14 DSC curve for B-5

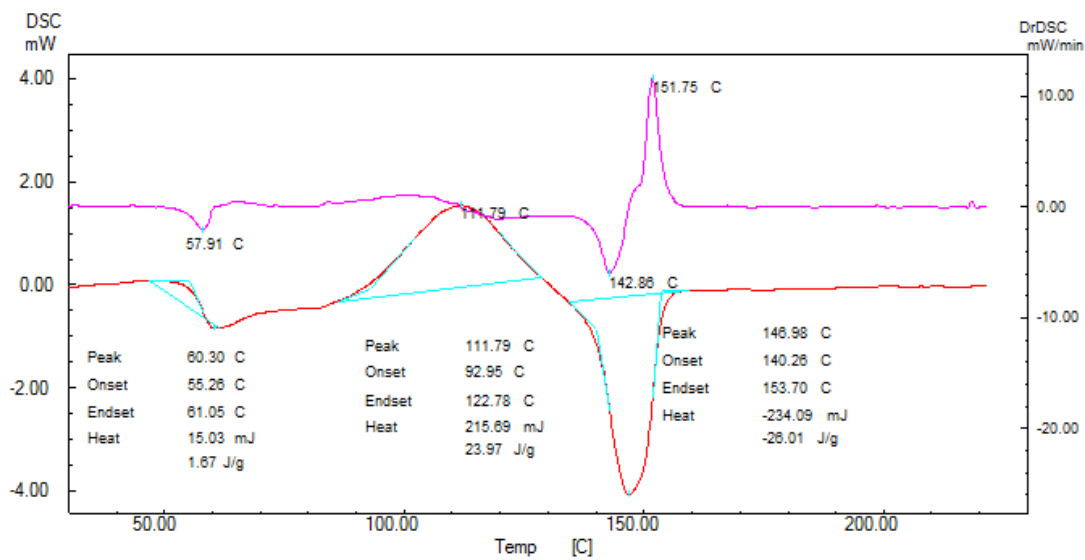


Figure C.15 DSC curve for C-1

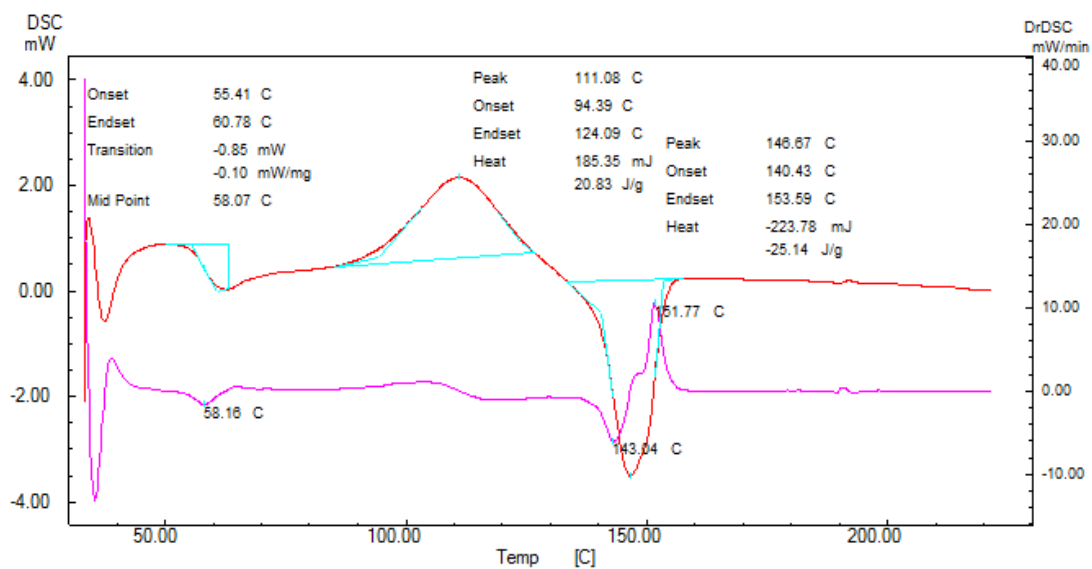


Figure C.16 DSC curve for C-2

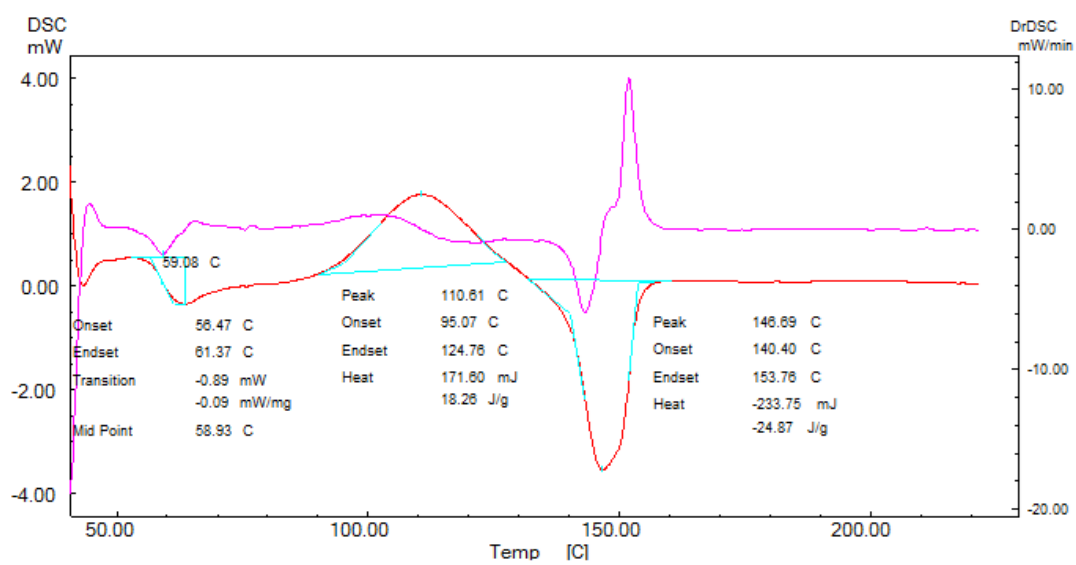


Figure C.17 DSC curve for C-3

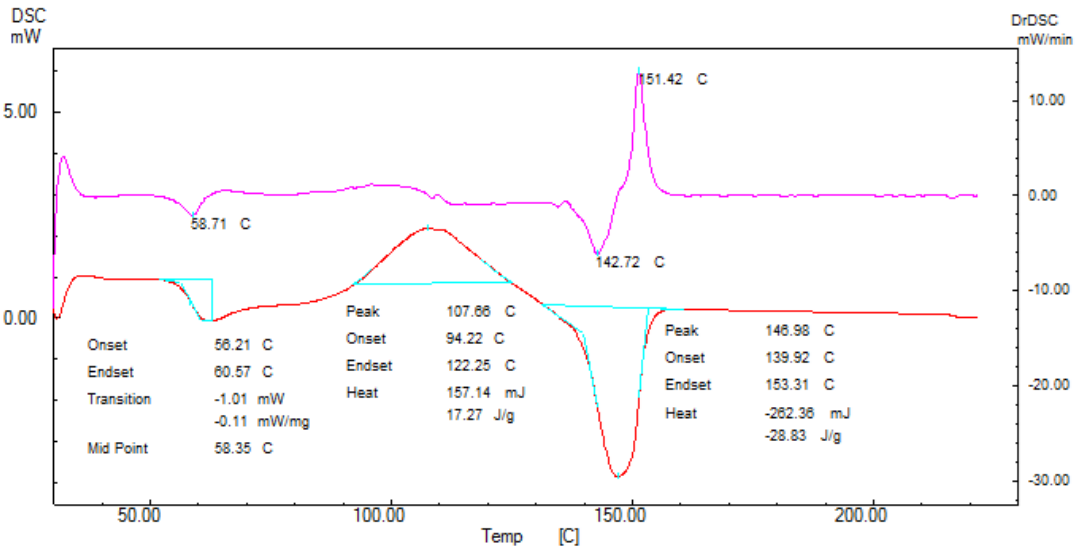


Figure C.18 DSC curve for C-4

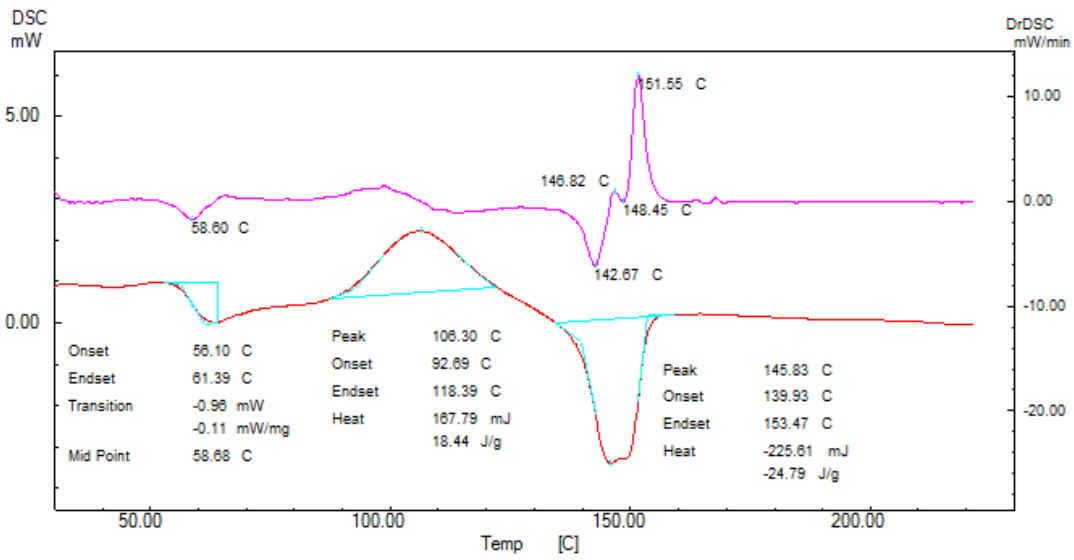


Figure C.19 DSC curve for C-5

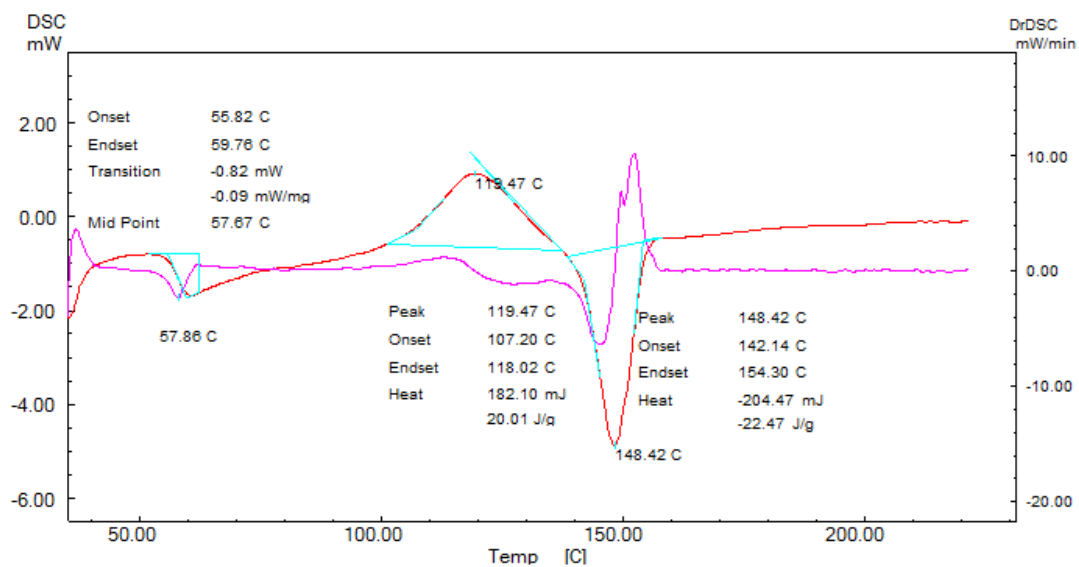


Figure C.20 DSC curve for E-0

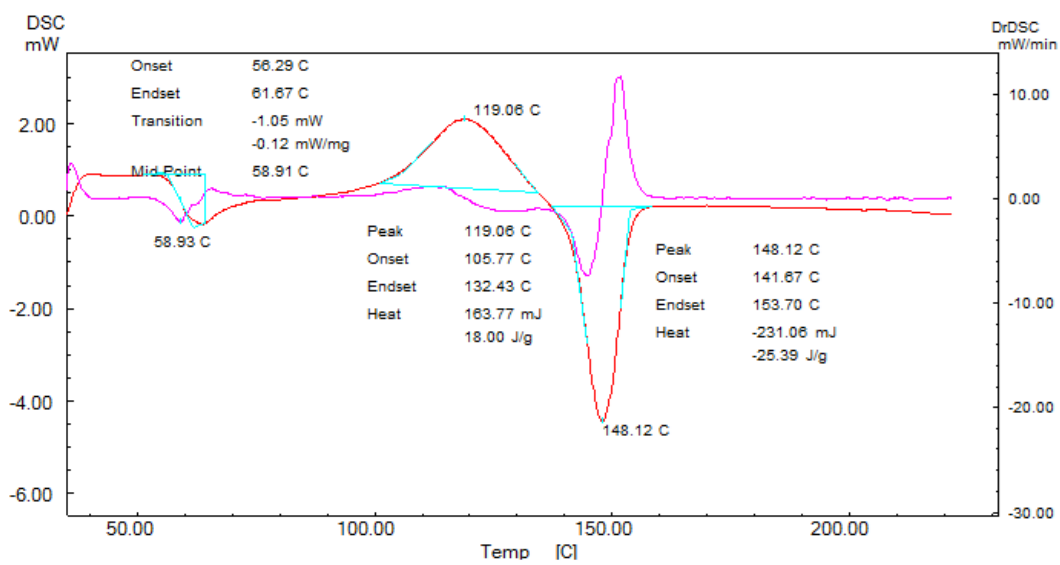


Figure C.21 DSC curve for E-1

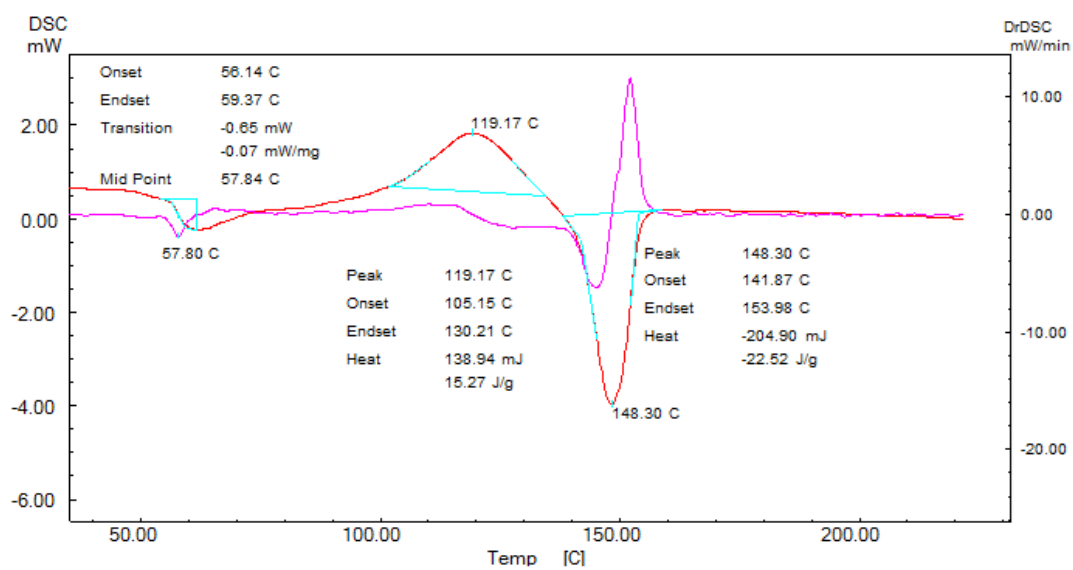


Figure C.22 DSC curve for E-2

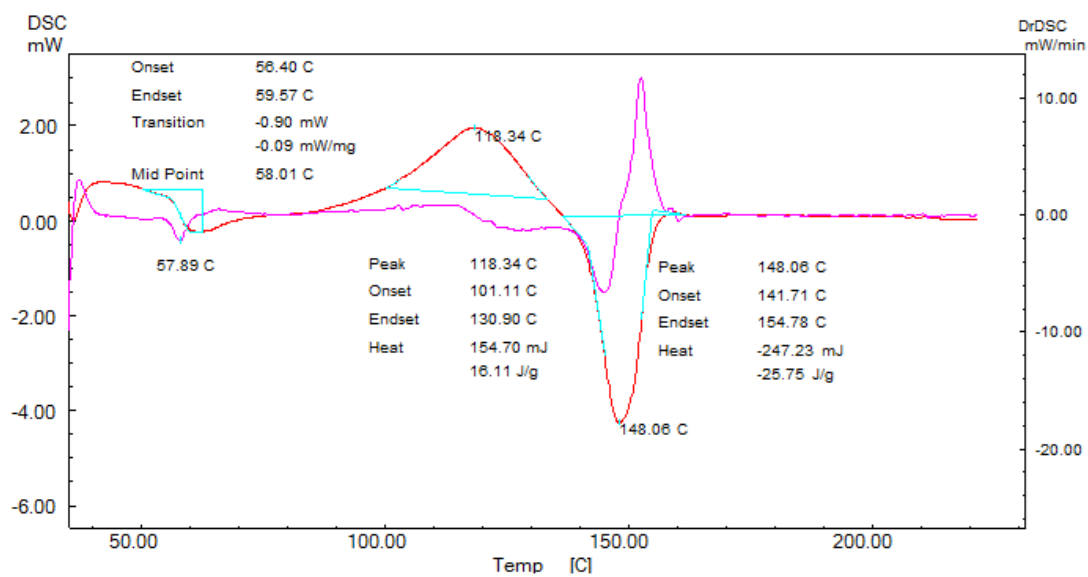


Figure C.23 DSC curve for E-3

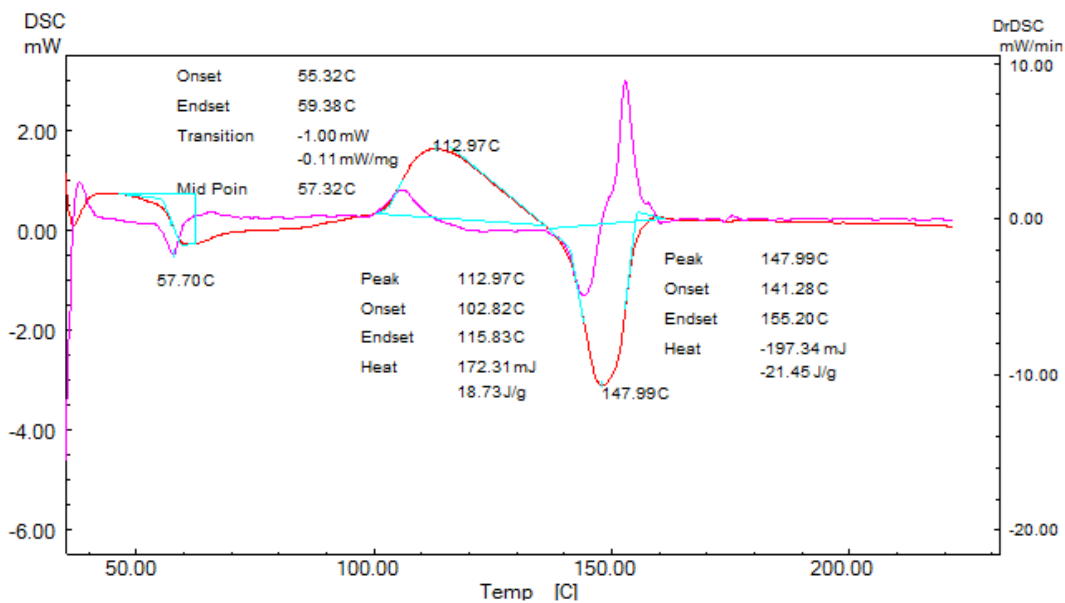


Figure C.24 DSC curve for E-4

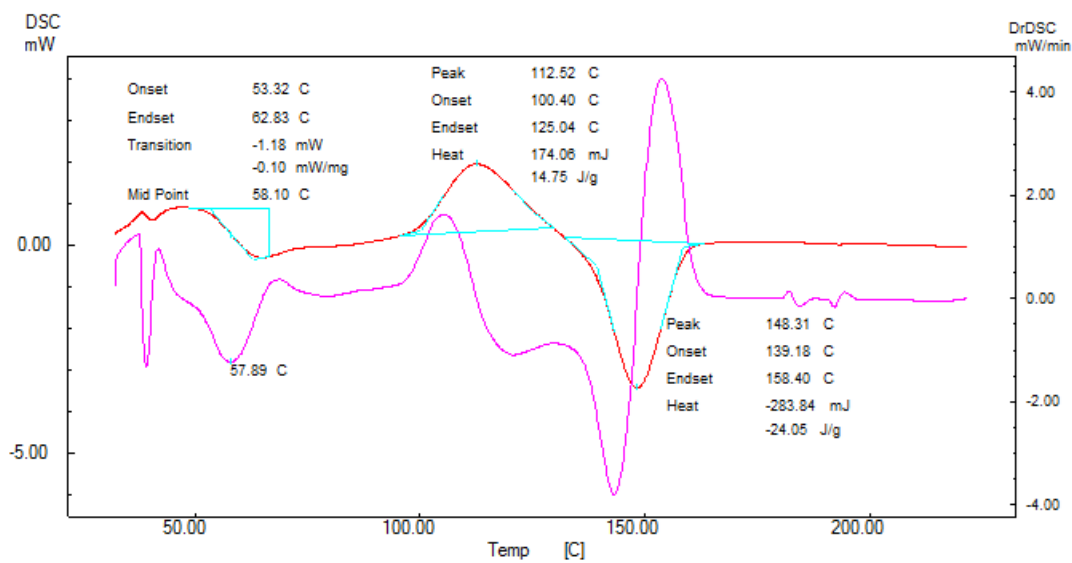


Figure C.25 DSC curve for E-5

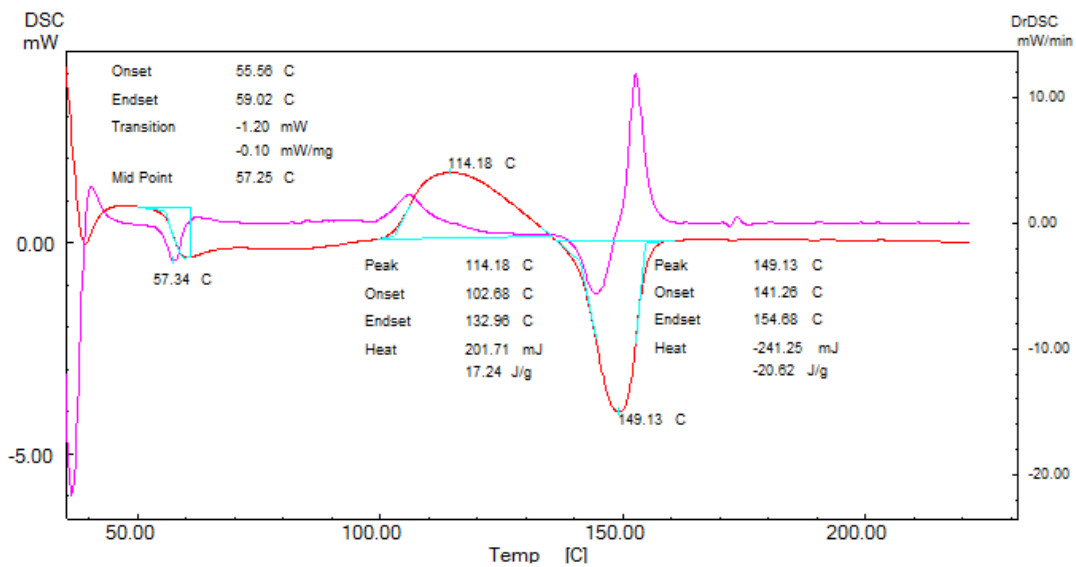


Figure C.26 DSC curve for E-6

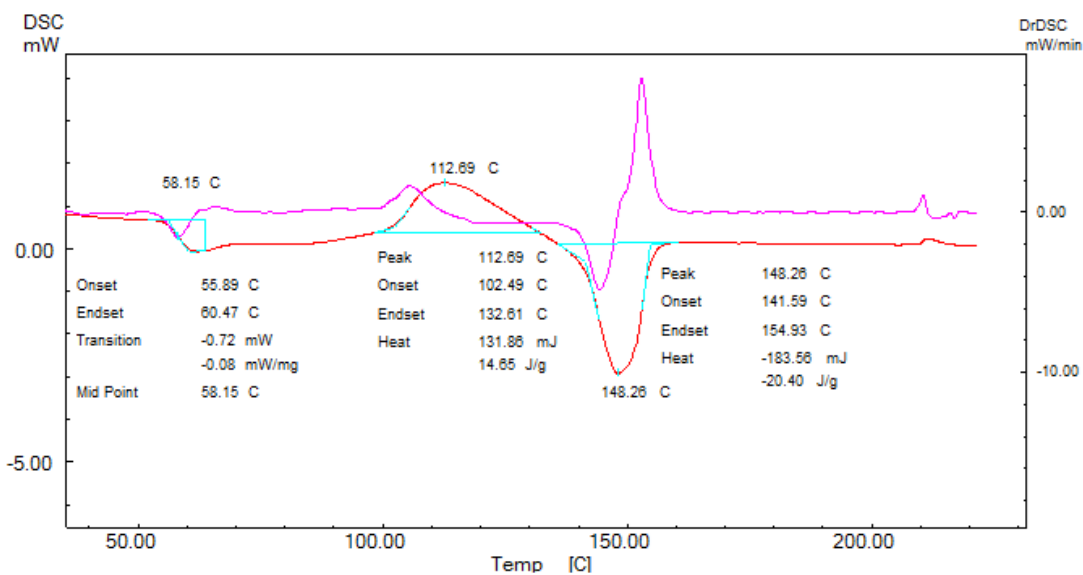


Figure C.27 DSC curve for E-7

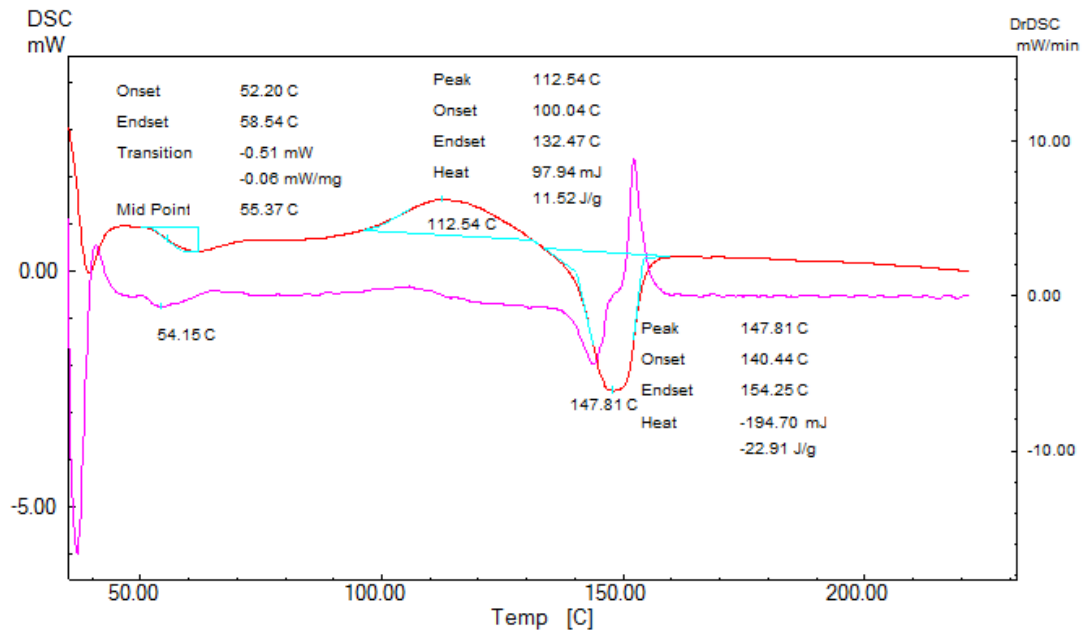


Figure C.28 DSC curve for S-1

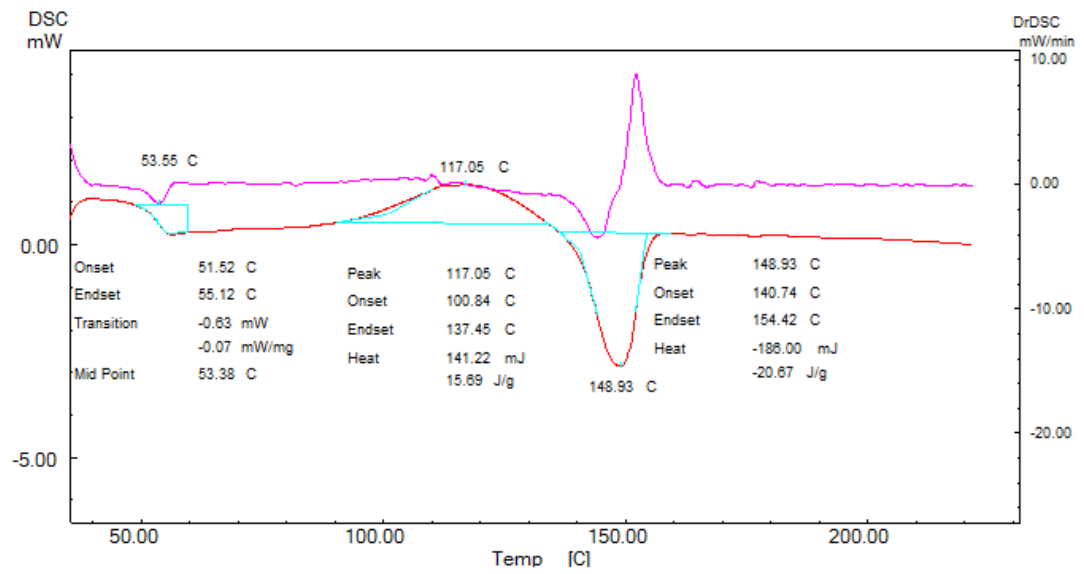


Figure C.29 DSC curve for S-2

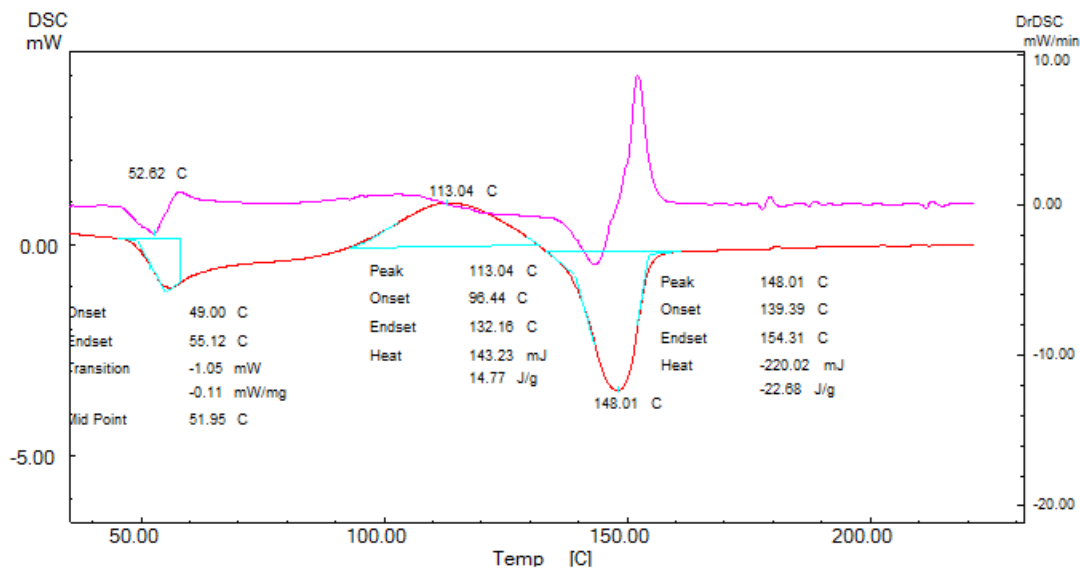


Figure C.30 DSC curve for S-3

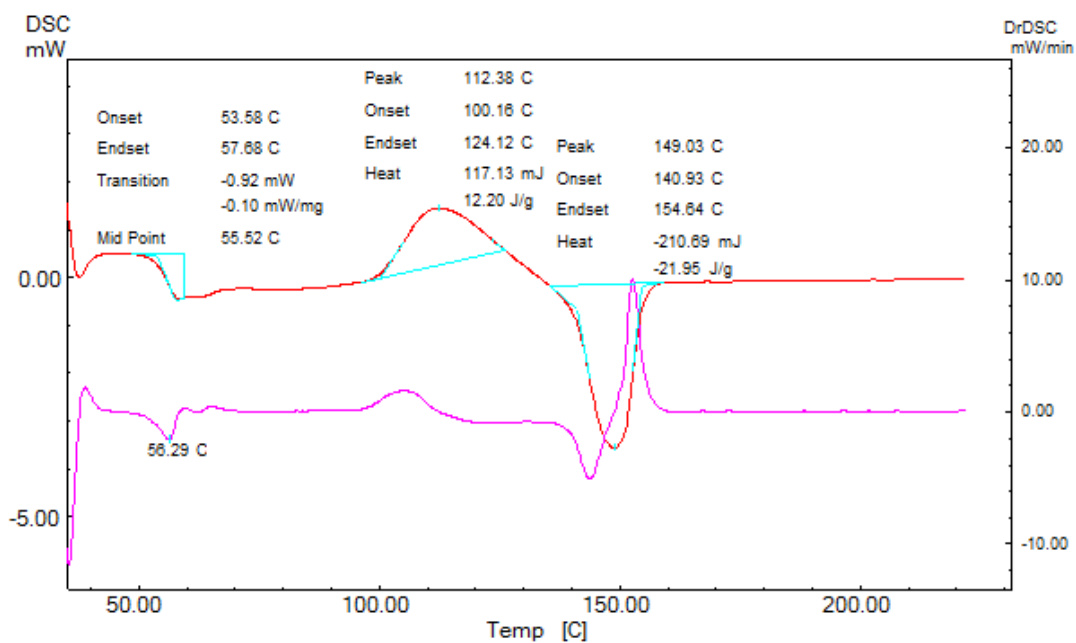


Figure C.31 DSC curve for S-5

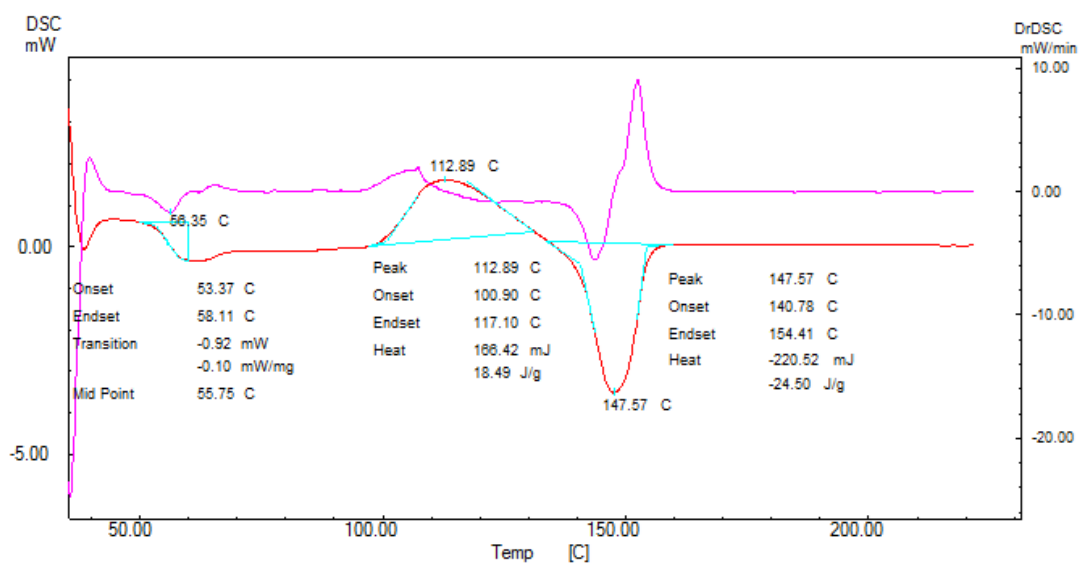


Figure C.32 DSC curve for S-6

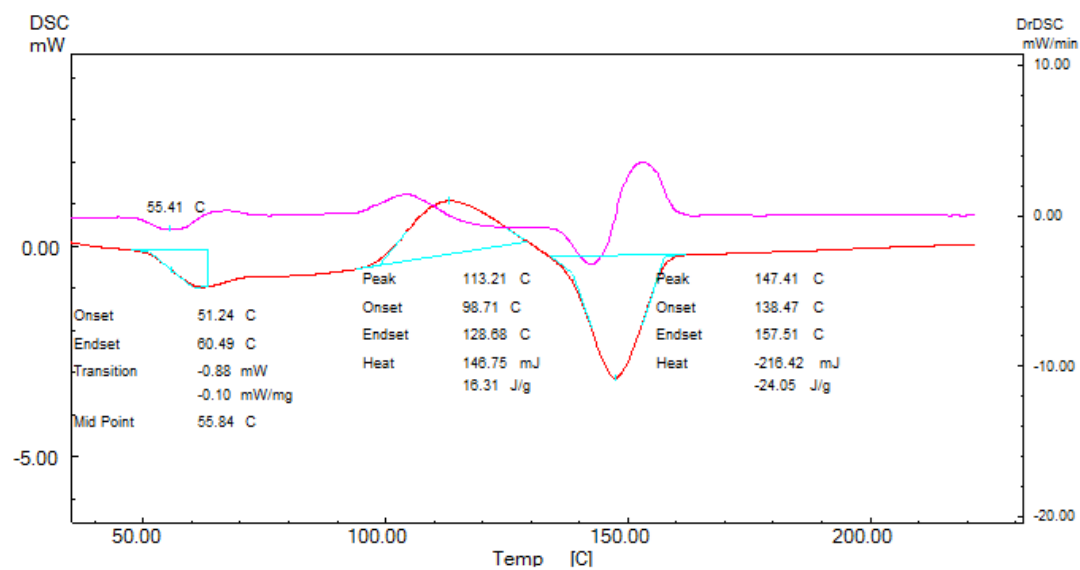


Figure C.33 DSC curve for S-7

APPENDIX D

DYNAMIC FREQUENCY TEST RESULTS

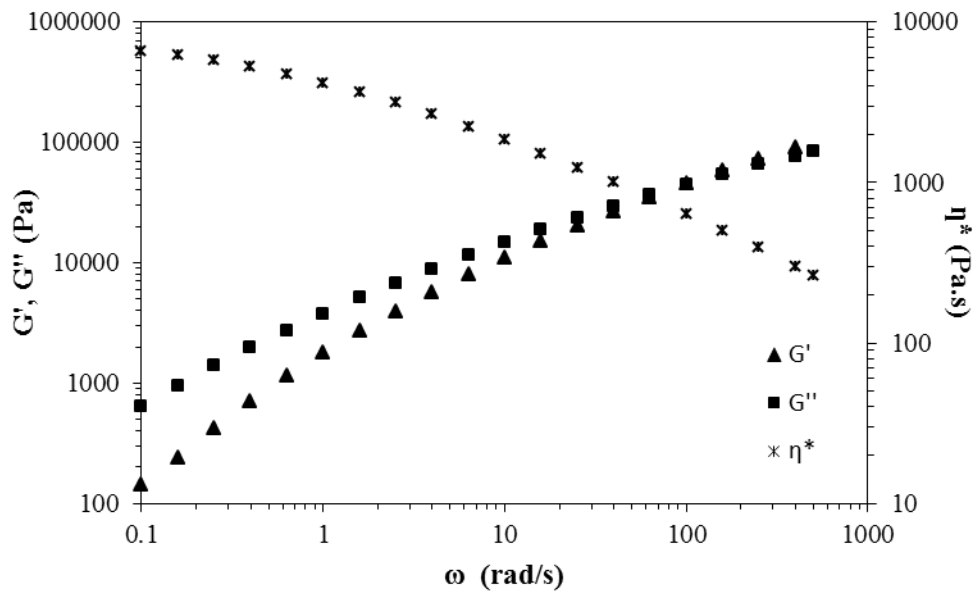


Figure D.1 Frequency dependence of G' , G'' and η^* of E-GMA

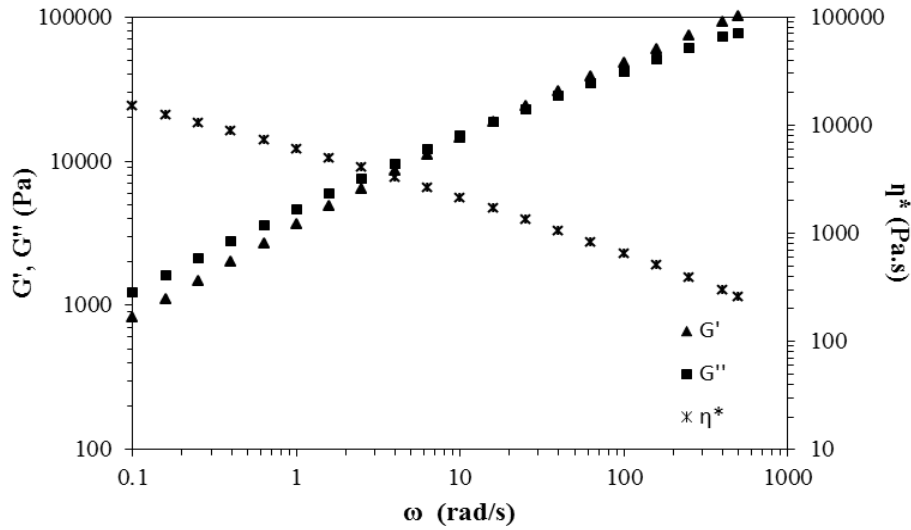


Figure D.2 Frequency dependence of G' , G'' and η^* of E-BA-MAH

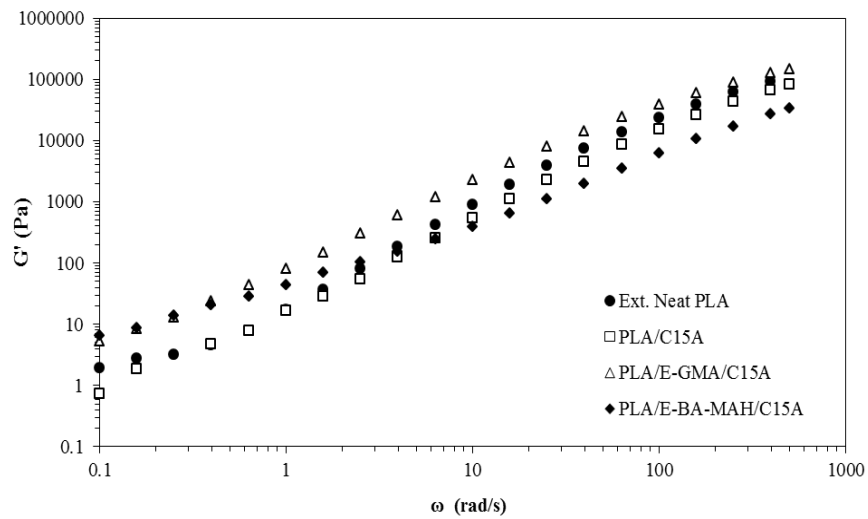


Figure D.3 Storage modulus as a function of frequency for neat PLA, and binary and ternary nanocomposites produced with C15A

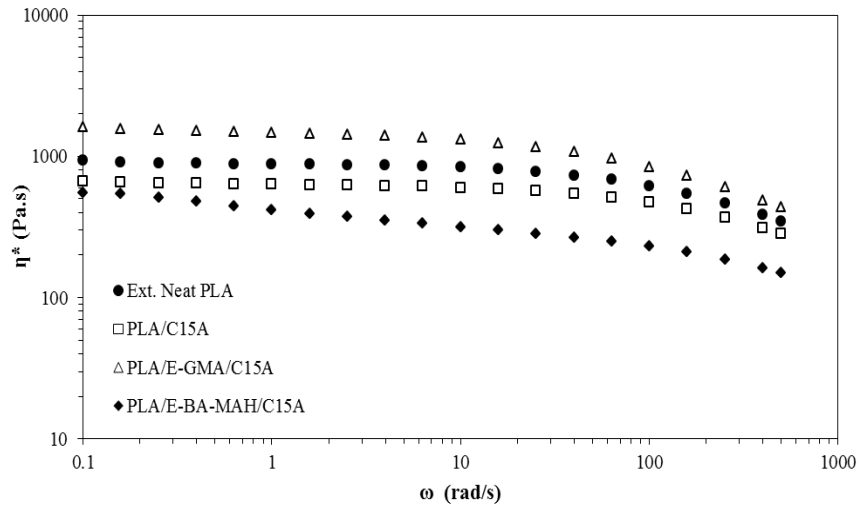


Figure D.4 Complex viscosity as a function of frequency for neat PLA, and binary and ternary nanocomposites produced with C15A

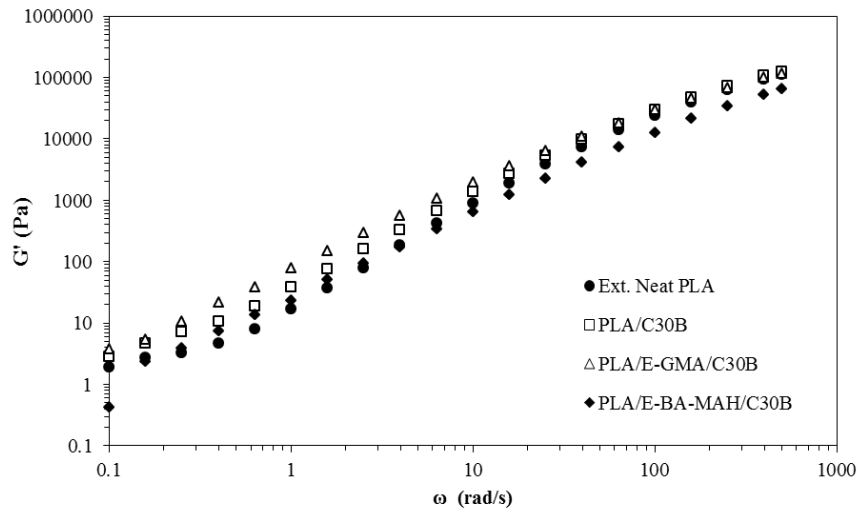


Figure D.5 Storage modulus as a function of frequency for neat PLA, and binary and ternary nanocomposites produced with C30B

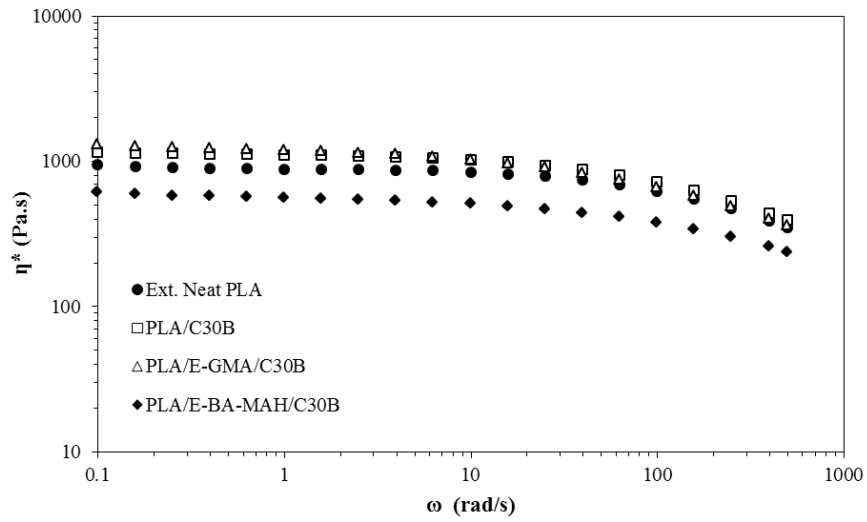


Figure D.6 Complex viscosity as a function of frequency for neat PLA, and binary and ternary nanocomposites produced with C30B

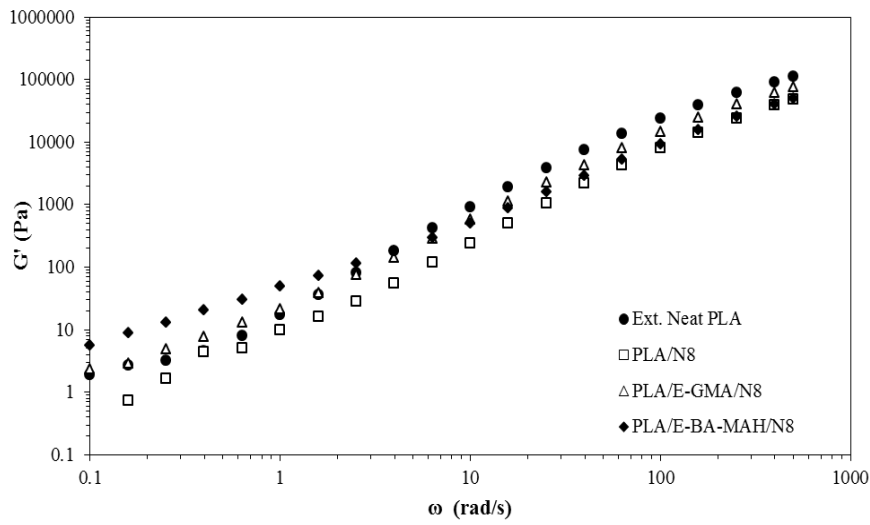


Figure D.7 Storage modulus as a function of frequency for neat PLA, and binary and ternary nanocomposites produced with N8

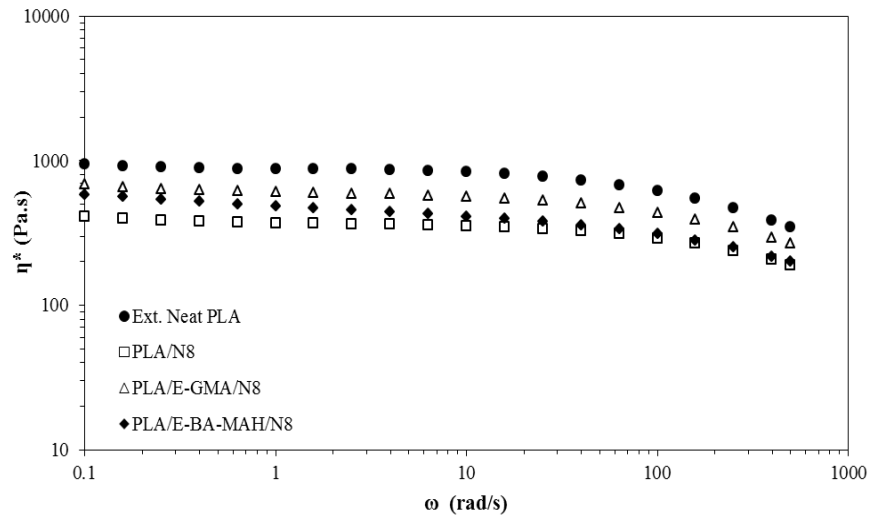


Figure D.8 Complex viscosity as a function of frequency for neat PLA, and binary and ternary nanocomposites produced with N8

APPENDIX E

IMAGE ANALYSES

SEM images of the blends and nanocomposites prepared in this study were investigated using the image analyses program, Image J. This program was primarily used to determine the average size of the dispersed phase (rubber domains) in the binary blends and ternary nanocomposites. At least three images with a magnification of x3000 were analyzed for each sample. The area of each hole in the samples was determined by using the image analysis software by transforming these black holes into ellipsoids and calculating the area of these ellipsoids. Then, the average domain size (average diameter) was calculated statistically with the box plot method. Details of these steps are given below.

- 1.** Image to be analyzed is selected. (File → Open)
- 2.** A straight line of the same length as the scale is drawn in order to identify the known length to the image analyses program. Then, this scale is defined with its given unit on the image to the corresponding number of pixels (Figure E.1).
- 3.** The area to be analyzed is selected and duplicated by right clicking on the selected region.

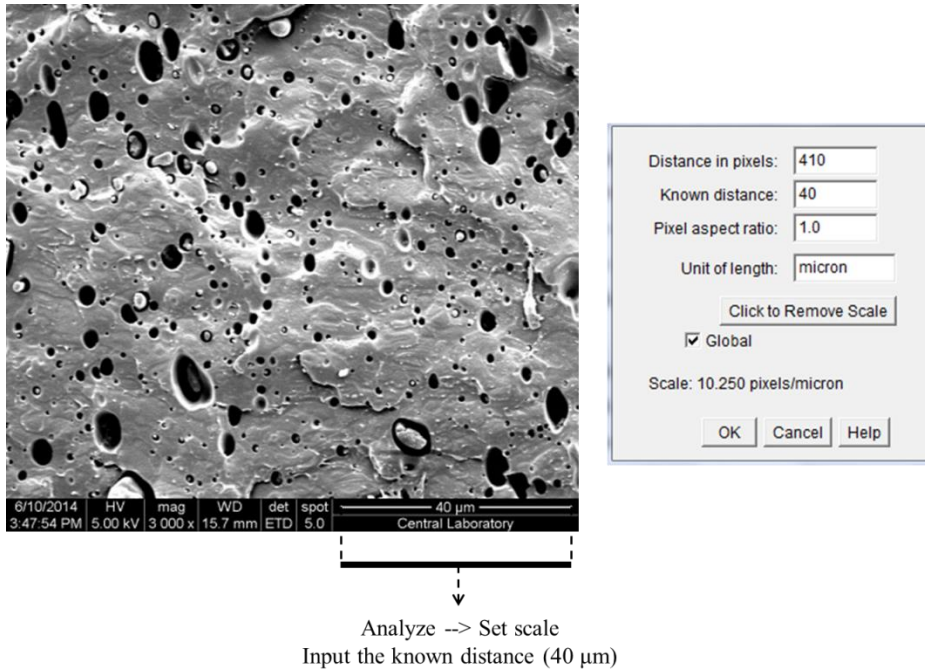


Figure E.1 SEM image of a binary blend with x3000 magnification

4. Following these steps on the software: Image → Adjust → Threshold, colors of the image can be adjusted. Threshold space should be selected as black and white (B&W) in order to identify the domains clearly. Threshold vales should be selected after the desired colors are obtained (Figure E.2).

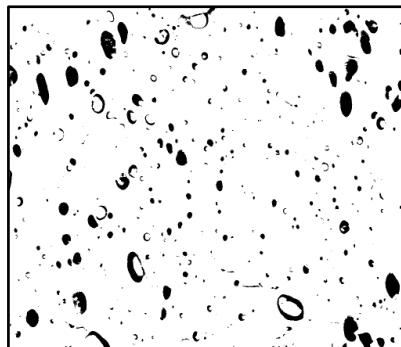


Figure E.2 SEM image of a binary blend after thresholding

5. On the threshold image, following these steps: Analyze → Analyze Particles → Ellipses; areas of all identified rubber domains can be found. The program gives the list of all domains and their areas. The identified ellipses can be seen in Figure E.3.

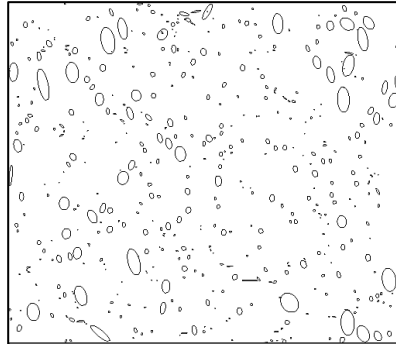


Figure E.3 SEM image of a binary blend with the identified rubber domains

6. There can be very large or small ellipses in the data set obtained from the image analyses software. These ellipses should be excluded from the data set before calculating the average domain size. In order to determine these outliers from the data set, box plot method was used.

7. The box plot is a graphical display that simultaneously describes several important features of a data set, i.e., center, departure from symmetry and identification of unusual observations or outliers.

A box plot displays the three quartiles, the minimum and the maximum data on a rectangular box, aligned either horizontally or vertically. The box encloses the interquartile range with the left edge at the first quartile (q_1), and the right edge at the third quartile (q_3). A line is drawn through the box indicating the second quartile or the median. A line (whisker) extends from each end of the box. The lower one is a line from the first quartile to the smallest data point within the 1.5 interquartile ranges from the first quartile. Similarly, the upper whisker is a line from the third quartile to the largest data point within the 1.5 interquartile from the third quartile. A

point beyond a whisker, but less than 3 interquartile ranges from the box edge, is called an outlier. A point more than 3 interquartile ranges from the box edge is called as an extreme outlier [186]. Illustration of the box plot method together with the definitions given here can be seen in Figure E.4

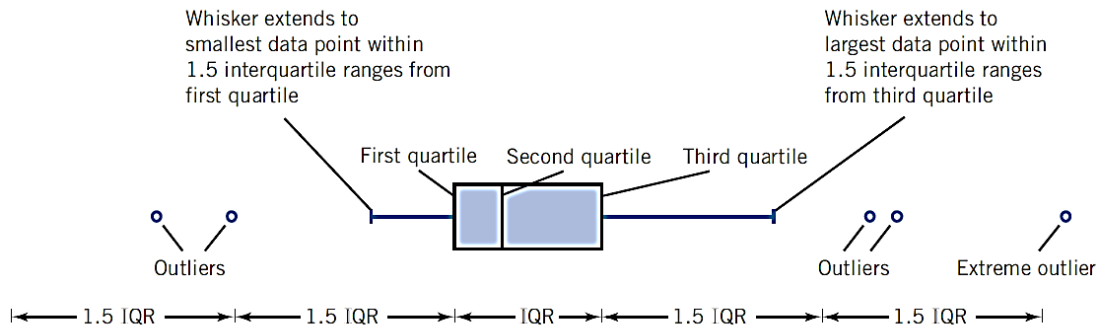


Figure E.4 Description of a box plot [186]

8. After determining the outliers and extreme outliers in the data set obtained from Image J software, the average droplet size is calculated using the remaining data.

CURRICULUM VITAE

PERSONAL INFORMATION

Surname, Name: Aık, Eda

Nationality: Turkish (TC)

Date and Place of Birth: 30 April 1984, Ankara

Marital Status: Single

E-mail: edaacik@gmail.com

EDUCATION

Degree	Institution	Year of Graduation
MS	METU Chemical Engineering	2009
BS	METU Chemical Engineering	2007
High School	Mehmet Emin Resulzade Anadolu Lisesi	2002

WORK EXPERIENCE

Year	Place	Enrollment
September 2007 - Now	METU, Chemical Engineering	Teaching Assistant
July 2013 - October 2013	University of Massachusetts Lowell, Chemical Engineering	Visiting Research Scholar
June 2006 - July 2006	Verbo Companies Group	Intern
August 2005 - September 2005	Set Ankara Cement Plant	Intern

FOREING LANGUAGES

Turkish – Native

English – Fluent

German – Beginner

PUBLICATIONS

Journal Articles Covered by Science Citation Index

P. Çalık, B. Bozkurt, G. H. Zerze, B. İnankur, E. Bayraktar, E. Boy, M. A. Orman, **E. Açık**, and T. H. Özdamar. “Effect of co-substrate sorbitol different feeding strategies on human growth hormone production by recombinant *Pichia pastoris*” *Journal of Chemical Technology & Biotechnology*, 85 (2), pp. 226-233 (2013)

P. Çalık, B. İnankur, E. Ş. Soyaslan, H. Taşpınar, **E. Açık**, and E. Bayraktar. “Fermentation and Oxygen Transfer Characteristics in Recombinant Human Growth Hormone Production by *Pichia pastoris* in Sorbitol Batch and Methanol Fed-Batch Operation” *Journal of Chemical Technology & Biotechnology*, 85 (2), pp. 226-233 (2010)

P. Çalık, E. Bayraktar, B. İnankur, E. Ş. Soyaslan, M. Şahin, H. Taşpınar, **E. Açık**, R. Yılmaz, and T. H. Tunçer. “Influence of pH on recombinant human growth hormone production by *Pichia pastoris*” *Journal of Chemical Technology & Biotechnology*, 85 (12), pp. 1628-1635 (2010)

Abstracts Published in Proceedings of National and International Conferences

E. Açık, Ü. Yilmazer. “Effects of Different Organoclays and Compatibilizers on Poly (Lactic Acid) Based Nanocomposites” 3rd Nano Today Conference, Biopolis, Singapore Poster Presentation (December 2013)

E. Açık, Ü. Yilmazer. “Effects of Processing Parameters and Nanofillers on Mechanical and Thermal Properties and Morphology of Impact Modified Poly(lactic acid)”, Materials Research Society Fall Meeting & Exhibit, Boston, USA. Poster Presentation (November 2012)

E. Açık, Ü. Yilmazer. “Effects of Different Organoclays and Compatibilizers on Poly (Lactic Acid) Based Nanocomposites”, 3rd International Polymeric Composites Symposium, Exhibition and Workshop, İzmir, Türkiye. Poster Presentation (November 2012)

E. Aık, Ü. Yilmazer. “Poli(Laktik Asit) Bazlı Nanokompozitler: Mekanik ve Isısal Özellikleri ile Morfolojisi”, 10. Ulusal Kimya Mühendisliđi Kongresi, İstanbul, Türkiye. Poster Presentation (September, 2012)

B. İnankur, **E. Aık**, E. Bayraktar, P. alık. “Effects of Bioprocess Operation Parameters on Recombinant Human Growth Hormone Production by *Pichia Pastoris*”. 6th Chemical Engineering Conference for Collaborative Research in Eastern Mediterranean Countries, Antalya, Türkiye. Poster Presentation (March 2010)

E. Aık, E. Bayraktar, P. alık. “Effects of Glycerol and Sorbitol on Human Growth Hormone Production by *Pichia Pastoris*”. International Symposium on Biotechnology: Developments and Trends, Ankara, Türkiye. Poster Presentation (September 2009)

PERSONAL INTERESTS

Air Cooled Volkswagens

Turkish Folk Dancing